TALLINN UNIVERSITY OF TECHNOLOGY
DOCTORAL THESIS
41/2019

Water Circulation in Gulf Type Regions of Freshwater Influence – the Gulf of Finland and Gulf of Riga

ILJA MALJUTENKO

TAL TECH PRESS

TALLINN UNIVERSITY OF TECHNOLOGY
School of Science
Department of Marine Systems
This dissertation was accepted for the defence of the degree 28 May 2019

Supervisor: Prof. Urmas Raudsepp
School of Science
Tallinn University of Technology
Tallinn, Estonia

Opponents: Ph.D. Tuomas Kärnä
Finnish Meteorological Institute
Helsinki, Finland

Prof. Emil V. Stanev
Institute of Coastal Research
University of Oldenburg; Helmholtz-Zentrum Geesthacht
Germany

Defence of the thesis: 2 July 2019, Tallinn

Declaration: Hereby I declare that this doctoral thesis, my original investigation and achievement, submitted for the doctoral degree at Tallinn University of Technology has not been submitted for doctoral or equivalent academic degree.

Ilja Maljutenko ……
signature

European Union
European Regional
Development Fund

Investing
in your future

ISSN 2585-6898 (publication)
ISBN 978-9949-83-460-0 (publication)
ISSN 2585-6901 (PDF)
ISBN 978-9949-83-461-7 (PDF)

TALLINNA TEHNIKAÜLIKOOL
DOKTORITÖÖ
41/2019

Vee tsirkulatsioon poolsuletud magevee mõjualas – Soome lahes ja Liivi lahes

ILJA MALJUTENKO

Contents

List of Publications

This is the list of publications on which the thesis is based on:

I Maljutenko I, Raudsepp U. 2019. Long-term mean, interannual and seasonal circulation in the Gulf of Finland — The wide salt wedge estuary or gulf type ROFI. J Mar Syst 195:1–19. Elsevier. doi:10.1016/J.JMARSYS.2019.03.004 (1.1)

II Maljutenko I, Raudsepp U. 2014. Validation of GETM model simulated long-term salinity fields in the pathway of saltwater transport in response to the Major Baltic Inflows in the Baltic Sea. Carroll J, editor. 2014 IEEE/OES Baltic International Symposium (BALTIC):23–31. Tallinn (3.2)

III Soosaar E, Maljutenko I, Raudsepp U, Elken J. 2014. An investigation of anticyclonic circulation in the southern Gulf of Riga during the spring period. Cont Shelf Res 78:75–84. (1.1)

IV Elken J, Raudsepp U, Laanemets J, Passenko J, Maljutenko I, Pärn O, Keevallik S. 2014. Increased frequency of wintertime stratification collapse events in the Gulf of Finland since the 1990s. J Mar Syst 129:47–55. Elsevier B.V. doi:10.1016/j.jmarsys.2013.04.015 (1.1)

V Raudsepp U, Legeais J-F, She J, Maljutenko I, Jandt S. 2018. Baltic Inflows. In: von Schuckmann K, Pierre-Yves Le T, Smith N, Pascual A, Brasseur P, Fennel K, Djavidnia S, editors. Copernicus Marine Service Ocean State Report, Issue 2. Journal of Operational Oceanography. p. 107–111. (1.1)

Author's Contribution to the Publications

I Setting up and running the modelling system. Manuscript writing. Analysis and post-processing of data. Preparation of figures.

II Setting up and running the modelling system. Manuscript writing. Data processing and analysis. Preparation of figures.

III Setting up and running the modelling system. Data processing and analysis. Preparation of figures. Contribution to manuscript writing.

IV Setting up and running the modelling system. Preparation of model results for analysis. Contribution to data analysis and manuscript writing.

V Data mining. Data processing and analysis. Preparation of figures. Contribution to manuscript writing.

List of abbreviations

3D	3-dimensional
2D	2-dimensional
AC	anticyclonic
BP	Baltic Proper
BS	Baltic Sea
GETM	General Estuarine Transport Model
GOTM	General Ocean Turbulence Model
GoF	Gulf of Finland
GoR	Gulf of Riga
LHCC	Left Hand Coastal Current
LSULW	Less Saline Upper Layer Water
MBI	Major Baltic Inflow
PCA	Principal Component Analysis
ROFI	Regions Of Freshwater Influence
SW	Salt Wedge
WCC	Westward Coastal Current

1 Introduction

The transition area between river and ocean, which have often been referred to as an estuary, offers a wide range of natural opportunities for different ecosystems to flourish and form one of the most productive and versatile habitats on Earth (Hansen and Rattray 1966, Aubrey and Friedrichs 1996, Kaiser et al. 2001). Urban habitats have been established near the large estuarine systems benefitting from their favorable conditions for fisheries, trading ports and agriculture where fertile plains are available (Barbier et al. 2011, Zapata et al. 2018). The mixing of riverine freshwater with underlying circulation creates a natural pathway for nutrients to reach offshore areas. Contrarily, strong stratification can suppress the mixing of oxygen to the bottom layers of the productive sea areas, creating vast zones of oxygen depletion. Therefore, estuarine ecosystems depend on the governing physical processes which may be distinctive for each estuary (Kaiser et al. 2001).

The basic concept of tidally averaged (also referred to as residual) estuarine circulation lies in the gravitational circulation of buoyant and dense water on the estuary head and mouth, respectively (Pritchard 1952, Hansen and Rattray 1965, MacCready and Geyer 2010, Geyer and MacCready 2013). The river inflow to the estuary head creates a barotropic pressure gradient towards the estuary mouth and increases longitudinal salinity gradient towards the estuary head, which results in barotropic net outflow from the estuary. The balance between the baroclinic pressure gradient from the longitudinal salinity gradient and vertical friction from the bidirectional flow system results in an exchange flow between the head and mouth of the estuary, where buoyant freshwater flows in the surface layer towards the estuary mouth and salty water in the lower layer towards the estuary head along the main axis of the estuary (Pritchard 1952, Hansen and Rattray 1965). Based on the strength and extent of the vertical stratification, four types of estuaries are recognized: salt wedge, partially mixed, vertically homogeneous and strongly stratified estuaries (Pritchard 1955). Recent findings of Burchard and Hetland (2010) and Burchard et al. (2011) challenge the assumption that forcing of the estuarine circulation arises from gravitational circulation by showing that tidal straining circulation is the dominant contributor to the classical estuarine circulation in tidally energetic estuaries (Geyer and MacCready 2014, Dijkstra et al. 2017). Cheng et al. (2013) suggested that the ratio between tidal excursion and salinity intrusion control whether the baroclinic or tidal forcing dominates the estuarine circulation.

The extent of saline water intrusion into the estuary sets the scale for longitudinal estuarine exchange (Geyer and MacCready 2014). The intrusion is often characterized as a salt wedge which is formed under the presence of a steady outflow which is gradually shrinking towards the estuary mouth above the inflow in a deeper layer towards the estuary head (Hansen and Rattray 1966). The intrusion length of the frictionally arrested salt wedge has been shown to be dependent on river discharge (Schijf and Schönfeld 1953) and estuarine convergence (Poggioli and Horner-Devine 2015); however, the realistic extent of salty water intrusion is greatly modified by tidal currents, prevailing wind forcing and the density structure of a particular estuary (Geyer and MacCready 2014).

The theory of a 2-dimensional (2D) estuarine circulation has shown to be applicable in many well-known estuaries eg. Columbia River, Juan de Fuca Strait, Mersey Narrows, James River (Hansen and Rattray 1965), Hudson River (Ralston et al. 2008), Merrimack river (Cheng et al. 2013), San Francisco Bay (Walters and Gartner 1985, Monismith et al. 1996, McCready 2004), Chesapeake Bay (Goodrich and Blumberg 1998), Mersey Estuary

(Bowden 1963, Bowden and Din 1966), Willapa Bay (Banas et al. 2004).

The rotational effects of the Earth become important when the width of the estuary becomes comparable with the internal Rossby radius and weak friction (Gill 1982, Winant 2004). The Kelvin number Ke, as a measure for Coriolis force in the estuary, is defined as the ratio between basin width W and internal Rossby deformation radius R_d, $Ke=W/R_d$, where $R_d= (g' D)^{0.5}/f$, where g' is reduced gravity, D is the thickness of the upper layer and f is the Earth's rotation frequency. In wide estuaries (Ke>1), the effect of Earth rotation causes a significant lateral shear with inflow along the left hand side and outflow along the right hand side of the estuary (Valle-Levinson 2008). This results in cyclonical (i.e anticlockwise) horizontal water circulation in the northern hemisphere (Valle Levinson et al. 2011). The inclusion of frictional effects accounted for the vertical Ekman number, $Ek= A_z/fH^2$, where A_z is vertical eddy diffusivity, f is Earth rotation frequency and H is characteristic water depth, results in a laterally sheared flow pattern with outflows along the coasts and an inflow along the central part of the estuary in case of moderate and high Ek (Kasai et al. 2000, Valle-Levinson 2008). Such a scheme in a shallow shoaling estuary head should result in an anticyclonic (i.e. clockwise) shear flow along the left hand side and a cyclonic shear along the right hand side of the estuary (e.g. Fischer 1972, Wong 1994, Wei et al. 2017). Several studies have demonstrated the existence of a persistent anticyclonic (AC) circulation gyre in the head of the wide estuary or the region of freshwater influence (ROFI) (James 1997, Johnson et al. 1997, Fujiwara et al. 1997, Kasai 2000, McClimans et al. 2000, Fujiwara 2003, Nielsen 2005, Panteleev et al. 2007, Malačič and Petelin 2009, Nakayama et al. 2014, Soosaar et al. 2014 , Lips et al. 2016a, Itoh et al. 2016, Yoon and Kasai 2017).

Freshwater outflow in the head of the wide estuary or ROFI typically forms a coastally trapped buoyant current along the right hand coast (Griffiths and Lenden 1981, Garvine 1987, Chapman and Lentz 1994, Horner-Devine et al. 2015). Under the geostrophic balance of pressure terms and favorable conditions, the fresh water can reach distances over hundreds of km, influencing coastal current systems of other estuaries (Geyer et al. 2004, Giddings and McCready 2017). The coastal current may be modified by external factors such as fluctuations of river discharge (Avicola and Huq 2003, Yankowski and Chapman 2005), winds (Geyer et al. 2004, Whitney and Garvine 2005, Choi and Wilkin 2007, Jurisa and Chant 2012), waves (Gerbi et al. 2013), tides (Halverson and Pawlowicz 2008) or ambient currents (Fong and Geyer 2002). It is shown in Soosaar et al. (2016) how external factors affect the coastal current and how ambient AC circulation causes river water to be transported along the left hand coast. Fujiwara et al. (1999) developed an analytical framework based on vorticity balance to study persistent AC circulation in Ise Bay (Japan). They showed that constant upward entrainment is the source of negative vorticity in the surface layer. The steady state cross-sectional model applied by Kasai et al. (2000) was able to explain the baroclinic inflow in the deep layer of Ise Bay, but the strong coastal current, which was part of the observed AC circulation, was absent in the model results. Thus, there are evidence of the AC circulation and coastal current at the left hand coast in natural marine systems, but no solid dynamical explanation is available.

The effect of wind has been found to either enhance or hinder estuarine circulation due to the additional surface momentum flux (Reyes-Hernandez and Valle-Levinson 2010, Li and Li 2011) and to induce barotropic pressure gradients (Gibbs et al. 2000, Elken et al. 2003). The effects of far-field processes have been shown to set up favorable conditions for reversals of the estuarine circulation by altering stratification in the mouth of the estuary (Giddings and MacCready 2018) or forcing ambient water inflows to the estuary

(Alvarez-Salgado et al. 2000, Lopez et al. 2001). There are many other indirect drivers for estuarine circulation like asymmetry of tidal currents and nonlinearities in momentum transport due to geometry of estuaries (Schultz et al. 2014, Beckerer et al. 2015).

The microtidal Baltic Sea (BS) offers a unique opportunity to study residual circulation of wide ROFIs and the underlying estuarine physical processes. The small tidal impact on hydrodynamical conditions of the BS enables research of the processes governing low frequency motions that are less contaminated with short-term variability of the currents and hydrography than in the tidally energetic estuaries. The depth of the BS sub-basins and their spatial temperature and salinity distributions are sufficient to manifest thermohaline circulation with a strong estuarine circulation component.

This study is focused on the two wide easternmost basins of the BS — the Gulf of Riga (GoR) and the Gulf of Finland (GoF). Those ROFIs differ by their unique basin morphologies, but share similar climatology of atmosphere and ambient boundary conditions from the Baltic Proper (BP). Large freshwater supply and exchange flow in the mouth in those gulfs sets the longitudinal density gradients which in turn give rise to baroclinicity of the currents. The large Kelvin number of those sub-basins suggest that the transversal currents are an important component in the prevailing circulation patterns. The results of the study are comparable to the circulation dynamics of any wide estuary.

The main goal of the thesis is to provide scientific evidence and build up a solid justification that AC, prominent coastal current at the left hand side of the estuary and estuarine exchange flow are essential components of the general circulation of the two easternmost ROFIs of the BS — GoF and GoR.

The following specific objectives are met:

- validity of long-term model simulation results is proven through comparison of the model results with the measurements (Paper **I**, **II**);
- simulated long-term mean surface current field and thermohaline fields suggested that seasonal variations of the surface layer currents and estuarine exchange along the thalweg are prevalent in the GoF (Paper **I**);
- basinwide AC circulation patterns are essential features in the GoF and GoR as derived from the validated and state-of-art long-term numerical model simulations (Paper **I**, **II**, **III**);
- realization of the AC gyres, the intensity of the left-hand coastal current and estuarine exchange flow is dependent on the strength of the zonal wind component until the generation of stratification collapses (Paper **I, III**, **IV**);
- possible mechanisms behind the dynamics of the LHCC and AC circulation is geostrophic baroclinic adjustment and upward entrainment of the salty water into the less saline upper layer (Paper **I**, **III**);
- salt wedge dynamics, LHCC and AC circulation are interrelated and affected by MBIs (Paper **I**).

The research is based on the numerical model simulations, where the validation of the model results is emphasised in Paper **II**. The results from the long-term model simulations are presented in Papers **I** and **III**. The long-term processes (Paper **III** and **I**) and short-term processes (Paper **IV**) are put in the context of the far field forcing via Major Baltic Inflows in the BP (Paper **V**).

The overview of study areas is given in Chapter 2. The description of GETM model and setups is presented in Chapter 3. The main results from the long-term mean and interannual investigations of different circulation features is presented in Chapter 4. In Chapter 5 discussion focuses on the underlying dynamics which force the water circulation in particular ROFIs. Conclusions in Chapter 6 summarize the main findings.

2 Study areas

2.1 The Baltic Sea

The Baltic Sea (BS) has been characterized as a shallow semi-enclosed intracontinental sea with a strong permanent stratification (Elken and Matthäus 2008, Leppäranta and Myrberg 2009). The surface area of the BS (including Kattegat) is 415 000 km^2 and the average depth is 55 m (Elken and Matthäus 2008). The extensive runoff from its vast catchment area, extending over 1 720 000 km^2, and inflows of saline water through the narrow Danish Straits in the west, create a strong vertical stratification with halocline extending into depths of 80—100 m. Geographically the BS is divided into multiple sub-basins that differ by their unique hydrographical and topographical peculiarities. They are connected to the BP via straits and sills where exchange flows form complicated horizontal fronts (Elken 1994, Pavelson et al. 1997, Lilover et al. 1998, Mattias et al. 2006).

The physical conditions can be related to the fjord type of estuary due to low mixing and occasional inflows of dense water over the shallow Danish Straits, which can be viewed as a sill between the North Sea and the Baltic Sea. However morphological description of a fjard [sic] (Perillo 1995) is better suited to describe the BS as it is a wide and shallow submerged glacial valley with low relief. According to Geyer and McCready (2014) the BS has been classified as a transition between a strongly stratified and fjord type estuary in scales of tidal mixing and freshwater velocity.

Döös et al. (2004) suggested the concept of a Baltic haline conveyor belt to characterize water circulation as a great meridional overturning cell extending from the Kattegat to the Bay of Bothnia. According to that the vertical circulation of the BS is described as a pathway of a dense water mass entering from the North Sea and extending to the depths of the BS sub-basins, where it is gradually mixed to the surface.

An important feature of the hydrographical conditions of the BS are the sporadic occurrences of the Major Baltic Inflows (MBI), which shape the thermohaline conditions and intensify stratification in all sub-basins (Matthäus and Franck 1992, Mohrholz 2018). The favorable conditions for MBI's occur when easterly winds have lowered the total volume of the BS and the following prevailing westerly winds force a large volume of salty water into the Arkona Basin (Lass and Matthäus 1996, Schinke and Matthäus 1998). Following the gravitational spread of dense water into the depths of the BP forces old brackish water to flush downstream or entrain into the surface layer, hence shifting the vertical isohalines in almost every sub-basin. Even intermediate inflows, which occur almost every winter (Mätthäus and Franck 1992, Lehmann et al. 2017), enhance transport within the halocline and influence the haline conditions of the downstream basins. Recent occurrences of dense water inflows to the BS have been described in Mohrholz et al. (2015) and Gräwe et al. (2015). In the Paper **V** of this study it was found that the recent MBI at the end of 2014 set favorable conditions for the following smaller inflows to reach the Gotland Deep.

A number of numerical model results show the dominance of the cyclonic mean horizontal water circulation in the BS (eg. Lehmann and Hinrichsen 2000, Lehmann et al. 2002, Meier 2007, Jedrasik 2008, Jedrasik and Kowalewski 2019). Lehmann et al. (2002) suggested that the geostrophic barotropic currents are topographically steered and form cyclonic circulation gyres around the deeps of the BP and in the Sea of Bothnia. The largest transports are found around the Gotland Basin and in the Gulf of Bothnia

(i.e the Sea of Bothnia and the Bay of Bothnia combined, see Fig. 1), while currents in the GoF and GoR show lower stability and strength (Meier 2007). Väli et al. (2013) showed that the volume transports in the BP undergo large interannual variations.

The surface currents averaged over the 40-year model run (Paper **I**) show average cyclonic circulation with strong boundary currents near the coasts in the BP and the Gulf of Bothnia (Fig. 1). There are several local scale circulation cells embedded in the main flow, which recirculate the inflowing and outflowing water. In the GoF and GoR the current field shows an anticyclonic tendency and extensive coastal currents near the southern and western coast, respectively. The currents have a higher persistency and velocity near the shoals compared to the open sea.

The tides are found to be negligible in the BS, remaining within a range of a few cm, due to shallowness and low connectivity with the ocean (Witting 1911, Magaard and Krauss 1966, Medvedev et al. 2013). Only in the GoF diurnal tidal currents may reach velocities up to 8 cm/s in the eastern part (Evdokimov et al. 1974) and 9.5 cm/s in the western part (Lilover 2012). Generally, other periodic processes, such as seiches and short term sea level variations, surpass the influence of tides (Alenius et al. 1998).

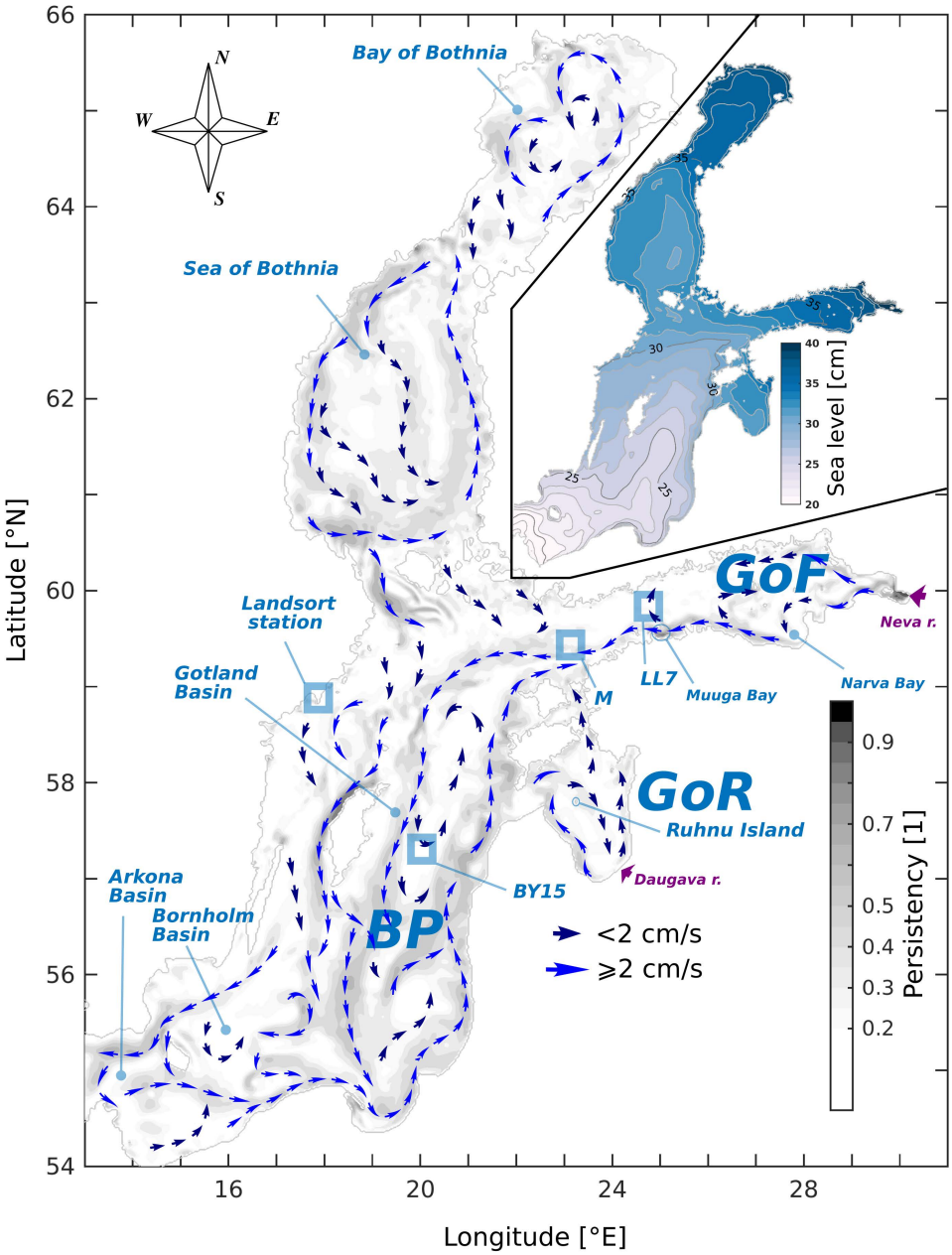

Figure 1. *The mean surface (0—10 m) current field redrawn from the vector field of long-term model simulation (Paper **I, II**). The stability of currents is underlaid in grayscale. Distribution of the mean sea level is shown in the upper-right inset.*

2.2 The Gulf of Finland

The Gulf of Finland (GoF) is a large (29 751 m^2 according to Alenius et al. (1998)) elongated sub-basin in the eastern part of the BS. It has an unrestricted connection with the BP without any sills in the western part of the gulf. The depth at the entrance to the GoF (at the 23^o E) reaches over 100 m meaning that the deep water of GoF is formed below the halocline in the BP. The southern slope is slightly steeper than the northern slope and therefore the thalweg is shifted southward from the main axis of the gulf. The coastline is irregular and characterized by many embayments and peninsulas at the southern coast and with many small islands at the northern coast.

Vertically the water column is stratified by the salinity, except for the summer months when seasonal thermocline has developed in the upper 15—20 m layer. The mean depth of quasi-permanent halocline was approximately 67 m during the summers of 1987—2008 (Liblik 2012). However, the halocline depth varies substantially near the entrance of the GoF (Elken et al. 2006). Over the longitudinal length of 400 km the salinity increases from 3—4 g/kg at the eastern part and up to 6—7 g/kg in the western part. The horizontal salinity gradient is maintained by the voluminous freshwater runoff in the eastern part of the GoF and the saline water transport to the gulf in the western part. During enhanced estuarine circulation saline water inflows to the gulf can increase salinity up to 10—11 g/kg below the halocline at the entrance of the gulf (Alenius et al. 1998, Liblik et al. 2018). The high-saline salt wedge has shown sensitivity to the westerly impulse which could result in a reversal of the estuarine circulation (Elken et al. 2003). Wind mixing and current-induced straining have shown to reduce vertical stratification significantly and even bring a water column to a mixed state during strong westerly wind impulses (Elken et al. 2003, Liblik and Lips 2012, Liblik et al. 2013). The wind has also been found to be responsible for the transverse variability of the pycnoclines (Liblik and Lips 2017) and the variability of the general flow field (Lilover et al. 2017). The ice is present in the GoF during winter time from December to April and covers the whole gulf during a severe winter (Sooäär and Jaagus 2007.

The earliest studies on the long-term average circulation in the GoF were made by Witting (1910) who introduced the concept of general cyclonic circulation (Fig. 2a). The following study by Palmèn (1930) and Hela (1952) analyzed multi-year observations from light-ships across the GoF conducted during ice free seasons. Although surface currents showed low stability, the mean cyclonic circulation was suggested (Fig. 2b). Later modelling studies of Andrejev et al. (2004) and Elken et al. (2011) confirmed the general cyclonic circulation and suggested a persistent Finnish coastal current on the northern flank of the GoF (Fig. 2 c-d).

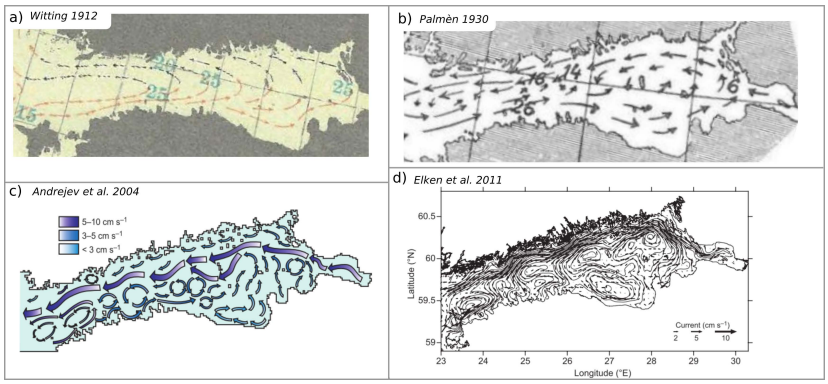

Figure 2. *Historical view of a mean circulation from fundamental studies of Witting (1912)* ***a)*** *and Palmèn (1930)* ***b)****. Surface circulation as shown in studies of Andrejev et al. (2004)* ***c)*** *and Elken et al. (2011)* ***d)****.* ***c)*** *and* ***d)*** *are reprinted from corresponding papers with the permission from the Boreal Environment Research Publishing Board.*

There have been studies based mainly on numerical model simulations, showing contradicting results with the main idea of cyclonic circulation. The anticyclonic mean circulation and indications of the persistent outflow on the southern flank of the GoF have been suggested in the modelling studies (Fig. 3) by Maljutenko et al. (2010), Soomere et al. (2011), Lagemaa (2014), Suhhova et al. (2015), Westerlund et al. (2018) and in Paper **I** of current study. Only a few studies based on measurements confirm the existence of a strong outflowing coastal current on the southern flank of the GoF (Raudsepp 1998, Suursaar 2010, Suhhova et al. 2015).

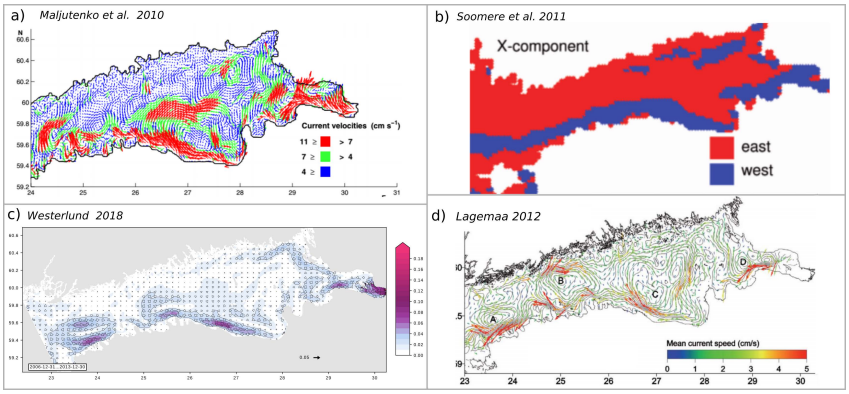

Figure 3. *Model studies of various authors depicting average surface layer circulation in the GoF. Plots replicated from corresponding studies are shown as Maljutenko et al. (2010)* ***a),*** *Soomere et al. (2011)* ***b),*** *Westerlund (2018)* ***c)*** *and Lagemaa (2012)* ***d)****.* ***b)*** *is reprinted from corresponding papers with the permission from the Boreal Environment Research Publishing Board.* ***a)*** *is reprinted with permission from author (©2010, IEEE).* ***c)*** *and* ***d)*** *are reprinted from corresponding studies with permission from author.*

2.3 The Gulf of Riga

The Gulf of Riga (GoR) is a circular shallow semi-enclosed basin in the eastern BS. It is connected with the BP via the shallow Irbe Strait, where the sill depth is 23 m, and with the Estonian Archipelago Sea via the Suur Strait with a sill depth of 5 m (Stipa et al. 1999). Therefore, only the surface water of the BP reaches the GoR under favorable conditions (Berzinsh 1995, Lilover et al. 1998). The basin is bowl-shaped with an average depth of 26 m and maximum depth of 66 m near the western coast (Stiebrins and Valing 1996). The deeper eastern part is separated from the shallower western part of the gulf by Ruhnu Island located in the central part of the GoR.

Relatively strong vertical stratification is maintained by the seasonal thermocline during summer by the buoyant freshwater flow from the rivers during springs and increased salinity below 20 m in summer (Stipa et al. 1999, Raudsepp 2001). During the period from December to March the thermal stratification is absent in the gulf. The longitudinal salinity gradient from the southern coast toward the northwestern Irbe strait is maintained by the runoff from the Daugava river and inflowing water from the BP. Ice is present in almost every winter, forming in December and lasting until April (Soosaar et al. 2010). The contribution of tides to the dynamics of currents and mixing is small as the largest tidal amplitudes of most energetic O_1 constituents have been 1.6 cm (Haritonova 2016).

Occasional inflow events into the GoR from the BP have been identified, both in measurements and modelling studies (Lilover et al. 1998, Raudsepp and Elken 1999). However, such inflow events could last over a considerable period of time. Lilover et al. (1998) suggests that on average the multilayer water exchange in the Irbe Strait is consistent with estuarine circulation. Further, they argue that the seasonal thermocline enhances the formation of dense bottom flows by reducing the wind mixing.

The circulation of the GoR has been predicted as cyclonic from the classical theory (Leppäranta and Myrberg 2008). However, several studies on salinity distributions and current measurements have revealed the anticyclonic nature of the surface circulation in the GoR (Lips et al. 1995, Paper **III**, Lips et al. 2016a). The new findings based on multi-year model simulations by Paper **III** and Lips et al. (2016a, 2016b) suggest that the mean circulation pattern can be characterized by basin-wide anticyclonic gyres with a northward current along the western flank of the GoR. Based on the vorticity conservation equation Lips et al. (2016a) drew the conclusion that a negative wind curl along with the bathymetry variations is responsible for the anticyclonic tendency in the GoR. The dynamics of basin scale topographic waves with characteristic double gyre circulation has been studied by Raudsepp et al. (2003).

The voluminous freshwater discharge of the Daugava River in the southern coast of the GoR creates a buoyant coastal current along the eastern coast of the GoR (Stipa et al. 1999, Lips et al. 2016a, Paper **III**). The coastal current is evident during the spring, but indistinguishable from ambient water in the late-summer (Stipa et al. 1999).

3 Model description and setups

The current study is based on a 3-dimensional hydrodynamic model, the General Estuarine Transport Model (GETM, Burchard and Bolding 2002). The model solves advection-diffusion equations for momentum, salinity and temperature. The sub-grid turbulence is parametrized by means of constant horizontal eddy viscosity and dynamic vertical eddy viscosity, which is calculated using two-equation κ-ε model via implementation of GOTM (General Ocean Turbulence Model, Umlauf and Burchard 2005). Arakawa-C grid is used for horizontal discretization. Adaptive bottom-following coordinate system is used for vertical discretization. Model is split into barotropic and baroclinic mode using the mode splitting technique. For the advection total variation the diminishing (TVD) scheme is used with directional split and P2-PDM limiter (Lax and Wendroff 1964, Pietrzak 1999, Klingbeil et al. 2014). Internal pressure has been parameterized according to Shchepetkin and McWilliams (2005). Ice cover, which limits heat and momentum fluxes at the surface, is assumed from when the water temperature reaches freezing temperature.

3.1 Long-term model setup

The GETM model (Paper **I** and **II**) with one nautical mile (nml) horizontal resolution was set up for the whole BS. Digital bathymetry of the BS was adopted from Seifert et al. (1995). We have used a simple 3x3 boxcar filter in order to smooth steep slopes, and adjusted water depths at the Danish Straits (Great Belt, Darss Sill). In the vertical direction, 40 bottom-following adaptive layers with adjustments parameters of alpha=0.2 and c_d=0.2 (Hofmeister et al. 2013) have been defined. Jerlov coastal water type 3 (Jerlov 1976) has been chosen for double exponential light attenuation parametrization following the adjustment of parameters by Stips (2010). The timestep for the barotropic mode of the model is 20 s and for the baroclinic mode 400 s.

The model was initialized from the average summertime salinity and temperature fields and constructed using the Data Assimilation System coupled with the Baltic Environmental Database (Wulff et al. 2013). Only a short spin-up period of a few weeks was possible from the zero velocity and sea level fields, otherwise a large-scale gravitational adjustment was beginning to cause unrealistic salinity and temperature conditions in the Southern BS. Atmospheric forcing for the BS region was prepared from the BaltAn65+ dataset, which is a dynamical downscaling of the ERA40 reanalysis using the HIRLAM model (Luhamaa et al. 2011). The atmospheric parameters were available on a spatial grid with a resolution of 0.1^{o} and at a temporal resolution of 6 hours. Monthly river runoff data of the 37 largest rivers from the Baltic catchment was adopted from the hindcast simulation of the E-HYPE hydrology model (Donnelly et al. 2016). The sea level at the open boundary in the Kattegat was prescribed using daily measurements from the Smøgen gauge station.

For realistic salinity data, we prescribed boundary conditions based on recorded salinity measurements made on Danish Lightships in Kattegat (Madsen et al. 2009) and used local wind conditions from BaltAn65+ to describe the tendency toward oceanic salinities during westerly wind impulses Gustafsson (1999). Detailed description of constructing boundary data is in Paper **II**. The monthly mean air temperature from the Kattegat was used as the surface water temperature boundary condition. When negative air temperatures occurred, $0^{o}C$ was used.

3.2 Process oriented setup

In the more process oriented studies of Paper **III** and **IV** we applied the 2 nml GETM model setup for period of 1997—2006 which was developed prior to 1 nml setup and therefore differs substantially by forcing and implementation of GETM model. In the vertical 25 sigma layers were defined. Extensive vertical mixing was suppressed by using the TVD advection scheme with Superbee limiter (Roe 1986, Pietrzak 1999, Klingbeil et al. 2014). For the open boundary, climatological monthly mean salinity and temperature profiles (Janssen et al. 1999) were used. The atmospheric forcing was adopted from the RCAO ERA40 reanalysis (Höglund et al. 2009, Meier et al. 2011).

3.3 Validation

The Landsort station at Sweden's eastern coast (Fig. 1) characterizes the overall mean sea level and the whole volume of the BS (Lehmann et al. 2017). The simulated sea level variations followed measurements with a correlation of 0.94 and RMSD of 7.4 cm. Recently, it was shown that the mean sea level derived from satellite altimetry is a good indicator for the inflows of saline water into the southern basins of the BS (Paper **III**). Therefore, simulated sea level quality also indicates the model's ability to reproduce in- and outflow events through the Danish straits and thermohaline conditions in the downstream basins.

The modelled profiles of the salinity and temperature comparison with the measured profiles for the period of 1993—2006 (Major Baltic Inflow Ocean Monitoring Indicator (MBI OMI), Paper **V**) show a good coherence of inflow signals in space and time (Fig. 4). For the overlapping period from 1993 to 2006 four deepwater inflows to the Gotland Deep are seen in the simulated and observed salinity and temperature data (Fig. 4). The inflowing saltier water increases bottom salinity from 11 g/kg close to 13 g/kg by the end of 2003. The temperature distributions also show inflows to the intermediate layer between depths of 80—150 m. These occasional inflows are crucial for the further spreading of the water masses into the GoF (Fig. 4bd). The model is a bit too sensitive to the inflows showing similar inflow patterns, but slightly overestimating the temperature values. For example, the inflow in 1997 is a prominent event in the model results, but is hardly seen in observations. In the surface layer, seasonal temperature cycle, interannual variations of salinity, upper mixed layer depth and cold intermediate layer are well reproduced by the model.

A detailed validation of the model results for physical parameters in various locations in the BP, GoR and GoF is provided in Paper **II**. Different aspects of the model results and observational data comparison are presented in Paper **V**.

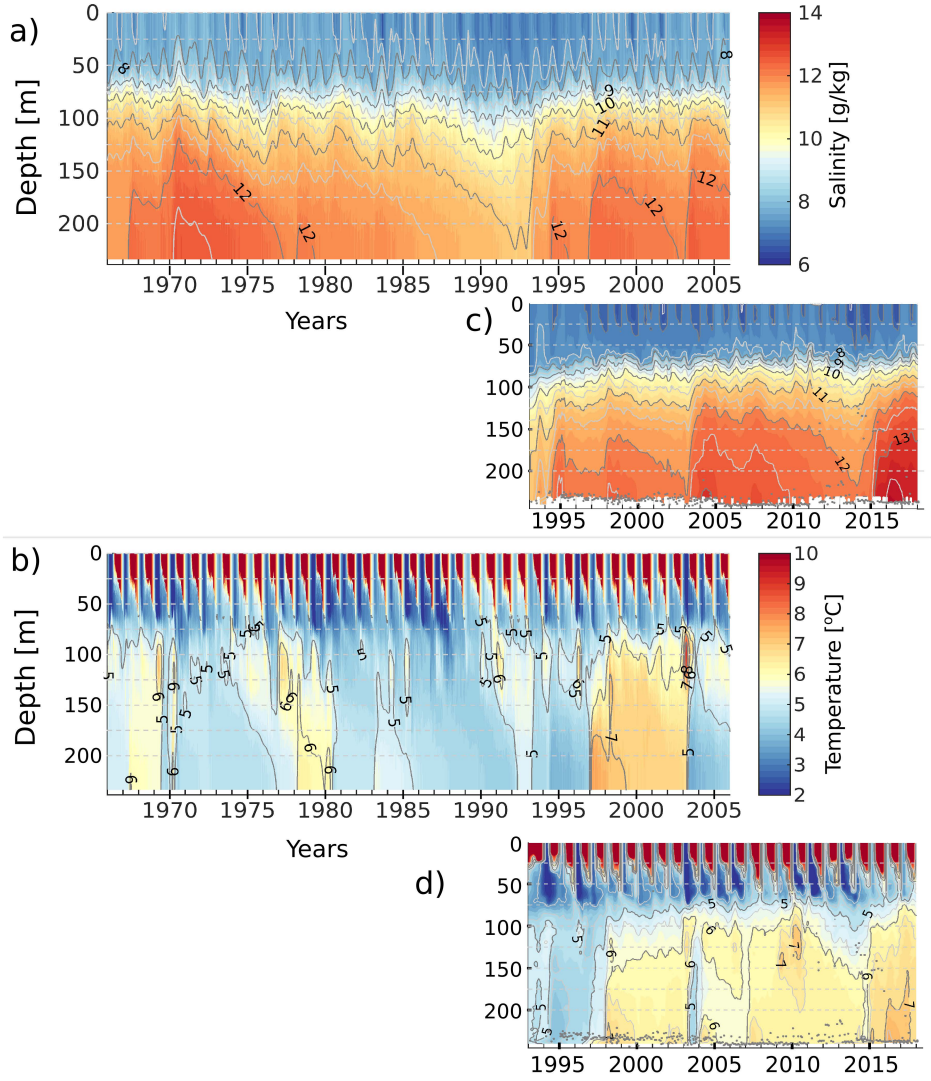

Figure 4. *Temporal evolution of vertical salinity and temperature profiles in the Gotland Deep (BY15 station). Results from long-term simulation are shown on the upper row* ***a,b)*** *and observation on bottom row* ***c,d)****.*

4 Results

4.1 Mean fields

The time-averaged salinity distributions show longitudinal asymmetry with a remarkable transversal gradient (Fig. 5a). In the western GoF a high salinity region can be seen at the southern coast, while at the northern coast approximately 1 g/kg lower salinities are evident. In the central part, the cross-shore salinity difference almost vanishes. The longitudinal gradients are higher in the eastern part of the gulf where major freshwater sources are located. Remarkable westward freshwater intrusions are evident on both the southern and the northern coast.

The average circulation field from the 40-year long-term model simulation reveals low average velocities in the major part of the GoF, except for the southern coast where the westward coastal current, which we call the Left-Hand Coastal Current (LHCC), stands out (Fig. 5b) (Paper **I**). The LHCC extends from the eastern part to the western part of the GoF, where the LHCC merges with the north-eastern loop of the cyclonic gyre of the BP. LHCC has multiple meanderings across the numerous peninsulas at the southern coast and forms multiple cross-shore extensions, which can be interpreted as anticyclonic circulation cells. The instabilities of the LHCC feed the weak eastward flow along the main axis of the gulf and therefore explain the eastward salinity intrusion in the central part of the GoF (Fig. 5a).

The general low persistency of the average current field (average of 0.28) indicates that the mean horizontal circulation pattern is more a statistical property, suggesting significant seasonality in current patterns. Higher persistency is evident over the whole span of the LHCC and in the eastern GoF where freshwater from the Neva Bay splits into the northward and southward branch.

The mean springtime circulation in the GoR (Paper **III**) has revealed an anticyclonic gyre on the left hand coast near the freshwater source along with a cyclonic gyre in the central part of the basin (Fig. 5c). The 40-year mean currents provide evidence of a well-developed LHCC and an AC gyre in the GoR (Fig. 1). Weak southward flow together with a narrow northward coastal current is evident on the eastern coast.

Sequential transects of zonal velocity show that the LHCC is associated with the bi-directional flow on the southern flank of the GoF (Fig. 6a). Such bi-directional flow is evident over the whole span of the LHCC system. The vertical extent of the westward flow extends to 20—30 m in the eastern part and up to 50 m in the western part of the GoF, where the current is shifted offshore. The salinity transects (Fig. 6b) do not show a strong freshwater intrusion along the LHCC, indicating that the LHCC has a significant source from the underlying salty water inflow, which is also confirmed from the pattern of average vertical advective flux (Paper **I**).

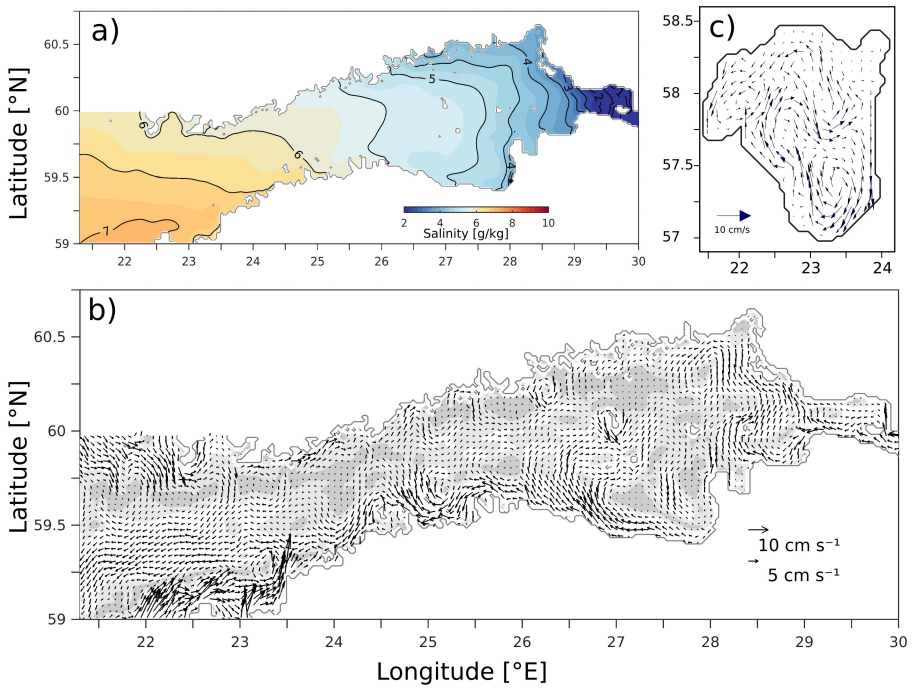

***Figure 5**. Time averaged upper-layer salinity **a)** and currents **b)** from the long-term simulation for the GoF. Mean velocity distribution at 5 m depth for the GoR **c)** averaged over the spring months from March to June from the 10-year simulation (1997—2006).*

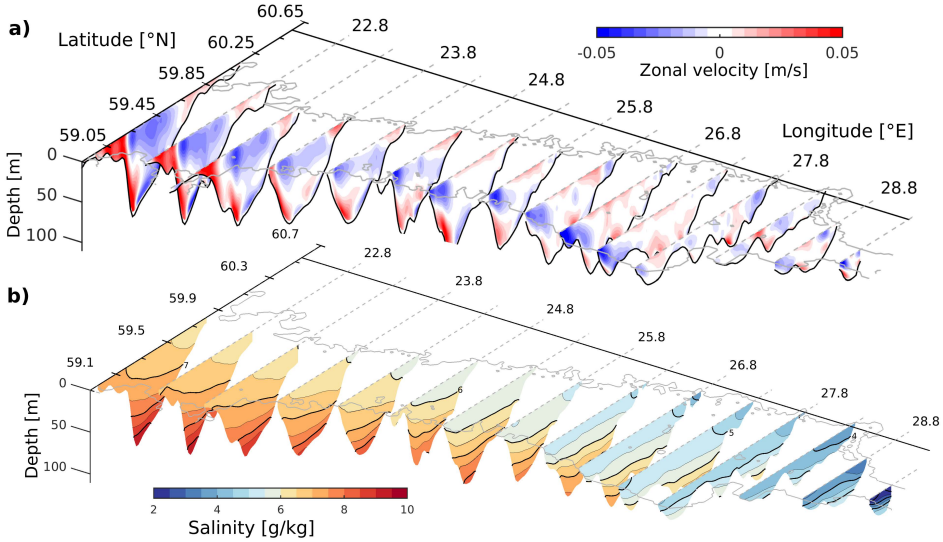

***Figure 6.** Sequential meridional transects of a 40-year mean zonal current **a)** and salinity field **b)**.*

4.2 Seasonality of the LHCC and AC gyre

Monthly climatology of the average current field in the GoF calculated from the long-term simulation shows a large seasonal variability in the upper layer of 0—10 m (Paper **I**). The series of monthly mean surface velocity patterns show that the strength of the LHCC varies within the year, being a dominant current feature during the spring months (Fig. 7a) and weakening in the second half of the year. During the period of February to May the westward current is also evident on the northern coast, where it is creating transversal salinity gradient between coastal and offshore regions. After July the cross-shore currents in the central part along with the eastward flow on the northern coast and the westward current on the southern coast form two basinwide AC gyres in September (Fig. 7b). The third, smaller gyre, is evident in the Narva Bay for most of the year. The AC gyre in the eastern part of the GoF diminishes in October due to the disappearance of LHCC, while the eastward current and southward cross-shore current in the central part maintain the western AC gyre. In November eastward velocities dominate the surface current field, without any distinctive gyre-system.

The visual inspection showed frequent occurrences of AC gyres and LHCC during the whole simulation period (Table 1). The development of LHCC during the spring months was less frequent during the periods of 1972—1982 and 1999—2003, but was continuously present over the period of 1983—1998. The development of AC gyres was less clear in the beginning of the simulation from 1966—1976, when the AC gyre dominated either in one or another part of the GoF. There are periods when development of AC gyres is not present (e.g 1982—1988, 1991—1992) and periods when a well-developed AC system could be identified in both the western and eastern part of the GoF (e.g 1980—1981, 1994—1997). The development of AC gyres is more frequent after 1993.

The existence of AC circulation in the GoR during the spring months has been analyzed using Principal Component Analysis (PCA) in Paper **III** (Fig. 8). The first mode, which embodied double gyre circulation with AC gyre in the southern part of the GoR, explained 46% of variability. For instance, the resemblance of the first PC with circulation pattern in April 1998 was 89%. The second mode, which explained 14% of variability, describes the occurrence of general cyclonic circulation embodying the strong coastal current on the right-hand coast. Third mode describes 10% of variability with basin wide anticyclonic circulation pattern. As the PCs describe symmetric flow schemes, depending on the sign of the PC amplitude, then the anticyclonic circulation pattern emerges for the positive 1st mode, negative 2nd mode and positive 3rd mode. The interannual occurrence of AC patterns is evident during the spring of all years, but most pronounced during the period from 1998 to 2005.

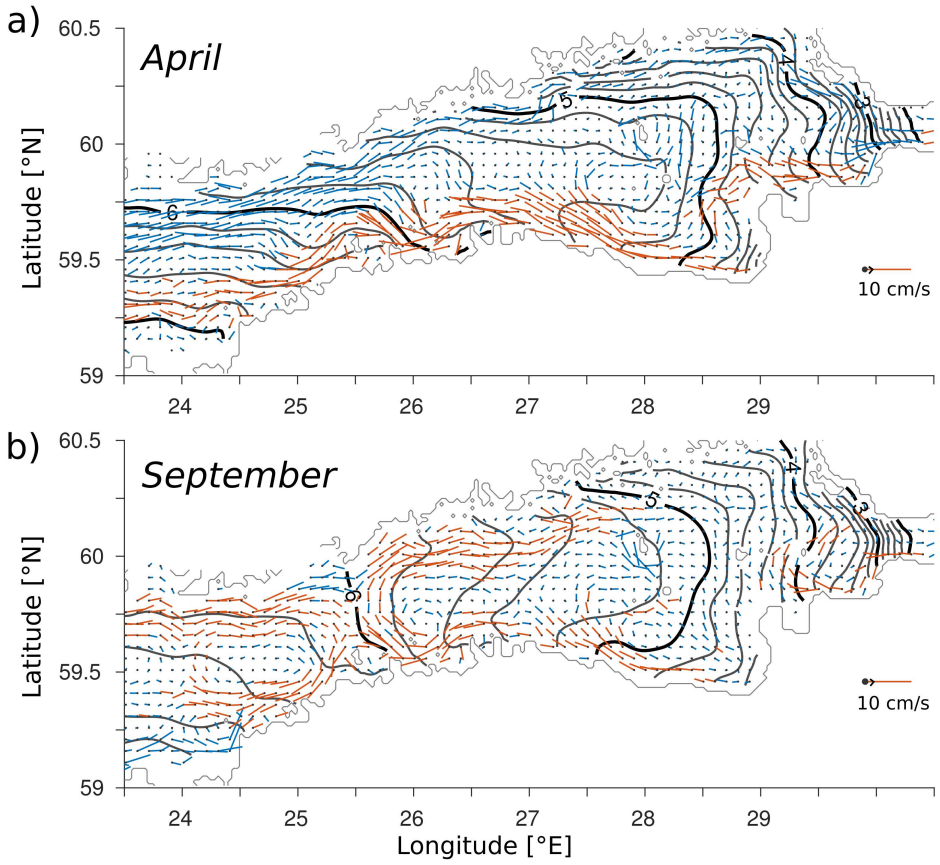

Figure 7. *Mean circulation of the upper surface layer (0—10 m) for April* ***a)*** *and September* ***b)****. LHCC and AC gyres are highlighted with red arrows. The contour lines correspond to the monthly mean upper layer salinity isohalines.*

Table 1. *The prevalence/occurrences of LHCC in the period from April to June and two basin scale anticyclonic (AC) gyres in the western (W) and eastern (E) part of the GoF during the period from July to September. The detection of LHCC and AC gyres is based on visual inspection of monthly mean circulation patterns. 1 - fully developed LHCC/AC; 2 - partially developed LHCC/AC; 3 - no WCC/AC has been identified. The last two digits of the years from 1966—2005 are shown in the first row.*

	YEAR	66	67	68	69	70	71	72	73	74	75	76	77	78	79	80	81	82	83	84	85
AMJ	LHCC	1	2	3	1	1	1	3	3	1	2	1	2	1	3	1	2	3	1	1	1
JAS	W-AC	1	2	3	1	1	2	3	2	3	2	2	1	2	3	1	1	2	3	3	3
JAS	E-AC	2	2	2	1	3	2	1	1	3	3	1	1	2	3	1	1	2	3	3	3

	YEAR	86	87	88	89	90	91	92	93	94	95	96	97	98	99	00	01	02	03	04	05
AMJ	LHCC	2	1	1	1	1	2	1	1	2	1	1	1	1	2	2	1	1	3	2	2
JAS	W-AC	3	2	3	1	3	3	3	3	3	1	1	1	2	1	1	3	1	2	3	2
JAS	E-AC	3	3	3	2	1	3	3	1	1	1	1	1	3	2	1	2	1	1	3	2

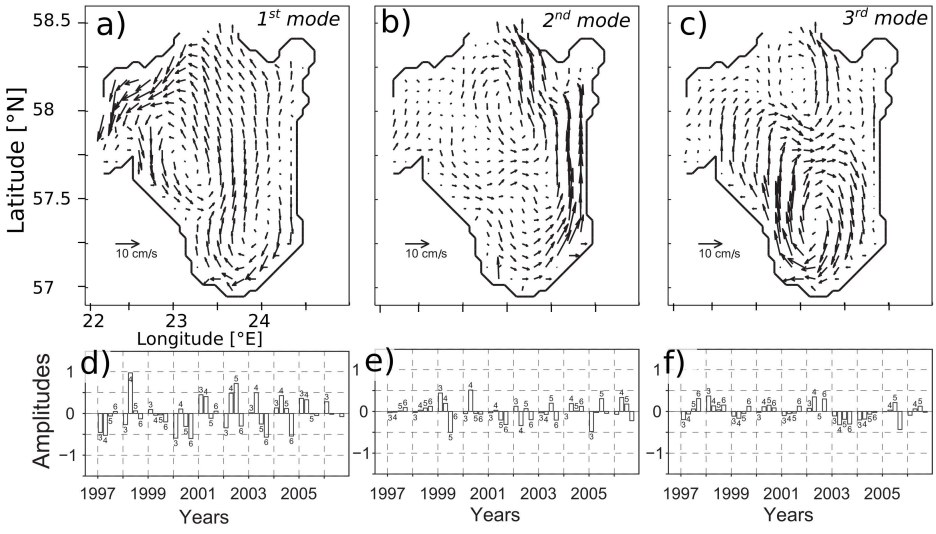

Figure 8. *First three PCA modes of spring time circulation variability in the GoR.* ***a), b)*** *and* ***c)*** *correspond to first, second and third mode respectively. Timeseries of amplitudes of first, second and third mode are shown on* ***d), e)*** *and* ***f)*** *respectively.*

4.3 Salt wedge dynamics

Monthly mean salinity transect along the thalweg (definition in Paper **I**) shows annual longitudinal variability of the estuarine circulation in the GoF (Paper **I**, Fig. 9). Longitudinal co-alignment of the isohalines 6.5 g/kg and 8 g/kg describes a winter situation in the GoF, which is characterised by strong convective and wind-induced mixing, which penetrates down to 50—60 m depth (Fig. 9a). The bottom-located isohaline of 8 g/kg is selected to describe the salt wedge's (SW) longitudinal movement and the surface isohaline of 6.5 g/kg is selected as the boundary for the low saline upper layer water (LSULW). The most inward (from west to east) location of SW and the most outward (from east to west) location of LSULW in July resemble the result of dominant estuarine circulation, where the upper layer and lower layer water have moved in the opposite directions. The climatological monthly variability of the longitudinal salinity distribution, as well as the locations of the 6.5 g/kg and 8 g/kg isohalines, is described in detail in Paper **I**. Two extreme positions of SW and LSULW are depicted on Fig. 9, showing the highest (Fig. 9b) and lowest (Fig. 9a) longitudinal separation.

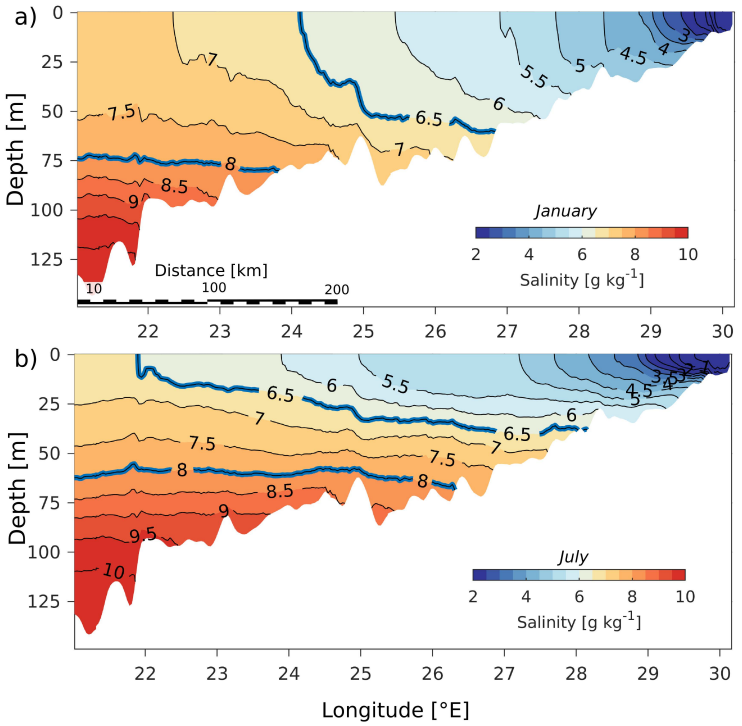

Figure 9*. The monthly mean salinity distribution along the thalweg of GoF for January* ***a)*** *and July* ***b)****. The bold blue lines represent boundaries for the less-saline upper layer and salt wedge.*

Temporal evolution of vertical salinity distribution at the location of 23 °E on the thalweg confirms the seasonal evolution of SW and LSULW (Fig. 10). The 8 g/kg isohaline reached up to 40—50 m during its shallowest position in the summer of 1969. The interannual course of salt wedge height is declining after the 1960s reaching its minimum in 1992. Since that more saline water reaches GoF and increases the height of the salt wedge until 2004. The seasonal destratification during the autumns often results

with the stratification collapse events during the winters of 1975/1976, 1977/1978, 1980/1981, 1991/1992, 1994/1995, 1999/2000 and 2004/2005, which are also evident in the measurements (Fig. 10b). The collapse in 1999/2000 was investigated in Paper **IV**, using the results from the process study model.

The salinity inflows to the GoR are intermittent due to the shallow sill, which hinders the saltier surface water of BP reaching the interior of the gulf (Lilover et al. 1998). In Paper **III** the sensitivity between zonal wind and salt flux through the Irbe strait was evaluated. The inflow of saltier water into the gulf was evident in case of negative and low positive zonal wind forcing. The inflows to the gulf were shown to increase the 3D stratification along the main axis of the gulf. Two components together, stronger density gradient and lower wind forcing, were shown to increase the anticyclonic shear in the head of the gulf.

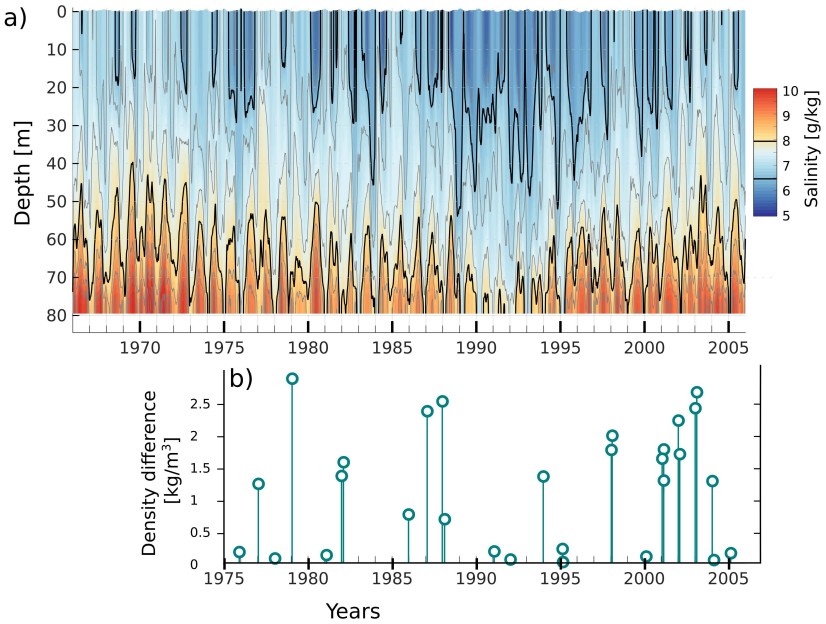

Figure 10. *Temporal evolution of vertical salinity profiles at the western part of the GoF (station **M**) **a)** and density difference between the surface and bottom layers at **LL7** station **b).** Black isohalines show 6.5 and 8 g/kg salinities which defines less saline upper water and salt wedge in the current study.*

4.4 The effect of wind on LHCC, AC and SW

The mean zonal wind calculated from observations at Kalbådagrund shows weak, north-eastward airflow of 2 m/s (Paper **I**). The positive zonal wind flow is consistent with the mean current speed at northern coast where the mean flow is eastward, however, the mean airflow is opposite to the westward waterflow on the southern coast. Annual climatology of the zonal wind is in the range of 0.5—1.5 m/s with the lowest values in April—May. The intensification of zonal wind is evident during the period from May to July, after which airflow reaches the maximum value of 1.5 m/s. Such conditions prevail from July until February and after that the wind speed starts to decrease toward its springtime minimum.

The seasonal intensification of the LHCC is simultaneous with decreasing zonal wind velocity in the beginning of the year. During the period of April—May, when the zonal wind is the weakest, the intensity of the LHCC is the highest. After June the positive zonal wind increases simultaneously with an increasing eastward current on the northern coast. This forms northern loops of two basin wide AC gyres which share extensive cross-shore bi-directional exchange in the center of the GoF.

The wind also has important influence on the interannual variability of the intensity of LHCC, development of the AC gyres and intensity of estuarine circulation (Paper **I**). During the years when zonal airflow is stronger, mean zonal currents are weaker along the southern coast, indicating weaker LHCC. However, weak zonal wind in the summer period does not completely destroy LHCC, while it enhances currents on the northern coast and development of AC gyres. Strong positive zonal wind suppresses both LHCC and AC systems. During the longer periods of relatively low zonal wind in spring (e.g. 1983—1989), the LHCC is well-developed each year.

The estuarine circulation is enhanced by down-estuary wind forcing (Li and Li 2002), therefore, larger separation of LSULW and SW in July has a high correlation with low annual positive zonal wind speed (Paper **I**). The most intensive separation of LSULW and SW takes place during the period when the zonal wind has its annual minimum in April. The retreat of the SW takes place during the second half of the year when zonal wind gains strength. In the interannual scale the maximum separation distance between LSULW and SW shows a negative correlation with the annual zonal wind speed as the intensity of estuarine circulation is hindered with a stronger up-estuary wind speed. In Paper **IV** it is shown that wintertime up-estuary wind impulses have increased since the 1990s and have further caused an increase in the number of stratification collapse events.

The position and shape of the GoR results in a slightly different wind/SW relationship. The inflow of saline water from BP is enhanced with negative and low zonal winds (Paper **III**). Such conditions are also favorable for the AC circulation pattern in the southern part of the GoR. Moreover, the sensitivity study showed that the negative zonal wind favors cyclonic circulation in the north-western part of the GoF, which transports saltier water further toward the southern part of GoR. In the study of Paper **III**, the mean circulation of April 1998, which showed AC gyre in the southern part of GoR, was investigated and sensitivity study was conducted using four forcing functions. The monthly mean zonal wind, which was negative in April 1998, resulted in a similar circulation pattern as was obtained using full forcing. The wind forcing alone did not produce the full extent of the LHCC and AC gyre. Therefore, it was suggested that the characteristic velocity field for April 1998 was a combination of density-driven and wind-induced circulation patterns.

5 Discussion

Basin-scale cyclonic circulation has been considered natural for stratified wide estuaries in terms of Kelvin and Ekman numbers (Valle-Levinson 2008). Dynamically cyclonic circulation pattern is explained by the balance between baroclinic and barotropic longitudinal pressure gradient, vertical friction and Coriolis' force (Valle-Levinson et al. 2003). The influence of longitudinal wind forcing has been found to either enhance, reduce or inverse density-driven flows (Reyes-Hernandez and Valle-Levinson 2010). Emery and Csanady (1972) have argued that the residual wind stress curl has to be positive in order to generate cyclonic mean circulation in a closed basin. In the steady state, cyclonic circulation could become a statistical property if seasonal variability of the circulation system prevails. In the basins of BS, cyclonic circulation has been shown to dominate in the BP, the Sea of Bothnia and the Bay of Bothnia (Lehmann and Hinrichsen 2000, Meier 2007, Jedrasik and Kowalewski 2019). In the GoF, the cyclonic circulation has been assumed, although already Witting (1912), Palmen (1930) and Hela (1952) emphasised that this could be only a statistical property. In the GoR the generalization of cyclonic circulation is suggested, based on the same early observations described in Witting and Palmen (Leppäranta and Myrberg 2008), however, recent investigations have shown that the cyclonic circulation is prevailing only during the cold seasons (Lips et al. 2016a). More recently, Westerlund et al. (2018) have questioned the dominance of the cyclonic circulation in the GoF and Lips et al. (2016a) have shown the dominance of cyclonic/anticyclonic circulation in the GoR during the cold seasons/calm periods respectively.

The AC circulation in the GoF has been found to be prevailing in the monthly average current field during the summertime (Paper **I**) and in GoR during spring and summer (Paper **III**, Lips et al. 2016a). In both cases, the AC gyres are well-developed in the estuary head. In the GoF the second AC gyre has formed in the mouth part of the estuary, but is less developed, has a shorter life-time and is inter-annually present less frequently. AC circulation has been reported in several wide gulf type ROFIs worldwide (e.g Fujiwara et al. 1997, Panteleev et al. 2007, Malačič and Petelin 2009). The dynamics of the AC gyres in the estuary/ROFI head have been explained by Fujiwara et al. (1997). Their two-layer vorticity balance theory suggests that the steady upward entrainment velocity generates negative vorticity tendency in the upper layer. Such vertical flux is maintained by longitudinal estuarine circulation. Similar mechanism for the formation and maintenance of the AC gyres has been suggested for the GoF and GoR (Paper **I**, **III**).

The GoF and GoR are strongly influenced by the freshwater inflow from Neva and Daugava rivers. It is well documented that an anticyclonically rotating bulge is formed in the close vicinity of the river outflow. Configuration of the GoR is very suitable for the formation of the Daugava River bulge compared to the Neva estuary. Development of the Daugava River bulge was well seen in the satellite remote sensing imagery and reproduced by the numerical model (Soosaar et al. 2016). The river bulge can contribute to the overall AC circulation in the estuary head, but the horizontal dimensions of the AC river bulge are much smaller and the dynamics are rather different than for the AC gyre. The sensitivity study by Westerlund et al. (2018) showed that increasing river runoff in GoF produced a larger river bulge and stronger velocities across the gulf, but did not change the pattern of dominant basinwide anticyclonic circulation.

In the GoR, the existence of the AC gyre has been explained by the negative wind curl (Lips et al. 2016b) and in relation to the 3D density difference (Paper **I**), which is more

consistent with the theory by Fujiwara et al. (1997). In Paper **III** it was shown that negative zonal wind enhances AC circulation in the GoR. It has been shown that wind-induced topographic waves could also generate basinwide AC gyres (Raudsepp 2001). In the GoF the existence of anticyclonic gyres is consistent with lower zonal wind speed. Negative zonal wind enhances the strength of the AC circulation, while strong positive zonal wind could destroy the anticyclonic circulation pattern.

The Left Hand Coastal Current (LHCC) has been obtained as a characteristic current feature for both the GoF and GoR (Fig. 1, 5). In the GoF, LHCC prevails during most of the months and has high persistency (Paper **I**). During the spring months, LHCC is the dominant current system in the GoR (Paper **III**). It is also an essential source of AC shear, which eventually develops into basinwide AC gyres in both gulfs. The LHCC has been shown in multiple model studies (Andrejev et al. 2010, Soomere et al. 2011, Lagemaa 2012, Lips et al. 2016a, Westerlund et al. 2018) and also in observations (Raudsepp 1998, Suursaar 2010, Suhhova et al. 2015).

The possible mechanism behind the LHCC could be geostrophic baroclinic density adjustment (Wake et al. 2004). The rotating lock-exchange experiment conducted by Wake et al. (2004) created a horizontal density jump in a rotating circular tank (Fig. 11). The advection of dyed water showed two coastal currents at the right hand and left hand sides of the tank and geostrophic flow along the front in the center of tank. Similar pattern is evident in the salinity distribution in April in the GoF (Fig. 4a), where there were strong coastal currents with northward cross-shore flow in the central part. The tank experiments are consistent with the numerical model experiments conducted for the GoR as LHCC prevails during the adjustment of the 3D density field both in experiments of Paper **III** and Lips et al. (2016b).

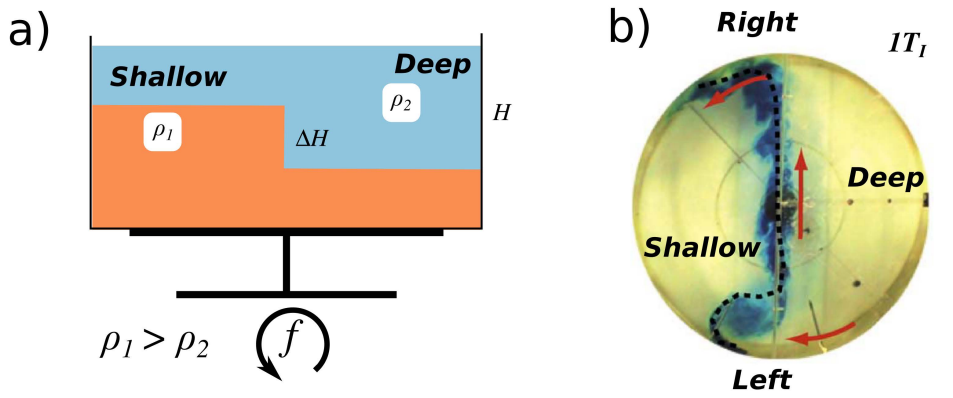

***Figure 11**. The scheme of lock-exchange experiment in a rotating tank with height H and rotation period f as conducted in the study of Wake et al. (2005) **a)** and the dye pattern and the location of potential vorticity (PV) front after 1 rotation period of density adjustment **b)**. The lower density ρ_1 water and higher density water with density ρ_2 forms an initial spatial density gradient due to a sharp density jump with interface displacement of ΔH and he dye was injected along the PV front. **b)** is reprinted from Wake et al. (2005) with permission from Elsevier.*

Both seasonal and inter-annual intensity of the LHCC in the GoF have shown to be dependent on the intensity of westerly winds (Lagemaa 2012, Paper **I**). The positive zonal wind reduces the LHCC by either suppressing the longitudinal flow in the GoR and/or enhancing wind circulation (Paper **III**). The negative zonal wind could also enhance the

LHCC due to development of the upwelling and following geostrophic adjustment on the southern coast of the GoF (Suursaar 2010, Laanemets et al. 2011). The sensitivity study in Westerlund et al. (2017) showed that increased river runoff in the GoF enhanced LHCC and related anticyclonic circulation patterns.

In the study of Kasai et al. (2000) and Fujiwara et al. (1997), a similar LHCC system is evident and is characterized as part of AC surface layer circulation in the Ise Bay. The observed current structure was similar to the ones obtained as long-term averages in GoF (Fig. 6a) where the bi-directional current structure was evident along the left-hand coast. The LHCC dynamics seems to be consistent with the longitudinal divergent flow in the surface layer (e.g Fujiwara et al. 1997). The vertical extent of the LHCC is smaller on the eastern side of the GoF (about 20 m), but extends up to 50 m in the western boundary of the GoF. The divergence in the surface layer is consistent with the positive vertical velocities on the southern coast of the GoF. During the period of strong estuarine circulation, the deep water inflow to the gulf is enhanced, which means that also the divergence in the upper layer is large. This results in stronger LHCC during the spring period or in the years when mean zonal wind is weaker. Low and negative zonal wind enhances also inflows to the GoR which in turn enhance LHCC along the western coast.

The seasonality of the LHCC has concurrent timing with the development of the seasonal thermocline, but also with decreasing mean sea levels across the GoF and GoR (Raudsepp et al. 1999). Development of the seasonal thermocline could suppress convection and wind-induced mixing allowing up-estuary advancement of the SW. Decreasing sea level creates a longitudinal sea-level gradient, which results in barotropic outflow and baroclinic water exchange enhancing estuarine circulation.

The SW shows a non-stationary position in the GoF through the full annual course. The dynamics of the halocline variability and thus SW mobility follow the dynamics described in Elken et al. (2006), which suggested that the deep water in- and outflow is associated with the baroclinic exchange, rising from the rapid volume changes in the GoF. The sea level variations have a detectable seasonal cycle (Raudsepp et al. 1999), thus it is straightforward that the barotropic water exchange has a similar seasonal cycle with an impact on the baroclinic component. In case of GoF the SW advancement toward the head is simultaneous with reducing mean sea level in the eastern BS (Raudsepp et al. 1999). The seasonal sea level variability in BS has been shown to be forced externally by the sea level variations in the North Sea, which in turn depend on the intensity of westerlies and the strength of the zonal air pressure gradient (Matthäus and Franck 1992). The invariant/steady variability of seasonal sea level variations as a driving force for seasonal SW extent could explain why the SW/LSULW maximum separation is not sensitive to salinity conditions. In the Irbe Strait, easterly wind impulses drive inflows of more saline BP surface water to the GoR, which subducts below buoyant surface water, when reaching the interior of GoR (Lilover et al. 1998, Raudsepp and Elken 1999, Paper **III**, Lips et al. 2016a). Such a gravitational current strengthens estuarine circulation in the southern part of the GoR.

The interannual SW extent in the GoF shows sensitivity to the salinity conditions in the BP. The MBIs in 1969, 1971, 1993, 1998 and 2003 have risen the mean depth of the halocline in BP. Since the depth range of thalweg in the entrance of the GoF coincides with the depths of the long-term halocline variability, the large variations in longitudinal SW extent can also be due to relatively small changes in halocline depth.

The maximum separation distance of SW and LSULW in July was shown to be sensitive to the mean annual zonal wind speed, although no long-term trends similar to salinity

trends were evident. This suggests that the MBIs set the longitudinal location for the LSULW/SW system, but do not influence the separation of LSULW/SW system or the general estuarine circulation.

Lower zonal winds have been shown to favor the inflow of saline water to the GoR (Lilover et al. 1998, Paper **I**). The inflows through the Irbe Strait have shown to occur when the sea level in the BP is higher than in GoR, which occurs during the easterly winds (Lilover et al. 1998). This is in accordance with the calculated salt flux relationship with zonal wind impulse (Paper **III**). Further propagation of dense water towards the head of the estuary as a geostrophic gravity current intensifies the estuarine circulation in the southern part of the GoR.

Both the LHCC and AC circulation have been shown to be an integral part of the normal/positive estuarine circulation. The intensification of the estuarine circulation has been evident in the seasonal course of SW and LSULW separation. The estuarine circulation inflicts natural upward entrainment/ divergence which was shown to dominate the left hand coast in the GoF (Paper **I**). All three circulation features - AC gyres, LHCC, SW - have shown similar sensitivity to the zonal-wind forcing, but are also essential parts of the dynamics described by both Fujiwara et al. (1997) and Wake et al. (2004). The important premise for AC circulation development is a strong LHCC, which forms southern loops of the AC gyres. Later development of the eastward current and cross shore exchange closes the loops and forms basin-wide gyres. The development of the LHCC is initiated simultaneously with advancement of SW towards the head since February. The location of the LHCC is consistent with the mean divergence pattern described in Paper **I**. The upward water/entrainment is necessary for development of both LHCC and the basinwide anticyclonic circulation (Fujiwara et al. 1997). In the GoF and GoR such entrainment could be either advective as a SW intrusion or related to mixing of deep water to the surface layer through boundary-, wind- and internal wave mixing.

The results of the current study rely on the results of multi-year simulations using the state of the art 3D numerical model, which enables to study the temporal dynamics of multidimensional processes. Moreover, application of 3D modelling has shown multiple advantages over simplified 1D or 2D models, which are unable to predict spatial density gradients and consequent baroclinic dynamics (e.g Kasai et al. 2000). Many features of the applied GETM model are necessary to simulate the estuarine dynamics in the GoF and GoR. The vertical discretization using temporarily varying stratification-adaptive and bottom-following coordinates is necessary for realistic propagation of the SW along the longitudinally varying slopes. The provided higher on-demand vertical resolution improves accuracy in the development of seasonal upper-layer stratification. Moreover, the higher-order advection schemes and state of art pressure gradient parametrization help to reduce both the numerical mixing and numerical scheme errors (Gräwe et al. 2013, Klingbeil et al. 2018).

It is important to note that the AC circulation patterns cannot be simulated using steady-state process models with reduced dimensionality (e.g. Valle-Levinson 2008, Kasai et al. 2000), but are evident in numerous simulations with 3D numerical models (Yanagi et al. 1998, Soomere et al. 2011, Lagemaa 2012, Westerlund et al. 2018). Multiple model studies have shown different circulation patterns in the GoF. In case of a too coarse vertical resolution resulting in a too shallow halocline, the SW would lose its longitudinal mobility and vertical entrainment would inflict AC circulation gyres in different locations, where the vertical estuarine circulation shows non-stationarity.

The validation of the model results show good agreement with observations and are comparable with other recent model studies (Placke et al. 2018, Jedrasik and Kowalewski 2019). The complexity of the simulations include also numerous uncertainties which are discussed in Paper **I**. The largest discrepancies between model and observations were due to the occasionally overestimated inflows to the BP and the following intensification of estuarine circulation.

Westerlund (2018) raises justified doubt in the accuracy of the numerical models as some of the processes have been included with the first order accuracy or through robust parametrizations. For example, the coupling of atmosphere-ice-water is absent in many of the studies and therefore, the momentum flux from the wind could have a higher uncertainty.

In the current thesis the momentum flux of long-term model simulation was limited using seawater freezing temperature. With a more realistic ice model, taking also into account ice volume, the momentum flux could be limited for a longer period in the spring resulting in a more realistic estuarine circulation. The results could be biased due to the uncoupled windwave and atmosphere effects, unresolved bathymetry (Andrejev et al. 2010) and ice-ocean dynamics (Roy et al. 2015).

6 Conclusions

This work emphasizes the importance of AC circulation, down-estuary LHCC and estuarine exchange flow along the thalweg during the annual course of the GoF. In the GoR, similar features are apparent or indicative in the multi-year study of the hydrography and the circulation. These sub-basins of the BS are both wide enough compared to the internal Rossby deformation radius, so that Coriolis force plays a significant role in the water circulation and shapes the hydrographic fields. Nonetheless, different morphology of these two basins has a significant role regarding how the considered features and underlying dynamics are realized. The GoF has an elongated shape and unrestricted connection to the BP, making it more an example of a classical wide estuary. The GoR has almost a circular shape and the water exchange with the BP is limited through the narrow Irbe Strait with a shallow sill, making it more like a gulf-type ROFI.

In both basins the mean climatological surface layer currents (residual circulation) are weak, <2 cm/s, but still the down-estuary coastal current at the left hand side with persistency up to 0.5 emerges. In the GoF the current extends to the central area of the gulf (24 °E), while it spans along the entire western coast in the GoR. The AC circulation gyre covers the southwestern part of the GoR, but is hardly seen in the south-eastern GoF. Seasonal variations of the surface layer circulation are shown to overwhelm mean circulation, emphasizing a highly energetic coastal current system and two AC circulation gyres in the GoF in spring and summer, respectively. In the GoR the dominance of AC circulation is presumed during spring and proven accordingly with a hint that this circulation feature can be more common in summer.

Zonal wind has shown to have a decisive effect on the coastal current and AC circulation in both sub-basins. Negative zonal wind component enhances the coastal current and AC circulation. Zero and even weak positive zonal wind enables the existence of the circulation patterns, but a stronger positive zonal wind destroys them.

Free connection between the GoF and BP enables the two-layer estuarine circulation to fully develop. During the first half of the year, SW in the bottom layer and less saline upper layer water are advancing up-estuary and down-estuary, respectively. During the second half of the year, the SW retreats and upper layer water is mixed down to the halocline. In case of favourable wind conditions, i.e. relatively strong positive zonal wind component, estuarine circulation reversals cause a collapse of the vertical stratification, the frequency of which has increased since the 1990s. Free estuarine circulation is hampered in the GoR due to the shallow sill in the Irbe Strait and saline water inflows to the gulf are intermittent. Still, the increase in the bottom layer salinity in the northwestern GoR and anticyclonic vorticity in the southern gulf are positively correlated. Negative zonal wind strengthens AC circulation in the southern GoR by itself, but forces inflow to the GoR through the Irbe Strait, which in turn drives AC vorticity tendency.

Salinity stratification in the BP is the far-field driver of the estuarine exchange flow in the GoF. The MBIs, which increase the stratification in and below the halocline, shift the estuarine exchange flow pattern towards the estuary head, while the estuarine exchange flow system is shifted towards estuary mouth during the stagnation period. Inside the gulf, the longitudinal travelling distance of the LSULW and SW are independent on the stratification in the BP, but affected by the strength and a sign of the zonal wind component. Dynamically, but so far speculatively, rapid advancement of the SW in the GoF and intermittent inflows to the GoR force LHCC through the baroclinic geostrophic

adjustment. In more steady estuarine circulation conditions, vertical entrainment of saline bottom layer water into the buoyant surface layer water and earth rotation drive AC circulation in the surface layer of the gulfs.

Although the analyses of this thesis are mainly based on the numerical model simulations, thorough validation of the model results and consistency with other published studies provide confidence that the conclusions of this study are valid for the GoF and the GoR, and could be exported to the other wide estuaries and gulf type ROFIs.

References

Alenius P, Myrberg K, Nekrasov A. 1998. The physical oceanography of the Gulf of Finland: A review. Boreal Environ Res 3(2):97–125.

Álvarez-Salgado XA, Gago J, Míguez BM, Gilcoto M, Pérez FF. 2000. Surface Waters of the NW Iberian Margin: Upwelling on the Shelf versus Outwelling of Upwelled Waters from the Rías Baixas. Estuar Coast Shelf Sci 51(6):821–837. doi:10.1006/ecss.2000.0714

Andrejev O, Myrberg K, Alenius P, Lundberg PA. 2004. Mean circulation and water exchange in the Gulf of Finland-a study based on three-dimensional modelling. Boreal Environ Res 9(1):1–16. http://www.borenv.net/BER/pdfs/ber9/ber9-001.pdf.

Andrejev O, Sokolov A, Soomere T, Värv R, Viikmäe B. 2010. The use of high-resolution bathymetry for circulation modelling in the Gulf of Finland. Est J Eng 16(3):187. doi:10.3176/eng.2010.3.01

Aubrey DG, Friedrichs CT. 1996. Buoyancy Effects on Coastal and Estuarine Dynamics. Aubrey D. G., Friedrichs CT, editors. Washington, D. C.: American Geophysical Union. (Coastal and Estuarine Studies; Vol. 53). doi:10.1029/CE053

Avicola G, Huq P. 2003. The role of outflow geometry in the formation of the recirculating bulge region in coastal buoyant outflows. J Mar Res 61(4):411–434. doi:10.1357/002224003322384870

Banas NS, Hickey BM, MacCready P, Newton JA. 2004. Dynamics of Willapa Bay, Washington: A Highly Unsteady, Partially Mixed Estuary. J Phys Oceanogr 34(11):2413–2427. doi:10.1175/jpo2637.1

Barbier EB, Hacker SD, Kennedy C, Koch EW, Stier AC, Silliman BR. 2011. The value of estuarine and coastal ecosystem services. Ecol Monogr 81(2):169–193. doi:10.1890/10-1510.1

Baugh TM, Day JW, Hall CAS, Kemp WM, Yáñez-Arancibia A. 1990. Estuarine Ecology. Estuaries 13(1):112. doi:10.2307/1351438

Becherer J, Stacey MT, Umlauf L, Burchard H. 2014. Lateral Circulation Generates Flood Tide Stratification and Estuarine Exchange Flow in a Curved Tidal Inlet. J Phys Oceanogr 45(3):638–656. doi:10.1175/jpo-d-14-0001.1

Berzinsh V. 1995. Hydrological regime. In: Ojaveer E, editor. *Ecosystem of the Gulf of Riga between 1920 and 1990*. Tallinn: Estonian Academy of Sciences.

Berzinsh V. 1995. Hydrology. Ecosystem of the Gulf of Riga between 1920 and 1990. Academia 5:7–8.

Bowden KF. 2013. the Mixing Processes in a Tidal Estuary. Adv Water Pollut Res 7: 329–346. doi:10.1016/b978-1-4832-8391-3.50054-3

Bowden KF, Din SHS El. 1966. Circulation, Salinity and River Discharge in the Mersey Estuary. Geophys J Int 10(4):383–399. doi:10.1111/j.1365-246X.1966.tb03066.x

Bowden KF. 1963. The mixing processes in a tidal estuary. Air Water Pollut 7:343–356.

Burchard H, Bolding K. 2002. Getm – a general estuarine transport model. Scientific documentation. Tech Rep EUR 20253 en, in press.

Burchard H, Hetland RD. 2010. Quantifying the Contributions of Tidal Straining and Gravitational Circulation to Residual Circulation in Periodically Stratified Tidal Estuaries. J Phys Oceanogr 40(6):1243–1262. doi:10.1175/2010JPO4270.1

Burchard H, Hetland RD, Schulz E, Schuttelaars HM. 2011. Drivers of Residual Estuarine Circulation in Tidally Energetic Estuaries: Straight and Irrotational Channels with Parabolic Cross Section. J Phys Oceanogr 41(3):548–570. doi:10.1175/2010JPO4453.1

Chapman DC, Lentz SJ. 1994. Trapping of a Coastal Density Front by the Bottom Boundary Layer. J Phys Oceanogr 24(7):1464–1479. doi:10.1175/1520-0485(1994)024<1464:TOACDF>2.0.CO;2

Cheng P, de Swart HE, Valle-Levinson A. 2013. Role of asymmetric tidal mixing in the subtidal dynamics of narrow estuaries. J Geophys Res Ocean 118(5):2623–2639. doi:10.1002/jgrc.20189

Choi B-J, Wilkin JL. 2007. The Effect of Wind on the Dispersal of the Hudson River Plume. J Phys Oceanogr 37(7):1878–1897. doi:10.1175/jpo3081.1

Dietze H, Löptien U, Getzlaff K. 2014. MOMBA 1.1 - a high-resolution Baltic Sea configuration of GFDL's Modular Ocean Model. Geosci Model Dev 7(4):1713–1731. doi:10.5194/gmd-7-1713-2014

Dijkstra YM, Schuttelaars HM, Burchard H. 2017. Generation of exchange flows in estuaries by tidal and gravitational eddy viscosity-shear covariance (ESCO). J Geophys Res Ocean 122(5):4217–4237. doi:10.1002/2016JC012379

Döös K, Meier HEM, Döscher R. 2004. The Baltic haline conveyor belt or the overturning circulation and mixing in the Baltic. Ambio 33(4–5):261–266. doi:10.1579/0044-7447-33.4.261

Elken J. 1994. Numerical study of fronts between the Baltic sub-basins. Proceedings of the 19th Conference of the Baltic Sea Oceanographers 1:438–446. Sopot: Institute of Oceanology, Polish Academy of Sciences.

Elken J, Mälkki P, Alenius P, Stipa T. 2006. Large halocline variations in the Northern Baltic Proper and associated meso- and basin-scale processes. Oceanologia 48(SUPPL.):91–117.

Elken J, Matthäus W. 2008. Baltic Sea Oceanography. In: H. von Storch, editor. *Assessment of Climate Change for the Baltic Sea Basin*. Springer-Verlag Berlin Heidelberg. p. 379–385.

Elken J, Nõmm M, Lagemaa P. 2011. Circulation patterns in the Gulf of Finland derived from the EOF analysis of model results. Boreal Environ Res 16(SUPPL. A):84–102.

Elken J, Raudsepp U, Lips U. 2003. On the estuarine transport reversal in deep layers of the Gulf of Finland. J Sea Res 49(4):267–274. doi:10.1016/S1385-1101(03)00018-2

Emery KO, Csanady GT. 1973. Surface Circulation of Lakes and Nearly Land-Locked Seas. Proc Natl Acad Sci U S A 70(1):93–97. National Academy of Sciences. http://www.jstor.org/stable/62274.

Evdokimov SN, Klevantsov YP, Sustatov YY. 1974. Analysis of dynamics of waters in the Gulf of Finland. Collect Work Leningr Hydrometeorol Obs [In Russ 8:155–164.

Fischer H. 1972. Mass transport mechanisms in partially stratified estuaries. J Fluid Mech 53(04):671. doi:10.1017/S0022112072000412

Fong DA, Geyer WR. 2002. The Alongshore Transport of Freshwater in a Surface-Trapped River Plume. J Phys Oceanogr 32(3):957–972. doi:10.1175/1520-0485(2002)032<0957:TATOFI>2.0.CO;2

Fonselius SH. 1970. On the stagnation and recent turnover of the water in the Baltic. Tellus 22(5):533–544. doi:10.1111/j.2153-3490.1970.tb00520.x

Fujiwara T, Sanford LP, Nakatsuji K, Sugiyama Y. 1997. Anti-cyclonic circulation driven by the estuarine circulation in a gulf type ROFI. J Mar Syst 12(1–4):83–99. doi:10.1016/S0924-7963(96)00090-5

Garcia-alba J, Zapata C, Puente A, Espinoza J. 2018. Assessment of ecosystem services of an urbanized tropical estuary with a focus on habitats and scenarios. :1–19.

Garvine RW. 1987. Estuary Plumes and Fronts in Shelf Waters: A Layer Model. Journal of Physical Oceanography. doi:10.1175/1520-0485(1987)017<1877:EPAFIS>2.0.CO;2

Gerbi GP, Chant RJ, Wilkin JL. 2013. Breaking Surface Wave Effects on River Plume Dynamics during Upwelling-Favorable Winds. J Phys Oceanogr 43(9):1959–1980. doi:10.1175/jpo-d-12-0185.1

Geyer WR, Signell RP, Fong DA, Wang J, Anderson DM, Keafer BA. 2004. The freshwater transport and dynamics of the western Maine coastal current. Cont Shelf Res 24(12):1339–1357. doi:10.1016/j.csr.2004.04.001

Geyer WR, MacCready P. 2013. The Estuarine Circulation. Annu Rev Fluid Mech 46(1):130829112240001. doi:10.1146/annurev-fluid-010313-141302

Geyer WR, MacCready P. 2014. The Estuarine Circulation. Annu Rev Fluid Mech 46(1):175–197. doi:10.1146/annurev-fluid-010313-141302

Gibbs MT, Bowman MJ, Dietrich DE. 2000. Maintenance of Near-Surface Stratification in Doubtful Sound, a New Zealand Fjord. Estuar Coast Shelf Sci 51(6):683–704. doi:10.1006/ecss.2000.0716

Giddings SN, MacCready P. 2017. Reverse Estuarine Circulation Due to Local and Remote Wind Forcing, Enhanced by the Presence of Along-Coast Estuaries. J Geophys Res Ocean 122(12):10184–10205. doi:10.1002/2016JC012479

Gienapp H. 1993. Seiches, tides and their subharmonics in the Baltic. Dtsch Hydrogr Zeitschrift 45(4):267–278. doi:10.1007/BF02226384

Gill AE. 2016. Atmosphere—Ocean Dynamics. Elsevier.

Goodrich DM, Blumberg AF. 1991. The fortnightly mean circulation of chesapeake bay. Estuar Coast Shelf Sci 32(5):451–462. doi:10.1016/0272-7714(91)90034-9

Gräwe U, Holtermann P, Klingbeil K, Burchard H. 2013. Advantages of vertically adaptive coordinates in numerical models of stratified shelf seas. Ocean Model 92:56–68. Elsevier Ltd. doi:10.1016/j.ocemod.2015.05.008

Gräwe U, Naumann M, Mohrholz V, Burchard H. 2015. Anatomizing one of the largest saltwater inflows into the Baltic Sea in December 2014. J Geophys Res Ocean 120(11):7676–7697. doi:10.1002/2015JC011269

Griffiths RW, Linden PF. 1981. The stability of buoyancy-driven coastal currents. Dyn Atmos Ocean 5(4):281–306. doi:10.1016/0377-0265(81)90004-X

Halverson MJ, Pawlowicz R. 2008. Estuarine forcing of a river plume by river flow and tides. J Geophys Res Ocean 113(9):1–15. doi:10.1029/2008JC004844

Hansen D V., Rattray M. 1965. Gravitational circulation in straits and estuaries. J Mar Res 23:104–122. doi:10.1098/rspb.2009.2214

Hansen D V., Rattray M. 1966. New Dimensions In Estuary Classification. Limnol Oceanogr 11(July).

Haritonova D. 2016. Sea Level Variations At The Latvian Coastal Hydrologic Stations. Geod Cartogr 42(2):31–38. doi:10.3846/20296991.2016.1198564

Hela I. 1952. Drift Currents and Permanent Flow. *Societas Scientiarum Fennica, Commentationes Physico-Mathematicae* XVI(14):1–27. Helsinki.

Höglund A, Meier HEM, Broman B, Kriezi E. 2009. Validation and correction of regionalised ERA-40 wind fields over the Baltic Sea using the Rossby Centre Atmosphere model RCA3.0. (97).

Höglund A, Meier HEM, Broman B, Kriezi E. 2009. Validation and correction of regionalised ERA-40 wind fields over the Baltic Sea using the Rossby Centre Atmosphere model RCA3.0. (97).

Horner-Devine AR, Hetland RD, MacDonald DG. 2015. Mixing and Transport in Coastal River Plumes. Annu Rev Fluid Mech, in press. doi:10.1146/annurev-fluid-010313-141408

Itoh S, Kasai A, Takeshige A, Zenimoto K, Kimura S, Suzuki KW, Miyake Y, Funahashi T, Yamashita Y, Watanabe Y. 2016. Circulation and haline structure of a microtidal bay in the Sea of Japan influenced by the winter monsoon and the Tsushima Warm Current. J Geophys Res Ocean 121(8):6331–6350. doi:10.1002/2015JC011441

James ID. 1997. A numerical model of the development of anticyclonic circulation in a gulf-type region of freshwater influence. Cont Shelf Res 17(14):1803–1816. doi:10.1016/S0278-4343(97)00052-6

Janssen F, Schrum C, Backhaus JO. 1999. A climatological data set of temperature and salinity for the Baltic Sea and the North Sea. Dtsch Hydrogr Zeitschrift 51(S9):5–245. doi:10.1007/BF02933676

Jedrasik J, Cieślikiewicz W, Kowalewski M, Bradtke K, Jankowski A. 2008. 44 Years Hindcast of the sea level and circulation in the Baltic Sea. Coast Eng 55(11): 849–860. doi:10.1016/j.coastaleng.2008.02.026

Jedrasik J, Kowalewski M. 2019. Mean annual and seasonal circulation patterns and long-term variability of currents in the Baltic Sea. J Mar Syst 193(November 2018):1–26. Elsevier. doi:10.1016/j.jmarsys.2018.12.011

Jerlov NG. 1976. Marine Optics. Elsevier. (Vol. 14).

Johnson DR, Mcclimans TA, King S, Grenness Ø. 1997. Fresh water masses in the Kara Sea during summer. J Mar Syst 12(1–4):127–145. doi:10.1016/S0924-7963(96)00093-0

Jönsson BF, Döös K, Myrberg K, Lundberg PA. 2011. A Lagrangian-trajectory study of a gradually mixed estuary. Cont Shelf Res 31(17):1811–1817. doi:10.1016/j.csr.2011.07.007

Jurisa JT, Chant RJ. 2013. Impact of Offshore Winds on a Buoyant River Plume System. J Phys Oceanogr 43(12):2571–2587. doi:10.1175/jpo-d-12-0118.1

Kaiser MJ, Williams PJ leB. 2011. Marine Ecology: Processes, Systems, and Impacts. Oxford University Press.

Kasai A, Hill AE, Fujiwara T, Simpson JH. 2000. Effect of the Earth's rotation on the circulation in regions of freshwater influence. J Geophys Res Ocean 105(C7): 16961–16969. doi:10.1029/2000JC900058

Keevallik S. 2008. Wind speed and velocity at three Estonian coastal stations 1969-1992. Est J Eng 14(3):209–219. doi:10.3176/eng.2008.3.02

Keevallik S, Soomere T. 2014. Regime shifts in the surface-level average air flow over the Gulf of Finland during 1981–2010. Proc Est Acad Sci 63(4):428. doi:10.3176/proc.2014.4.08

Kikas V, Lips U. 2016. Upwelling characteristics in the Gulf of Finland (Baltic Sea) as revealed by Ferrybox measurements in 2007–2013. Ocean Sci 12(3):843–859. doi:10.5194/os-12-843-2016

Klingbeil K, Lemarié F, Debreu L, Burchard H. 2018. The numerics of hydrostatic structured-grid coastal ocean models: State of the art and future perspectives. Ocean Model 125(January):80–105. Elsevier. doi:10.1016/j.ocemod.2018.01.007

Klingbeil K, Mohammadi-Aragh M, Gräwe U, Burchard H. 2014. Quantification of spurious dissipation and mixing – Discrete variance decay in a Finite-Volume framework. Ocean Model 81:49–64. Elsevier Ltd. doi:10.1016/j.ocemod.2014.06.001

Laanearu J, Lips U, Lundberg P. 2000. On the application of hydraulic theory to the deep-water flow through the Irbe Strait. J Mar Syst 25(3–4):323–332. Elsevier. doi:10.1016/S0924-7963(00)00025-7

Laanemets J, Väli G, Zhurbas V, Elken J. 2011. Simulation of nutrient transport from different depths during an upwelling event in the Gulf of Finland. Oceanologia 53(1-TI):431–448. doi:10.5697/oc.53-1-TI.431

Lagemaa P. 2012. Operational forecasting in Estonian marine waters. [Tallinn]: TUT Press. http://digi.lib.ttu.ee/i/?714.

Lass HU, Matthäus W. 1996. On temporal wind variations forcing salt water inflows into the Baltic Sea. Tellus, Series A: Dynamic Meteorology and Oceanography. doi:10.3402/tellusa.v48i5.12163

Lax PD, Wendroff B. 1964. Difference Schemes for Hyperbolic Equations with High Order of Accuracy. Commun Pure Appl Math 17:381–398. doi:10.1002/cpa.3160170311

Lehmann A, Hinrichsen HH. 2000. On the thermohaline variability of the Baltic Sea. J Mar Syst 25(3–4):333–357. doi:10.1016/S0924-7963(00)00026-9

Lehmann A, Höflich K, Post P, Myrberg K. 2017. Pathways of deep cyclones associated with large volume changes (LVCs) and major Baltic inflows (MBIs). J Mar Syst 167(December 2014):11–18. doi:10.1016/j.jmarsys.2016.10.014

Lehmann A, Krauss W, Hinrichsen HH. 2002. Effects of remote and local atmospheric forcing on circulation and upwelling in the Baltic Sea. Tellus, Ser A Dyn Meteorol Oceanogr 54(3):299–316. doi:10.1034/j.1600-0870.2002.00289.x

Leppäranta M, Myrberg K. 2009. Physical Oceanography of the Baltic Sea. Berlin, Heidelberg: Springer Berlin Heidelberg. doi:10.1007/978-3-540-79703-6

Levinson AV, Li C, Royer TC, Atkinson LP. 1998. Flow patterns at the Chesapeake Bay entrance. Cont Shelf Res 18(10):1157–1177. doi:10.1016/S0278-4343(98)00036-3

Li Y, Li M. 2012. Wind-driven lateral circulation in a stratified estuary and its effects on the along-channel flow. J Geophys Res Ocean 117(C9). doi:10.1029/2011JC007829

Liblik T. 2012. Variability of thermohaline structure in the Gulf of Finland in summer. Tallinn University of Technology. https://digi.lib.ttu.ee/i/?709

Liblik T, Laanemets J, Raudsepp U, Elken J, Suhhova I. 2013. Estuarine circulation reversals and related rapid changes in winter near-Bottom oxygen conditions in the Gulf of Finland, Baltic Sea. Ocean Sci 9(5):917–930. doi:10.5194/os-9-917-2013

Liblik T, Lips U. 2012. Variability of synoptic-scale quasi-stationary thermohaline stratification patterns in the Gulf of Finland in summer 2009. Ocean Sci 8(4):603–614. doi:10.5194/os-8-603-2012

Liblik T, Lips U. 2017. Variability of pycnoclines in a three-layer, large estuary : the Gulf of Finland. Boreal Environ Res 22:27–47.

Liblik T, Naumann M, Alenius P, Hansson M, Lips U, Nausch G, Tuomi L, Wesslander K, Laanemets J, Viktorsson L. 2018. Propagation of Impact of the Recent Major Baltic Inflows From the Eastern Gotland Basin to the Gulf of Finland. Front Mar Sci 5(July):1–23. doi:10.3389/fmars.2018.00222

Lilover M-J, Lips U, Laanearu J, Liljebladh B. 1998. Flow regime in the Irbe Strait. Aquat Sci 60(3):253–265. doi:10.1007/s000270050040

Lilover M-J. 2012. Tidal currents as estimated from ADCP measurements in “practically non-tidal” Baltic Sea. Ocean Past, Present Futur - 2012 IEEE/OES Balt Int Symp Balt 2012:1–4. doi:10.1109/BALTIC.2012.6249181

Lilover M-J, Elken J, Suhhova I, Liblik T. 2017. Observed flow variability along the thalweg, and on the coastal slopes of the Gulf of Finland, Baltic Sea. Estuar Coast Shelf Sci 195:23–33. Elsevier Ltd. doi:10.1016/j.ecss.2016.11.002

Lips U, Lilover M-J, Raudsepp U, Talpsepp L. 1995. Water renewal processes and related hydrographic structures in the Gulf of Riga. EMI Rep Ser 1:1–34.

Lips U, Zhurbas V, Skudra M, Vali G. 2014. Features of summertime circulation in the Gulf of Riga (A numerical simulation). 2014 IEEE/OES Baltic International Symposium (BALTIC):1–9. IEEE. doi:10.1109/BALTIC.2014.6887846

Lips U, Zhurbas V, Skudra M, Väli G. 2016a. A numerical study of circulation in the Gulf of Riga, Baltic Sea. Part II: Mesoscale features and freshwater transport pathways. Cont Shelf Res 115:44–52. Elsevier. doi:10.1016/j.csr.2015.12.018

Lips U, Zhurbas V, Skudra M, Väli G. 2016b. A numerical study of circulation in the Gulf of Riga, Baltic Sea. Part I: Whole-basin gyres and mean currents. Cont Shelf Res 112:1–13. doi:10.1016/j.csr.2015.11.008

MacCready P. 2004. Toward a unified theory of tidally-averaged estuarine salinity structure. Estuaries 27(4):561–570. doi:10.1007/BF02907644

MacCready P, Geyer WR. 2010. Advances in estuarine physics. Ann Rev Mar Sci 2:35–58. doi:10.1146/annurev-marine-120308-081015

Madsen KS, Højerslev NK. 2009. Long-term temperature and salinity records from the Baltic Sea transition zone. Boreal Environ Res 14(1):125–131.

Magaard L, Krauss W. 1966. Spektren der wasserstandsschwankungen der Ostsee im jahre 1958. Kieler Meeresforsch 22(2):155–162.

Malačič V, Petelin B. 2009. Climatic circulation in the gulf of trieste (northern Adriatic). J Geophys Res Ocean 114(7):1–15. doi:10.1029/2008JC004904

Maljutenko I, Raudsepp U. 2019. Long-term mean, interannual and seasonal circulation in the Gulf of Finland — The wide salt wedge estuary or gulf type ROFI. J Mar Syst 195:1–19. Elsevier. doi:10.1016/J.JMARSYS.2019.03.004

Markus Meier HE. 2007. Modeling the pathways and ages of inflowing salt- and freshwater in the Baltic Sea. Estuar Coast Shelf Sci 74(4):717–734. doi:10.1016/j.ecss.2007.05.019

Markus Meier HE, Höglund A, Döscher R, Andersson H, Löptien U, Kjellström E. 2011. Quality assessment of atmospheric surface fields over the Baltic Sea from an ensemble of regional climate model simulations with respect to ocean dynamics. Oceanologia 53(1-TI):193–227. doi:10.5697/oc.53-1-TI.193

Matthäus W, Franck H. 1992. Characteristics of major Baltic inflows - a statistical analysis. Cont Shelf Res 12(12):1375–1400. doi:DOI: 10.1016/0278-4343(92)90060-W

Mattias Green JA, Liljebladh B, Omstedt A. 2006. Physical oceanography and water exchange in the Northern Kvark Strait. Cont Shelf Res 26(6):721–732. Pergamon. doi:10.1016/J.CSR.2006.01.012

Mcclimans TA, Johnson DR, Krosshavn M, King SE, Carroll J. 2000. Transport processes in the Kara Sea Pechora. 105.

Medvedev IP, Rabinovich AB, Kulikov EA. 2013. Tidal oscillations in the Baltic Sea. Oceanology 53(5):526–538. doi:10.1134/S0001437013050123

Mohrholz V. 2018. Major Baltic Inflow Statistics – Revised. Front Mar Sci 5(October):1–16. doi:10.3389/fmars.2018.00384

Mohrholz V, Naumann M, Nausch G, Krüger S, Gräwe U. 2015. Fresh oxygen for the Baltic Sea — An exceptional saline inflow after a decade of stagnation. J Mar Syst 148:152–166. Elsevier B.V. doi:10.1016/j.jmarsys.2015.03.005

Monismith SG, Burau J, Stacey. M. 1996. Stratification Dynamics and Gravitational Circulation in Northern San Francisco Bay. San Fr Bay Ecosyst Ecosyst J T Hollibaugh, Ed(American Association for the Advancement of Science):123–153.

Monismith SG, Burau J, Stacey. M. 1996. Stratification Dynamics and Gravitational Circulation in Northern San Francisco Bay. San Fr Bay Ecosyst Ecosyst J T Hollibaugh, Ed(American Association for the Advancement of Science):123–153.

Seas. J Hydraul Eng 123:362–373. doi:10.1061/(ASCE)0733-9429(1997)123:4(362)

Nakatsuji K, Fujiwara T. 1997. Residual Baroclinic Circulations in Semienclosed Coastal Seas. J Hydraul Eng 123:362–373. doi:10.1061/(ASCE)0733-9429(1997)123:4(362)

Nakayama K, Shintani T, Shimizu K, Okada T, Hinata H, Komai K. 2014. Horizontal and residual circulations driven by wind stress curl in Tokyo Bay. J Geophys Res Ocean 119(3):1977–1992. doi:10.1002/2013JC009396

Nielsen MH. 2005. The baroclinic surface currents in the Kattegat. J Mar Syst 55(3–4): 97–121. doi:10.1016/j.jmarsys.2004.08.004

Panteleev G, Proshutinsky A, Kulakov M, Nechaev DA, Maslowski W. 2007. Investigation of the summer Kara Sea circulation employing a variational data assimilation technique. J Geophys Res Ocean 112(4):1–21. doi:10.1029/2006JC003728

Pavelson J, Laanemets J, Kononen K, Nõmmann S. 1997. Quasi-permanent density front at the entrance to the Gulf of Finland: Response to wind forcing. Cont Shelf Res 17(3):253–265. doi:10.1016/S0278-4343(96)00028-3

Perillo GME. 1995. Chapter 1: Geomorphology and sedimentology of estuaries: An introduction. Dev Sedimentol 53(C):1–16. doi:10.1016/S0070-4571(05)80021-4

Pietrzak J. 1998. The Use of TVD Limiters for Forward-in-Time Upstream-Biased Advection Schemes in Ocean Modeling. Mon Weather Rev 126(3):812–830. doi:10.1175/1520-0493(1998)126<0812:TUOTLF>2.0.CO;2

Placke M, Meier HEM, Gräwe U, Neumann T, Frauen C, Liu Y. 2018. Long-Term Mean Circulation of the Baltic Sea as Represented by Various Ocean Circulation Models. Front Mar Sci 5(September):1–20. doi:10.3389/fmars.2018.00287

Poggioli AR, Horner-Devine AR. 2015. The Sensitivity of Salt Wedge Estuaries to Channel Geometry. J Phys Oceanogr 45(12):3169–3183. doi:10.1175/JPO-D-14-0218.1

Pritchard DW. 1952. Salinity Distribution and Circulation in the Chesapeake Bay Estuarine System. J Mar Res 15:33–42. https://books.google.ee/books?id=XxrYHwAACAAJ.

Pritchard DW. 1955. Estuarine circulation patterns. Proc Am Soc Civ Eng 81(717):1–11.

Ralston DK, Geyer WR, Lerczak JA. 2008. Subtidal Salinity and Velocity in the Hudson River Estuary: Observations and Modeling. J Phys Oceanogr 38(4):753–770. doi:10.1175/2007JPO3808.1

Raudsepp U. 1998. Current Dynamics of Estuarine Circulation in the Lateral Boundary Layer. Estuar Coast Shelf Sci 47(6):715–730. doi:10.1006/ecss.1998.0390

Raudsepp U. 2001. Interannual and seasonal temperature and salinity variations in the Gulf of Riga and corresponding saline water inflow from the Baltic Proper. Hydrol Res 32(2):135–160. International Water Association.

Raudsepp U. 2001. Wind-driven circulation in the Gulf of Riga. University of Tartu.

Raudsepp U, Beletsky D, Schwab DJ. 2003. Basin-Scale Topographic Waves in the Gulf of Riga. J Phys Oceanogr 33(5):1129–1140. doi:10.1175/1520-0485(2003)033<1129:btwitg>2.0.co;2

Raudsepp U, Elken J. 1999. Application of the Bryan-Cox-Type Ocean Model to reproduce synoptic and mesoscale variability of the Irbe Strait salinity front. Dtsch Hydrogr Zeitschrift 51(4):477–488.

Raudsepp U, Legeais J-F, She J, Maljutenko I, Jandt S. 2018. Report, The Copernicus Marine Environment Monitoring Service Ocean State. In: von Schuckmann K, editor The Copern. Taylor & Francis. p. 107–111. doi:10.1080/1755876X.2018.1489208

Reyes-Hernández C, Valle-Levinson A. 2010. Wind Modifications to Density-Driven Flows in Semienclosed, Rotating Basins. J Phys Oceanogr 40(7):1473–1487. doi:10.1175/2010JPO4230.1

Roe P. 1986. Characteristic-Based Schemes for the Euler Equations. Annu Rev Fluid Mech 18(1):337–365. doi:10.1146/annurev.fluid.18.1.337

Roy F, Chevallier M, Smith GC, Dupont F, Garric G, Lemieux J, Lu Y, Fraser D. 2015. Citation for: Arctic sea ice and freshwater sensitivity to the treatment of the atmosphere-ice-ocean surface layer. J Geophys Res Ocean 120(6):4392–4417. doi:10.1002/2014JC010677

Schijf JB, Schönfled JC. 1953. Theoretical considerations on the motion of salt and fresh water.

Schinke H, Matthäus W. 1998. On the causes of major Baltic inflows - An analysis of long time series. Cont Shelf Res 18(1):67–97. doi:10.1016/S0278-4343(97)00071-X

Schulz E, Schuttelaars HM, Gräwe U, Burchard H. 2015. Impact of the Depth-to-Width Ratio of Periodically Stratified Tidal Channels on the Estuarine Circulation. J Phys Oceanogr 45(8):2048–2069. doi:10.1175/jpo-d-14-0084.1

Seifert T, Kayser B. 1995. A high resolution spherical grid topography of the Baltic Sea. Meereswissenschaftliche Berichte 9:72–88.

Shchepetkin AF. 2003. A method for computing horizontal pressure-gradient force in an oceanic model with a nonaligned vertical coordinate. J Geophys Res 108(C3):1–34. doi:10.1029/2001JC001047

Shchepetkin AF, McWilliams JC. 2003. A method for computing horizontal pressure-gradient force in an oceanic model with a nonaligned vertical coordinate. J Geophys Res 108(C3):3090. doi:10.1029/2001JC001047

Sooäär J, Jaagus J. 2007. Long-term changes in the sea ice regime in the Baltic Sea near the Estonian coast. Proc Est Acad Sci Eng 13(3):189–200.

Soomere T, Delpeche N, Viikmäe B, Quak E, Meier HEM, Döös K. 2011. Patterns of current-induced transport in the surface layer of the Gulf of Finland. Boreal Environ Res 16(SUPPL. A):49–63.

Soosaar E, Maljutenko I, Raudsepp U, Elken J. 2014. An investigation of anticyclonic circulation in the southern Gulf of Riga during the spring period. Cont Shelf Res 78:75–84. Elsevier. doi:10.1016/j.csr.2014.02.009

Soosaar E, Maljutenko I, Uiboupin R, Skudra M, Raudsepp U. 2016. River bulge evolution and dynamics in a non-tidal sea – Daugava River plume in the Gulf of Riga, Baltic Sea. Ocean Sci 12(2):417–432. doi:10.5194/os-12-417-2016

Soosaar E, Sipelgas L, Raudsepp U. 2010. Simple model calculations of the ice thickness for complementing satellite remote sensing of ice extent. 2010 IEEE/OES US/EU Balt Int Symp Balt 2010:1–9. IEEE. doi:10.1109/BALTIC.2010.5621637

Stacey MT, Burau JR, Monismith SG. 2001. Creation of residual flows in a partially stratified estuary. J Geophys Res Ocean 106(C8):17013–17037. doi:10.1029/2000JC000576

Stipa T. 2004. Baroclinic adjustment in the Finnish coastal current. Tellus, Ser A Dyn Meteorol Oceanogr 56(1):79–87. doi:10.1111/j.1600-0870.2004.00041.x

Stipa T, Tamminen T, Seppälä J. 1999. On the creation and maintenance of stratification in the Gulf of Riga. J Mar Syst 23(1–3):27–49. doi:10.1016/S0924-7963(99)00049-4

Stips AK. 2010. Fitting measured irradiance of Jerlov water types to double exponential functions using R. JRC Tech Notes. doi:10.2788/80912

Striebinš O, Väling P. 1996. Bottom sediments of the Gulf of Rīga. Explanatory note to the bottom sediment map, scale 1: 200 000. Riga: Geol. Surv. Latvia & Geol. Surv. Estonia, Riga. p. 54.

Suhhova I, Liblik T, Lilover MJ, Lips U. 2018. A descriptive analysis of the linkage between the vertical stratification and current oscillations in the Gulf of Finland. Boreal Environ Res 23(February):83–103.

Suursaar Ü. 2010. Waves, currents and sea level variations along the Letipea - Sillamäe coastal section of the southern Gulf of Finland. OCEANOLOGIA 52(3):391–416. doi:10.5697/oc.52-3.391

Torres López S, Varela RA, Delhez E. 2001. Residual circulation and thermohaline distribution of the Ría de Vigo: A 3-D hydrodynamical model. Sci Mar 65(S1): 277–289. doi:10.3989/scimar.2001.65s1277

Umlauf L, Burchard H. 2005. Second-order turbulence closure models for geophysical boundary layers. A review of recent work. Cont Shelf Res 25(7–8):795–827. doi:10.1016/j.csr.2004.08.004

Väli G, Meier HEM, Elken J. 2013. Simulated halocline variability in the baltic sea and its impact on hypoxia during 1961-2007. J Geophys Res Ocean 118(12):6982–7000. doi:10.1002/2013JC009192

Valle-Levinson A. 2011. Classification of Estuarine Circulation. In: Wolanski E, McLusky D, editors. *Treatise on Estuarine and Coastal Science*. Waltham: Elsevier. p. 75–86. doi:10.1016/B978-0-12-374711-2.00106-6

Valle-Levinson A. 2008. Density-driven exchange flow in terms of the Kelvin and Ekman numbers. J Geophys Res 113(C4):C04001. doi:10.1029/2007JC004144

Valle-Levinson A, Reyes C, Sanay R. 2003. Effects of Bathymetry, Friction, and Rotation on Estuary–Ocean Exchange. J Phys Oceanogr 33(11):2375–2393. doi:10.1175/1520-0485(2003)033<2375:EOBFAR>2.0.CO;2

Wake GW, Ivey GN, Imberger J, McDonald NR. 2005. The temporal evolution of a geostrophic flow in a rotating stratified basin. Dyn Atmos Ocean 39(3–4):189–210. doi:10.1016/j.dynatmoce.2004.12.002

Wake GW, Ivey GN, Imberger J, McDonald NR, Stocker R. 2004. Baroclinic geostrophic adjustment in a rotating circular basin. J Fluid Mech 515:63–86. doi:10.1017/S0022112004000230

Walters RA, Gartner JW. 1985. Subtidal sea level and current variations in the northern reach of San Francisco Bay. Estuar Coast Shelf Sci 21(1):17–32. doi:10.1016/0272-7714(85)90003-4

Wei X, Kumar M, Schuttelaars HM. 2017. Three-Dimensional Salt Dynamics in Well-Mixed Estuaries: Influence of Estuarine Convergence, Coriolis, and Bathymetry. J Phys Oceanogr 47(7):1843–1871. doi:10.1175/jpo-d-16-0247.1

Westerlund A. 2018. Modelling circulation dynamics in the northern Baltic Sea. University of Helsinki. http://hdl.handle.net/10138/264606.

Westerlund A, Tuomi L, Alenius P, Miettunen E, Vankevich RE. 2018. Attributing mean circulation patterns to physical phenomena in the Gulf of Finland. Oceanologia 60(1):16–31. doi:10.1016/j.oceano.2017.05.003

Whitney MM, Garvine RW. 2005. Wind influence on a coastal buoyant outflow. J Geophys Res Ocean 110(C3). doi:10.1029/2003JC002261

Winant CD. 2004. Three-Dimensional Wind-Driven Flow in an Elongated, Rotating Basin. J Phys Oceanogr 34(2):462–476. doi:10.1175/1520-0485(2004)034<0462:twfiae>2.0.co;2

Witting R. 1911. Tidvattnet i Östersjön och Finska viken. Fennia 24(2):84.

Witting R. 1910. Rannikkomeret, Karttalehdet Nr. 6b, 7, 8, 9,. Suom Kartasto (Finn. Inst. Mar. Res., Helsinki).

Witting R. 1912. Zusammenfassende Übersicht der Hydrographie des Bottnischen und Finnischen Meerbusens und der nördlichen Ostsee nach den Untersuchungen bis Ende 1910. Finnländische Hydrogr Untersuchungen 7.

Wong K-C. 1994. On the nature of transverse variability in a coastal plain estuary. J Geophys Res 99(C7):14209. doi:10.1029/94JC00861

Wulff F, Sokolov A, Savchuk O. 2013. Nest – a Decision Support System for Management of the Baltic Sea. A User Manual.

Yanagi T, Kuroda M, Ishimaru T, Saino T. 1998. Residual flow in Ise Bay during summer. Bull Coast Oceanogr 35(2):185–191. The Oceanographic Society of Japan (OSJ). http://ci.nii.ac.jp/naid/110007999190/en/.

Yankovsky AE, Chapman DC. 1997. A Simple Theory for the Fate of Buoyant Coastal Discharges. J Phys Oceanogr 27(7):1386–1401. doi:10.1175/1520-0485(1997)027<1386:ASTFTF>2.0.CO;2

Yoon S, Kasai A. 2017. Relative contributions of external forcing factors to circulation and hydrographic properties in a micro-tidal bay. Estuar Coast Shelf Sci 198: 225–235. doi:10.1016/j.ecss.2017.09.017

Acknowledgements

I would like to thank the community of GETM developers who have created and maintained probably the best model in the world (j*). Working with the GETM model has taught me much more than just how the water circulates in the sea.

My sincere appreciation goes to the co-authors of the publications of the current thesis: Prof. Jüri Elken, Prof. Sirje Keevallik, Ph.D. Jaan Laanemets, M.Sc. Jelena Passenko, Ph.D. Ove Pärn, Ph.D. Jean-Francois Legaise, Ph.D. Jun She, M.Sc. Simon Jandt, Ph.D. Edith Soosaar.

Sometimes a tiny seed which you drop into the soil may grow into something unexpectedly big. A brief discussion or short question which you have asked, and maybe forgotten right after our meeting, might have grown into a big fruitful tree of ideas. Thank you to Victor Alari, Jüri Elken, Madis-Jaak Lilover, Adolf Stips, Jaan Laanemets, Germo Väli, Gennadi Lessin for planting many scientific seeds along my path. Thank you Kairi Kasemets for setting up that path.

My dear friends who never get tired of asking me about my progress with my thesis. Sincerely, thank you all for caring! I thank my charming colleagues for cheering up my supervisor's mood whenever he stepped into our office. A friend in need is a friend indeed!

I'm most grateful to Mari Karlson for her unfailing support with literally everything. Thanks for keeping me on the right track.

Last, but not least. My deepest gratitude are for my supervisor Prof. Urmas Raudsepp. Without his guidance, boldness and perseverance this work would have been much less intriguing and therefore unbearably boring. Thank you for such a unique opportunity to work with numerical marine models. I am deeply grateful for that.

The work was financially supported by institutional research funding IUT (19-6) of the Estonian Ministry of Education and Research, Estonian Science Foundation grants ETF9382, ETF9278, Estonian national project "EstKliima" and Tallinn University of Technology. The computational resource of TalTech HPC was used in Paper **I**, **II** and preparing data for Paper **V**. MSI cluster was used in Paper **III** and **IV**. I would like to acknowledge the tools which I have been using through the writing of this thesis: CDO, MATLAB, Inkscape, Overleaf, Mendeley and cloud services from Google Drive.

Abstract

Water Circulation in Gulf Type Regions of Freshwater Influence — the Gulf of Finland and Gulf of Riga

The thesis questions the validity of the cyclonic surface layer circulation in the Gulf of Finland and in the Gulf of Riga. The prevailing cyclonic circulation scheme proposed by Witting (1912), Palmèn (1930) and Hela (1952) as a statistical property has been picked up as a fact by a number of researchers. Still, there have been new measurements and modelling studies that do not agree with this circulation scheme that has been used for the past century. This study relies on a long-term numerical simulations of 40-years, which have been conducted by using the 3-dimensional hydrodynamical model. Numerous state of the art parametrization and numerical techniques have made it possible to perform long-term model simulations with reasonable quality without data assimilation. The comparison with measurements has shown that model has reproduced the main characteristics of the short-term and long-term thermohaline variability.

The current thesis provides scientific evidence that a seasonal cycle of the surface layer circulation and the salt wedge dynamics are prevalent over the mean climatology in the Gulf of Finland. Basinwide anticyclonic circulation patterns are evident in the seasonal climatology as well as in yearly realizations in the Gulf of Finland. In the Gulf of Riga anticyclonic circulation emerges in the southwestern part in the climatological mean fields and monthly realizations in spring and summer. A new unrecognized feature of the surface layer circulation, down-estuary directed left hand coastal current, is proven to exist in the Gulf of Finland and Gulf of Riga. This current has a higher persistency than the anticyclonic gyres and it exists at the estuary head throughout the year. Seasonal cycle of estuarine exchange flow comprises down-estuary transport of less saline upper layer water and up-estuary transport of the salt wedge in summer and retreat in winter. Under favourable wind conditions, reverse estuarine circulation may culminate with stratification collapse in the central Gulf of Finland. Wind forcing, especially zonal wind component, can enhance or destroy anticyclonic circulations, left hand coastal current and estuarine exchange flow. In the Baltic Sea scale, the Major Baltic Inflows shift less saline upper layer water and salt wedge system towards the estuary head, while the system is shifted towards the estuary mouth during the stagnation period. It is suggested in the thesis that the left hand coastal current and anticyclonic circulation are driven by salt wedge transport. The dynamics could be explained by baroclinic geostrophic adjustment and the mutual effect of vertical entrainment of the saline bottom layer water into buoyant surface layer water and earth rotation. Still, solid scientific justification remains the subject of forthcoming research.

Lühikokkuvõtte

Vee tsirkulatsioon poolsuletud magevee mõjualas — Soome lahes ja Liivi lahes

Käesolev töö seab kahtluse alla tsüklonaalse tsirkulatsiooni kehtivuse Soome- ja Liivi lahe pinnakihis. Tsüklonaalset tsirkulatsiooni, mis on varasemalt esitatud Wittingi (1912), Palmèni (1930) ja Hela (1952) töödes kui statistilist hoovusvälja karakteristikut, on paljudes uuringutes käsitletud kui püsivat vee horisontaalset liikumist. Siiski on paljud mõõtmised ja mudeluuringud näidanud vastuolu juba sajand tagasi pakutud tsirkulatsiooni skeemiga. Ka käesolev töö on tugineb pikaajalisel simulatsioonil kasutades numbrilist kolmemõõtmelist hüdrodünaamika mudelit GETM. Mudelis on kasutatud mitmeid uusi parametriseeringuid ja uuenduslike numbrilisi võtteid, mis võimaldavad teostada pikkaajalisi simulatsioone rahuldava kvaliteediga, samas kasutamata mõõtmisandmete assimileerimist. Mudel näitas võrdluses mõõtmistega head kooskõla vaadeldud termohaliinsete väljade lühi- ja pikaajalise muutlikuses.

Käesolev töö pakub teaduslike tõendeid, et sessoonne käik domineerib pinnakihi tsirkulatsioonis ning vertikaalses estuaarses veevahetuses/soolakeele dünaamikas. Mudeli tulemustest selgub, et sesoonne hoovuste ja soolsuse muutlikkus on Soome lahes olulisem kui vastavad pikaajalised keskmised. Antitsüklonaalne tsirkulatsioon ilmneb Soome lahes nii kuude keskmistatud klimatoloogias kui ka erinevate aastate hoovusvälja mustrites. Liivi lahes domineerib antitsüklonaalne tsirkulatsioon lahe lõunaosa pinnakihis nii kevad-suvisel ajal kui ka pikaajalistes keskmistes hoovusväljades. Oluliseks hoovusvälja iseärasuseks Soome ja Liivi lahes ilmnes püsiv päri-estuaari suunatud vasema kalda hoovus. See hoovustesüsteem näitas suuremat püsivust kui antitsüklonaalne tsirkulatsioon ning eksisteeris jõe suudme aladel aasta ringi. Sesoonne estuaarne veevahetus kujutab endast magedama veemassi liikumist estuaari suudme suunas ja soolakeele tungimist jõe suudme poole suvel samas kui sügis-talvel on need liikumised vastupidised. Tugevamate püsivate lääne-tuulte korral võib Soome lahe keskosas estuaarse voolu pöördumisega kaasneda ka veesamba täieliku segunemist. On näidatud, et tuul ning eriti selle tsonaalse komponendi tugevus, soodustab või lõhub antitsüklonaalset tsirkulatsiooni, vasema kalda hoovust ja estuaarset veevahetust. Suuremas pildis, suured soolase vee sissevoolud Läänemerde nihutavad soolakeelt ja magedaveelist ülakihti jõgede suudmete suunas ning stagnatsiooni perioodide korral estuaari suudme poole. Töös on küll pakutud, et kujunenud antitsüklonaalsust ja vasema kalda hoovust võiksid tekitada tihedusvälja barokliinsest geostroofilisest kohanemisest ja alumise kihi vertikaalsest kaasa hardest tingitud negatiivse pööriselisuse kasv ülemises veekihis, kuid täpsema teadusliku põhjenduse peavad välja selgitama tulevased uuringud.

Appendix

Paper I

Maljutenko I, Raudsepp U. 2019. Long-term mean, interannual and seasonal circulation in the Gulf of Finland — The wide salt wedge estuary or gulf type ROFI. J Mar Syst 195:1–19. Elsevier. doi:10.1016/J.JMARSYS.2019.03.004 (1.1)

Dataset used to prepare Paper I

Maljutenko I, Raudsepp U. 2018. Dataset from long-term model simulation of the Gulf of Finland, the Baltic Sea, v2
http://dx.doi.org/10.17632/b3my8b4dwc.2

Journal of Marine Systems 195 (2019) 1–19

Contents lists available at ScienceDirect

Journal of Marine Systems

journal homepage: www.elsevier.com/locate/jmarsys

Long-term mean, interannual and seasonal circulation in the Gulf of Finland — The wide salt wedge estuary or gulf type ROFI

Ilja Maljutenko*, Urmas Raudsepp

Tallinn University of Technology, Department of Marine Systems, Akadeemia tee 15a, 12611 Tallinn, Estonia

ARTICLE INFO

Keywords:
Estuarine circulation
Seasonal currents
Numerical modelling
Gulf of Finland
Baltic Sea
Long-term circulation
ROFI

ABSTRACT

Circulation of the wide gulf type ROFI or salt wedge estuary, the Gulf of Finland (GoF), was studied using a numerical 3D hydrodynamic model with 1 nmi horizontal resolution and 40 vertically adaptive layers for a period of 40 years. The results show an extensive down estuary or westward coastal current (WCC) on the left hand flank of the GoF. The WCC is more vigorous during the spring and summer months when longitudinal positive estuarine circulation with salt wedge up estuary transport and less saline upper layer water (LSULW) down estuary transport prevails. In the beginning of summer, the coastal current forms an extensive northward cross-shore current in the center of the gulf, giving rise to two basin-wide anticyclonic circulation gyres. The intensity of the WCC, anticyclonic gyres and estuarine transport vary interannually. The zonal wind component averaged over the period of the dominance of a particular feature — April–June for the WCC, July–September for the anticyclonic gyres and annual for estuarine exchange flow — modulates the strength of these circulation patterns. A negative/positive zonal wind supports/destroys the WCC and increase/decrease the intensity of the salt wedge and LSULW transport. The anticyclonic gyres are well developed during weak positive zonal wind, mainly.

1. Introduction

The circulation in wide estuaries and gulfs has attracted researchers for a long time. Relatively easy access to the water has made it possible to collect measurements there. The variety of the estuaries where measurements have been performed and a desire to generalize the results brought about the need to classify them. Cameron and Pritchard (1963) defined an estuary as a semi-enclosed and coastal waterbody that has an open connection with the ocean and exhibits a significant density gradient between mouth and head of the estuary. This is the most widely accepted definition of an estuary. Estuaries are classified based on geomorphology, water balance, vertical salinity structure and hydrodynamics (Valle-Levinson, 2011).

Simpson (1997) defined the Region Of Freshwater Influence (ROFI) as the region where buoyancy input by rivers is comparable to or exceeds the seasonal input of buoyancy as heat and gave the classification of different ROFIs. The main dynamical difference between wide estuaries and ROFIs is that pressure gradient forcing caused by river discharge is the main driver in the estuary, while being negligible in ROFIs. The main forcing there comes from spatial density gradients caused by interaction between buoyancy input by rivers and stirring mechanisms (Simpson, 1997).

The Gulf of Finland (GoF) is a very good example of a wide non-tidal positive coastal plain salt wedge estuary or a gulf-type ROFI (Elken et al., 2003; Liblik and Lips, 2011; Liblik et al., 2013). The current velocity measurements date back over a century. In the GoF, classical longitudinal density gradient, surface outflow and net inflow underneath as described by Valle-Levinson (2011) is maintained due to freshwater discharge at the head and open connection with more saline Baltic Proper at the mouth of the estuary. Circulation studies relying on measurements or numerical modelling have been performed in the past to investigate the current dynamics of the GoF (Andrejev et al., 2004; Elken et al., 2011; Jönsson et al., 2011; Palmén, 1930; Witting, 1912). They have concluded that the mean circulation, although low in speed, is cyclonic in the GoF, with inflow near the southern coast and outflow near the northern coast. Over the last decade, several authors have started to question the validity of this circulation in light of more recent findings (Delpeche-Ellmann et al., 2016; Soomere et al., 2011; Suursaar, 2010; Westerlund et al., 2017). Recent analyses of the ADCP measurements on the southern slope of the GoF show mean outflow in the surface layer of 20-m (Lilover et al., 2017; Suursaar, 2010) which is opposite to the cyclonic circulation scheme.

Both vertical stratification and horizontal gradients of density in the GoF undergo large seasonal variability due to the seasonal dominance

* Corresponding author.
E-mail address: ilja.maljutenko@taltech.ee (I. Maljutenko).

https://doi.org/10.1016/j.jmarsys.2019.03.004
Received 5 February 2018; Received in revised form 5 March 2019; Accepted 18 March 2019
Available online 22 March 2019

of different types of forcing (Alenius et al., 1998). Generally, the surface temperature distribution does not show large gradients due to uniform solar heating, except during occasional upwelling events (Myrberg et al., 2008). An additional longitudinal pressure gradient in spring can arise from a difference of heating between the shallower eastern GoF and the deeper western GoF (Alenius et al., 1998). The seasonal course of thermal stratification is ruled by the solar irradiation cycle, while salinity stratification is determined by wind modifications to estuarine circulation (Elken et al., 2003; Liblik and Lips, 2012; Lips et al., 2016a) and by convective mixing (Liblik et al., 2013; Lips et al., 2016a). This mixed state results in a longitudinal salinity gradient which is highly unstable and generates an energetic state for buoyancy-driven baroclinic currents (Alenius et al., 1998).

The general view is that water movement in a positive stratified estuary is characterized as relaxation of the longitudinal density gradient, where buoyant water outflow takes place in the surface layer and dense water inflow in the bottom layer. Implications of basin geometry, friction and Earth rotation can induce horizontally sheared flows. The width of the GoF is far beyond the internal Rossby radius, thus, the Earth's rotation gives rise to significant transverse pattern of the estuarine circulation (Valle-Levinson, 2008). With a high Kelvin number $O[10]$ and a low Ekman number $O[10^{-4}]$, the GoF should possess an inflow on the left-hand coast and an outflow on the right-hand coast from the perspective of the head of the estuary. In aparticular estuary, various factors such as tides, waves and prevailing winds modify the general circulation scheme (Geyer and MacCready, 2013).

In a finite basin with a gradual bottom slope, the characteristics of saline water inflow can be inflow length or the point of overturning. Salt wedge intrusion is greatly hindered by longitudinal estuarine convergence (Poggioli and Horner-Devine, 2015). Liblik et al. (2013) suggested that the salt wedge intrusion in the central part of the GoF can be hindered by topographic irregularities.

Recent estuarine circulation studies have focused on the implications of tides on residual circulation in tidally energetic estuaries. Geyer and MacCready (2013) suggested to scale estuaries according to the ratio of tidal and vertical mixing timescales, which places the GoF as a part of the Baltic Sea into a category of microtidal estuary. Despite the absence of significant tidal oscillations, Lips et al. (2016a) scaled the GoF using (atmospheric forcing generated) self-oscillation velocities and placed the GoF into the stratified estuary class. Burchard and Hetland (2010) found that in a well-mixed estuary tidal straining induced circulation can dominate over gravitational circulation.

Evidence suggests that circulation in a ROFI type estuary could be anticyclonic instead of cyclonic (Fujiwara et al., 1997; Lips et al., 2016b; Soosaar et al., 2014). Kasai et al. (2000) conceded that conventional study conducted on a transverse section assuming a steady state balance between Coriolis, pressure and friction terms is unable to explain important anticyclonic circulation features in the Ise Bay, which were observed by Fujiwara et al. (1997). The anticyclonic circulation in Ise Bay was reproduced by the diagnostic numerical model by Yanagi et al. (1998). The circulation pattern during the spring months in the Gulf of Riga (GoR) was found to be driven by a horizontal density gradient with prevailing wind conditions either enhancing or reversing it (Soosaar et al., 2014).

Main aim of this study is to investigate seasonal climatology of the upper layer water circulation and the salinity distribution along the thalweg of the GoF. This research was motivated by the uncertainties about the circulation scheme as both the model and measurement studies listed above show evidence of the cyclonic and anticyclonic basin-scale mean circulation depending largely on the averaging period or numerical model used. The 40-year mean circulation and salinity distribution as shown from our model simulation forms the background for seasonal climatology. A prominent feature of the upper layer circulation is an intensive westward coastal current along the left-hand side of the estuary, which transforms into two anticyclonic circulation gyres lined along the estuary. Therefore, one objective is to study interannual variations of these current features. Seasonal variation of the salinity distribution along the thalweg is the other prominent feature in the seasonal climatology. Therefore, the other objective is to study interannual variations of the intensity of the salt wedge and less saline upper layer water (LSULW) transports, i.e. estuarine circulation. Based on the dominant features of the upper layer circulation we argue that the GoF could be classified as wide gulf type ROFI (Fujiwara et al., 1997), but focusing on the seasonal variations of the salinity distribution along the thalweg the GoF could be classified as salt wedge estuary (Hansen and Rattray, 1966). The effect of the wind on the WCC, anticyclonic gyres and salinity variations along the thalweg is presented and discussed.

2. Methods

2.1. Numerical model description

Our hindcast simulation was carried out using the General Estuarine Transport Model (GETM) (Burchard and Bolding, 2002), which is a numerical 3D circulation model developed for coastal and estuarine applications (Gräwe et al., 2013a; Hofmeister et al., 2011; Holtermann et al., 2014). GETM solves nonlinear Navier-Stokes equations under Boussinesq and hydrostatic approximation in a 3D space based on the Arakawa C-staggered grid system. Horizontal spherical and vertical adaptive coordinate systems were used for spatial discretization. Compared to the fixed σ-layer grid, the adaptive vertical coordinate system has been shown to produce less numerical dissipation (Gräwe et al., 2013b) by offering a better resolution for stratification and the bottom boundary layer (Hofmeister et al., 2011). Temporal discretization was done using the volume conserving time-split technique which split the model into baroclinic and barotropic modes. The third order monotone P2-PDM advection scheme was applied using the directional split approach (Pietrzak, 1998). Klingbeil et al. (2014) showed that this scheme had smaller numerical dissipation compared to the other high order schemes. Internal pressure was parameterized using the z-interpolation method proposed by Shchepetkin (2003). Vertical turbulence is prescribed using the two-equation $\kappa - \epsilon$ model coupled with the algebraic second-moment turbulence closure via GOTM (Canuto et al., 2001; Umlauf and Burchard, 2005). Background diffusivity was set to $10^{-6}\,\mathrm{m^2\,s^{-1}}$, which is in good agreement with previous observations, e.g. Holtermann et al. (2014). Subgrid-scale horizontal turbulence was parameterized by means of a horizontal viscosity coefficient of $10\,\mathrm{m^2\,s^{-1}}$. The choice was made based on the considerations by Wallcraft et al. (2005). Heat and momentum fluxes through the surface were calculated using bulk formulas by Kondo (1975). We applied a simple rigid lid approach to mimic the ice coverage in the Baltic Sea when sea surface temperature reached freezing point. That reduced latent heat flux and wind stress at the surface.

2.2. Model setup and forcing

The model domain with one nautical mile grid step covers the Baltic Sea with an open boundary in Kattegat, where sea level elevation, temperature and salinity are prescribed. Digital bathymetry of the BS with a resolution of 1 nautical mile (nmi) was adopted from Seifert and Kayser (1995). Adjustments of initial bathymetry were necessary to reduce artificial mixing near steep-sloped and enhanced saline water inflows through the Danish straits. Therefore, we have used a simple 3×3 boxcar filter in order to smooth steep slopes and adjusted depths at the Danish Straits (Great Belt, Darss Sill). In vertical, 40 bottom-following adaptive layers have been defined, ensuring vertical resolution below 5 m. We use the tendency parameters described in Hofmeister et al. (2013), with the adjustments of $\alpha_{hor} = 0.2$ and $c_d = 0.2$. The timestep for the barotropic mode was chosen as 20 s and for the baroclinic mode as 400 s. We have stored daily mean values of main prognostic variables for the analysis if not stated otherwise.

The initial conditions of salinity and temperature for our simulation period of 1966–2006 were compiled using observation data from the Baltic Environmental Database (BED; http://nest.su.se/bed), which comprise long-term measurements of salinity, temperature and other hydrophysical parameters from various institutions around the Baltic Sea (Gustafsson and Medina, 2011; Wulff et al., 2013). The data is quality checked and is therefore widely used for model validations (e.g. Placke et al., 2018; Väli et al., 2013). The spin-up period was two weeks to enable fast gravitational adjustment of the initial temperature and salinity (density) and the velocity field. Hindcast atmospheric forcing for the Baltic Sea region was prepared from the BaltAn65+ dataset, which is a dynamical downscaling of the ERA40 reanalysis using the HIRLAM model (Luhamaa et al., 2011). The atmospheric parameters were available on a spatial grid with a resolution of 0.1° and at a temporal resolution of 6 h. Monthly river runoff data of 37 largest rivers from the Baltic catchment was adopted from the hindcast simulation of the *E*-HYPE hydrology model (Donnelly et al., 2015). The sea level at the open boundary in the Kattegat was prescribed using daily measurements from Smøgen gauge station. For realistic salinity data, we prescribed boundary conditions based on recorded salinity measurements made on Danish Lightships in Kattegat and used local wind conditions from BaltAn65+ to describe the tendency toward oceanic salinities during westerly wind impulses (Gustafsson, 1999). Monthly mean air temperature from the Kattegat was used as the surface water temperature boundary condition. When negative air temperatures occurred, 0 °C was used. Details of constructing boundary data are given by Maljutenko and Raudsepp (2014).

2.3. Defining thalweg

The characteristic distribution of salinity and estuarine exchange is often described as a vertical section along the thalweg of the estuary (Lilover et al., 2017; Lips et al., 2016a). However, unlike conventional drowned river estuaries and fjords where the main erosion direction aligns with the main gulf axis, the sea bed of the GoF is shaped by erosion of the last ice age and river runoff, thus, the gulf is characterized by many underwater depressions and mounds. This makes it hard to define one continuous line combining the deepest points as a thalweg. We have defined a thalweg as 10% of the deepest grid points along the selected meridional transect. The grid points defining the thalweg are shown in Fig. 1b.

3. Results

3.1. Model validation

Here, we briefly summarize the model validation results presented in detail in Maljutenko and Raudsepp (2014). The statistical comparison of measured and simulated sea levels has been conducted in three sea level observing stations at Landsort, Dirham and Narva-Jõesuu (Fig. 1a). Sea level in Landsort station, characterizing the total volume of the Baltic Sea, has been simulated with a high correlation ($R = 0.94$) and a small root mean square difference (RMSD = 7.5 cm). Sea levels in Dirham ($R = 0.94$, RMSD = 8.8 cm) and Narva-Jõesuu ($R = 0.96$, RMSD = 8.2 cm) stations show validity of basin wide barotropic pressure gradient forcing in the GoF. The quality of our simulation results was comparable to other long-term modelling results (e.g. 8.9 cm by Jędrasik et al., 2008).

Comparison of the simulated and observed time-series for the bottom and surface salinity from the Gotland Basin (BY15) and the GoF (LL7) is shown in Fig. 2a, b. In the time-series plots, monthly mean data from the Baltic Environment Database (Wulff et al., 2013) and daily mean values from the model were compared. The monthly mean values from the database were used because of scarcity of data on the one hand and because of large scattering of temperature and salinity values, when several measurements fall into short time interval and mesoscale and sub-mesoscale features dominate in the area, on the other hand.

Measured surface salinity in the Gotland Basin shows a steady increase up until the end of the 70's, which is followed by a decrease up until the mid-90's and a slight increase thereafter (Fig. 2a). A similar tendency is less pronounced in the GoF. In the model, the salinity level is rather steady until the end of the 70's because the initial salinity level is already higher compared to observed salinity values. The model salinities and observed salinities even out after the first 10 years of the simulation, and the following decrease in salinity starting with the beginning of the 80's is well reproduced by the model. Since 1995, the model gives statistically significant linear salinity trend of 0.03 g kg^{-1} year^{-1} and 0.04 g kg^{-1} year^{-1} in the Gotland Basin and in the GoF, respectively, while there are no trends in the measured salinity values. The seasonal salinity cycle is well-reproduced both in timing and in range. The latter does not exceed 1 g kg^{-1} in the BY15, while being around 2 g kg^{-1} in the GoF. Low salinity values are observed in summer. This is caused by the development of vertical stratification and less mixing.

At the beginning of the simulation, the initial salinity is about 1 g kg^{-1} lower than observed in the bottom layer of the Gotland basin (Fig. 2a). This affects the salinity until the Major Baltic Inflow (MBI) in 1993. The maximum salinity difference between the model and

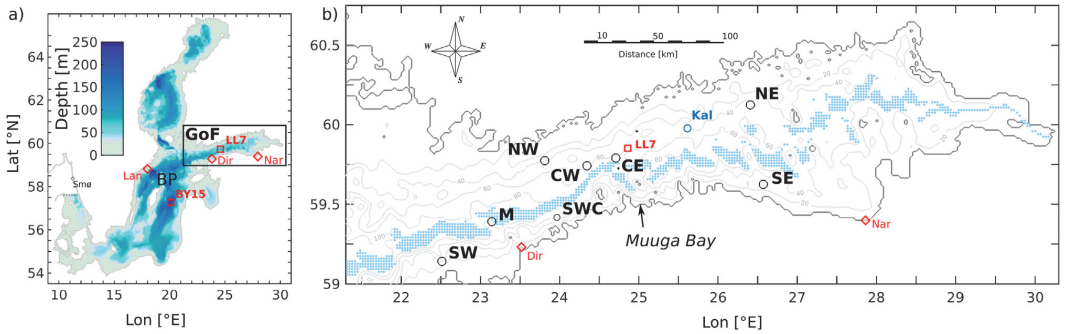

Fig. 1. Map of model domain and area showing location of the Baltic Proper (BP) and the Gulf of Finland (GoF) on (a). Map of study area with locations of current observations and selected stations (b). The red diamonds on (a) and (b) show locations of sea level gauges and red squares show locations of salinity and temperature monitoring stations. Black circles on (b) show the selected stations. Light blue dots show the thalweg location of depths below 90 percentile on the corresponding meridional transect. (For interpretation of the references to color in this figure legend, the reader is referred to the web version of this article.)

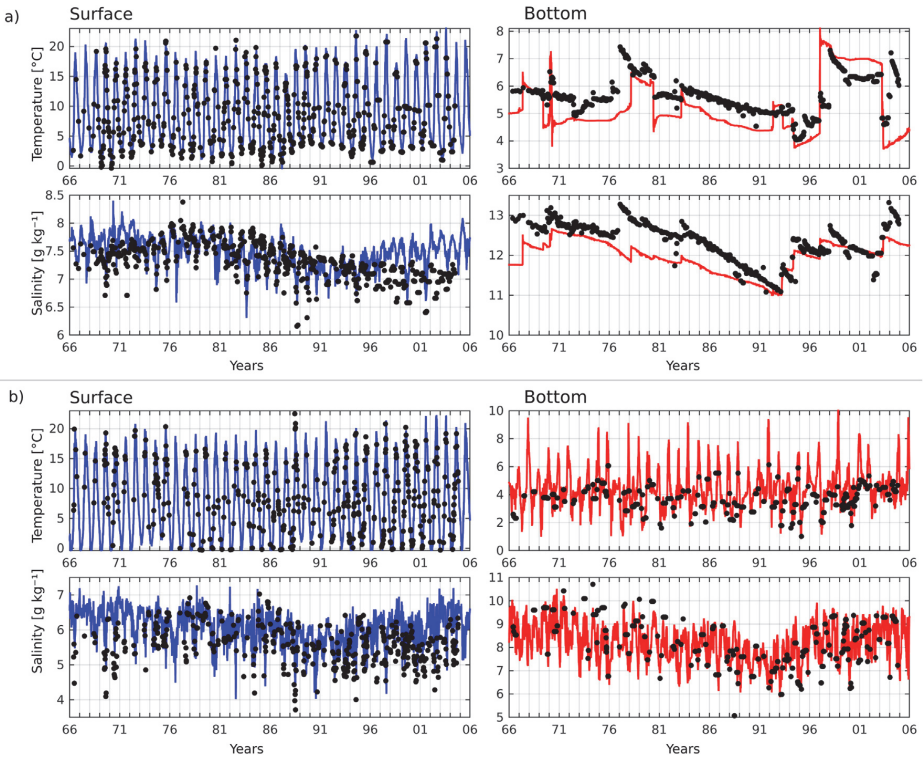

Fig. 2. Time-series of salinity and temperature at stations BY15 (a) and LL7 (b). Measurements are plotted as black dots and daily mean modelled values as continuous lines. The values for surface are on the left and bottom values on the right panels.

observations of 1.5 g kg^{-1} is evident in 1977 because the model does not have a signal from the moderate MBI in 1976. By the end of the stagnation period in 1993, both model and observed salinities reached 11 g kg^{-1}, which shows that the freshening of the bottom layer in the Gotland Deep between the MBIs in 1976 and in 1993 is slower in the model than in nature. Model results show artificial inflows to the Gotland Basin in 1978 and 1980, which reduce observed salinity decrease. Model results show oversensitivity to some smaller inflows reaching the Gotland Basin, e.g. the inflows of 1996 and 1997 have hindered the inflow signal in 1998, which is visible in the measurements. Thus, with some exceptions, the model reproduces the dynamics of MBIs and the following transport of saline water from the Danish Straits to the Gotland Deep rather well.

The seasonal signal in the GoF is overwhelming in the bottom salinity variations, with a range of up to 3 g kg^{-1} and 2.5 g kg^{-1} in the observations and model, respectively. High salinity conditions prevail in summer, followed by low salinity in winter. This indicates that the estuarine circulation is more pronounced in summer than in winter. In late autumn and winter, intense vertical mixing due to convection and estuarine flow reversals (Elken et al., 2014; Liblik et al., 2013) reduce vertical salinity stratification in the GoF. Long-term salinity variations that had a clear signal in the surface layer of the Gotland Basin are obvious in the bottom salinities in the GoF. The long-term trends of bottom salinity decrease in the 70's and 80's, and the following increase after the MBI in 1993 are well-simulated by model.

A simple rigid lid formulation for ice reproduced maximum ice extent for the Baltic Sea in mild winters but underestimated ice extent in severe winters, while interannual variations were simulated well (Maljutenko and Raudsepp, 2014).

A more detailed validation of the results from the current simulation has been presented in Maljutenko and Raudsepp (2014).

3.2. Mean fields

Spatial pattern of 40-year mean wind vectors is uniform with the direction being predominantly south-west and the speed of about 2 m s^{-1} over the GoF (not shown). This is in agreement with Isemer et al. (2008), Keevallik (2008) and Keevallik and Soomere (2014).

As a proxy for the mean circulation, mean surface salinity characterizes fresh and saline water exchange between the mouth and head area of GoF (Figs. 3a, 4a). Over the longitudinal length of 400 km, salinity changes from 6 g kg^{-1} to 2 g kg^{-1}, which results in a mean salinity gradient of 0.01 g kg^{-1} km^{-1} (or 10^{-5} g kg^{-1} m^{-1}). The salinity gradient is somewhat steeper in the north-eastern part of the GoF where freshwater from Kymi and Neva rivers are major contributors. In the eastern part of the gulf, distorted isohalines show a westward intrusion of freshwater at the north-eastern and south-eastern coast and eastward spread of saline water in the central part (Fig. 3a). This is consistent with the dominant westward coastal current (WCC) at the southern coast and weak eastward flow in the central part (Fig. 4a). In the eastern part of the gulf, detachments of the WCC from the coast are merging with a weak eastward flow at the center of the gulf, which can be easily interpreted as an anticyclonic circulation gyre. Significant transformation of WCC takes place near the mouth area where WCC merges with coastal inflow from BP and continues as an outflow near the central axis of the gulf. This results in a well-known cyclonic circulation pattern and a transversal salinity gradient.

The persistency of surface currents (Fig. 4b) is calculated as a ratio

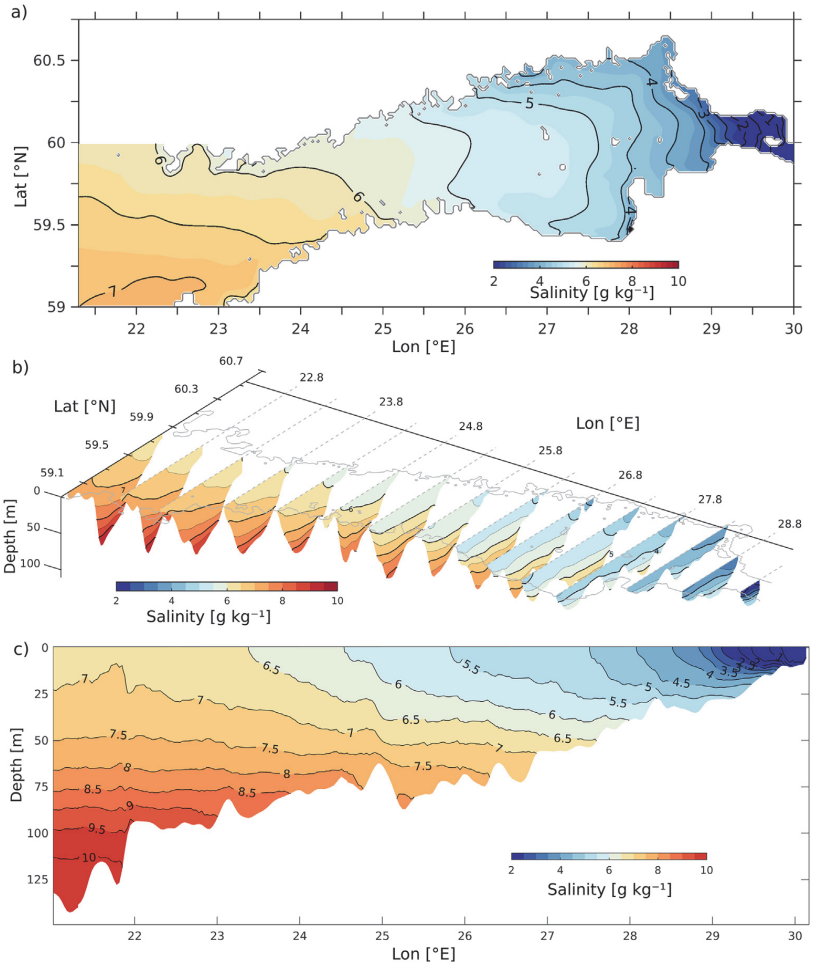

Fig. 3. Mean salinity distribution of average upper 10 m (a), transverse transections (b) and the mean salinity transect along thalweg (c).

of mean vectorial and scalar current velocities,

$$|\overrightarrow{u} + \overrightarrow{v}|/|\overrightarrow{u} + \overrightarrow{v}|, \quad (1)$$

where u is the zonal current component and v is meridional current component. The mean persistency, calculated from daily mean velocity fields, over the gulf area (0.28, std. 0.05, median 0.22) reflects a low stability of the general current pattern. However, the stability of WCC is above 0.28 over the whole length of GoF. The current system associated with the Neva River outflow in the eastern part of the GoF reveals a persistency above 0.28 and occasionally above 0.5.

Sequential meridional transects in Figs. 3b and 4c reveal the vertical structure of the salinity and zonal velocity fields. From the surface down to about 15 m isohalines tend to be vertical, which is a sign of a mixed upper layer. In the intermediate layers/deep layers of the western part of the GoF, isohalines decline/incline toward the northern coast, resulting in stronger vertical stratification on the northern slope than on the southern slope of the GoF. However, in the eastern part of the gulf, transverse isohalines are horizontally more flat.

The WCC extends over the upper 20–30 m in the eastern part of the GoF and reaches 50 m in the western part, where it detaches from the southern coast. The eastward current extends over the entire water column in the western part and submerges below the WCC as the WCC attaches to the coast. Although the WCC originates from the less saline eastern GoF, it does not cause a low salinity area similar to the northeastern coast of the GoF. Higher salinity could be explained by an entrainment of saline water from the deep inflow current. In order to investigate vertical advective flux, the integral of mean vertical velocity

$$\frac{1}{D}\int_D^{\eta} \overrightarrow{w}\, dz, \quad (2)$$

where D is depth, η is sea level and w is vertical velocity, is plotted on Fig. 4d. The patchy distribution of vertical velocity (e.g. Meier, 2007; Myrberg and Andrejev, 2003) is smoothed twice using a moving average horizontal filter over a 4 × 4 cell in order to reveal larger regions of vertical advective fluxes. The average vertical velocities over the whole GoF area are positive but two orders of magnitude lower than local values. The regions with upward and downward fluxes are alternating sequentially, revealing that vertical advective flux mostly has a local nature. However, the southern slope is characterized by a relatively uniform upward flux, which is contradicting the results by Myrberg and Andrejev (2003). This area overlaps with WCC, suggesting there is a significant vertical salt flux along its longitudinal extension.

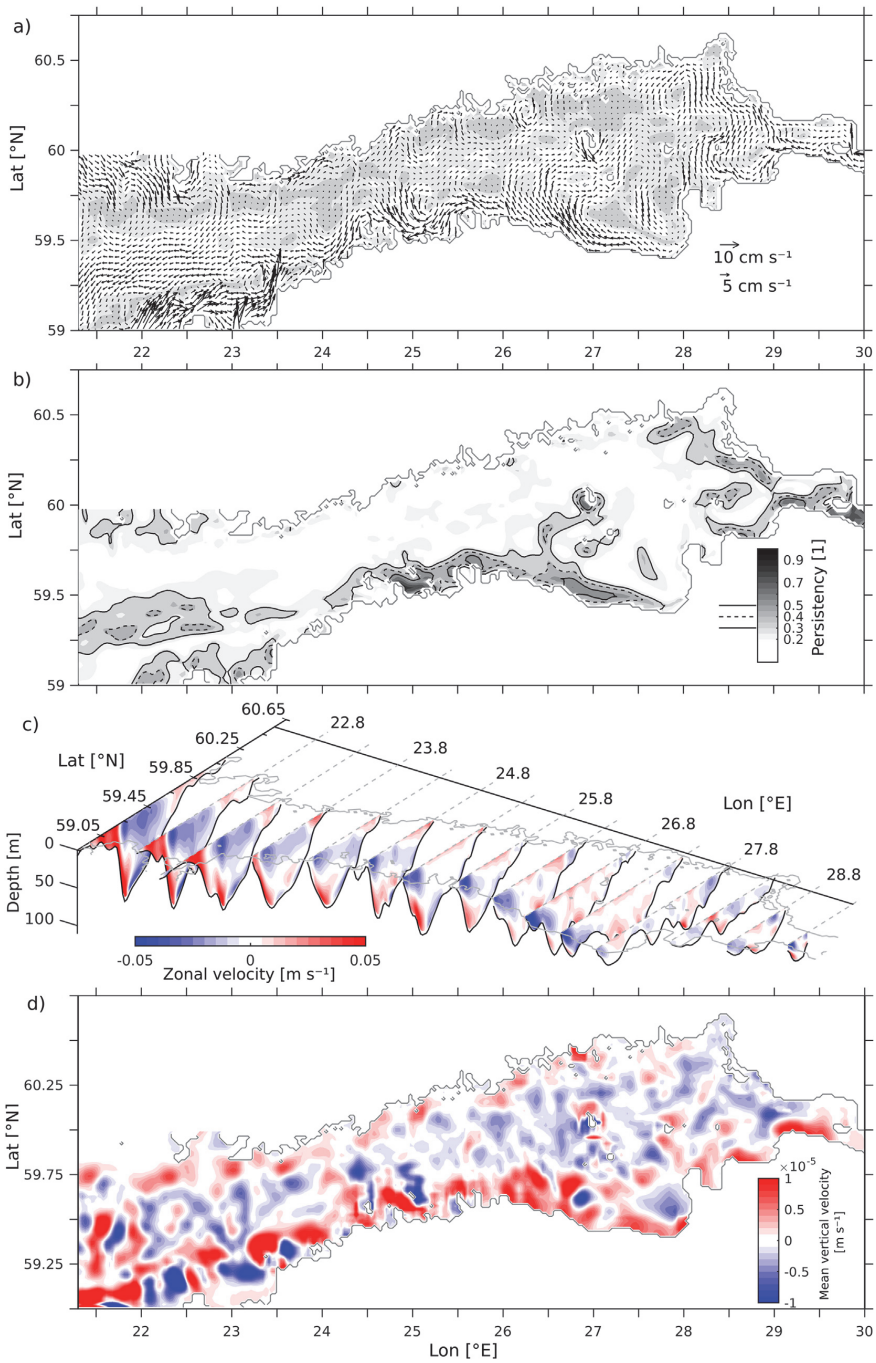

Fig. 4. Mean surface layer (0–10 m) current field with shaded persistency < 0.2 on (a) and every 2nd arrow shown. Surface layer persistency is shown on (b). Zonal velocity transects are plotted on (c). Depth averaged mean vertical velocity distribution calculated using Eq. (2) on (d).

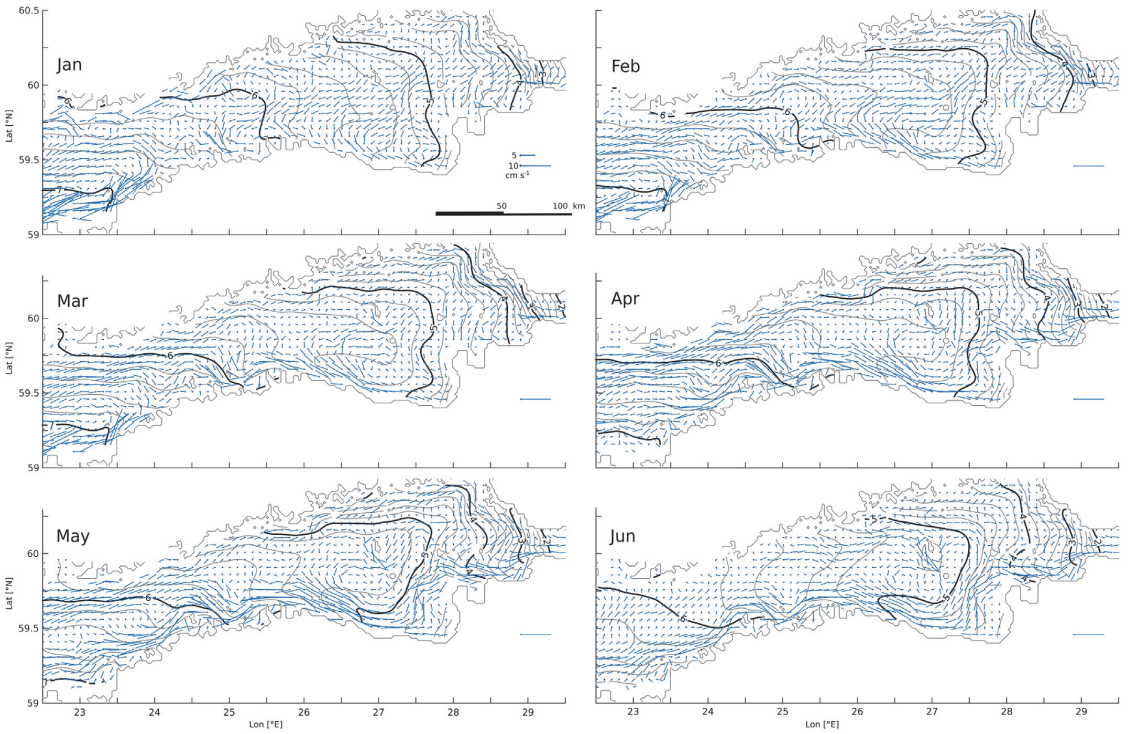

Fig. 5. Monthly mean surface layer current field averaged over depth of 0–10 m. Every 3rd velocity gridpoint is shown for better visibility. Monthly mean salinity distribution averaged over same depth range is shown as black and grey isohalines.

The subducting area near the southern coast of the western GoF marks the sinking of saline inflow near the surface. Farther offshore, mostly a downward flux dominates until the northern coast where isolated areas of upwelling appear in the vicinity of peninsulas near the northern coast. The latter is consistent with the results by Myrberg and Andrejev (2003). There is no significant difference in spatial distribution of vertical advective flux through the different layers i.e. 10-m, 20-m, 40-m, 60-m layer (not shown), compared to the vertical velocity averaged over the whole water column.

3.3. Seasonal climatology

Monthly mean upper layer (0–10 m) circulation patterns are plotted in Fig. 5 showing significant annual surface current field variability. The inflow in the western part of the gulf near the southern coast is the dominant current structure over the course of the months from November to January. This inflow begins to form in September/October and disappears in April as WCC starts to prevail and becomes the dominating current in May and June. Only a weak inflow is evident during July and August. The strength of WCC varies within the year, being strongest during spring months. First signs of developing WCC are evident in February when the coastal current forms in the eastern part of the GoF. During the period from April to June, the coastal current stretches from the eastern edge of the gulf and extends further into the Baltic Proper along the southern coast. In July, the WCC weakens due to extensive cross-shore transport and transforms into two basin-wide anticyclonic gyres. Weakening of the gyres takes place in autumn and they disappear by November. The small-scale anticyclonic loop is present in the Narva Bay during all months.

A westward current along the northern coast starts to develop in February being most intensive in April–May. The latter coincides with the period of high river discharge (Donnelly et al., 2015). The current is stronger in the western part due to a substantial cross-shore exchange originating from the WCC in the central part of the gulf. In June, the current reforms into an inflow which lasts from July to October.

The seasonal climatology of dominant current that features the WCC and two anticyclonic gyres is also evident on the Hovmöller diagrams, i.e. temporal variability of vertical distribution of current velocity components at the selected locations (daily mean climatology smoothed once over 13 days). Temporal variability of vertical distribution of daily climatology of unsmoothed zonal velocity component at the SW and SE locations shows that WCC is a prominent feature in the surface layer of 20 m from April to June (Fig. 6c, f). During that period, the WCC breaks inflow at the SW location which is otherwise strong and vertically unidirectional.

At the NW location, there is an outflow period from February to June over the upper 30 m layer and weak inflow below (Fig. 6a). The outflow is reversed to inflow in the surface layer while extending over the rest of the water column in June. The inflow layer deepens and the outflow layer shrinks in time until inflow covers the whole water column by November. The bi-directional flow is strong from July to October, which corresponds to a dominating anticyclonic circulation in the upper layer over the western Gulf. A low southwards meridional velocity component at the CW location (Fig. 6b) confirms existence of anticyclonic circulation that extends to 20 m depth in July and August. Occasionally, zonal flow at the SW location is negative during that period. Comparing velocities at the NW, SW and CW locations indicates a cyclonic circulation in a depth ranging from 20 to 40 m, i.e. below the anticyclonic circulation pattern. From September to October, the anticyclonic circulation extends over the entire water column but is

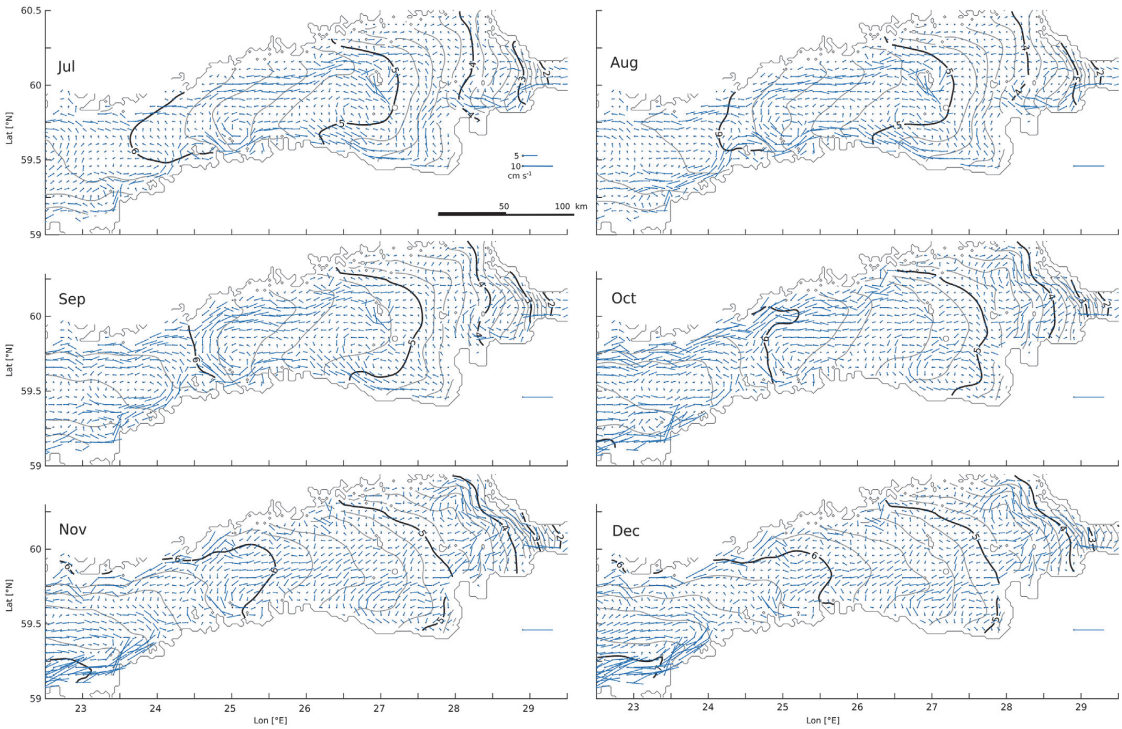

Fig. 5. (*continued*)

pushed offshore due to increasing inflow at the SW location.

A similar anticyclonic circulation starts to develop over the eastern part of the Gulf in June. Then, the WCC transitions smoothly into the southern part of anticyclonic circulation. The flow at the SE location is continuously westward (Fig. 6f). The meridional flow at CE location is northward, although relatively weak (Fig. 6e). We like to note that at the adjacent CW location, the mean flow is southward (Fig. 6b). At the NE location, the flow is eastward (Fig. 6d), thus forming the northern

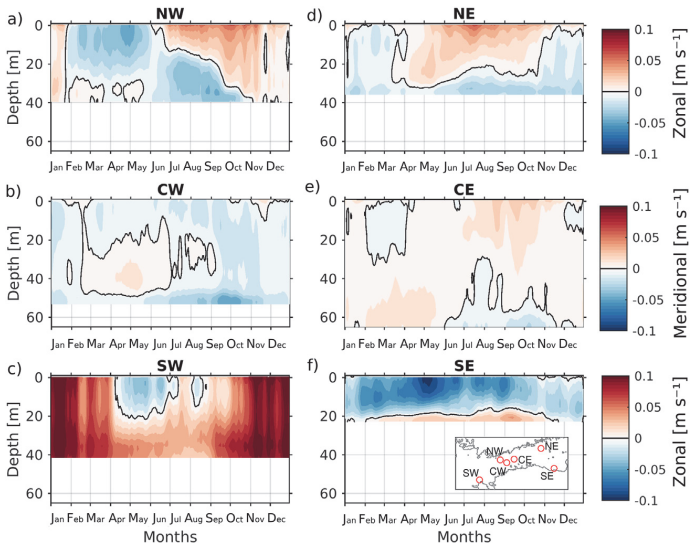

Fig. 6. Hovmöller diagrams of daily mean meridional and zonal velocity components for selected stations (a)–(f). The locations of selected stations have been shown in Fig. 1.

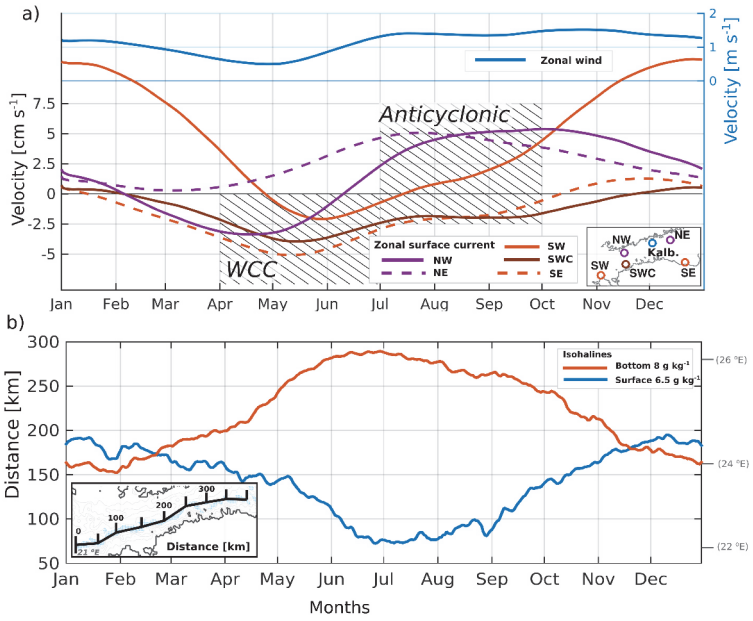

Fig. 7. Daily mean climatology of residual zonal current speed at surface layer and zonal wind speed at Kalbådagrund (a). The purple lines correspond to the stations at the northern coast and red lines correspond to stations located at southern coast. Solid and dashed lines correspond to the western and eastern stations respectively. The hatcheted area labeled WCC corresponds to the period when the westward coastal current is the dominating feature of surface circulation field. The anticyclonic hatcheted area shows the months during when the WCC diminishes and the basin wide anticyclonic gyres develop. Daily mean climatology of the salt wedge (8 g kg^{-1} isohaline) extent toward the head of the GoF and the less saline upper layer water (6.5 g kg^{-1} isohaline) extent toward the mouth of the GoF (b). The distance is calculated from longitude of 21°E and the longitudes are shown on right-hand side axis. (For interpretation of the references to color in this figure legend, the reader is referred to the web version of this article.)

part of anticyclonic circulation. It should be noted that in spring the NE location is outside the coastal current of the river plume. Initially, anticyclonic circulation is weak, but it extends over the thick upper layer of about 30 m. While strengthening, the anticyclonic circulation shrinks in depth as cyclonic circulation in the bottom layer increases.

To summarize the seasonal climatology of the dominant current structures, the WCC and two anticyclonic gyres, we have depicted seasonal course of the surface zonal current velocity and zonal wind speed at the selected locations in Fig. 7 (daily climatology of zonal current and wind speed which is twice smoothed over 61 days). The zonal current velocity at the SE and SWC locations describe the strength of WCC, at the SW location the north-eastern branch of cyclonic circulation in the Baltic Proper and at the NE and NW locations the existence of the anticyclonic gyres. The full 40-year time series are presented in Fig. 8 to show that seasonal climatology is not a statistical property only. The zonal wind is included because of the mean wind although small in magnitude plays significant role in the modification of the WCC and affecting the development of the anticyclonic circulation gyres. The zonal velocity at the SW location is dominantly positive, which is consistent with the general cyclonic circulation in the Baltic Proper (Lehmann and Hinrichsen, 2000; Meier, 2007). At the SWC and SE locations, the zonal flow is mainly negative which supports the existence of WCC and southern part of anticyclonic gyres. At the NW location, mean zonal flow is weakly positive, but persistently positive at the NE location in the support of northern part of the anticyclonic gyres. The zonal wind is mainly positive, thus the dominating flow at the northern GoF is consistent with zonal wind, but the zonal flow at the southern coast is opposite to the zonal wind.

The correlation coefficients between the zonal currents and zonal wind calculated from unsmoothed daily mean values are presented in Table 1. Zonal wind component has strong correlation with zonal current velocity of WCC and zonal velocities of the northern parts of anticyclonic gyres (Fig. 8). This shows that wind has significant role in reducing (positive zonal wind component) the intensity or enhancing (negative zonal wind component) the intensity of the WCC. In case of the western anticyclonic gyre, the positive zonal wind drives the eastward flow at the northern part of the GoF, which is needed to form the anticyclonic loop. In case of the eastern anticyclonic gyre, the positive zonal wind increases eastward flow and intensifies northern part of anticyclonic gyre. Considering zonal current velocities at the selected location, we would like to emphasize the high correlations between the flow at the southern coast on the one hand and at the northern coast, on the other hand. For the WCC, it means that cyclonic circulation in the Baltic Proper influences the strength of the WCC and vice versa. For the anticyclonic gyres, it means that both of them exist simultaneously.

In the seasonal scale, the development phase of the WCC from February coincides with the decrease of the zonal positive wind velocity (Fig. 7a). The most intensive WCC in April–May falls into the period where zonal wind is in its minimum. Since June, the WCC reforms into anticyclonic circulations as the zonal wind increases simultaneously. Since July until October 2, anticyclonic gyres dominate the circulation in the surface layer of the GoF in response to the positive zonal wind. From October–November to January–February, vertical mixing due to wind and thermal convection due to surface cooling, as well as ice coverage affect the circulation in the GoF, but remain out of the scope of current study. Besides, we would like to mention that the circulation in the entrance area to the GoF is strongly influenced by the main cyclonic circulation of the Baltic Proper.

The monthly mean salinity distributions along the transect of the thalweg of the GoF describe estuarine circulation in general (Fig. 9). Seasonal salinity dynamics resemble advancement of salt wedge toward the head of the estuary during the period from February to June and the retreat of the salt wedge from July to October. We defined lower salinity of the salt wedge as 8 g kg^{-1} and higher salinity of less saline upper layer water (LSULW) as 6.5 g kg^{-1}. The choice was made because during the period of the most intensive mixing these isohalines share approximately the same location on the thalweg (Figs. 7b, 11b). From November until January, salinity distribution is relatively stable (Fig. 7b). The upper mixed layer reaches about 40 m in the eastern part and up to 60 m in the western part of the GoF, followed by a stratified water column below. The following development of a seasonal salinity stratification due to the freshwater discharge and solar heating reduce the mixed layer depth to 10 m. The period from February to June is characterized by a westward transport of LSULW, which is most

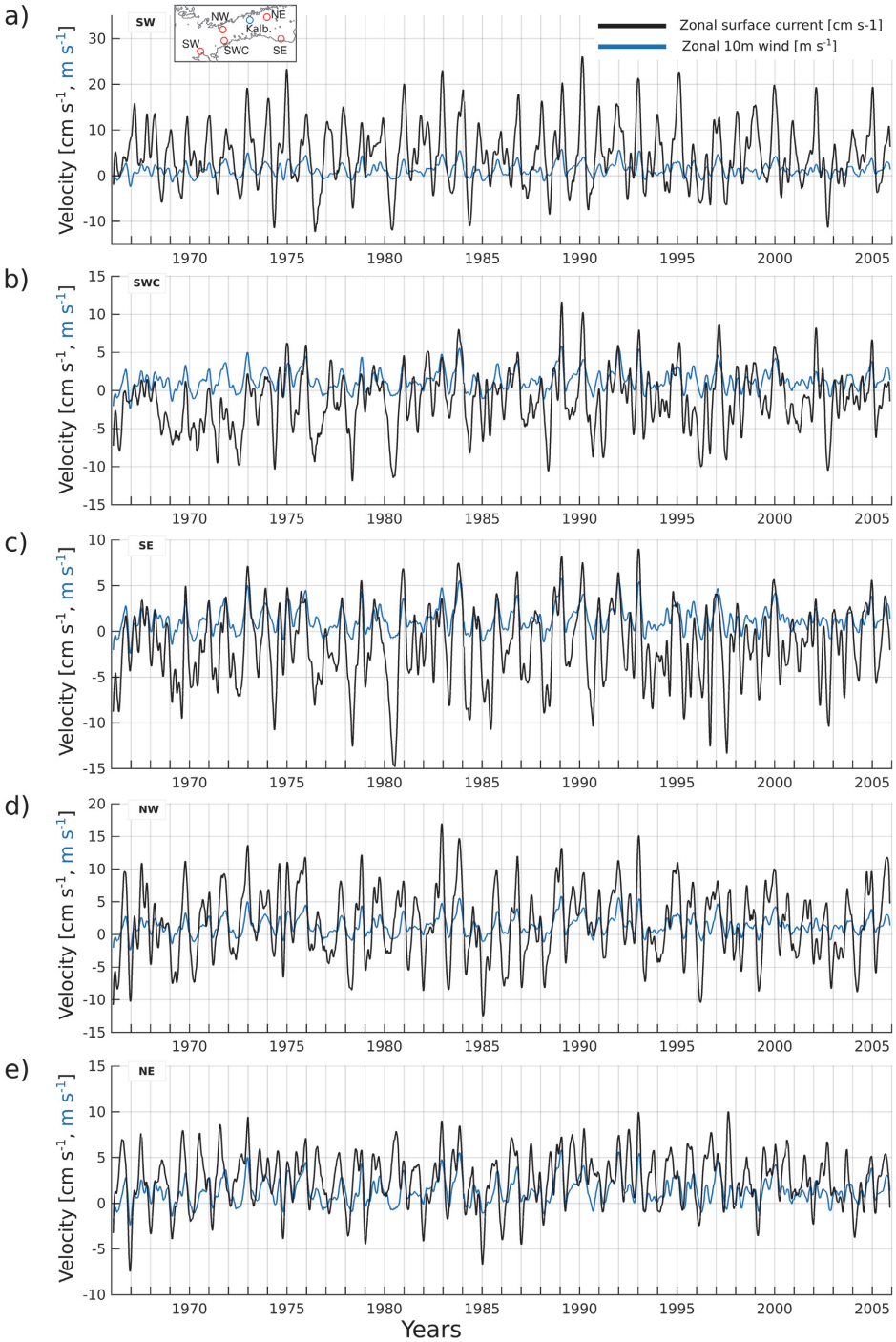

Fig. 8. Time-series of 60-day residual zonal wind (from Kalbådagrund) and current velocity components from selected stations SW (a), SWC (b) SE (c), NW (d) and NE (a).

Table 1
Correlation matrix of 60-days running mean zonal wind flow in Kalbådagrund and zonal surface current speed at five stations (Fig. 1b).

	Wind	SE	SW	SWC	NW	NE
Wind	1.					
SE	0.782	1.				
SW	0.467	0.719	1.			
SWC	0.711	0.794	0.763	1.		
NW	0.837	0.681	0.406	0.515	1.	
NE	0.582	0.238	−0.034	0.159	0.733	1.

intensive in May and June. The water with salinity of 6.5 g kg^{-1} reaches the longitude of about 22°E making the travelling distance of about 120 km. Simultaneously, a strong eastward saline water transport takes place in the lower water column from February to June. Maximum eastward extension of the salt wedge, to 26.30°E which is about 140 km in distance, is achieved in June. The most intensive eastward/westward advancement of the salt wedge/LSULW is during low wind period (Fig. 7a). In late summer, from July to September, the shifts of the surface and near-bottom salinity isohalines resemble weak reverse estuarine circulation without drastic changes in the depth of the mixed layer. In October and November, continuous mixing increases upper layer salinity over the entire gulf.

3.4. Interannual variations

We divide the annual period into two sub-periods: one from April to June (Fig. 10a) and the other from July to September (Fig. 10b). These periods correspond to the dominance of the WCC and two anticyclonic gyres respectively. The low or high wind periods of the three month mean zonal wind in spring (Fig. 10a) and summer (Fig. 10b) do not coincide. As low zonal wind favors both the WCC and anticyclonic gyres, then we do not expect these two phenomena to be strong during the same year. The exceptions are the years of 1979 and 1980, when the zonal wind component was high and low during both periods, respectively. The WCC and the anticyclonic gyres were absent in 1979, but well-developed in 1980. We have visually checked the current structures for each year, and the subjective estimates of the rate of the development are presented in the panel in Fig. 10c. Besides the intensive WCC, well-established anticyclonic gyres existed in 1969, 1995–1997 and 2002, but the correlation with the wind is not so obvious.

The WCC emerges in the zonal velocities (3-month mean calculated from daily mean values) at the selected locations of the southern coast of the GoF, especially at SWC and SE locations (Fig. 10a). There, the negative zonal velocity shows the existence and intensity of the WCC. In case of a very intensive WCC, the WCC extends to the NE Baltic Proper and negative velocity is visible at SW location. Until 1989, there is very good correlation with the intensity of WCC and the wind strength. Low wind speed or even very small negative wind corresponds to intensive WCC and high positive wind destroys WCC, except in 1976. During the period from 1969 to 1972, the wind is low and the WCC is intensive every year except in 1972. Since then until 1981, the years with strong and weak WCC follow each other. The period from 1983 until 1989 has relatively low wind speed and the WCC is well-developed. Since that period until the end of the simulation, the coincidence between wind speed and intensity of WCC is not so strong. The WCC exists almost every year, but does not extend so far west as it was during 70's. There are several publications showing regime shift of the airflow over the GoF in 1989 (Elken et al., 2014; Keevallik and Soomere, 2014; Soomere et al., 2015).

The anticyclonic gyres emerge on the zonal velocities at the locations on the southern as well as on the northern coast (Fig. 10b) (3-month mean calculated from daily mean values). The velocities on the southern coast should be negative similar to the period of the WCC, but positive on the northern coast. The higher absolute values of the zonal velocity components indicate more established and more intensive anticyclonic gyres. During summer months, the stronger zonal wind favors stronger currents at the northern coast of the GoF (Fig. 10b). The correlation is especially good at the NW location. On the other hand, stronger wind weakens westward current at the southern coast or even reverses it. The westward currents are the strongest when the wind is weak. In general, anticyclonic gyres are present when zonal wind is weak, but may not exist when zonal wind is strong. Since the start of the simulation until 1979, the established anticyclonic gyres exist during the summers with moderate wind (Fig. 10b, c). In 1980–81, we have strong anticyclonic gyres at both locations simultaneously. From 1982 to 1988, the anticyclonic gyres do not establish during summer as this period is characterized with relatively strong westward zonal wind. Since 1993, the anticyclonic gyres occur more frequently, also the zonal wind is lower than during the 60–80's. The changes in the frequency of occurrence and intensity of the WCC and anticyclonic gyres before year 1990 and after could be related to the changes in the zonal wind component (Elken et al., 2014; Keevallik and Soomere, 2014; Soomere et al., 2015). Before 1990, the three month mean zonal wind was stronger in summer than in spring, but equalized after 1990, in general. There are some years, when the wind favors the WCC or anticyclonic circulation, but they are absent or are weak, and vice versa. This leaves the possibility that in some cases the structures are hindered/suppressed by the physical processes not tackled in this paper.

The Hovmöller diagram, i.e. the temporal variability of vertical distribution for salinity, confirms the seasonal nature of estuarine exchange flow in the GoF (Fig. 11a). Salinity stratification begins strengthening during the spring with increasing bottom layer salinity and decreasing surface layer salinity. Maximum height of the salt wedge as well as the easternmost extent of it is achieved by the end of June (Fig. 7b). Following destratification during autumn and winter has two different mechanisms, vertical mixing and reverse estuarine circulation. The latter results in stratification collapses in winters of 1975/1976, 1977/1978, 1980/1981, 1991/1992, 1994/1995, 1999/2000, 2004/2005, which coincide with the years of a very small density difference calculated from the measurements (Elken et al., 2014).

Interannual variations of the height of salt wedge at the entrance to the GoF (Fig. 11a) and its eastward transport along the thalweg (Fig. 11b) as well as thickness and westward transport of the LSULW are consistent with the bottom salinity variations in the Gotland Deep (Fig. 2a). After the MBIs and following high-saline water period the salt wedge extends up to 40–50 m depth from the bottom and reaches about 27°E. Since the beginning of 1970's the height of the salt wedge slowly decreases, its wintertime location shifts westward as well as the eastward extent decreases accordingly. The MBI in 1976 as well as moderate inflow in 1982 cause some recovery of the salt wedge height, location and eastward distance. The stagnation period in the Baltic Sea until the MBI in 1993, has a substantial effect to the salinity variations in the GoF. The salt wedge becomes weak, it remains in the entrance area and reaches the longitude of 24°E during its maximum extent in 1990–91. At the same time, LSULW is pushed much more westward reaching 21°E during summer and remaining at 23°E in winter. Following MBIs and moderate inflows in 1993, 1994, 1998 and 2003 restore the situation with salt wedge and LSULW that was characteristic to the end of 60's and beginning of 70's.

Although MBIs and moderate saline water inflows that increase the salinity in the Gotland Deep set the scenery for the salt wedge variation and estuarine circulation in the GoF, the mean zonal wind component considerably modifies salt wedge and LSULW dynamics. The distance between salt wedge and LSULW do not have obvious trends during their maximum separation (Fig. 11c). Interannual variations cover a wide range being < 100 km in 1979 to 310 km in 1980 for instance. The maximum distance between salt wedge and LSULW is strongly dependent on annual mean zonal wind component in the way that stronger positive zonal wind reduces the distance between the isohalines. Dynamically, eastward zonal wind works against the westward movement

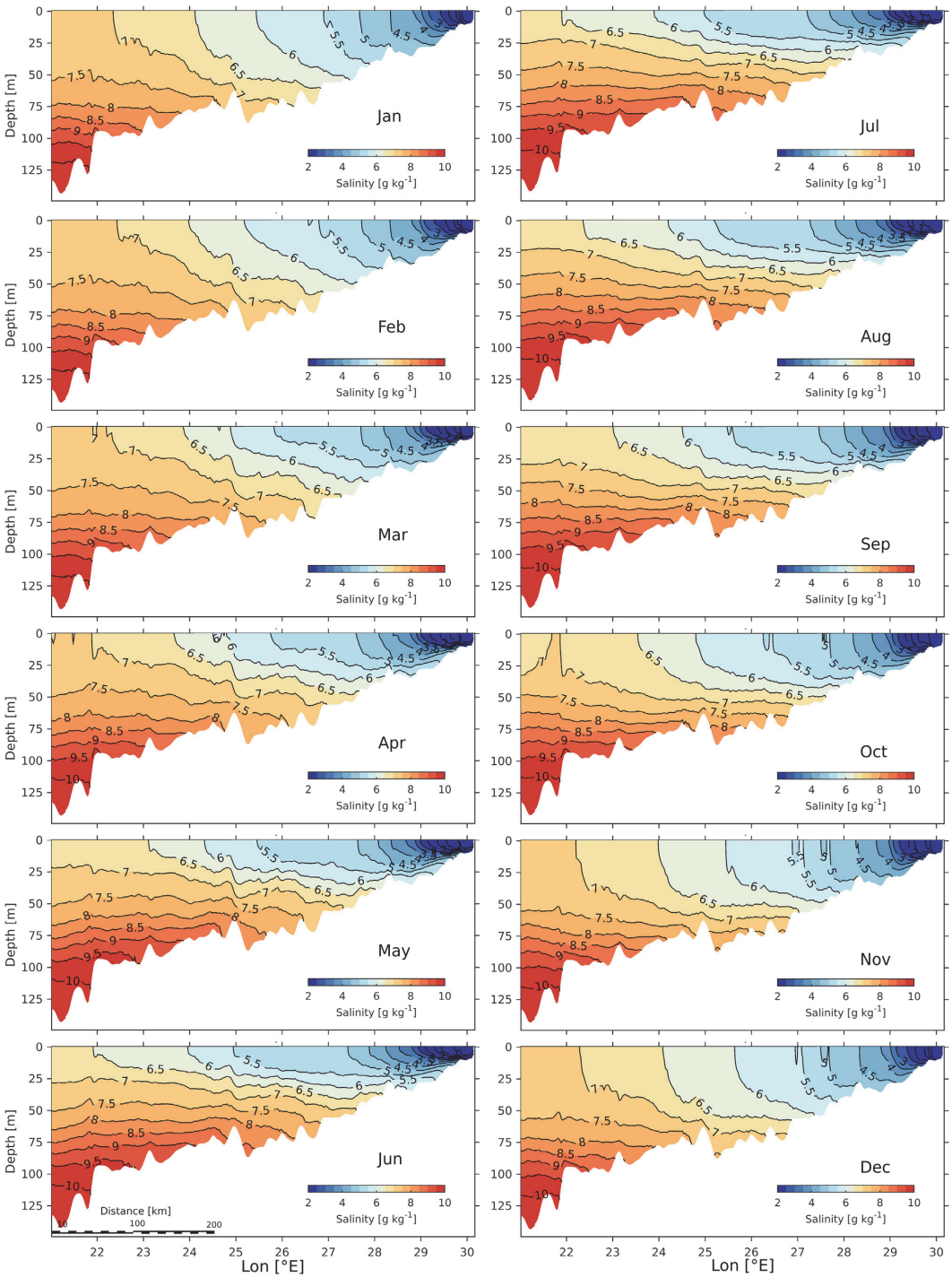

Fig. 9. Vertical distribution of monthly mean salinity along the thalweg.

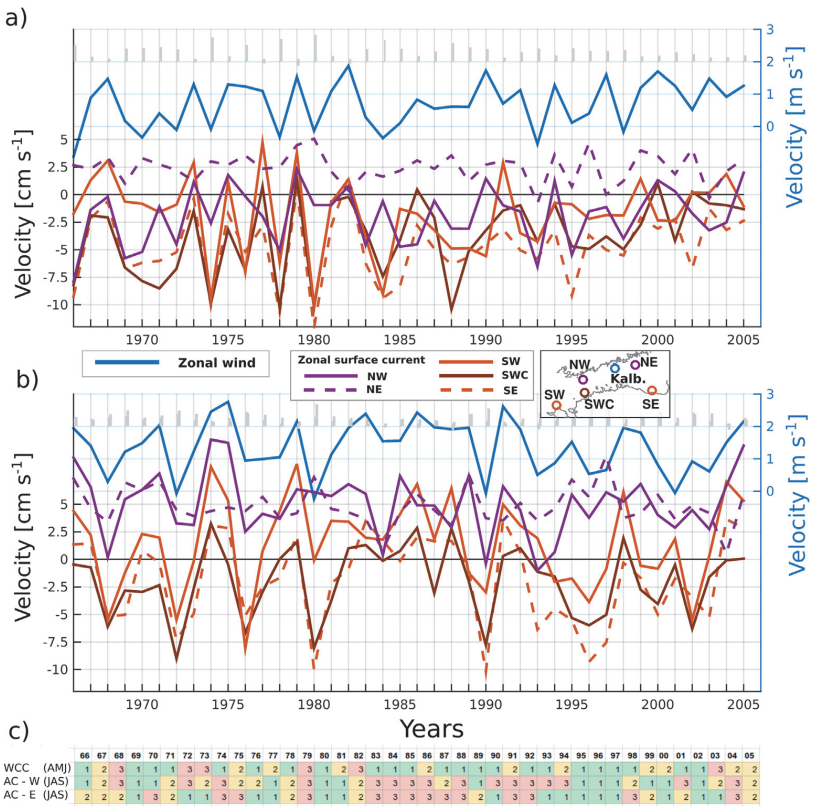

Fig. 10. Mean zonal current speed and zonal wind speed in upper part for periods of April–June (a) and July–September (b) at selected stations (Fig. 8). The solid and dashed lines correspond to western and eastern stations respectively. Color shade shows station location on northern and southern coast. Identification of WCC and anticyclonic (AC) circulation cells based on visual inspection of monthly mean surface circulation field on (c). Numbers correspond to: 1 as fully developed WCC/AC, 2 as partially developed WCC/AC and 3 as no WCC/AC has been identified. (For interpretation of the references to color in this figure legend, the reader is referred to the web version of this article.)

of LSULW and the pressure gradient which is set up at the head of the GoF does not allow eastward penetration of the salt wedge. The estuarine circulation and corresponding eastward transport of saline water and westward transport of LSULW is most intensive with low zonal wind. We like to note that there is no difference when mean zonal wind of spring period is used instead of annual mean zonal wind.

Although we have considered the WCC and salt wedge dynamics separately, they are connected anyhow. The WCC has low intensity during the peak of stagnation period from 1986 to 1994 in general, but 1989–1992 in particular. Indeed, during the last period zonal wind component is relatively high, which reduces the WCC. The WCC is relatively strong after the MBI in 1993. Investigation of the interrelationship between the WCC and salt wedge dynamics is the scope of a future paper.

4. Discussion

Numerous previous studies have explicitly stated that mean circulation is cyclonic in the GoF (Delpeche-Ellmann et al., 2016; Jönsson et al., 2011; Kullenberg, 1981; Laanemets et al., 2004; Lessin and Raudsepp, 2006; Lilover and Talpsepp, 2014; Omstedt et al., 2014; Pavelson et al., 1997; Raudsepp, 1998; Vahtera et al., 2005) based on the data interpretation by Hela (1952), Palmén (1930), and Witting (1912).

On the other hand, many authors (e.g. Alenius et al., 1998; Andrejev et al., 2004) have stated that the generalization of anti-clockwise circulation with low persistency is rather a statistical property than a permanent feature. Our model study shows that mean circulation comprises a mixture of dominant and more persistent currents which are shifted over time. It was also noted by Palmén (1930) that current persistency was much larger within seasons than over the course of the whole year, suggesting that specific seasonal currents do exist. Recently, there have been several studies discussing the seasonality of the currents in the GoF e.g. Jędrasik and Kowalewski (2019), Lilover et al. (2017), Soomere et al. (2011), and Westerlund (2018).

We have shown that WCC is a dominant feature in the surface layer of 20 m at the southern coast of the GoF during April–June, but starts to develop in February and transforms into a southern branch of the anticyclonic gyre in summer. The current measurements at the Muuga Bay during two periods, 23–28.07 and 2–6.08, in 1994 by Raudsepp (1998) showed extensive WCC in the upper layer and reverse flow below seasonal pycnocline over the whole bay, although the interpretation of the dynamics of the flow might not be valid, today. Visual inspection of model results for April–June and July–September 1994 confirmed the qualitative consistency of the current model results and the measurements. The analyses of the WCC dynamics indicated that wind could modify the WCC. The WCC is well-developed during a calm period and weak positive zonal wind component. Strong positive zonal wind reduces the intensity or even destroys the WCC, while negative zonal wind enhances the WCC. In spring and summer 1994, the zonal wind was moderate (Fig. 10), but weak during the measurement period in particular (Raudsepp, 1998).

The physical mechanism of the enhancement of the WCC by negative zonal wind component could be due to the development of the coastal upwelling at the southern coast. Cross-shore pressure gradient associated with coastal upwelling favors the development of alongshore coastal current in the direction of the wind (Csanady, 1982). In several cases, measurements and model studies show a strong WCC current

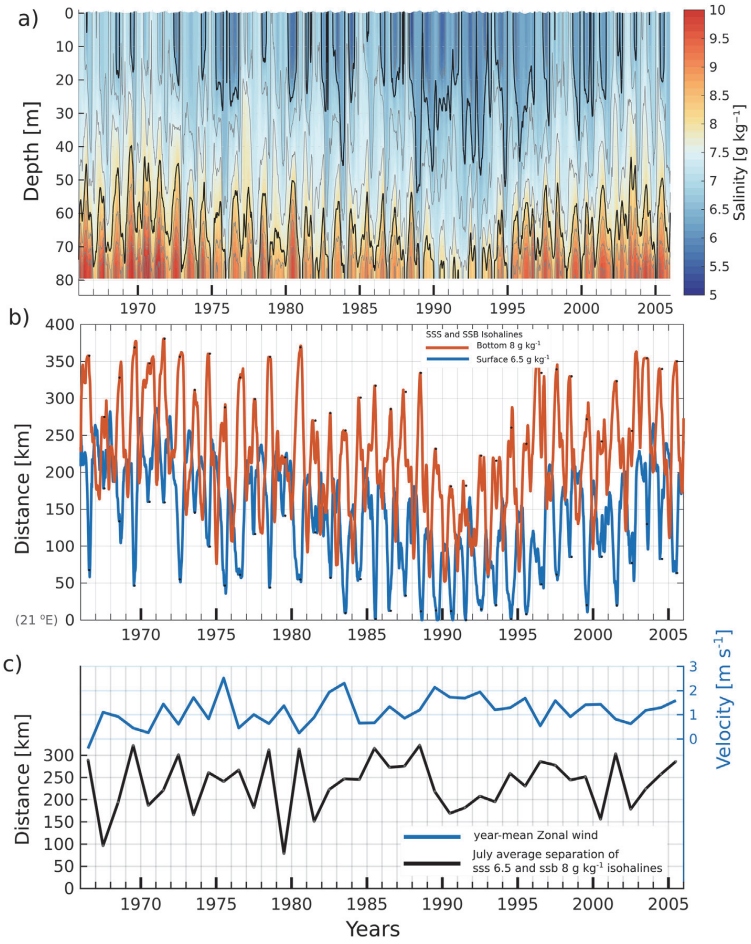

Fig. 11. Temporal variability of vertical salinity distribution at the mouth of the GoF (location M in Fig. 1) on (a). Longitudinal extent (from longitude of 21°E) along thalweg of the LSULW and salt wedge (b) and separation/difference during July on (c). Annual mean zonal wind speed from Kalbådagrund is shown on (c).

during the coastal upwelling events (Laanemets et al., 2011; Suursaar, 2010; Suursaar and Aps, 2007). Equally well, there are measurements and model studies that show the existence of the westward currents at the southern coast that could not be explained by the upwellings (Höglund and Meier, 2012; Jędrasik et al., 2008; Lagemaa, 2012; Lagemaa et al., 2010; Raudsepp, 1998; Soomere et al., 2011; Suursaar, 2010; Westerlund et al., 2017).

In the mean fields, we have shown that the upward flux dominates at the southern coast. Indeed, development of coastal upwellings supports this upward flux, but statistical analyses show that upwelling events are more frequent at the northern coast than at the southern coast of the GoF (Lehmann et al., 2012; Myrberg and Andrejev, 2003; Uiboupin and Laanemets, 2009). Myrberg and Andrejev (2003) use vertical velocity to define the upwelling index, which is similar to our study, but their model setup accounts for mainly the wind effect, on the forcing of vertical velocity which varies from year to year. In our study, we speculate that the upward flux at the southern coast is mainly entrainment velocity caused by the eastward transport of the salt wedge, which feeds the WCC. To confirm this, the summer periods of the years 1979–1988 are characterized with relatively high positive zonal wind component (Fig. 10b), which is not favorable for upwelling, but WCC is evident. The mean wind vector, calculated over the whole modelling period is toward northeast, which favors upwellings at the northern coast and mean downward flux at the southern coast. In spring and summer, mean zonal winds for different years of the modelling periods show dominating positive zonal wind, once again not supporting the WCC and southern branches of the anticyclonic gyres, as well as upward flux at the southern coast.

Indeed, there could still be debates about the role of negative zonal wind component in the forcing of a coastal upwelling and their relationship to the WCC, but the detailed research of the dynamics of the WCC remains the subject of forthcoming papers. For instance, recently, Westerlund et al. (2017) has explained the WCC as the result of accumulation of the upwellings at the southern coast of the GoF. The alongshore barotropic currents show exponential decay already within one day after ceasing of the favorable winds for an upwelling (Zhurbas et al., 2006). Following relaxation of the upwelling, the front induces baroclinic alongshore flows, which reach their maximum velocity within a time period of a week unless diminished by growing baroclinic instabilities or by the consecutive wind impulse.

The second, relatively new feature that emerges in this study is the double anticyclonic gyre system, one in the eastern and the other in the

western part of the GoF. The existence of recurrent anticyclonic circulation cells in the GoF has been shown in previous modelling studies (Andrejev et al., 2004; Elken et al., 2011; Lagemaa, 2012; Soomere et al., 2011; Westerlund et al., 2017). The anticyclonic gyres could exist separately, but also simultaneously (Fig. 10c). The eastern anticyclonic gyre is usually better developed than the western one. These two gyres are separated in the longitude of about 24.50°E. This longitudinal area is characterized with intensive cross-shore exchange (Delpeche-Ellmann et al., 2017; Delpeche-Ellmann et al., 2016; Elken et al., 2011; Lagemaa, 2012; Lips et al., 2017; Soomere et al., 2011; Viikmäe et al., 2012). The current velocity measurements, which fall into this area, show relatively variable currents with even stronger meridional component compared to the zonal velocity component (Hela, 1952; Liblik and Lips, 2012; Lilover et al., 2011).

The effect of the wind in relation to the anticyclonic circulation is not straightforward. Stronger zonal wind component results in stronger eastward currents at the northern coast (Fig. 10b). Simultaneously, if the wind is too strong, it destroys the westward current at the southern coast, so that no anticyclonic gyre can emerge. As the mean eastward flow is characteristic of the northern coast in summer, the establishment of the anticyclonic circulation gyres depends on the strength of the zonal wind. Currently, we cannot provide quantitative estimates about the thresholds of the wind speeds in relation to the existence of anticyclonic gyres, which will be the subject of forthcoming studies. When we look at the seasonal course of the anticyclonic gyres and salt wedge transport, we can argue that anticyclonic gyres start to develop when the salt wedge has reached its maximum eastward extent, becomes steady and is slowly retreating (Fig. 7). The period of eastward advection of the salt wedge coincides with the period of intensive WCC. A hint for the dynamics of the eastern anticyclonic gyre could be obtained from the paper by Soosaar et al. (2014). In the conclusion, they suggest that anticyclonic circulation in the Gulf of Riga is caused by the 3-dimensional estuarine type density gradient and maintained by upward entrainment of lower layer water into the upper layer (Fujiwara et al., 1997) due to continuous inflow of saline water into the estuarine basin. Soosaar et al. (2014) showed that in the Gulf of Riga anticyclonic circulation is either enhanced by the wind impulse from the east, destroyed or reversed to cyclonic circulation by the wind impulse from the west, which is similar to the effect of the zonal wind in the GoF. The coastline configuration and peculiarities of bottom topography could support the separation of the WCC from the southern coast and intensive transverse exchange flow at the longitude of about 24.5°E, and the formation of two anticyclonic gyres (e.g. Geyer and MacCready, 2013; Peffley and O'Brien, 1976). In general, the existence of the WCC and two anticyclonic gyres describes the GoF as a gulf type ROFI.

A seasonal course of the salinity stratification manifests the significance of estuarine exchange flow along the thalweg of the GoF. Usually vertical salinity stratification in the deeper (> 70 m) part of the gulf has been characterized as a two-layer structure in winter and three-layer structure in summer, with quasi-permanent halocline at the depth of 50–80 (Alenius et al., 1998; Liblik and Lips, 2011; Liblik and Lips, 2017). Our modelling study as well as several recently published studies (Elken et al., 2014; Liblik et al., 2013; Liblik and Lips, 2017) show that quasi-permanent halocline, as well as the entire vertical salinity stratification, is highly dynamic. The up-estuary penetration of the salt wedge and down-estuary spreading of a LSULW during the first half of the year, as seen on the hydrography measurements along the thalweg (Liblik et al., 2013; Lips et al., 2017), support the concept of a salt wedge estuary for the GoF. There are multiple recent studies of salt wedge dynamics that were based on ADCP measurements near the thalweg of the GoF (Liblik et al., 2013; Liblik and Lips, 2012; Lilover et al., 2017; Lips et al., 2017).

To study the dynamics of the salt wedge, we have selected $8\ g\ kg^{-1}$ isohaline as the lower limit of the salt wedge. The choice was somehow arbitrary, but we expect that spatio-temporal variations of the water mass with $S \geq 8\ g\ kg^{-1}$ is more influenced by advection than vertical mixing. There is indirect evidence, that wind and convective mixing alone does not penetrate to the depth of the corresponding water mass. Although there are calculations of the wind-mixing penetration depth (Laanemets et al., 2004), there are no estimates about the depth of convective mixing, that depends on the stratification of the water column in the GoF. This choice, as well as the selection of $6.5\ g\ kg^{-1}$ isohaline for the upper limit of the LSULW, is supported by the measurements (Lips et al., 2017).

The range of travel distance of the salt wedge along the thalweg is up to 200 km during the phase of estuarine circulation, but could be up to 250 km during reversal estuarine circulation, like in 1974 and 1980 (Fig. 10b). The transport of salt wedge and LSULW is not symmetrical, either during estuarine circulation phase or retreatment phase, which is straightforward as the water masses at the surface layer are directly influenced by wind transport and mixing, as well as by convective mixing. Interannual variations of the seasonal course of the salt wedge and LSULW could not be directly related to the annual mean zonal wind. Situation is different for the distance between corresponding isohalines. Annual mean zonal wind is positive, thus not favorable for the estuarine transport. This results in the larger distance between the selected isohalines when annual mean zonal wind is weak, but smaller distance otherwise. The distance could vary from 70 km in one year to 320 km in the following year, like in 1979 and 1980 (Fig. 10c). Estuarine exchange flow has been explained by the decrease of cumulative along-gulf wind stress (Lips et al., 2017), as well as retreat of the salt wedge and weakening (or even collapse) of the stratification by the increase of cumulative along-gulf wind stress (Elken et al., 2014; Elken et al., 2003; Liblik et al., 2013; Lips et al., 2017). Our results indicate that variability of wind forcing is not a single factor explaining variability of estuarine circulation and its reversal, but the interannual variations of the zonal longitudinal pressure gradient forcing should be considered also, a detailed study of which is left for the forthcoming paper.

The salt wedge dynamics on the other side are strongly related to the Major Baltic Inflows. Lessin et al. (2014) and Liblik et al. (2018) have showed reshaping of the salinity distribution in the northwestern Baltic Proper by the MBIs. A comparison of $7.5\ g\ kg^{-1}$ isohaline in Fig. 10a and bottom salinity in Gotland Deep in Fig. 2a shows the shallowing of $7.5\ g\ kg^{-1}$ isohaline in the GoF after the inflows in 1969, 1976, 1993, 1998 and 2003. In general, the LSULW-salt wedge system is pushed more/further eastward from the entrance of the GoF, following the MBIs to the Baltic Sea, but retreated westward during stagnation period (Fig. 10b). As a result, the salt wedge penetrates further to the east during estuarine circulation phase in case of higher salinity in the Gotland basin and northern Baltic Proper, than in case of low salinity there. We like to note that intensity of estuarine circulation, i.e. maximum distance between the selected isohalines (Fig. 10c), does not depend on the salinity conditions in the open Baltic Sea. For instance, at the end of stagnation period the salt wedge extends to 190 km eastward from 21°E, but the separation of selected isohalines is still about 200 km, which is close to the mean yearly maximum distance over the 40-year period. Seemingly, after the MBIs estuarine circulation is more dominant in terms of salt wedge transport, while during the stagnation period in terms of LSULW transport.

Model results are sensitive to the forcing, which is applied to the boundaries. The atmospheric forcing for current study is based on downscaling of ERA-40 reanalysis using HIRLAM (Unden and Rontu, 2002) atmospheric model which has been described and briefly validated by Luhamaa et al. (2011). Here, we present comparison with measured and modelled wind velocities at Kalbådagrund (Fig. 1) for the overlapping period of 1981–2005. The modelled mean airflow was directed northeast $(1.73,\ 1.28)\ m\ s^{-1}$, which is consistent with the average airflow from measurements $(1.52,\ 1.21)\ m\ s^{-1}$. The average model wind direction is deflected by 2 degrees clockwise from the measurements. In some periods, the difference between model and measured wind direction can be larger (Keevallik et al., 2010; Keevallik

and Soomere, 2010). The correlation coefficient between measured and simulated zonal wind component is 0.89 and RMSD 2.7 m s^{-1}. Monthly mean zonal wind followed the seasonal cycle of measured wind, which was lowest in April and highest during January and October with positive bias (reanalysis minus measurements) up to 0.6 m s^{-1} in February.

Having realistic runoff volumes of freshwater is essential to correct the estuarine circulation; therefore, calibrated and validated data from the hindcast simulation of hydrology model *E*-HYPE (Donnelly et al., 2015) have been used. The model takes into account different land use and soil type for the whole Baltic Sea catchment area. River runoff values estimated from the direct measurements could be of variable quality, also Stalnacke et al. (1999). However, Westerlund et al. (2017) argued that the simulated river discharges could differ from measurements by up to 28%, but our preliminary check of E-HYPE data does not confirm their argument.

Prescribed boundary data in our case involves sea level, temperature and salinity at the Kattegat (see Fig. 1 for the location of model open boundary). While the sea level data could be readily obtained for the Kattegat, prescription of the temperature and salinity sections could pose a problem, especially for the correct simulation of the MBIs. Madsen and Højerslev (2009) have shown that salinity conditions in Kattegat during MBI events differ considerably from climatological averages used by Jędrasik et al. (2008) and Meier (2007). After numerous mid-term tests with different boundary conditions for the model open boundary and in order to obtain realistic temperature and salinity fields for inflowing water masses, the salinity and temperature conditions were parameterized based on long-term salinity and temperature observations (Madsen and Højerslev, 2009) as described by Maljutenko and Raudsepp (2014). Besides, we adjusted initial bathymetry at the Danish Sounds, which is rather common procedure (Büchmann et al., 2011; Dietze et al., 2014; Hordoir et al., 2019; Stips et al., 2008). The other possibilities used for the Baltic Sea modelling are applying coupled North Sea–Baltic Sea model with a nesting approach in Kattegat-southern Baltic area (Büchmann et al., 2011; Gräwe and Burchard, 2012; Holtermann et al., 2014), using data assimilation in the Baltic Sea (Placke et al., 2018; von Schuckmann et al., 2016; von Schuckmann and Traon, 2018) or focusing on the GoF with prescribed boundary fields at the entrance to the GoF (Andrejev et al., 2004; Vankevich et al., 2016; Westerlund et al., 2017).

The horizontal and vertical resolutions of the models have been stated to be one of the biggest shortcomings of models that have been applied in the GoF (Myrberg et al., 2010). Internal Rossby radius is in the range of 2–6 km in the GoF (Alenius et al., 2003). Thus, to resolve mesoscale features properly, the horizontal grid step should be at least two times lower than the local deformation radius (Sein et al., 2017; Soomere et al., 2008). In long-term numerical studies, it sets severe limit to the choice of the length of the modelling period versus horizontal resolution of the modelling studies. The numerical modelling studies that use eddy-resolving horizontal grid in the GoF show increased number of submesoscale vortices and filaments with more detailed internal structure (e.g. Andrejev et al., 2010; Väli et al., 2017; Vankevich et al., 2016; Westerlund et al., 2017). Considering existence of the WCC, this feature is present in low horizontal resolution model results (Jędrasik et al., 2008; Soomere et al., 2011; Westerlund et al., 2017), as well as in high resolution model results (Andrejev et al., 2010; Westerlund et al., 2017). The WCC, anticyclonic circulation gyres and salt wedge advection are basin scale features, which occurrence should be resolved by the models that have horizontal resolution lower than needed for the eddy resolving models.

Our results suggest that intensity of the WCC and development of the anticyclonic gyres depends on the salt wedge dynamics. In the numerical model studies, these three features should be acceptably reproduced by the model. Besides, the wind affects the dynamics of all these features. Myrberg et al. (2010) have stated that low vertical resolution can cause severe inaccuracies in the results of the model simulations. The salt wedge dynamics could be accurately simulated with the model which resolves vertical structure of the salinity and temperature fields, especially their strong vertical gradients. The vertical resolution is higher near the surface layer in almost all recently published hindcast simulations setups (Andrejev et al., 2004; Dietze et al., 2014; Elken et al., 2011; Hordoir et al., 2019; Meier, 2007; Placke et al., 2018). Such approach allows to properly resolve the upper Ekman layer dynamics and the evolution of seasonal thermocline at reduced computational cost. In the GoF along the thalweg, the depth of the halocline associated with the salt wedge varies between 50 and 100 m seasonally (Figs. 3c, 9) (Elken et al., 2006; Liblik and Lips, 2017). Dense water overflows and further gravitational spread near the bottom need special treatment due to spurious mixing during advection which could significantly change the properties of inflown water masses (Beckmann and Döscher, 1997; Hordoir et al., 2015). The adaptive coordinate system used in the present study has shown advantages in the representation of thermocline distribution (Gräwe et al., 2013b) and dense water inflows into the Baltic Sea (Hofmeister et al., 2011) by significantly reducing numerical mixing. In the case of the GoF, the locations where salinity shows a seasonally varying halocline over the complex topography (Fig. 9), such an adaptive vertical mesh is a great advantage in representing the bottom boundary layer and the longitudinal movement of the salt wedge. In the GoF, Andrejev et al. (2010) and Westerlund et al. (2017) have shown that WCC can be modelled using the 1 m vertical resolution. However, even the coarse scale model of Jędrasik et al. (2008) shows a sign of WCC with only 18 bottom-following layers, but with enhanced resolution toward the upper- and bottom boundary.

The 40-year mean surface layer circulation field (Fig. 4a) conceals the WCC and the anticyclonic gyres, which are dominant features in the seasonal climatology fields (Fig. 5). Only the eastern part of the WCC with several cross-shore branches and medium scale anticyclonic circulation cells is obvious on the mean circulation field. Comparison of the model results by Elken et al. (2011) and by Lagemaa (2012) shows that the mean velocity scheme in the sub-surface layer (4–8 m depth) of the northern GoF could be completely different if the averaging periods were different and comprised only a few years, although the model used and the setup were similar. If the models and their setups are different then the contradictory results on the same field could be obtained for the similar period (Fig. 3, (Soomere et al., 2011) and Fig. 8, (Andrejev et al., 2004)). The surface layer (0–10 m) currents from our model averaged over the period 1987–1991, which coincides with the period by Soomere et al. (2011), are similar to the 40-year mean currents (Fig. 4a) and show qualitatively similar circulation pattern to Soomere et al. (2011), but have different current speeds. An explanation of the differences in the model results requires a detailed comparison of the models, their setup, forcing and averaging procedure, which is not straightforward and is beyond the scope of this paper. To resolve the discrepancies in the different model results and to show validity of our results we suggest that simultaneous ADCP measurements should be performed at several locations along the northern GoF and western part of the southern GoF covering the period from March to November.

Another aspect to mention is that using adaptive vertical coordinates decreases numerical mixing by quarter compared to the sigma coordinates (Gräwe et al., 2013b). They suggested that these improvements are needed for inclusion of the subgrid scale processes (e.g. Langmuir circulation, internal waves) in the future models. The bias of surface salinity in the GoF at the end of our simulation period (Fig. 2) could hint that either mixing or salt water transport to the GoF is slightly overestimated in our simulation. Validation has shown overventilation of mid-layers during the medium inflows to the Baltic Sea (Fig. 4 of Maljutenko and Raudsepp, 2014). Still, we may argue that this has not changed the dynamics of estuarine circulation (Fig. 10c), i.e. the variability of salinity in the bottom layer of GoF (Fig. 2b) substantially. The most notable shortcoming of the current model study could be that we have overestimated the intensity of estuarine circulation and

following surface circulation patterns. The study of Westerlund et al. (2017) has shown that the exaggerating river runoff, which should induce increased estuarine circulation, leads to amplification of the WCC current system, but does not change the current directions. Our results may also have some uncertainties due to uncoupled wavefield interactions (e.g. Raudsepp et al., 2011; Staneva et al., 2017; Tuomi et al., 2018), unresolved bathymetry features (Andrejev et al., 2010), decoupled air-ocean interactions which could alter atmospheric forcing (Tisler et al., 2008), and surface ice-ocean boundary layer dynamics during the ice-season (e.g. Roy et al., 2015).

5. Conclusions

The long-term salinity distribution and circulation of the GoF were studied with a 40-year numerical model simulation using regional atmospheric forcing. The validity of the forcing fields for the model was briefly discussed. Model results were in close agreement with the observations of the sea level, salinity and temperature during the simulation period.

The results of our model study confirmed that the mean circulation and salinity distribution could be considered as statistical properties, while the seasonal variations of the circulation and salinity distribution are significant in the GoF. The seasonal climatology shows that WCC along the southern coast of the GoF and two anticyclonic gyres, one on the eastern and the other on the western part of the GOF separated at the longitude of about 24.5°E, are dominant circulation features from March to September. The WCC starts to develop in March and transforms into an anticyclonic circulation in July. The existence of these features supports the concept that the GoF can be characterized as a wide gulf type ROFI. The seasonal variations of the salinity distribution along the thalweg classify the GoF as a salt wedge estuary.

Interannual variations of the circulation and salinity distributions prove that the WCC and estuarine exchange flow are modified by zonal wind. In general, negative/positive zonal wind supports/destroys the WCC and increase/decrease the intensity of the estuarine exchange flow. The intensity of the estuarine exchange flow is defined by the maximum distance between the LSULW and the salt wedge. The salinity increase/decrease in the Gotland Deep following the MBIs/stagnation period shifts the LSULW-salt wedge estuarine system toward the head/mouth of the GoF. The effect of the wind to the anticyclonic gyres is more complex and is not quantified in this study. Positive zonal wind favors stronger eastward currents at the northern coast, but destroys westward current at the southern coast. Our study shows that anticyclonic gyres are well-developed during small positive zonal wind, mainly. There could be years when neither the WCC nor anticyclonic gyres exist, but also years when all three features are present.

Current study enables us to outline the following dynamical scheme, which couples salt wedge estuarine circulation, and the WCC and anticyclonic circulations of the wide gulf type ROFI. The estuarine circulation and the development of the WCC correspond to the baroclinic geostrophic adjustment (Wake et al., 2004). The up-estuary transport of the salt wedge feeds the WCC through upward entrainment. When the salt wedge reaches its maximum up-estuary distance and starts to retreat slowly, the WCC transforms into anticyclonic gyres maintained by continuous upward entrainment of lower layer water into the upper layer (Fujiwara et al., 1997). The detailed study of the outlined dynamics of the system remains the subject of forthcoming papers, as well as tests of the sensitivity of these circulation features to the horizontal and vertical resolution of the numerical model.

Acknowledgements

This study was partly supported by institutional research funding IUT 19-6 from the Estonian Ministry of Education and Research. The study was also supported by the Estonian Science Foundation grants ETF9382, ETF9278 and by the Estonian national project “EstKliima”. We are grateful to GETM community for the code development and maintenance of GETM. An allocation of computing time from the High Performance Computing cluster at the TalTech is gratefully acknowledged. We would like to thank the two anonymous reviewers for their suggestions and comments.

References

Alenius, P., Myrberg, K., Nekrasov, A., 1998. The physical oceanography of the Gulf of Finland: a review. Boreal Environ. Res. 3, 97–125.
Alenius, P., Nekrasov, A., Myrberg, K., 2003. Variability of the baroclinic Rossby radius in the Gulf of Finland. Cont. Shelf Res. 23, 563–573. https://doi.org/10.1016/S0278-4343(03)00004-9.
Andrejev, O., Myrberg, K., Alenius, P., Lundberg, P.A., 2004. Mean circulation and water exchange in the Gulf of Finland — a study based on three-dimensional modelling. Boreal Environ. Res. 9, 1–16.
Andrejev, O., Sokolov, A., Soomere, T., Värv, R., Viikmäe, B., 2010. The use of high-resolution bathymetry for circulation modelling in the Gulf of Finland. Est. J. Eng. 16, 187. https://doi.org/10.3176/eng.2010.3.01.
Beckmann, A., Döscher, R., 1997. A method for improved representation of dense water spreading over topography in geopotential-coordinate models. J. Phys. Oceanogr. 27, 581–591. https://doi.org/10.1175/1520-0485(1997)027<0581:AMFIRO>2.0.CO;2.
Büchmann, B., Hansen, C., Söderkvist, J., 2011. Improvement of hydrodynamic forecasting of Danish waters: impact of low-frequency North Atlantic barotropic variations. Ocean Dyn. 61, 1611–1617. https://doi.org/10.1007/s10236-011-0451-2.
Burchard, H., Bolding, K., 2002. GETM — A General Estuarine Transport Model. Scientific Documentation. Technical Report EUR 20253 en.
Burchard, H., Hetland, R.D., 2010. Quantifying the contributions of tidal straining and gravitational circulation to residual circulation in periodically stratified tidal estuaries. J. Phys. Oceanogr. 40, 1243–1262. https://doi.org/10.1175/2010JPO4270.1.
Cameron, W.M., Pritchard, D.W., 1963. Estuaries. In: Hill, M.N. (Ed.), The Sea: Ideas and Observations on Progress in the Study of the Seas. The Composition of Sea Water, Comparative and descriptive Oceanography, vol. 2. Wiley Interscience, New York, pp. 306–324.
Canuto, V.M., Howard, A., Cheng, Y., Dubovikov, M.S., 2001. Ocean turbulence. Part I: one-point closure model—momentum and heat vertical diffusivities. J. Phys. Oceanogr. 31, 1413–1426. https://doi.org/10.1175/1520-0485(2001)031<1413:OTPIOP>2.0.CO;2.
Csanady, G.T., 1982. Circulation in the Coastal Ocean. Springer Netherlands, Dordrecht. https://doi.org/10.1007/978-94-017-1041-1.
Delpeche-Ellmann, N., Torsvik, T., Soomere, T., 2016. A comparison of the motions of surface drifters with offshore wind properties in the Gulf of Finland, the Baltic Sea. Estuar. Coast. Shelf Sci. 172, 154–164. https://doi.org/10.1016/j.ecss.2016.02.009.
Delpeche-Ellmann, N., Mingelaitė, T., Soomere, T., 2017. Examining Lagrangian surface transport during a coastal upwelling in the Gulf of Finland, Baltic Sea. J. Mar. Syst. 171, 21–30. https://doi.org/10.1016/j.jmarsys.2016.10.007.
Dietze, H., Löptien, U., Getzlaff, K., 2014. MOMBA 1.1 — a high-resolution Baltic Sea configuration of GFDL's Modular Ocean Model. Geosci. Model Dev. 7, 1713–1731. https://doi.org/10.5194/gmd-7-1713-2014.
Donnelly, C., Andersson, J.C., Arheimer, B., 2015. Using flow signatures and catchment similarities to evaluate the E-HYPE multi-basin model across Europe. Hydrol. Sci. J. 61, 255–273. https://doi.org/10.1080/02626667.2015.1027710.
Elken, J., Raudsepp, U., Lips, U., 2003. On the estuarine transport reversal in deep layers of the Gulf of Finland. J. Sea Res. 49, 267–274. https://doi.org/10.1016/S1385-1101(03)00018-2.
Elken, J., Mälkki, P., Alenius, P., Stipa, T., 2006. Large halocline variations in the northern Baltic Proper and associated meso- and basin-scale processes. Oceanologia 48, 91–117.
Elken, J., Nõmm, M., Lagemaa, P., 2011. Circulation patterns in the Gulf of Finland derived from the EOF analysis of model results. Boreal Environ. Res. 16, 84–102.
Elken, J., Raudsepp, U., Laanemets, J., Passenko, J., Maljutenko, I., Pärn, O., Keevallik, S., 2014. Increased frequency of wintertime stratification collapse events in the Gulf of Finland since the 1990s. J. Mar. Syst. 129, 47–55. https://doi.org/10.1016/j.jmarsys.2013.04.015.
Fujiwara, T., Sanford, L., Nakatsuji, K., Sugiyama, Y., 1997. Anti-cyclonic circulation driven by the estuarine circulation in a gulf type ROFI. J. Mar. Syst. 12, 83–99. https://doi.org/10.1016/S0924-7963(96)00090-5.
Geyer, W.R., MacCready, P., 2013. The estuarine circulation. Annu. Rev. Fluid Mech. 46, 130829112240001. https://doi.org/10.1146/annurev-fluid-010313-141302.
Gräwe, U., Burchard, H., 2012. Storm surges in the Western Baltic Sea: the present and a possible future. Clim. Dyn. 39, 165–183. https://doi.org/10.1007/s00382-011-1185-z.
Gräwe, U., Friedland, R., Burchard, H., 2013a. The future of the western Baltic Sea: two possible scenarios. Ocean Dyn. 63, 901–921. https://doi.org/10.1007/s10236-013-0634-0.
Gräwe, U., Holtermann, P., Klingbeil, K., Burchard, H., 2013b. Advantages of vertically adaptive coordinates in numerical models of stratified shelf seas. Ocean Model 92, 56–68. https://doi.org/10.1016/j.ocemod.2015.05.008.
Gustafsson, B., 1999. High frequency variability of the surface layers in the Skagerrak during SKAGEX. Cont. Shelf Res. 19, 1021–1047. https://doi.org/10.1016/S0278-4343(99)00008-4.
Gustafsson, B.G., Medina, M.R., 2011. Validation data set compiled from Baltic

environmental database, version 2. In: Technical Report 2. Baltic Nest Institute.
Hansen, D.V., Rattray, M., 1966. New dimensions in estuary classification. Limnol. Oceanogr. 11, 319–326. https://doi.org/10.4319/lo.1966.11.3.0319.
Hela, I., 1952. Drift Currents and Permanent Flow. Societas Scientiarum Fennica, pp. 1–27 Commentationes Physico-Mathematicae XVI.
Hofmeister, R., Beckers, J.M., Burchard, H., 2011. Realistic modelling of the exceptional inflows into the central Baltic Sea in 2003 using terrain-following coordinates. Ocean Model 39, 233–247. https://doi.org/10.1016/j.ocemod.2011.04.007.
Hofmeister, R., Bolding, K., Hetland, R.D., Schernewski, G., Siegel, H., Burchard, H., 2013. The dynamics of cooling water discharge in a shallow, non-tidal embayment. Cont. Shelf Res. 71, 68–77. https://doi.org/10.1016/j.csr.2013.10.006.
Höglund, A., Meier, H.E.M., 2012. Environmentally safe areas and routes in the Baltic Proper using Eulerian tracers. Mar. Pollut. Bull. 64, 1375–1385. https://doi.org/10.1016/j.marpolbul.2012.04.021.
Holtermann, P.L., Burchard, H., Gräwe, U., Klingbeil, K., Umlauf, L., 2014. Deep-water dynamics and boundary mixing in a nontidal stratified basin: a modeling study of the Baltic Sea. J. Geophys. Res. Oceans 119, 1465–1487. https://doi.org/10.1002/2013JC009483.
Hordoir, R., Axell, L., Löptien, U., Dietze, H., Kuznetsov, I., 2015. Influence of sea level rise on the dynamics of salt inflows in the Baltic Sea. J. Geophys. Res. Oceans 120, 6653–6668. https://doi.org/10.1002/2014JC010642.
Hordoir, R., Axell, L., Höglund, A., Dieterich, C., Fransner, F., Gröger, M., Liu, Y., Pemberton, P., Schimanke, S., Andersson, H., Ljungemyr, P., Nygren, P., Falahat, S., Nord, A., Jönsson, A., Lake, I., Döös, K., Hieronymus, M., Dietze, H., Löptien, U., Kuznetsov, I., Westerlund, A., Tuomi, L., Haapala, J., 2019. Nemo-Nordic 1.0: a NEMO-based ocean model for the Baltic and North seas — research and operational applications. Geosci. Model Dev. 12, 363–386. https://doi.org/10.5194/gmd-12-363-2019.
Isemer, H.J., Russak, V., Tuomenvirta, H., 2008. A.1.2 atmosphere. In: Bolle, H.J., Menenti, M., Rasool, I. (Eds.), Assessment of Climate Change for the Baltic Sea Basin. Springer, Berlin, Heidelberg, Berlin, Heidelberg. chapter Annexes, pp. 386–392. https://doi.org/10.1007/978-3-540-72786-6.
Jędrasik, J., Kowalewski, M., 2019. Mean annual and seasonal circulation patterns and long-term variability of currents in the Baltic Sea. J. Mar. Syst. 193, 1–26. https://doi.org/10.1016/j.jmarsys.2018.12.011.
Jędrasik, J., Cieślikiewicz, W., Kowalewski, M., Bradtke, K., Jankowski, A., 2008. 44 years hindcast of the sea level and circulation in the Baltic Sea. Coast. Eng. 55, 849–860. https://doi.org/10.1016/j.coastaleng.2008.02.026.
Jönsson, B.F., Döös, K., Myrberg, K., Lundberg, P.A., 2011. A Lagrangian-trajectory study of a gradually mixed estuary. Cont. Shelf Res. 31, 1811–1817. https://doi.org/10.1016/j.csr.2011.07.007.
Kasai, A., Hill, A.E., Fujiwara, T., Simpson, J.H., 2000. Effect of the Earth's rotation on the circulation in regions of freshwater influence. J. Geophys. Res. Oceans 105, 16961–16969. https://doi.org/10.1029/2000JC900058.
Keevallik, S., 2008. Wind speed and velocity at three Estonian coastal stations 1969–1992. Est. J. Eng. 14, 209–219. https://doi.org/10.3176/eng.2008.3.02.
Keevallik, S., Soomere, T., 2010. Towards quantifying variations in wind parameters across the Gulf of Finland. Est. J. Earth Sci. 59, 288. https://doi.org/10.3176/earth.2010.4.05.
Keevallik, S., Soomere, T., 2014. Regime shifts in the surface-level average air flow over the Gulf of Finland during 1981–2010. Proc. Est. Acad. Sci. 63, 428. https://doi.org/10.3176/proc.2014.4.08.
Keevallik, S., Mannik, A., Hinnov, J., 2010. Comparison of HIRLAM wind data with measurements at Estonian coastal meteorological stations. Est. J. Earth Sci. 59, 90. https://doi.org/10.3176/earth.2010.1.07.
Klingbeil, K., Mohammadi-Aragh, M., Gräwe, U., Burchard, H., 2014. Quantification of spurious dissipation and mixing — discrete variance decay in a finite-volume framework. Ocean Model 81, 49–64. https://doi.org/10.1016/j.ocemod.2014.06.001.
Kondo, J., 1975. Air-sea bulk transfer coefficients in diabatic conditions. Bound.-Layer Meteorol. 9. https://doi.org/10.1007/BF00232256.
Kullenberg, G., 1981. Physical oceanography. In: Voipio, Aarno (Ed.), The Baltic Sea, pp. 135–181. https://doi.org/10.1016/S0422-9894(08)70140-5. Chapter 3.
Laanemets, J., Kononen, K., Pavelson, J., Poutanen, E.L., 2004. Vertical location of seasonal nutriclines in the western Gulf of Finland. J. Mar. Syst. 52, 1–13. https://doi.org/10.1016/j.jmarsys.2004.03.003.
Laanemets, J., Väli, G., Zhurbas, V., Elken, J., 2011. Simulation of nutrient transport from different depths during an upwelling event in the Gulf of Finland. Oceanologia 53, 431–448. https://doi.org/10.5697/oc.53-1-TI.431.
Lagemaa, P., 2012. Operational Forecasting in Estonian Marine Waters. Ph.D. thesis. Tallinn University of Technology, Tallinn.
Lagemaa, P., Suhhova, I., Nõmm, M., Pavelson, J., Elken, J., 2010. Comparison of current simulations by the state-of-the-art operational models in the Gulf of Finland with ADCP measurements. In: 2010 IEEE/OES Baltic International Symposium (BALTIC). IEEE, pp. 1–11. https://doi.org/10.1109/BALTIC.2010.5621656.
Lehmann, A., Hinrichsen, H.H., 2000. On the thermohaline variability of the Baltic Sea. J. Mar. Syst. 25, 333–357. https://doi.org/10.1016/S0924-7963(00)00026-9.
Lehmann, A., Myrberg, K., Höflich, K., 2012. A statistical approach to coastal upwelling in the Baltic Sea based on the analysis of satellite data for 1990–2009. Oceanologia 54, 369–393. https://doi.org/10.5697/oc.54-3.369.
Lessin, G., Raudsepp, U., 2006. Water quality assessment using integrated modeling and monitoring in Narva Bay, Gulf of Finland. Environ. Model. Assess. 11, 315–332. https://doi.org/10.1007/s10666-006-9045-7.
Lessin, G., Raudsepp, U., Stips, A.K., 2014. Modelling the influence of major Baltic inflows on near-bottom conditions at the entrance of the Gulf of Finland. PLoS One 9, e112881. https://doi.org/10.1371/journal.pone.0112881.
Liblik, T., Lips, U., 2011. Characteristics and variability of the vertical thermohaline structure in the Gulf of Finland in summer. Boreal Environ. Res. 16, 73–83.
Liblik, T., Lips, U., 2012. Variability of synoptic-scale quasi-stationary thermohaline stratification patterns in the Gulf of Finland in summer 2009. Ocean Sci. 8, 603–614. https://doi.org/10.5194/os-8-603-2012.
Liblik, T., Lips, U., 2017. Variability of pycnoclines in a three-layer, large estuary: the Gulf of Finland. Boreal Environ. Res. 22, 27–47.
Liblik, T., Laanemets, J., Raudsepp, U., Elken, J., Suhhova, I., 2013. Estuarine circulation reversals and related rapid changes in winter near-bottom oxygen conditions in the Gulf of Finland, Baltic Sea. Ocean Sci. 9, 917–930. https://doi.org/10.5194/os-9-917-2013.
Liblik, T., Naumann, M., Alenius, P., Hansson, M., Lips, U., Nausch, G., Tuomi, L., Wesslander, K., Laanemets, J., Viktorsson, L., 2018. Propagation of impact of the recent Major Baltic inflows from the eastern Gotland Basin to the Gulf of Finland. Front. Mar. Sci. 5, 1–23. https://doi.org/10.3389/fmars.2018.00222.
Lilover, M.J., Talpsepp, L., 2014. On the vertical structure of the low-frequency oscillations of currents in the Gulf of Finland. In: Measuring and Modeling of Multi-Scale Interactions in the Marine Environment. IEEE/OES Baltic International Symposium 2014, BALTIC 2014. pp. 1–6. https://doi.org/10.1109/BALTIC.2014.6887844.
Lilover, M.J., Pavelson, J., Kõuts, T., 2011. Wind forced currents over the shallow Naissaar Bank in the Gulf of Finland. Boreal Environ. Res. 16, 164–174.
Lilover, M.J., Elken, J., Suhhova, I., Liblik, T., 2017. Observed flow variability along the thalweg, and on the coastal slopes of the Gulf of Finland, Baltic Sea. Estuar. Coast. Shelf Sci. 195, 23–33. https://doi.org/10.1016/j.ecss.2016.11.002.
Lips, U., Kikas, V., Liblik, T., Lips, I., 2016a. Multi-sensor in situ observations to resolve the sub-mesoscale features in the stratified Gulf of Finland, Baltic Sea. Ocean Sci. 12, 715–732. https://doi.org/10.5194/os-12-715-2016.
Lips, U., Zhurbas, V., Skudra, M., Väli, G., 2016b. A numerical study of circulation in the Gulf of Riga, Baltic Sea. Part I: whole-basin gyres and mean currents. Cont. Shelf Res. 112, 1–13. https://doi.org/10.1016/j.csr.2015.11.008.
Lips, U., Laanemets, J., Lips, I., Liblik, T., Suhhova, I., Suursaar, Ü., 2017. Wind-driven residual circulation and related oxygen and nutrient dynamics in the Gulf of Finland (Baltic Sea) in winter. Estuar. Coast. Shelf Sci. 195, 4–15. https://doi.org/10.1016/j.ecss.2016.10.006.
Luhamaa, A., Kimmel, K., Mannik, A., Room, R., 2011. High resolution re-analysis for the Baltic Sea region during 1965–2005 period. Clim. Dyn. 36, 727–738. https://doi.org/10.1007/s00382-010-0842-y.
Madsen, K.S., Højerslev, N.K., 2009. Long-term temperature and salinity records from the Baltic Sea transition zone. Boreal Environ. Res. 14, 125–131.
Maljutenko, I., Raudsepp, U., 2014. Validation of GETM model simulated long-term salinity fields in the pathway of saltwater transport in response to the Major Baltic Inflows in the Baltic Sea. In: Carroll, J. (Ed.), 2014 IEEE/OES Baltic International Symposium (BALTIC). IEEE/OES, Tallinn, pp. 23–31. https://doi.org/10.1109/BALTIC.2014.6887830.
Meier, H.E.M., 2007. Modeling the pathways and ages of inflowing salt- and freshwater in the Baltic Sea. Estuar. Coast. Shelf Sci. 74, 717–734. https://doi.org/10.1016/j.ecss.2007.05.019.
Myrberg, K., Andrejev, O., 2003. Main upwelling regions in the Baltic Sea — a statistical analysis based on three-dimensional modelling. Boreal Environ. Res. 8, 97–112.
Myrberg, K., Lehmann, A., Raudsepp, U., Szymelfenig, M., Lips, I., Lips, U., Matciak, M., Kowalewski, M., Krężel, A., Burska, D., Szymanek, L., Ameryk, A., Bielecka, L., Bradtke, K., Gałkowska, A., Gromisz, S., Jędrasik, J., Kaluźny, M., Kozłowski, Ł., Krajewska-Sołtys, A., Ołdakowski, B., Ostrowski, M., Zalewski, M., Andrejev, O., Suomi, I., Zhurbas, V., Kauppinen, O.K., Soosaar, E., Laanemets, J., Uiboupin, R., Talpsepp, L., Golenko, M., Golenko, N., Vahtera, E., 2008. Baltic Sea upwelling coastal-open sea biogeochemistry. Oceanologia 50, 95–113.
Myrberg, K., Ryabchenko, V., Isaev, A., Vankevich, R., Andrejev, O., Bendtsen, J., Erichsen, A., Funkquist, L., Inkala, A., Neelov, I., Rasmus, K., Medina, M.R., Raudsepp, U., Passenko, J., Söderkvist, J., Sokolov, A., Kuosa, H., Anderson, T.R., Lehmann, A., Skogen, M.D., 2010. Validation of three-dimensional hydrodynamic models of the Gulf of Finland. Boreal Environ. Res. 15, 453–479.
Omstedt, A., Elken, J., Lehmann, A., Leppäranta, M., Meier, H.E.M., Myrberg, K., Rutgersson, A., 2014. Progress in physical oceanography of the Baltic Sea during the 2003—2014 period. Prog. Oceanogr. 128, 139–171. https://doi.org/10.1016/j.pocean.2014.08.010.
Palmén, E.H., 1930. Untersuchungen über die strömungen in den Finnland umgebenden meeren. Comm. Phys. Math./Soc. Sci. Fennica 12, 93.
Pavelson, J., Laanemets, J., Kononen, K., Nõmmann, S., 1997. Quasi-permanent density front at the entrance to the Gulf of Finland: response to wind forcing. Cont. Shelf Res. 17, 253–265. https://doi.org/10.1016/S0278-4343(96)00028-3.
Peffley, M.B., O'Brien, J.J., 1976. A Three-Dimensional Simulation of Coastal Upwelling off Oregon. https://doi.org/10.1175/1520-0485(1976)006<0164:ATDSOC>2.0.CO;2.
Pietrzak, J., 1998. The use of TVD limiters for forward-in-time upstream-biased advection schemes in ocean modeling. Mon. Weather Rev. 126, 812–830. https://doi.org/10.1175/1520-0493(1998)126<0812:TUOTLF>2.0.CO;2.
Placke, M., Meier, H.E.M., Gräwe, U., Neumann, T., Frauen, C., Liu, Y., 2018. Long-term mean circulation of the Baltic Sea as represented by various ocean circulation models. Front. Mar. Sci. 5, 1–20. https://doi.org/10.3389/fmars.2018.00287.
Poggioli, A.R., Horner-Devine, A.R., 2015. The sensitivity of salt wedge estuaries to channel geometry. J. Phys. Oceanogr. 45, 3169–3183. https://doi.org/10.1175/JPO-D-14-0218.1.
Raudsepp, U., 1998. Current dynamics of estuarine circulation in the lateral boundary layer. Estuar. Coast. Shelf Sci. 47, 715–730. https://doi.org/10.1006/ecss.1998.0390.
Raudsepp, U., Laanemets, J., Haran, G., Alari, V., Pavelson, J., Kõuts, T., 2011. Flow, waves and water exchange in the Suur Strait, Gulf of Riga. Oceanologia 53, 35–56.

Roy, F., Chevallier, M., Smith, G.C., Dupont, F., Garric, G., Lemieux, J., Lu, Y., Fraser, D., 2015. Arctic sea ice and freshwater sensitivity to the treatment of the atmosphere-ice-ocean surface layer. J. Geophys. Res. Oceans 120, 4392–4417. https://doi.org/10.1002/2014JC010677.

Seifert, T., Kayser, B., 1995. A high resolution spherical grid topography of the Baltic Sea. Meereswissenschaftliche Berichte 72–88.

Sein, D.V., Koldunov, N.V., Danilov, S., Wang, Q., Sidorenko, D., Fast, I., Rackow, T., Cabos, W., Jung, T., 2017. Ocean modeling on a mesh with resolution following the local Rossby radius. J. Adv. Model. Earth Syst. 9, 2601–2614. https://doi.org/10.1002/2017MS001099.

Shchepetkin, A.F., 2003. A method for computing horizontal pressure-gradient force in an oceanic model with a nonaligned vertical coordinate. J. Geophys. Res. 108, 1–34. https://doi.org/10.1029/2001JC001047.

Simpson, J., 1997. Physical processes in the ROFI regime. J. Mar. Syst. 12, 3–15. https://doi.org/10.1016/S0924-7963(96)00085-1.

Soomere, T., Myrberg, K., Leppanranta, M., Nekrasov, A., 2008. The progress in knowledge of physical oceanography of the Gulf of Finland: a review for 1997–2007. Oceanologia 50, 287–362.

Soomere, T., Delpeche, N., Viikmäe, B., Quak, E., Meier, H.E.M., Döös, K., 2011. Patterns of current-induced transport in the surface layer of the Gulf of Finland. Boreal Environ. Res. 16, 49–63.

Soomere, T., Bishop, S.R., Viška, M., Räämet, A., 2015. An abrupt change in winds that may radically affect the coasts and deep sections of the Baltic Sea. Clim. Res. 62, 163–171. https://doi.org/10.3354/cr01269.

Soosaar, E., Maljutenko, I., Raudsepp, U., Elken, J., 2014. An investigation of anticyclonic circulation in the southern Gulf of Riga during the spring period. Cont. Shelf Res. 78, 75–84. https://doi.org/10.1016/j.csr.2014.02.009.

Stalnacke, P., Grimvall, A., Sundblad, K., Tonderski, A., 1999. Estimation of riverine loads of nitrogen and phosphorus to the Baltic Sea, 1970–1993. Environ. Monit. Assess. 58, 173–200. https://doi.org/10.1023/A:1006073015871.

Staneva, J., Alari, V., Breivik, Ø., Bidlot, J.R., Mogensen, K., 2017. Effects of wave-induced forcing on a circulation model of the North Sea. Ocean Dyn. 67, 81–101. https://doi.org/10.1007/s10236-016-1009-0.

Stips, A.K., Bolding, K., Lilover, M.J., 2008. In: Scenario Simulations of Recent Baltic Sea Inflows Using the Hydrodynamic Transport Model GETM. US/EU-Baltic International Symposium: Ocean Observations, Ecosystem-Based Management and Forecasting — Provisional Symposium Proceedings. BALTIC. https://doi.org/10.1109/BALTIC.2008.4625527.

Suursaar, Ü., 2010. Waves, currents and sea level variations along the Letipea-Sillamäe coastal section of the southern Gulf of Finland. Oceanologia 52, 391–416. https://doi.org/10.5697/oc.52-3.391.

Suursaar, Ü., Aps, R., 2007. Spatio-temporal variations in hydro-physical and -chemical parameters during a major upwelling event off the southern coast of the Gulf of Finland in summer 2006. Oceanologia 49, 209–228.

Tisler, P., Vihma, T., Müller, G., Brümmer, B., 2008. Modelling of warm-air advection over Arctic sea ice. Tellus, Series A: Dynamic Meteorology and Oceanography 60 A, 775–788. doi: https://doi.org/10.1111/j.1600-0870.2008.00316.x.

Tuomi, L., Vähä-Piikkiö, O., Alenius, P., Björkqvist, J.V., Kahma, K.K., 2018. Surface Stokes drift in the Baltic Sea based on modelled wave spectra. Ocean Dyn. 68, 17–33. https://doi.org/10.1007/s10236-017-1115-7.

Uiboupin, R., Laanemets, J., 2009. Upwelling characteristics derived from satellite sea surface temperature data in the Gulf of Finland, Baltic Sea. Boreal Environ. Res. 14, 297–304.

Umlauf, L., Burchard, H., 2005. Second-order turbulence closure models for geophysical boundary layers. A review of recent work. Cont. Shelf Res. 25, 795–827. https://doi.org/10.1016/j.csr.2004.08.004.

Unden, P., Rontu, L., Järvinen, H., Lynch, P., Calvo, J., Cats, G., Cuxart, J., Eerola, K., Fortelius, C., Garcia-Moya, J.A., Jones, C., Geert, Lenderlink, G., Mcdonald, A., Mcgrath, R., Navascues, B., Nielsen, N.W., Degaard, V., Rodriguez, E., Rummukainen, M., Sattler, K., Sass, B.H., Savijarvi, H., Schreur, B.W., Sigg, R., The, H., 2002. HIRLAM-5 scientific documentation. In: Technical Report December. SMHI, Norrköping. https://doi.org/10.1007/s00254-002-0712-y.

Vahtera, E., Laanemets, J., Pavelson, J., Huttunen, M., Kononen, K., 2005. Effect of upwelling on the pelagic environment and bloom-forming cyanobacteria in the western Gulf of Finland, Baltic Sea. J. Mar. Syst. 58, 67–82. https://doi.org/10.1016/j.jmarsys.2005.07.001.

Väli, G., Meier, H.E.M., Elken, J., 2013. Simulated halocline variability in the Baltic Sea and its impact on hypoxia during 1961–2007. J. Geophys. Res. Oceans 118, 6982–7000. https://doi.org/10.1002/2013JC009192.

Väli, G., Zhurbas, V., Lips, U., Laanemets, J., 2017. Submesoscale structures related to upwelling events in the Gulf of Finland, Baltic Sea (numerical experiments). J. Mar. Syst. 171, 31–42. https://doi.org/10.1016/j.jmarsys.2016.06.010.

Valle-Levinson, A., 2008. Density-driven exchange flow in terms of the Kelvin and Ekman numbers. J. Geophys. Res. 113, C04001. https://doi.org/10.1029/2007JC004144.

Valle-Levinson, A., 2011. 1.05 — classification of estuarine circulation. In: Wolanski, E., McLusky, D. (Eds.), Treatise on Estuarine and Coastal Science. Academic Press, Waltham, pp. 75–86. https://doi.org/10.1016/B978-0-12-374711-2.00106-6.

Vankevich, R.E., Sofina, E.V., Eremina, T.E., Ryabchenko, V.A., Molchanov, M.S., Isaev, A.V., 2016. Effects of lateral processes on the seasonal water stratification of the Gulf of Finland: 3-D NEMO-based model study. Ocean Sci. 12, 987–1001. https://doi.org/10.5194/os-12-987-2016.

Viikmäe, B., Torsvik, T., Soomere, T., 2012. Analysis of the structure of currents in the Gulf of Finland using the Okubo-Weiss parameter. In: Ocean: Past, Present and Future. 2012 IEEE/OES Baltic International Symposium. BALTIC 2012. https://doi.org/10.1109/BALTIC.2012.6249184.

von Schuckmann, K., Traon, P.Y.L., Smith, N., Pascual, A., Brasseur, P., Fennel, K., Djavidnia, S., 2018. Copernicus marine service ocean state report. J. Oper. Oceanogr. 11, S1–S142. https://doi.org/10.1080/1755876X.2018.1489208.

von Schuckmann, K., Traon, P.Y.L., Alvarez-Fanjul, E., Axell, L., Balmaseda, M., Breivik, L.A., Brewin, R.J.W., Bricaud, C., Drevillon, M., Drillet, Y., Dubois, C., Embury, O., Etienne, H., Sotillo, M.G., Garric, G., Gasparin, F., Gutknecht, E., Guinehut, S., Hernandez, F., Juza, M., Karlson, B., Korres, G., Legeais, J.F., Levier, B., Lien, V.S., Morrow, R., Notarstefano, G., Parent, L., Pascual, A., Pérez-Gómez, B., Perruche, C., Pinardi, N., Pisano, A., Poulain, P.M., Pujol, I.M., Raj, R.P., Raudsepp, U., Roquet, H., Samuelsen, A., Sathyendranath, S., She, J., Simoncelli, S., Solidoro, C., Tinker, J., Tintoré, J., Viktorsson, L., Ablain, M., Almroth-Rosell, E., Bonaduce, A., Clementi, E., Cossarini, G., Dagneaux, Q., Desportes, C., Dye, S., Fratianni, C., Good, S., Greiner, E., Gourrion, J., Hamon, M., Holt, J., Hyder, P., Kennedy, J., Manzano-Muñoz, F., Melet, A., Meyssignac, B., Mulet, S., Nardelli, B.B., O'Dea, E., Olason, E., Paulmier, A., Pérez-González, I., Reid, R., Racault, M.F., Raitsos, D.E., Ramos, A., Sykes, P., Szekely, T., Verbrugge, N., 2016. The Copernicus marine environment monitoring service ocean state report. J. Oper. Oceanogr. 9, s235–s320. https://doi.org/10.1080/1755876X.2016.1273446.

Wake, G.W., Ivey, G.N., Imberger, J., McDonald, N.R., Stocker, R., 2004. Baroclinic geostrophic adjustment in a rotating circular basin. J. Fluid Mech. 515, 63–86. https://doi.org/10.1017/S0022112004000230.

Wallcraft, A.J., Kara, A.B., Hurlburt, H.E., 2005. Convergence of Laplacian diffusion versus resolution of an ocean model. Geophys. Res. Lett. 32, 1–4. https://doi.org/10.1029/2005GL022514.

Westerlund, A., 2018. Modelling Circulation Dynamics in the Northern Baltic Sea. Ph.D. thesis. University of Helsinki.

Westerlund, A., Tuomi, L., Alenius, P., Miettunen, E., Vankevich, R.E., 2017. Attributing mean circulation patterns to physical phenomena in the Gulf of Finland. Oceanologia. https://doi.org/10.1016/j.oceano.2017.05.003.

Witting, R., 1912. Zusammenfassende Übersicht der Hydrographie des Bottnischen und Finnischen Meerbusens und der nördlichen Ostsee nach den Untersuchungen bis Ende 1910. Finnländische hydrographisch-biologische Untersuchungen 7.

Wulff, F., Sokolov, A., Savchuk, O., 2013. Nest — A Decision Support System for Management of the Baltic Sea. A User Manual. 10 Baltic Nest Institute.

Yanagi, T., Kuroda, M., Ishimaru, T., Saino, T., 1998. Residual flow in Ise Bay during summer. Bull. Coas. Oceanogr. 35, 185–191.

Zhurbas, V., Oh, I.S., Park, T., 2006. Formation and decay of a longshore baroclinic jet associated with transient coastal upwelling and downwelling: a numerical study with applications to the Baltic Sea. J. Geophys. Res. 111, C04014. https://doi.org/10.1029/2005JC003079.

Paper II

Maljutenko I, Raudsepp U. 2014. Validation of GETM model simulated long-term salinity fields in the pathway of saltwater transport in response to the Major Baltic Inflows in the Baltic Sea. Carroll J, editor. 2014 IEEE/OES Baltic International Symposium (BALTIC):23–31. Tallinn: IEEE/OES. doi:10.1109/BALTIC.2014.6887830 (3.1)

Validation of GETM model simulated long-term salinity fields in the pathway of saltwater transport in response to the Major Baltic inflows in the Baltic Sea

Ilja Maljutenko, Urmas Raudsepp
Marine Systems Institute
Akadeemia tee 15a
12618, Tallinn, Estonia

***Abstract*-The hydrodynamic model GETM was used to simulate the hydrographic conditions in the Baltic Sea for the hindcast period from 1966 to 2005. Time series of surface and bottom salinity and bottom temperature at four monitoring stations belonging to the Bornholm Basin, Gotland Basin, the Gulf of Finland and the Gulf of Riga were used for model validation. The model has reproduced realistic conditions through the simulation period that was characterized by stagnation period in the 80s and numerous Major Baltic Inflow events. The simulated salinity and temperature at different depths were in good agreement with measurements. Also, the sea level and maximum ice extent were compared with observations.**

I. INTRODUCTION

There have been numerous long-term modelling studies of the circulation and ecosystem dynamics in the Baltic Sea during the last decade by [1], [2], [3], [4] etc. The validation of model results is essential when numerical models are used for climate change studies. It is rather common to use the hindcast period from early sixties until mid 2000 for model validation. Reference [5] has validated MOM for the period 1960-2000. Simulated sea surface salinity (SSS) and sea surface temperature (SST) were underestimated in the Gotland Basin in their model results. Reference [6] compared the performance of 2 nm setup of the Rossby Centre Ocean model (RCO) with observations from the period of 1961–2007. They found that the model overestimated the long-term surface salinity median, underestimated the depth of the halocline and overestimated the strength of stratification in the Baltic Proper. At the northern and western BS the bottom salinities were overestimated. Reference [7] compared simulated and observed bottom salinities at three stations in the western Baltic Sea for the period 1971-2000. They showed that GETM can reproduce bottom salinity statistics rather well. It is especially challenging to correctly simulate Major Baltic Inflows (MBI). The MBIs influence long term salinity and oxygen variations in the NE subbasins of the Baltic Sea. Therefore, the validation of model simulation results in the Bornholm Basin, Gotland Basin, the Gulf of Finland and the Gulf of Riga is performed.

II. MODEL DESCRIPTION AND SETUP

For the simulation of the Baltic Sea hydrodynamics the 3D circulation model GETM (General Estuarine Transport Model) has been used [8]. The GETM solves numerically primitive ocean equations using hydrostatic and Boussinesq approximation and eddy viscosity assumption. For the advection total variation the diminishing (TVD) P2-PDM scheme has been applied [9] and internal pressure has been parameterized according to [10]. The vertical mixing is parameterized using the coupled GOTM (General Ocean Transport Model) model [11]. Two equation k-ε model with algebraic second-moment closures have been applied for this study. The model is missing the dynamical ice model, thus the artificial ice (which is limiting both heat exchange and wind stress) has been applied when water temperature reaches freezing point.

The GETM model was applied to the BS for the simulation period from the January 1st, 1966 to December 31st, 2005. The spatial discretization has a horizontal resolution of 1 x 1 nautical mile and 40 layers in vertical. The layer distribution has both spatial and temporal adaptation to the density and velocity fields, which allows good reproducibility of inflow events to the BS [12]. Bathymetry data have been adopted from the BS digital topography by [13]. Maximum depths have been limited with 260 m and depths in the Danish straits have been slightly adjusted to enhance water flow through narrow straits. Initial salinity and temperature fields have been interpolated from climatic mean fields that have been constructed using the Data Assimilation System coupled with the Baltic Environmental Database at Stockholm University (http://nest.su.se/das) [14].

Atmospheric forcing has been adopted from BaltAn65+ dataset which is result of regional downscaling of ERA-40 and ERA-INTERIM re-analysis using HIRLAM atmospheric model [15]. The horizontal resolution of this dataset is 11 km and 6 hours in temporal scale. The river discharge has been adopted from the hindcast simulation of the Balt-HYPE hydrological model [16]. The

total number of the 37 rivers has been taken into account. At the open boundary in northern Kattegat, sea levels from the measurements at Smøgen were prescribed. The boundary conditions for salinity and temperature have been parameterized using monthly zonal wind stress and air temperature data from the BaltAn65+ dataset.

Boundary data

Recently, data from the Danish Lightships have been made available for scientific research by DMI [17]. Despite the long time series the data still contains many temporal gaps which restrain us from using direct measurements for boundary forcing. Jakobson [18] has shown that salinity at the entrance of the northern Kattegat is sensitive to westerly wind forcing. Thus we derive the monthly mean salinity from monthly wind impulse calculated from BaltAn65+ dataset at Kattegat at 58 ºN 14' and 10 ºE 15'.

Monthly wind impulse I_w is defined as

$$I_w = C_d * \rho_a \int W_{10} * U_{10}\, dt, \quad (1)$$

where $C_d = 1.2 * 10^{-3}$ is drag coefficient, $\rho_a = 1.22$ kg/m^3 is air density, W_{10} is wind speed and U_{10} is zonal wind speed at 10 m.

The monthly salinity at surface SSS is calculated by normalizing the wind impulse to the measured monthly mean salinity at the Skagens Rev. lightship at 58 ºN 46' and 10 ºE 46' during the period of available data (1966 – 1979) as

$$SSS = \max\{ \min\{ (I_w - mI_w) / \mathrm{std}(I_w) * \mathrm{std}(S_{obs}) + mS_{obs}, 34\}, 25\}, \quad (2)$$

where $mI_w = 3.9 * 10^4$ is mean wind impulse over the forcing period of 1966 – 2005, $\mathrm{std}(I_w) = 6.1 * 10^4$ is standard deviation of the wind impulse, $\mathrm{std}(S_{obs}) = 2.5$ is standard deviation of observed monthly mean salinity and $S_{obs} = 30.5$ is mean of the monthly mean observed salinity. The calculated correlation between observed monthly mean and calculated salinity is 0.55 and RMSD 2.1 g/kg.

The monthly salinity at the bottom SBS is calculated as

$$SBS = \max\{ 0.1 * (SSS - mSSS) + 33.5, SSS\}, \quad (3)$$

where mSSS is time averaged (2). The hyperbolic tangent function (4) with zs=25 as the depth of the halocline and cs=0.2 as the smoothness parameter

$$Fs(z) = \tanh((z - zs) * cs) \quad (4)$$

is used to derive the smooth salinity profile

$$S(z) = (SSS + SBS) / 2 + Fs(z) * (SBS - SSS) / 2. \quad (5)$$

Monthly sea surface temperature SST have been constructed using limited monthly mean air temperature T_a data from the same location

$$SST = \max\{T_a, 0\}. \quad (6)$$

The correlation between measured and calculated sea surface temperature is 0.98 and RMSD 1 K.

The bottom temperature SBT is calculated as,

$$SBT = \max\{0.4*(SST - mSST) + 7.5, 0\}, \quad (7)$$

where mSST is the time average over the calculated SST from (6).

Similar to the salinity profile the slightly sharper (ct = 0.4) and seasonally varying (zt= 25 – 0.6*SST) thermocline is defined using a hyperbolic tangent function as following

$$Ft(z) = \tanh((z - zt) * ct), \quad (8)$$

$$T(z) = (SST + SBT) / 2 + Ft(z) * (SBT - SST) / 2. \quad (9)$$

If the density profile is unstable, the temperature profile is recalculated with adjusted bottom temperature

$$SBT' = SBT * 0.5 \quad (10)$$

III. RESULTS

1. *Sea level elevation*

Two stations along the southern coast of the GoF and one at Landsort have been selected for the validation of simulated sea levels. Narva-Jõesuu and Dirham represent the sea levels in the eastern and western GoF, respectively, while Landsort station is situated on the eastern coast of Sweden, thus representing the sea level of the open Baltic Proper (Fig. 1). Daily mean sea levels have been used for comparison. The comparison between modelled and measured sea level elevations at these three stations indicates that the model can reproduce sea level variations accurately (Table I.). In general, RMSD between simulated and observed sea level do not exceed 9 cm, but the variability is somehow higher in the model than in observations.

TABLE I. MAIN STATISTICS OF DAILY SEALEVEL ELEVATIONS.

	Landsort	Dirham	Narva-J
CORR (R)	0.94	0.94	0.96
RMSD, cm	7.5	8.8	8.2
STD obs., cm	19.8	23.8	26.3
STD mod., cm	22.5	26.9	29.1

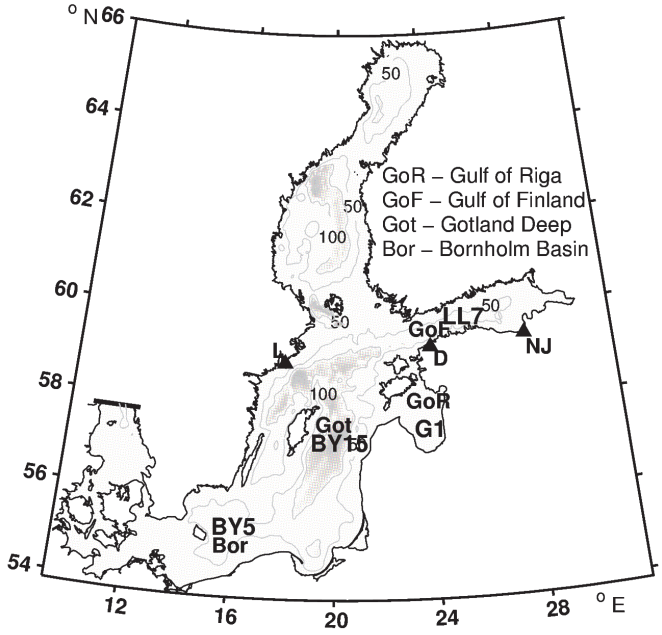

Fig. 1 The model domain and location of the monitoring stations. Sea level stations are marked with triangles.

2. Salinity and temperature timeseries

The validation of thermohaline fields has been done for 4 monitoring stations (Fig. 1) belonging to the Bornholm Basin, the Gotland Basin, the Gulf of Finland and the Gulf of Riga. Hydrographic data were extracted from the Baltic Environment Database [20] which combines the monitoring data adopted from the various databases around the BS. Monthly mean data are extracted over the period of 1966 – 2005.

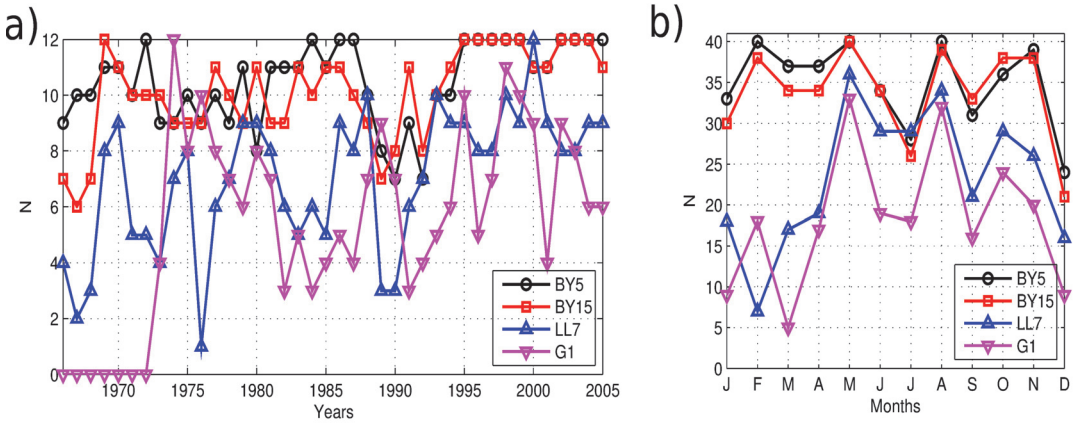

Fig. 2 Number of months covered with observations for each year (a) and for each month (b).

A distribution of measurement data over time is presented in Fig. 2. In the Bornholm and Gotland Basin the yearly data availability from the database is relatively uniform over time. In general, the data availability has improved in the Gulf of Finland with time. Data coverage for different years varies considerably in the Gulf of Riga. The data is lacking completely until 1973.

Monthly data coverage is more uniform for the Bornholm and Gotland Basin than for the Gulf of Finland and the Gulf of Riga. The latter two are frequently covered with ice during winter and early spring, which has complicated data acquisition during that period.

In the visual comparison of salinity and temperature time series daily mean values from the model have been used.

Long term variations show steady increase of surface salinity until the end of the 70s following decrease until mid 90s and slight increase thereafter (Fig. 3). These changes are more pronounced in the southern and central Baltic Sea, but less in the Gulf of Finland and the Gulf of Riga. The salinity increase during the first period is not so obvious in the model results because the initial salinity level is already higher compared to observed salinity values. After the first 10 years of the simulation the model salinities and observed salinities equalize and the following decrease in salinity is well reproduced by the model. The salinity increase during the last period is overestimated by the model. Interannual and seasonal variations are well reproduced by the model in all sub-basins. The range of short-term salinity variability is wider in the model because daily mean values are plotted in the model time series, but monthly mean values from the observations.

Surface temperatures (not shown) follow natural seasonal cycle without any remarkable deviations and bias from observed values ($R > 0.95$).

At BY5 the dynamics of saline water inflows is well reproduced by the model (Fig. 4). Some of the inflow salinities are overestimated and some are underestimated. During the inflows of 1983, 1992 and 2003 the model has overestimated the salinity values by more than 2 g/kg, while during the inflows in 1972 and 1977 salinity values are underestimated. In the bottom layer of the Gotland basin (BY15) the salinities are underestimated by about 1 – 1.5 g/kg from the beginning of the simulation until the end of the stagnation period in 1993. This discrepancy could be attributed partly to the errors in the initial salinity field in the model, as at the beginning of the simulation period the model salinity is about 1 g/kg lower than observed. By the end of the stagnation period in 1993 both model and observed salinities reached 11 g/kg. This indicates that the freshening of the bottom layer in the Gotland Deep between MBIs is slower in the model than in nature. The following cascade of inflows increases observed salinity values up to 13 g/kg, which is also evident in the simulation results. The MBI in 1977 is not reproduced by the model. Model results show an artificial inflow to the Gotland basin in 1997. The seasonal signal is dominant in the bottom salinity variations in the Gulf of Finland (LL7). The amplitude of the variability is well reproduced by the model for the entire simulation period. Until 1984, high values of bottom salinity during summer are slightly underestimated by the model. Oppositely, the model overestimates salinity in summer since the period from 1995. The stagnation period is reflected in the bottom salinities in the Gulf of Finland at the end of 80s and beginning of 90s. This period and following increase in salinity is well reproduced by the model. The model results also show dominant seasonal signal in bottom salinity time series of the Gulf of Riga (G1). This variability is not so obvious in the measurements due to the scarcity and irregularity of the observations in the gulf. Interannual variations are reproduced relatively well. As in the Gulf of Finland, the model underestimates salinity level until 1984 and overestimates it starting from 1998. The salinity during the intermediate period is reproduced very well.

The temperature variations in the bottom layer of southern and central BS (stations BY5 and BY15) are mainly guided by the inflowing water temperatures (Fig. 5). The simulated temperature variability is slightly overestimated at BY5, overestimating warmer and underestimating colder inflows. At BY15 stations we see that all inflows own their characteristic temperature. The model has captured all inflows with a correct temperature change towards observed values. At the G1 and LL7 stations the model has captured high seasonal variability and characteristic mixing events in autumn and winter. Well-mixed states, where cold water reaches the bottom layer, have been also well reproduced by the model.

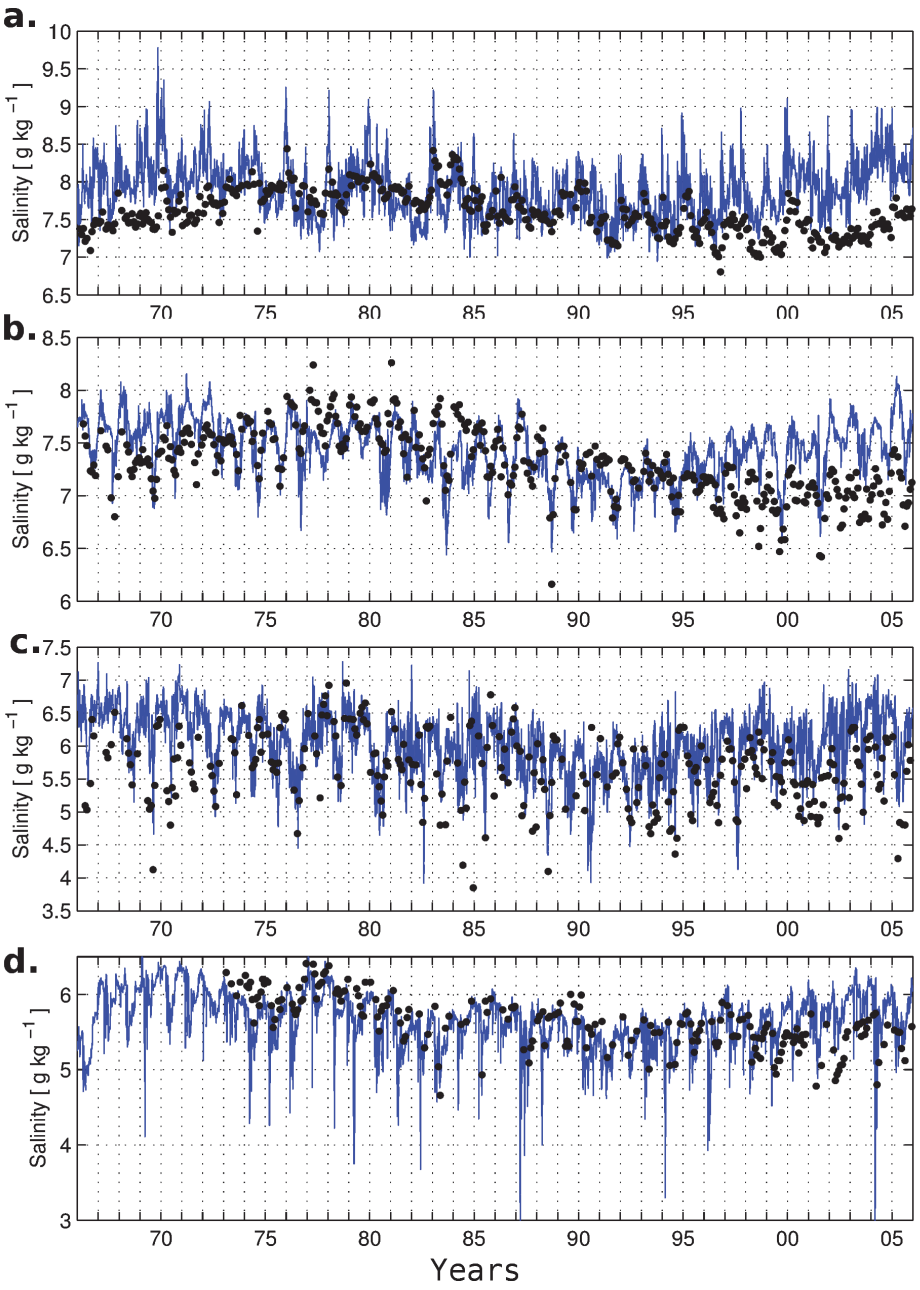

Fig. 3 Surface salinity at four monitoring stations of the BS - a) BY5, b) BY15, c) LL7 and d) G1.

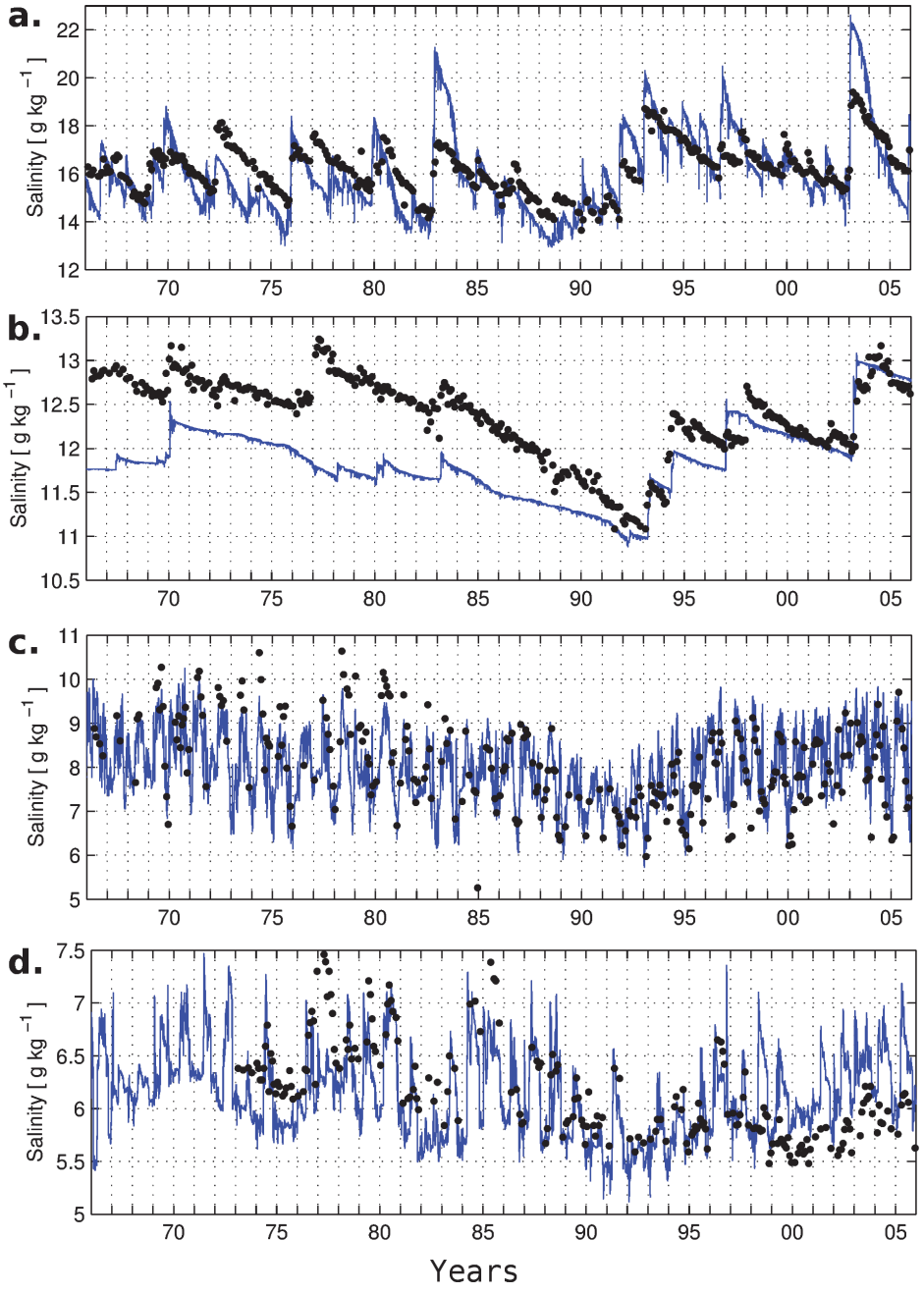

Fig. 4 Bottom salinity at four monitoring stations of the BS - a) BY5, b) BY15, c) LL7 and d) G1.

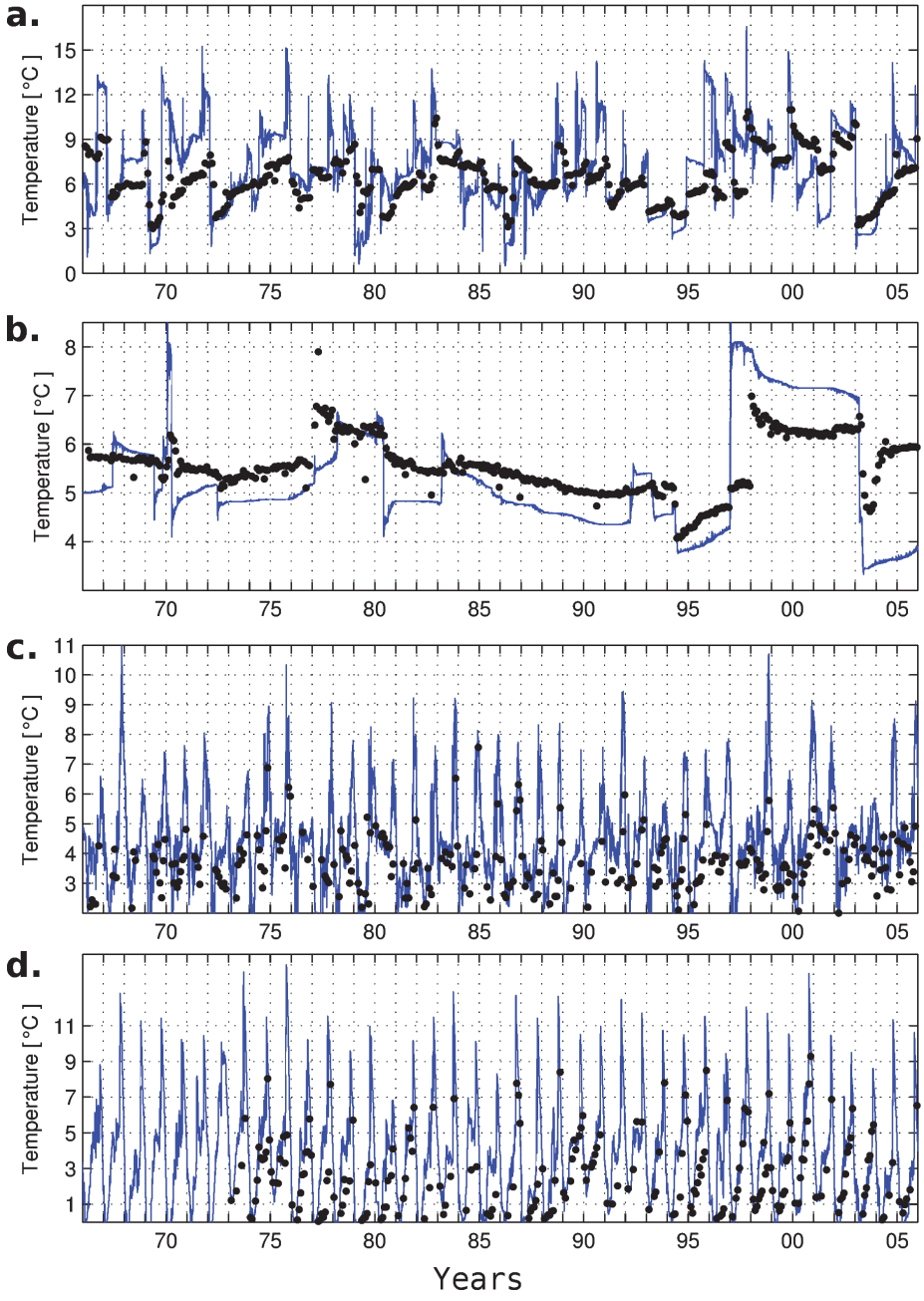

Fig. 5 Bottom temperature at four monitoring stations of the BS - a) BY5, b) BY15, c) LL7 and d) G1.

Another way to validate modelling results is to use the cost function defined by [20]. The score is defined as bias between observed and modelled value divided by the standard deviation of observed values. According to [20] the model has given good agreement with observations when the score is 1 or less, values of 1 - 2 indicate reasonable quality and score over 3 is poor. The BY15 and G1 station have given the best cost function score for surface layer. At station LL7 the salinities are in good accordance through all levels. The poorest results are simulated at the G1 bottom layer, BY5 mid layers and BY15 bottom layer. At G1 the model has given lower score due to higher bias from observations. The temperature in the whole water column had good agreement with observations.

3. Ice coverage

The ice coverage in the Gulf of Finland and the Gulf of Riga may affect the evolution of thermohaline fields to a large extent. Air-sea heat exchange and momentum transfer are restrained in case of ice coverage. A simple approach is used for the modelling of ice conditions. A so called rigid lid approximation is implemented in the model. When sea surface temperature is equal to freezing temperature, the model grid cell is assumed to be covered with ice. The observation data are adopted from compiled observations [21] and covers the whole Baltic Sea including Skagerrak. The model reproduces interannual variations of maximum ice extent well (Fig. 7), but has a clear tendency to underestimate it. The error between the simulated and observed maximum ice extent increases with the severity of the winter.

The snapshot of spatial ice coverage on February 24th, 1996 illustrates the disparities between model results and observations. The Gulf of Finland and the Gulf of Riga are both covered with ice. Also, the model is able to reproduce ice coverage at the coasts of the central and southern Baltic Sea. The model underestimates the ice extent over the deeper parts in the northeastern Baltic Sea where the water column holds more heat and thus does not cool down rapidly enough below freezing temperature. Thus, the difference between the maximum ice extent in the model compared to the observations increases when the ice edge progresses southward in the Baltic Proper.

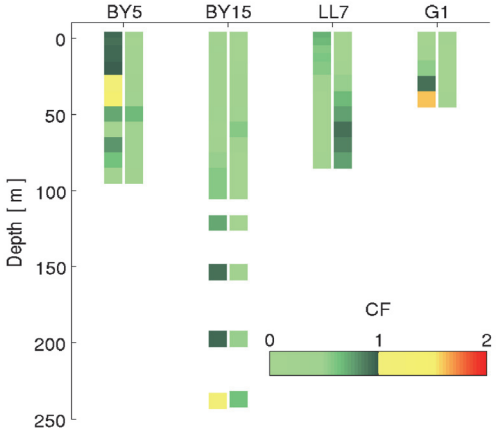

Fig. 6 Cost function values of salinities (left column) and temperature (right column) at different stations.

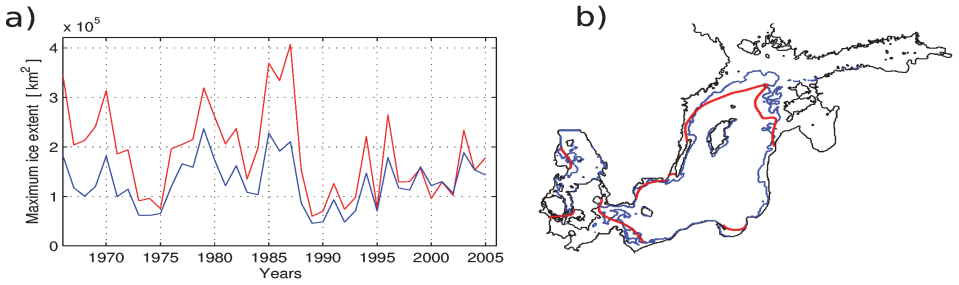

Fig. 7 a) Yearly maximum ice extent (red - observations, blue – simulation). b) Ice extent on 24th February 1996 (red - ice extent redrawn from the ice chart by EMHI, blue – model).

IV. Conclusions

The GETM was used for the simulation of the Baltic Sea hydrodynamics during the hindcast period 1966-2006. Simulated sea level, salinity, temperature and ice extent were compared with observation data. The correlation coefficients and RMSDs between simulated and measured sea level at three location in the NE Baltic Sea were higher than 0.94 and lower than 9 cm, respectively. The temporal course of surface and bottom salinity and temperature in the Bornholm Basin, Gotland Basin, the Gulf of Finland and the Gulf of Riga was well reproduced by the model. The MBIs were captured by the model as well as the stagnation period in the Gotland Deep at the end of 80s and beginning of 90s. According to the cost function values [21] the quality of the simulated temperature and salinity was good with only a few exceptions. The model reproduces the interannual variations of maximum ice extent well, although no dynamic ice model was used.

Acknowledgment

This research was partially supported by the project EstKliima funded by the Environmental protection and technology programme No 3.2.0802.11-0043 of the European Regional Fund. The model results would have been much worse without the enthusiastic developers team of the GETM, salinity data from DMI and helpful hints from Jüri Elken.

References

1. K. Eilola, B.G. Gustafsson, I. Kuznetsov, H.E.M. Meier, T. Neumann, O.P. Savchuk, “Evaluation of biogeochemical cycles in an ensemble of three state-of-the-art numerical models of the Baltic Sea”, *Journal of Marine Systems*, 88(2), pp 267-284, 2011.
2. H. E. M. Meier, B.Müller-Karulis, H. C. Andersson, C. Dieterich, K. Eilola, B. G. Gustafsson, et al., “Impact of Climate Change on Ecological Quality Indicators and Biogeochemical Fluxes in the Baltic Sea: A Multi-Model Ensemble Study”, *Ambio*, 41, pp 558-573, DOI 10.1007/s13280-012-0320-3, 2012.
3. U. Daewel, C. Schrum, “Simulating long-term dynamics of the coupled North Sea and Baltic Sea ecosystem with ECOSMO II: Model description and validation”, *Journal of Marine Systems*, Volumes 119–120, pp 30-49, 2013.
4. H. E. M. Meier, A. Hoglund, R. Doscher, H. Andersson, U. Loptien, E Kjellstrom, “Quality assessment of atmospheric surface fields over the Baltic Sea from an ensemble of regional climate model simulations with respect to ocean dynamics”, *Oceanologia* , 53(1), pp 193–227, 2011.
5. T. Neumann,“Climate-change effects on the Baltic Sea ecosystem: a model study”, *Journal of Marine Systems*, 81(3), pp 213–224, 2010
6. G. Väli, H. E. M. Meier, J. Elken, “Simulated halocline variability in the Baltic Sea and its impact on hypoxia during 1961–2007”, *J. Geophys. Res. Oceans*, 118,pp 6982–7000, doi:10.1002/2013JC009192, 2013.
7. U. Gráwe, R. Friedland, H. Burchard, “The future of the western baltic sea: two possible scenarios,” *Ocean Dynamics*, vol. 63, no. 8, pp. 901-921, 2013
8. H. Burchard and K. Bolding, “GETM – a general estuarine transport model – scientific documentation”, *European Commission, Tech. Rep.* EUR 20253 EN, pp 157, 2002.
9. J. Pietrzak, “The use of TVD limiters for forward-in-time upstream-biased advection schemes in ocean modeling”, *Mon. Weather Rev.*, 126 , pp 812–830., 1998
10. A. F. Shchepetkin, J. C. McWilliams, “A method for computing horizontal pressure- gradient force in an oceanic model with a nonaligned vertical coordinate”, *J. Geophys. Res.- Oceans*, 108, doi:10.1029/2001JC001047, 2003.
11. L. Umlauf, H. Burchard,K. Bolding, “General Ocean Turbulence Model. Source code documentation”, *Technical Report 63. Tech. rep., Baltic Sea Research Institute Warnemünde.*, 2006.
12. R. Hofmeiste, J.-M. Beckers, H. Burchard, “Realistic modelling of the major inflows into the central Baltic Sea in 2003 using terrain-following coordinates”, *Ocean Modelling,* 39 (3-4), pp 233–247, 2011.
13. T. Seifert and B. Kayser, “A high resolution spherical grid topography of the Baltic Sea”, *Scientific report series, Institute Baltic Sea Research Warnemünde*, 9, pp 73-88, 1995.
14. A. Sokolov, O. Andrejev, F.Wulff and M.Rodriguez Medina, “The Data Assimilation System for Data Analysis in the Baltic Sea”, *Systems Ecology Contributions*, 3, , pp 66, 1997,
15. A. Luhamaa, K. Kimmel,A. Männik, R. Rõõm, “High resolution re-analysis for the Baltic Sea region during 1965-2005 period”, *Climate Dynamics,* 36 (3), pp 727-738, 2011.
16. B. Arheimer, J. Dahné, C. Donnelly, G. Lindström, J. Strömqvist, “Water and nutrient simulations using the HYPE model for Sweden vs. the Baltic Sea basin – influence of input data quality and scale”. *Hydrology Research special issue*, 2010.
17. K. S. Madsen, N. K. Højerslev, “Long-term temperature and salinity records from the Baltic Sea transition zone”, *Boreal Environmental Research,* 14, pp 125-131, 2009.
18. F. Jakobsen, “Hydrographic investigation of the northern Kattegat front”, *Continental Shelf Research,* 17, pp. 533–554, 1997.
19. F. Wulff, A. Sokolov, O. Savchuk, “Nest – a decision support system for management of the Baltic Sea. A user manual.”, *Baltic Nest Institute, Stockholm University Baltic Sea Centre, Technical Report No. 10,* ISBN: 978-91-86655-09-9, 2013.
20. K. Eilola, H. E. M. Meier, E Almroth, “On the dynamics of oxygen, phosphorus and cyanobacteria in the Baltic Sea; A model study”, *Journal of Marine Systems*, 75, pp 163–184, 2009.
21. A. Seinä, E. Palosuo, “The classification of the maximum annual extent of ice cover in the Baltic Sea 1720–1995”, *Meri, Report Series of the Finnish Institute of Marine Research*, vol. 20, pp. 79–910, 1996. (reviewed in 2011, by J. Vainio,ISSN: 1239-0291)

Paper III

Soosaar E, Maljutenko I, Raudsepp U, Elken J. 2014. An investigation of anticyclonic circulation in the southern Gulf of Riga during the spring period. Cont Shelf Res 78: 75–84. Elsevier. doi:10.1016/j.csr.2014.02.009 (1.1)

Continental Shelf Research 78 (2014) 75–84

Contents lists available at ScienceDirect

Continental Shelf Research

journal homepage: www.elsevier.com/locate/csr

Research papers

An investigation of anticyclonic circulation in the southern Gulf of Riga during the spring period

Edith Soosaar*, Ilja Maljutenko, Urmas Raudsepp, Jüri Elken

Marine Systems Institute at Tallinn University of Technology, Akadeemia 15a, 12618 Tallinn, Estonia

ARTICLE INFO

Article history:
Received 20 December 2012
Received in revised form
29 October 2013
Accepted 8 February 2014
Available online 22 February 2014

Keywords:
Anticyclonic circulation
ROFI
Vorticity
River discharge
Numerical modeling
Gulf of Riga

ABSTRACT

Previous studies of the gulf-type Region of Freshwater Influence (ROFI) have shown that circulation near the area of freshwater inflow sometimes becomes anticyclonic. Such a circulation is different from basic coastal ocean buoyancy-driven circulation where an anticyclonic bulge develops near the source and a coastal current is established along the right hand coast (in the northern hemisphere), resulting in the general cyclonic circulation. The spring (from March to June) circulation and spreading of river discharge water in the southern Gulf of Riga (GoR) in the Baltic Sea was analyzed based on the results of a 10-year simulation (1997–2006) using the General Estuarine Transport Model (GETM). Monthly mean currents in the upper layer of the GoR revealed a double gyre structure dominated either by an anticyclonic or cyclonic gyre in the near-head southeastern part and corresponding cyclonic/anticyclonic gyre in the near-mouth northwestern part of the gulf. Time series analysis of PCA and vorticity, calculated from velocity data and model sensitivity tests, showed that in spring the anticyclonic circulation in the upper layer of the southern GoR is driven primarily by the estuarine type density field. This anticyclonic circulation is enhanced by easterly winds but blocked or even reversed by westerly winds. The estuarine type density field is maintained by salt flux in the northwestern connection to the Baltic Proper and river discharge in the southern GoR.

1. Introduction

Fresh water from rivers contributes significant amounts of buoyancy to large areas of the coastal sea. The region where buoyancy input by rivers is comparable to or exceeds the seasonal input of buoyancy as heat is called ROFI (Region Of Freshwater Influence; a term adapted by Simpson (1997)). Buoyancy input results in a circulation pattern where lower density water from river output forms a circulating bulge near the source and a coastal current along the right hand coast (in the northern hemisphere) (Yankovsky and Chapman, 1997). Such a circulation pattern is believed to be the result of the combined effect of the inertial and Coriolis forces and is confirmed by multiple in situ measurements and laboratory and numerical simulations (Horner-Devine et al., 2006; Yankovsky and Chapman, 1997).

Local winds, tides and ambient currents modify the spreading of buoyant plume (see Osadchiev and Zavialov, 2013 and reference therein). Regarding local effects, winds that favor downwelling (towards the buoyant coastal current) compress the plume to the coast (Whitney and Garvine, 2006) and enhance the coastal current (Jurisa and Chant, 2012). Winds that favor upwelling (opposite to the buoyant coastal current) spread buoyant water offshore and can reverse the coastal current (Whitney and Garvine, 2006), so that new discharged water is transported leftwards from the source (Choi and Wilkin, 2007). On the basin scale of large lakes and enclosed seas, spatially uniform wind drives barotropic circulation with downwind currents at the coast and return flow in the center of the basin (Bennett, 1974).

A study by Fujiwara et al. (1997) shows theoretically that when an estuary is wider than the internal Rossby deformation radius, the combination of classical longitudinal estuarine circulation and the Earth's rotation may cause the surface circulation to become anticyclonic at the estuary head. In the northern hemisphere, this circulation will eventually transport fresh water from the river along the left hand coast. Anticyclonic residual circulation has been observed at the estuary head in Ise Bay, Osaka Bay and Tokyo Bay (Fujiwara et al., 1997). The presence of an anticyclonic circulation in the ROFIs is also confirmed by an observational study in the Kattegat–Skagerrak region, which is a transition area between the brackish Baltic Sea and the saline North Sea (Nielsen, 2005).

* Correspondence to: Marine System Institute at Tallinn University of Technology. Akadeemia tee 15a-321, Tallinn, Estonia.
E-mail address: edith.soosaar@msi.ttu.ee (E. Soosaar).

http://dx.doi.org/10.1016/j.csr.2014.02.009
0278-4343 © 2014 Published by Elsevier Ltd.

Measurements in the Kara Sea show the presence of an anticyclonic circulation in the Ob River discharge region in the late summer period (McClimans et al., 2000). The process was reproduced by numerical simulations (Panteleev et al., 2007). In the Gulf of Trieste, in the northern Adriatic, an anticyclonic gyre covers the surface layer during the stratified season (Malačič and Petelin, 2009). In all of these cases, the salinity distribution consists of vertical stratification, i.e. a brackish upper layer and a more saline lower layer, and a horizontal salinity gradient in the surface layer.

The morphological characteristics and hydrographic conditions in the Gulf of Riga (GoR) in the eastern Baltic Sea are well suited for the emergence of an anticyclonic circulation in the GoR head. The GoR is an almost bowl-shaped brackish-water semi-enclosed estuarine sub-basin (Fig. 1a). The area of the GoR is about 18,000 km^3 (140 km in length and 110 km in width), with a maximum depth of 56 m and mean depth of 22 m. The Daugava River located in the south-eastern part of the GoR is the main fresh water source. The river discharge ranges from 200 m^3 s^{-1} in late summer to 2500 m^3 s^{-1} in spring. The GoR has two openings connecting it to the Baltic Sea: the Irbe Strait (with a sill depth of 25 m and a minimum cross-section area of 0.4 km^2) in the west and the Virtsu Strait (with a sill depth of 5 m and a minimum cross-section area of 0.04 km^2) in the north (Fig. 1b).

As the GoR is shallow, water is usually well mixed throughout the period from December to March (Raudsepp, 2001). Ice is formed in the GoR every winter. The annual ice extent as well as duration of ice season has a wide range of variation determined by the severity of the winter (Soosaar et al., 2010). During severe winters ice starts to form in December and may last until the end of April. Increased freshwater discharge from the melting of snow and ice in early spring (March–April) stabilizes the surface layer and contributes to the seasonal stratification, resulting in a more or less two-layered salinity structure (Stipa et al., 1999). In summer and autumn the stratification is mostly maintained by temperature fluxes from the atmosphere. The tides are negligible in the GoR, which simplifies the problem by eliminating one cause of mixing.

Thus, the aim of our study is to investigate the springtime water circulation in the southern GoR, which is well preconditioned for the formation of anticyclonic circulation and is characterized by high river discharge. The input of freshwater buoyancy exceeds the input of buoyancy as heat, which is in accordance with the formal definition of ROFI by Simpson (1997). As there are no extensive field measurements of currents and salinity distribution available, we mainly rely on the results of numerical model simulations. Sparse in situ measurement data that are used in this study are available for May 1994 and 2006.

2. Materials and methods

2.1. Numerical model

In this study we use the fully baroclinic and hydrostatic ocean model GETM (General Estuarine Transport Model (Burchard and Bolding, 2002)) that is coupled with the GOTM (General Ocean Turbulence Model (Umlauf and Burchard, 2005)) which is used for vertical turbulence parameterization. The GETM uses a spherical coordinate system in the horizontal plane and a bottom-following vertical coordinate system. Using the mode splitting technique, GETM solves water dynamics on the Arakawa C grid (Arakawa and Lamb, 1977). The GETM is characterized by the advanced numerical techniques of advection schemes and internal pressure discretization schemes that minimize computational errors (Stips et al., 2004; Burchard and Rennau, 2008). Here we used the total variance diminishing (TVD) advection scheme for salinity, temperature and momentum (Pietrzak, 1998) and internal pressure parameterization suggested by Shchepetkin and McWilliams (2003).

For the current model simulations, the model domain covers the whole Baltic Sea (Fig. 1a). The bathymetry has been interpolated to the 2 nautical mile grid from the digital topography by Seifert et al. (2001). Depths have been adjusted so that the maximum depth is 260 m in the deepest areas of the Baltic Sea. The vertical water column is split into 25 sigma layers, where z_k is the layer depth and D is the depth of the water column.

The model simulation covers the period from 1 January 1997 to 31 December 2006. Initial salinity and temperature fields were interpolated from the climatic mean field constructed using the Data Assimilation System coupled with the Baltic Environmental Database at Stockholm University (http://nest.su.se/das). Initial sea surface elevation was set to zero. Atmospheric forcing was

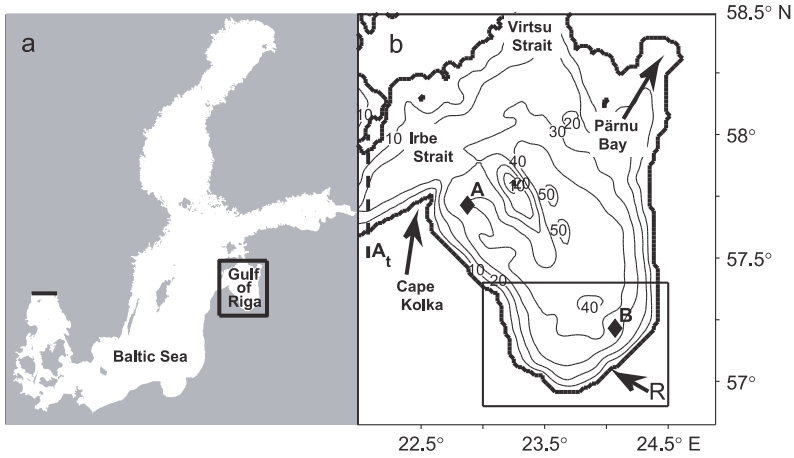

Fig. 1. Map showing the location of the Gulf of Riga (a) and its topography (b). R and arrow mark the location of the Daugava River outflow, At is the location of the north–south transect for the calculation of salt flux, A and B are sites where density is calculated (a depth of 30 m for A and 5 m for B).The box shows the area over which spatially averaged relative vorticity is calculated.

adopted from the ERA40 re-analysis data which had been dynamically down-scaled with the Rossby Centre Atmosphere Ocean (RCAO) model (Döscher et al., 2002, 2010). Wind gustiness had been added to wind fields, according to Höglund et al. (2009). For open boundary sea level elevations, data from measurements in Smögen (Sweden) was used. Salinity and temperature at the open boundary was adopted from Janssen et al. (1999) climatological mean fields. River runoff was obtained from the hydrological model HYPE (Lindström et al., 2010). Validation of the model in terms of temperature and salinity has been presented by Passenko et al. (2010). The root mean square error (RMSE) for sea surface temperature at three stations in the Gulf of Finland varied between 0.3 and 0.4, and the RMSE for surface salinity was between 0.7 and 0.9. The corresponding values for bottom temperature and salinity were 0.5–0.9 and 0.9–1.1, respectively.

2.2. PCA

To assess the circulation patterns in the southern GoR over a longer time period, the principal component analysis (PCA) of monthly mean horizontal velocity vectors from March to June in 1997–2006 was performed. The velocity vectors were extracted at a depth of 5 m. At first, a time-averaged velocity field was subtracted from the original data, before applying the PCA (Fig. 2). In general, the mean current velocities were low. The strongest current (0.03 m s^{-1}) was obtained at the river mouth. The velocities of the coastal current along the eastern coast of the gulf and over the interior of the gulf did not exceed 0.02 m s^{-1} and 0.015 m s^{-1}, respectively. The data was analyzed in the S-mode of the PCA where eigenvectors, $E_k(\vec{x})$, represent different modes of the velocity vector field and principal amplitudes (PA), $A_k(t_n)$, display temporal variations of the corresponding mode (Preisendorfer and Mobley, 1988), where k refers to mode number, t_n is time in months and $\vec{x}$ is location in the horizontal plane. The horizontal velocity vectors can be reproduced from the orthogonal modes as

$$\vec{U}(t_n, \vec{x}) = (u, v)(t_n, \vec{x}) = \sum_{k=1}^{K} A_k(t_n) E_k(\vec{x}), \quad (1)$$

where (u,v) are current velocity components in x and y directions, respectively, and K is the total number of orthogonal modes. The corresponding PA shows how dominant this mode is for a particular month. Positive amplitude values show circulation in the same direction as shown by the mode. When amplitude values are negative, corresponding circulation is opposite in direction.

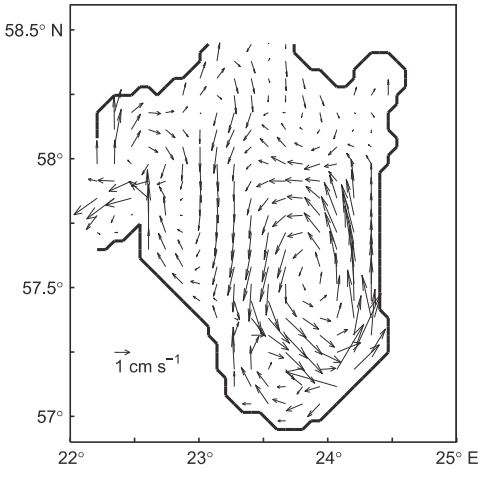

Fig. 2. Mean velocity at a depth of 5 m calculated over the four spring months (March–June) and covering a simulation period of ten years (1997–2006).

The coefficient of determination, r^2, shows how well a particular mode explains the corresponding monthly mean circulation and is defined as

$$r_k^2(t_n) = 1 - \frac{\sum_{i,j}\{[u_{i,j}^m(t_n) - A_k(t_n)u_{i,j}^k(t_n)]^2 + [v_{i,j}^m(t_n) - A_k(t_n)v_{i,j}^k(t_n)]^2\}}{\sum_{i,j}[u_{i,j}^{m^2}(t_n) + v_{i,j}^{m^2}(t_n)]}, \quad (2)$$

where superscript m refers to the model and k to the principal component. The subscripts i and j refer to the location in the model grid in x and y directions.

3. Results

The model data for the GoR was extracted from the model simulation for the whole Baltic Sea for the period 1997–2006. We use monthly mean velocity and salinity data for the four months of March, April, May and June during each model year. These months comprise the period of the melting of ice in the GoR and high river runoff (Soosaar et al., 2010), which cause stratification of the water column due to salinity (Raudsepp, 2001; Stipa et al., 1999) and represent the gulf-type ROFI according to the definition by Simpson (1997).

3.1. The cases of anticyclonic and river plume circulations

From the whole model data set, we present horizontal salinity and velocity distribution at a depth of 5 m together with salinity and the cross-section velocity component along the transect in the southern part of the GoR for April 1998 and 2006 (Figs. 3 and 4). We analyzed monthly mean salinity profiles from the southern GoR and a 5-m depth was chosen because this depth represents the upper layer in the two layer approximation of the water column stratification during all the months considered, and is within the river plume thickness. April 1998 (Fig. 3) represents a combination of wind induced double gyre circulation that can be driven by persistent winds from the east (monthly mean wind speed was 3.2 m s^{-1}) and anticyclonic circulation as described by Fujiwara et al. (1997). April 2006 (Fig. 4) represents river plume circulation (Yankovsky and Chapman, 1997) that is supported by weak wind from the south (monthly mean wind speed was 1.6 m s^{-1}). In April 1998 low saline water has spread anticyclonically from the mouth of the Daugava River (Fig. 3a). There is a notable southeast-northwest salinity gradient along the line from Daugava River mouth to Cape Kolka (0.7×10^{-4} g kg^{-1} m^{-1} as the mean value within the river plume up to 11 km from the coast, and 0.09×10^{-4} g kg^{-1} m^{-1} over the rest of the line), which is typical for an estuarine type gulf with its main freshwater sources in the gulf head and an open connection to the sea. A well-established anticyclonic gyre covers the southern part of the GoR (Fig. 3b). The currents are strongest (0.07 m s^{-1}) on the southwestern side of the gyre and drop to a negligible value on the northeastern side. A stagnation point can be identified at the eastern coast of the GoR (57.98°N, 24.34°E) where the flow reaching the coast splits into northward and southward currents. A prominent cyclonic gyre resides in the northwestern part of the GoR (Fig. 3b).

Salinity and cross-section velocity distribution on the east–west transect across the anticyclonic gyre show that the gyre extends down to a depth of 20–25 m and is confined by a halocline below (Fig. 3c and d). Below the halocline, the cross-section velocity is directed to the south over the entire transect. Within the gyre, the vertical salinity distribution is nearly homogeneous (maximum potential energy anomaly (PEA) of 1.83 J m^{-3} between

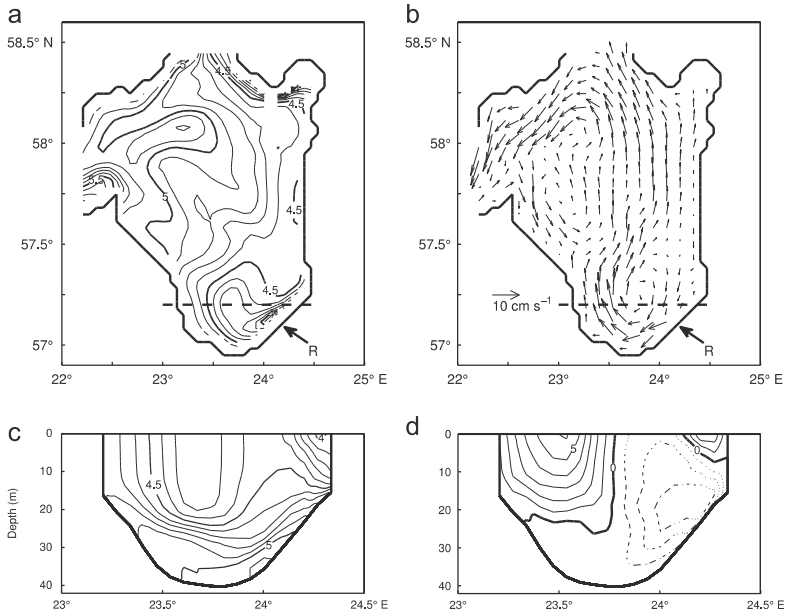

Fig. 3. Monthly mean horizontal salinity (a) and velocity (b) distributions at a depth of 5 m in the GoR in April 1998. Dashed line shows the cross-section for salinity and cross-section velocity distribution. Salinity (c) and cross-section velocity (d) on the east–west transect (solid lines show northward and dashed lines southward velocity).

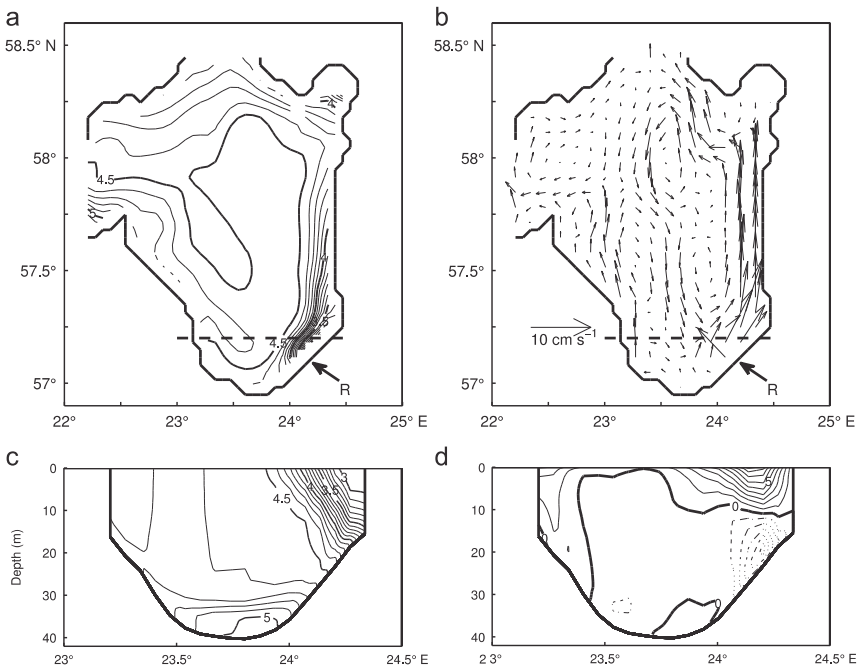

Fig. 4. As in Fig. 3, but for April 2006.

a depth of 0–20 m and longitude of 23.3–23.94°E). PEA, φ, is defined as the integral of the product of the buoyancy force and distance from the reference level

$$\varphi = \frac{1}{H}\int_{-H}^{0} g(\overline{\rho}-\rho)z\,dz \quad (3)$$

where g is gravity constant, H is water depth, z is the layer depth and $\overline{\rho}$ is average density of the water column

$$\overline{\rho} = \frac{1}{H}\int_{-H}^{0} \rho(z)\,dz. \quad (4)$$

The northward currents are strongest at the surface (0.06 m s^{-1}) and decrease with depth. The southward currents on the eastern side of the gyre do not exceed 0.02 m s^{-1} at the surface due to the merging of the gyre with the northward flowing river water in the upper 8-m thick layer at the eastern coast. The return flow is established below the river water with a maximum southward velocity of 0.04 m s^{-1} at a depth of 19 m.

In April 2006, low saline water from the Daugava River has spread along the right hand coast from the river mouth and extends almost to Pärnu Bay (Fig. 4a). There is a strong coastal current of up to 0.08 m s^{-1} over the same area (Fig. 4b). The mean salinity gradient along the line between Daugava River mouth and Cape Kolka is 1.3×10^{-4} g kg^{-1} m^{-1} within the river plume (up to 11 km offshore) and 0.06×10^{-4} g kg^{-1} m^{-1} along the rest of the line. The circulation pattern consists of 2 cyclonic and 2 anticyclonic circulation cells (Fig. 4b). Except for the river water belt, the water column is well mixed down to a depth of 30 m, the maximum PEA is 3 J m^{-3} between a depth of 0–30 m and a longitude of 23.3–23.94°E. The cross-section flow to the south is slow ($\leq$0.01 m s^{-1}) and vertically uniform, except on the water surface. A considerable surface layer current with a northward direction is present in the frontal zone of the river water. This flow is strongest at the surface (0.08 m s^{-1}) and extends to a depth of 10 m while decreasing in speed. Below, a southward countercurrent exists with a maximum flow of 0.05 m s^{-1} on the bottom slope.

Two snapshots of the measured salinity distribution in the surface layer are available for the southern GoR in May 1994 and 2006 (Fig. 5). The salinity distribution in May 1994 shows that fresh water from the river has spread offshore and a bulge-like structure has formed close to the river mouth. The salinity gradient over the gulf is mainly south-north directed. This salinity distribution indicates the presence of anti-cyclonic circulation near the river mouth. Monthly mean wind of 2.3 m s^{-1} was from the south in May 1994. In May 2006 there is a strong east–west salinity gradient at the eastern coast of the GoR and a much more homogeneous salinity distribution in the offshore area. The salinity distribution corresponds to the circulation scheme of a buoyancy-driven coastal current. Monthly mean wind of 0.8 m s^{-1} was from the southwest in May 2006.

3.2. Circulation patterns in the upper layer

The first three modes from the PCA analysis of the period from March to June in 1997–2006 explain 43%, 14% and 10% of the total variability in the model, respectively. These modes with corresponding time series of the principal amplitudes are presented in Fig. 6. The first mode (Fig. 6a) shows a double gyre circulation pattern where the anticyclonic circulation is located in the southeastern and cyclonic gyre in the northwestern part of the GoR. This pattern matches the circulation pattern in April 1998 (Fig. 3b) with r^2=0.87. The circulation pattern of the second mode (Fig. 6b) shows general cyclonic circulation in the whole GoR. There is a strong along-coast current at the eastern coast of the GoR, extending from the mouth of the Daugava River to the Virtsu Strait, and decreasing anticyclonic shear offshore. The coefficient of determination between simulated mean circulation in April 2006 (Fig. 4b) and that explained by the second mode is r^2=0.53. In the case of the third mode, a large anticyclonic/cyclonic gyre covers most of the GoR area extending to 58°N (Fig. 6c).

In addition to the principal amplitude (PA), we calculated the coefficient of determination according to (2) for each month (Fig. 7). As there is no exact linear relationship between PA and r^2, we use the threshold value $r^2\geq0.5$ to define whether monthly mean circulation is dominated by a particular mode or not. The threshold value was selected after visual inspection of all monthly mean circulation patterns. According to this criterion, the anticyclonic circulation explained by the first mode in the southern GoR is dominant in April 1998 (r^2=0.87), March and April 2001 (r^2=0.63 and 0.63), May 2002 (r^2=0.83), April 2003 (r^2=0.51) and April 2005 (r^2=0.65), i.e. in six cases. A similar flow structure, but with opposite direction of current vectors, i.e. cyclonic circulation in the southern GoR (negative PA) prevails in March and April 1997 (r^2=0.51 and 0.70), March, May and June 2000 (r^2=0.76, 0.61 and 0.79), June 2003 (r^2=0.61) and June 2004 (r^2=0.66), i.e. in seven cases. The circulation pattern explained by the second mode with a positive PA prevails in March 1999 (r^2=0.66), April 2000 (r^2=0.64) and April 2006 (r^2=0.53). The second mode with a negative PA explains the flow pattern in May 1999 (r^2=0.63), only. There is only one occasion

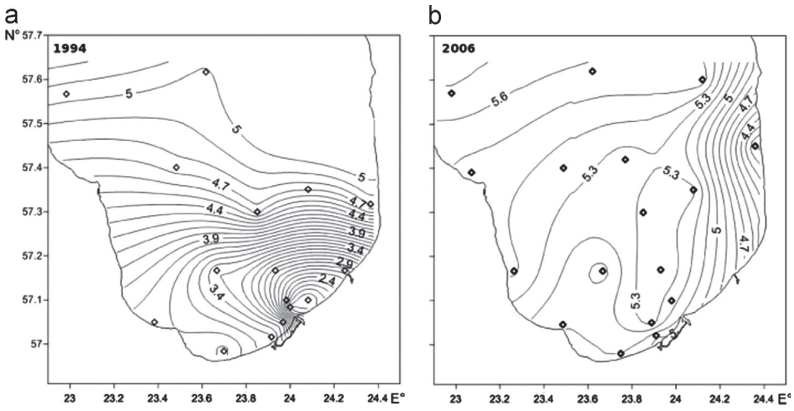

Fig. 5. Measured salinity distribution at a depth of 1 m in the southern GoR in May 1994 (left) and in May 2006 (right). The rhombuses mark locations of stations.

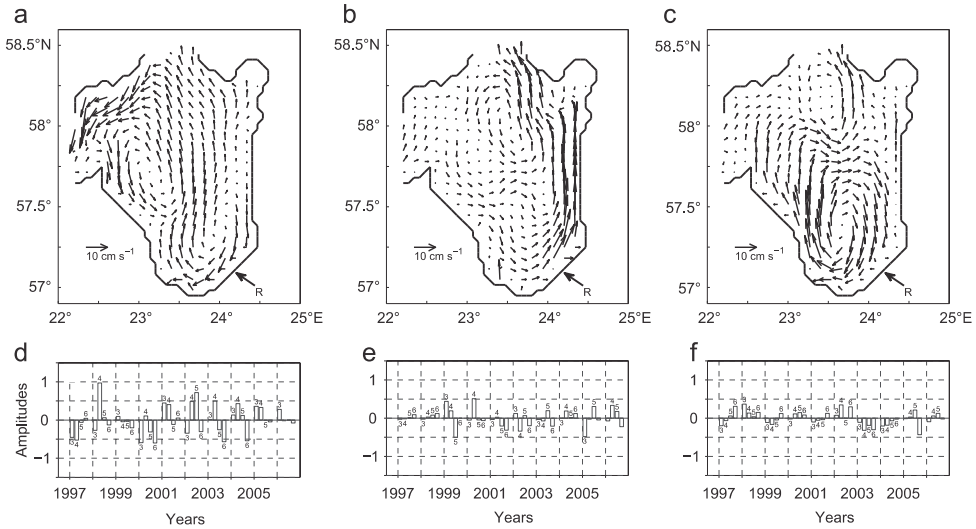

Fig. 6. The first (a), second (b) and third (c) circulation modes at a depth of 5 m for March, April, May and June in 1997–2006 and the amplitudes for the corresponding modes (d), (e) and (f), respectively.

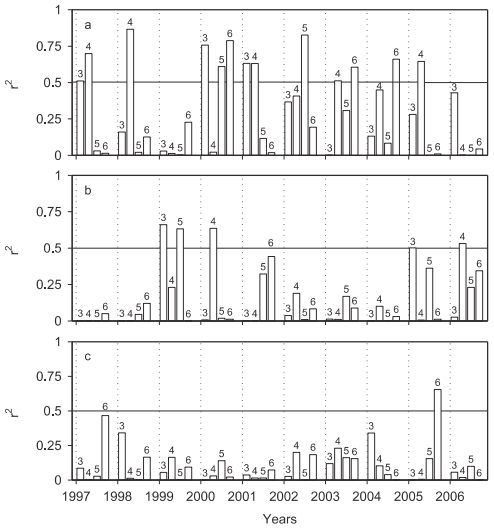

Fig. 7. Coefficients of determination, R^2, for the first (a), second (b) and third principal components compared to corresponding monthly mean water circulation at a depth of 5 m. R^2 is calculated according to Eq. (2).

when the third mode exceeds the threshold value, i.e. in June 2005 ($r^2=0.66$) with PA < 0.

3.3. Model sensitivity tests

To analyze the factors that may cause anticyclonic circulation we focus on April 1998 when anticyclonic gyre is strongly present in the southern GoR. Water exchange through the Irbe Strait and Suur Strait, the effect of river discharge, wind forcing and density-driven circulation were considered. All simulation runs were made over a period of two months (March and April), but only the mean circulation in April was analyzed.

Comparing monthly mean circulations, with the Irbe and Suur straits being either closed or opened, only minor differences emerge that occur mostly in the northern part of the gulf near the straits (Figs. 8a and 3b). The coefficient of determination between the two cases for April 1998 is $R^2=0.93$. Hence, we use closed boundaries for the three idealized simulations with 3-dimensional initial density gradient forcing, wind forcing and river discharge forcing accordingly.

To separate density-driven circulation, the simulation was initiated with salinity and temperature fields from the numerical model simulation results of 28 February 1998. Wind forcing and river discharge were excluded. Monthly mean circulation for April shows large anticyclonic circulation over the entire southern GoR reaching up to 57.75°N and a cyclonic loop in the northern part of the gulf (Fig. 8b).

In order to separate wind-driven circulation, simulation was initiated with uniform water density. Wind forcing from March and April 1998 was applied, while river discharge was switched off. Resulting circulation shows a double-gyre pattern with an anticyclonic loop in the southeastern part and a large cyclonic gyre over the central and northwestern parts (Fig. 8c). Wind in April 1998 was mainly from the east and northeast.

To separate river circulation, a simulation was initiated with a uniform ambient salinity of 5 g kg^{-1}. Wind forcing was switched off. The Daugava River discharge from March and April 1998 was applied. The resulting monthly mean circulation for April shows a river water bulge near the river mouth and a cyclonic coastal current along the eastern coast. Rest of the GoR is covered by weak cyclonic circulation (Fig. 8d). Monthly mean river discharge was 1700 $m^3\ s^{-1}$ and 1188 $m^3\ s^{-1}$ in March and April 1998, respectively.

The sensitivity tests show that wind forcing dominantly from the east as well as 3-dimensional density gradient forcing result in anticyclonic circulation at a depth of 5 m in the southern GoR in April 1998. Moreover, when we used initial 3-dimensional density distribution from 28 February 2006, the result was once again an anticyclonic circulation pattern in the southern GoR. The buoyancy input by the river does not produce anticyclonic circulation, but

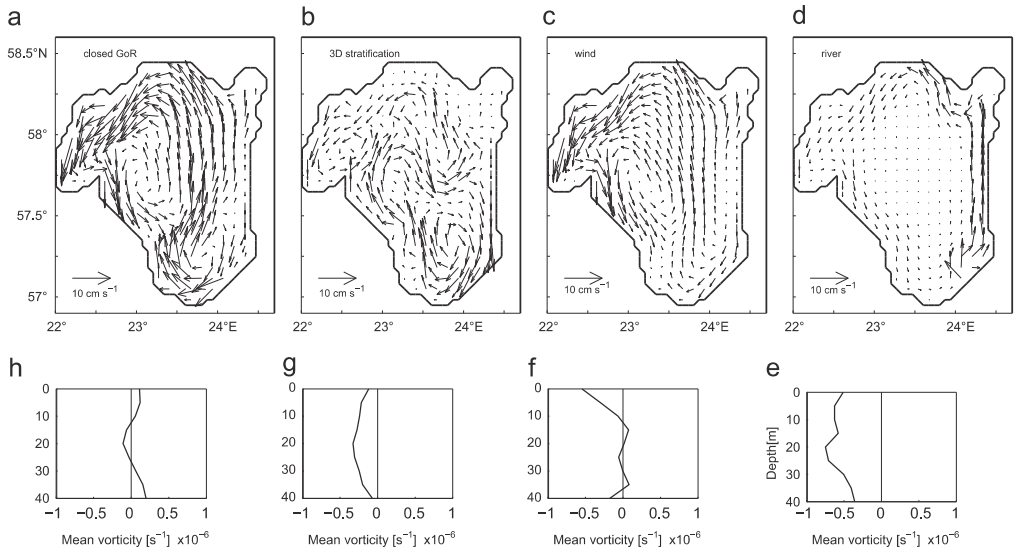

Fig. 8. (a)–(d) Monthly mean velocity patterns at a depth of 5 m (in April 1998) from the idealized simulations. (a) Closed boundary at the Irbe and Suur straits, (b) 3-dimensional density gradient forcing, (c) wind forcing from March and April 1998, (d) river discharge forcing in March and April 1998, and (e)–(h) respective vertical profiles of the relative vorticity averaged over the south-eastern part of the GoR (see Fig. 1 for the area).

merely contributes to the anticyclonic shear within the river bulge area. Obviously, this particular realization is not the result of a single factor, but a combination of them.

3.4. Relative vorticity

We study the rotation patterns further by using monthly mean relative vorticity. The PCA modes represent orthogonal flow patterns at a depth of 5 m over the whole GoR. Spatially averaged relative vorticity provides evidence for the presence of either anticyclonic or cyclonic circulation in the southern part of the GoR (see Fig. 1 for the area). The area was selected to capture the anticyclonic circulation according to the flow scheme of the first mode in the southeastern GoR (Fig. 6a). First, vertical profiles of horizontally averaged relative vorticity at 5 m depth intervals were calculated over the southern part of the gulf. Then, the relative vorticity profiles were vertically averaged while presuming that relative vorticity is homogeneous in the 5-m thick layers.

In the southern part of the GoR negative mean vorticity is clearly dominant during the spring period (Fig. 9). Frequency as well as average and maximum values are higher in the case of negative vorticity. Thus, when we use relative vorticity for describing the circulation in the southern GoR, we get "asymmetric" temporal occurrence of cyclonic and anticyclonic circulation. On the other hand, when we use the circulation pattern of the first principal mode for describing the circulation in the GoR, we get "symmetric" temporal occurrence of cyclonic and anticyclonic circulations. Still, there is a statistically significant linear relationship between the mean vorticity and the PA of the first mode ($R^2=0.62$, $p<0.001$) (Figs. 6a, d and 9).

Vertical profiles of relative vorticity were calculated from the idealized test cases over the same area in the southern GoR. Relative vorticity is negative all over the water column when the GoR is closed (Fig. 8e). Vertically averaged vorticity is close to the value of the continuous run in April 1998, being $-0.56\times10^{-6}\,s^{-1}$ and $-0.50\times10^{-6}\,s^{-1}$ in the case of the straits closed and opened, respectively. In the case of 3-dimensional density gradient forcing,

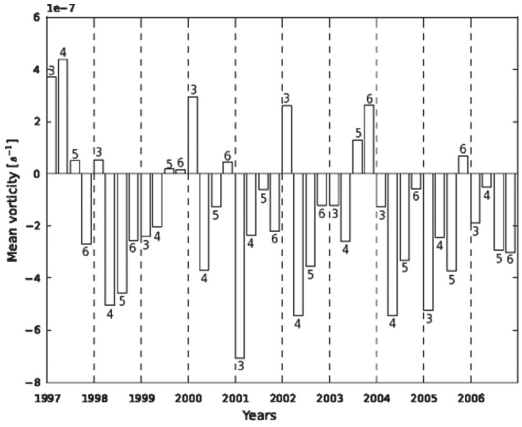

Fig. 9. Monthly mean relative vorticity averaged over the southern part of the GoR (see Fig. 1 for the area) from March, April, May and June 1997–2006.

relative vorticity is negative in the upper 10-m layer and around zero below (Fig. 8f), so that vertically averaged vorticity is negative, $-0.11\times10^{-6}\,s^{-1}$. Wind forcing results in negative vorticity over the whole water column with a vertically averaged value of $-0.2\times10^{-6}\,s^{-1}$ (Fig. 8g). Buoyancy forcing caused by river inflow results in positive vorticity in the upper and lower 10-m thick layers, while being negative in the intermediate layer (Fig. 8h). Vertically averaged vorticity is $0.06\times10^{-6}\,s^{-1}$.

3.5. Linear regression model for vorticity time series

The monthly mean values of PEA, river discharge, Q_R, wind mixing, monthly accumulated salt flux through transect in the Irbe Strait, S_f, east–west and north–south components of monthly accumulated wind impulses, I_x and I_y, and density difference

between northwestern and southeastern GoR, $\Delta\rho$, were considered as potential factors affecting cyclonic/anticyclonic circulation in the southern GoR. Positive salt flux means that salt is transported into the GoR. Monthly mean density values at atmospheric pressure have been calculated from two sites and at different depths. The northwestern site is located at 57°42' N 22° 52' E where the density has been calculated at a depth of 30 m, and the southeastern site is located at 57° 13' N 24° 4' E where the density has been calculated at a depth of 5 m. Only monthly mean salinity values were extracted from the numerical model while the temperature was kept constant with the value of 10 °C. Choosing the density difference between these locations and depth levels will take both the horizontal density gradient as well as the vertical stratification into account, thus being a proxy for the 3-dimensional density gradient.

At first, a multiple regression model for the dependent variable of vertically averaged vorticity, ω, that included all above listed independent variables was applied. Obviously, this model was an exaggeration of the physical factors that could affect vertically averaged vorticity in the southern GoR. The rough model revealed that zero hypothesis can be rejected for the east–west wind impulse and density difference. Therefore, a new multiple linear regression model including these two independent variables was built. Model sensitivity tests showed that both wind with a mean vector from the east as well as the 3-dimensional density gradient can drive anti-cyclonic circulation in the southern GoR (Fig. 8b and c). Overall goodness of fit of the model for monthly mean spatially averaged relative vorticity in the southern GoR

$$\omega = a_1 I_x + a_2 \Delta\rho \tag{5}$$

($a_1 = 4.23 \times 10^{-10}$ s kg^{-1}, $a_2 = -3.4 \times 10^{-7}$ kg g^{-1} s^{-1}) is rather high ($R^2 = 0.77$, $p < 10^{-4}$). A t-test for separate coefficients has $p < 10^{-4}$ for both coefficients. Density difference between selected locations is maintained by river discharge in the gulf head (Daugava River) and salt flux in the gulf mouth (Irbe Strait), so that we obtain the multiple linear regression model for $\Delta\rho$

$$\Delta\rho = b_1 Q_R + b_2 S_f \tag{6}$$

($b_1 = 5.5 \times 10^{-4}$ g kg^{-1} s m^{-3}, $b_2 = 3.17 \times 10^{-13}$ s m^{-3}) with $R^2 = 0.67$ ($p < 10^{-4}$). The p-values for Q_R and S_f are $p < 10^{-4}$ and $p = 0.016$, respectively. Salt flux in Irbe Strait is related to the east–west wind impulse

$$S_f = c_1 I_x + c_2 \tag{7}$$

($c_1 = -1.2 \times 10^9$ g s m^3 kg^{-2}, $c_2 = 2.74 \times 10^{11}$ g m^3 kg^{-1} s^{-1})($R^2 = 0.62$, $p < 10^{-4}$). The scatterplots of dependent variables versus independent variables in (5), (6) and (7) are shown in Fig. 10. We have presented values calculated from the model results. Negative vorticity persists even at positive values of east–west wind impulse, while positive vorticity can be produced if east–west wind impulse, in case of our parameters, exceeds 500 kg s^{-2}. (Fig. 10a). There is a tendency towards higher difference in density between southeastern and northwestern GoR being in favor of negative vorticity (Fig. 10b). River discharge contributes to the density difference but does not dominate in the process of setting up the density difference between southeastern and northwestern GoR (Fig. 10c). Positive salt flux in the Irbe Strait supplies saline water into the GoR and increases the density difference (Fig. 10d). Low values of density difference are related to negative salt flux. Salt flux is clearly negative when wind impulse is positive and exceeds the value of 500 kg s^{-2} (Fig. 10e). At lower values of positive wind impulse salt flux can be either positive or negative, while negative wind impulse mainly supports salt flux into the GoR.

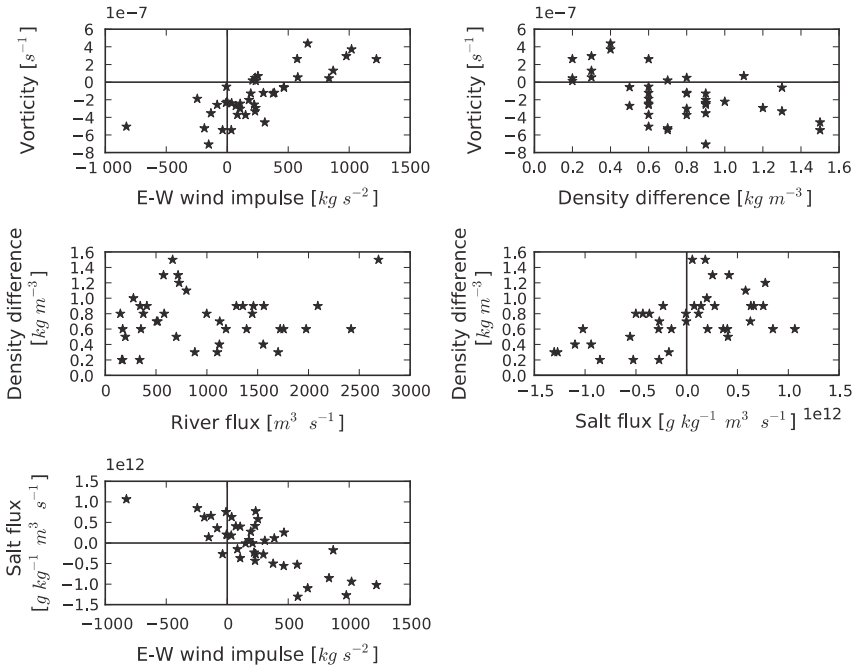

Fig. 10. Scatterplots of monthly mean (a) wind impulse and vorticity, (b) density difference and vorticity, (c) river flux and density difference, (d) salt flux and density difference, and (e) wind impulse and salt flux for the March–June periods of 1997–2006.

4. Discussion

The results of a model simulation covering a period of ten years were analyzed to investigate circulation in the southern GoR in spring, when the GoR can be considered a gulf-type ROFI.

Our results show that double gyre circulation is the most prominent circulation pattern in the upper layer of the GoR. It may be either anticyclonic or cyclonic in the southeastern gulf and the opposite in the northwestern part. This pattern corresponds to the classical wind-forced double gyre circulation scheme in large lakes (Bennett, 1974) when there is steady wind from the east or west. Due to shallowness of the GoR, double-gyre wind-driven circulation is readily excited in the GoR (Raudsepp, 2001; Raudsepp et al., 2003). In addition to wind forcing, anticyclonic circulation in the southern GoR can be forced by three-dimensional density distribution. Baroclinic geostrophic adjustment in a rotating circular basin consists of a geostrophic component in the form of a basin-scale double gyre (Wake et al., 2004). In the case of the GoR, the anticyclonic gyre should reside over the southern and the cyclonic gyre over the northern gulf. The main connection of the GoR to the Baltic Sea is through the Irbe Strait with a sill depth of 22 m. This limits the water and salt exchange between the gulf and the Baltic Sea. After an inflow event in the Irbe Strait, we may treat the GoR as a closed circular basin where baroclinic geostrophic adjustment results in anticyclonic circulation in the southern gulf. According to theoretical considerations by Fujiwara et al. (1997), anticyclonic circulation is generated at the head of a wide estuary with a two-layer salinity stratification and a longitudinal salinity gradient. To preserve the latter, upward entrainment of lower layer water into the upper layer is required. The primary difference between baroclinic geostrophic adjustment and anticyclonic circulation driven by estuarine circulation is that when using potential vorticity formulation the horizontal divergence in the upper layer is in the case of the former caused by changes in layer thickness (Wake et al., 2004) and in the case of the latter by upward entrainment (Fujiwara et al., 1997). In the case of continuous salt transport to the GoR through the Irbe Strait, we presume that anticyclonic circulation is forced by the mechanism described by Fujiwara et al. (1997). Both mechanisms support the occurrence of anticyclonic circulation in the southern GoR. In the present study we are not trying to separate these two mechanisms.

McClimans et al. (2000) speculated that the anticyclonic circulation in the Kara Sea ROFI is caused by increased river discharge during previous months. Freshwater accumulated in the ROFI zone during intensive river discharge acts as a zonal barrier, directing the flow to the left during reduced discharge months. Idealized numerical experiments in the Kara Sea show that the absence of baroclinic effects (using uniform salinity and temperature distribution) results in cyclonic circulation (Panteleev et al., 2007). An observational study in the Kattegat–Skagerrak region (Nielsen, 2005) confirms the presence of strong anticyclonic circulation in that area. Although there is a strong horizontal density front separating the brackish Baltic Sea water in the upper layer and the North Sea saline water in the lower layer, he concluded that wind-generated vertical entrainment is the primary driving agent for the anticyclonic circulation.

The cyclonic/anticyclonic circulation in the southern GoR was accounted for through spatially averaged relative vorticity. Negative vorticity (anticyclonic circulation) is forced by the winds from the east and by the 3-dimensional density distribution that vertically takes into account the two layer stratification and horizontally the estuarine salinity distribution. Positive vorticity (cyclonic circulation) is forced by winds from the west. River discharge may contribute to negative or positive vorticity in the southern GoR. Previous simulations and laboratory experiments of buoyant discharges have shown that buoyant water can form a large surface-trapped anticyclonic bulge (Garvine, 2001; Yankovsky and Chapman, 1997) near the river mouth, which has also been observed in the field (Huq, 2009; Horner-Devine et al., 2008). The formation of an anticyclonic bulge contributes to negative vorticity, while a coastal current contributes to positive vorticity. A bulge is expected to form if $h/D \leq 0.25$ (Huq, 2009), where $h = (2Qfg'^{-1})^{1/2}$ is depth scale, D is ambient water depth, Q is river flow rate and g' is reduced gravity. Rough estimates of h with a river discharge rate between 500 and 2500 $m^3 s^{-1}$, and a density difference between 1 and 5 $kg m^{-3}$, give values in the range of 1.5 to 7.5 m. Thus, we may expect that in certain months the anticyclonic buoyant bulge is well established, while in certain months river water is just deflected to the right from the river mouth. Our results showed that there is no significant relationship between the river discharge rate and the relative vorticity in the southern GoR, which indicates that the buoyancy input by Daugava River contributes to positive/negative vorticity in the southern GoR.

Taking into account potential forcing mechanisms and calculated monthly mean spatially averaged relative vorticity, we may conclude that there is asymmetry in the realization of either cyclonic or anticyclonic circulation in the southern GoR. The present study shows that negative mean vorticity is more frequent in the southern GoR than a positive one. A relatively strong positive east–west monthly accumulated wind impulse is needed to reverse anticyclonic circulation in the southern GoR.

Most previous studies assume that with little or no wind forcing river water will spread along the right hand coast, which is indeed the case when ambient water density is homogeneous. The present study supplements the common understanding of river water circulation by taking into account anticyclonic circulation caused by three-dimensional density stratification that transports river water to the left and offshore from the river mouth. Furthermore, nutrients as well as dissolved and particulate matter discharged by the river may be transported from the river mouth along the left hand coast. A numerical model study by Andrejev et al. (2010) for the Gulf of Finland shows anticyclonic circulation forming near the Neva River mouth and fresher water from the river discharge being partly transported along the left hand coast. While summarizing the measurement results, Wassman and Tamminen (1999) stated that the southwestern part in the GoR in spring was more influenced by the freshwater flow from the Daugava River than the south-eastern part and as a consequence phytoplankton bloom was more pronounced there.

5. Conclusions

The spring (from March to June) circulation and spreading of river discharge water in the southern GoR was analyzed based on the results of a 10-year simulation (1997–2006) using the GETM for the entire Baltic Sea. Three basic circulation schemes prevail in the upper layer of the GoR in spring. Dominant circulation patterns in spring were the anticyclonic/cyclonic gyre in the souhteastern and cyclonic/anticyclonic gyre in the northwestern part of the Gulf of Riga. The spreading of Daugava River water along the eastern coast of the GoR took place less frequently.

The anticyclonic/cyclonic circulation was accounted for with the spatially averaged relative vorticity in the southern GoR. There is asymmetry in the realization of cyclonic or anticyclonic circulation in the southern GoR. The present study shows that in the spring period anticyclonic circulation is far more frequent than cyclonic circulation.

The 3-dimensional estuarine type density field drives the anticyclonic circulation in the upper layer of the southern GoR in spring. The forming of circulation is either enhanced by the wind impulse from the east or destroyed or reversed to cyclonic circulation by the

wind impulse from the west. The 3-dimensional estuarine type density field is maintained by the salt flux in the Irbe Strait and by the freshwater discharge from the Daugava River. The wind impulse from the east directly drives the salt flux through the Irbe Strait into the GoR.

Our results suggest that anticyclonic circulation is a natural phenomenon in the wide ROFI caused by the 3-dimensional estuarine type density gradient, which is realized either by baroclinic geostrophic adjustment (Wake et al., 2004) in the case of an event like the supply of saline water, or by upward entrainment of lower layer water into the upper layer (Fujiwara et al., 1997) due to continuous inflow of saline water into the estuarine basin.

Acknowledgments

This research was partially supported by the Estonian Science Foundation Grant nos. ETF8968 and ETF9278, BONUS+ECOSUPPORT Project and Project EstKliima funded by the Environmental Protection and Technology Programme No 3.2.0802.11-0043 of the European Regional Fund.

References

Andrejev, O., Sokolov, A., Soomere, T., Värv, R., Viikmäe, B., 2010. The use of high-resolution bathymetry for circulation modelling in the Gulf of Finland. Est. J. Eng. 16, 187–210.

Arakawa, A., Lamb, V.R., 1977. Computational design of the basic dynamical processes of the UCLA General Circulation Model. Methods Comput. Phys., 173–263.

Bennett, J.R., 1974. On the dynamics of wind-driven lake currents. J. Phys. Oceanogr. 4, 400–414.

Burchard, H., Bolding, K., 2002. GETM – a general estuarine transport model. Scientific docu-mentation. Technical Report EUR 20253 EN, European Commission.

Burchard, H., Rennau, H., 2008. Comparative quantification of physically and numerically induced mixing in ocean models. Ocean Model. 20, 293–311.

Choi, B.J., Wilkin, J.L., 2007. The effect of wind on the dispersal of the Hudson River plume. J. Phys. Oceanogr. 37, 1878–1897.

Döscher, R., Willen, U., Jones, C., Rutgersson, A., Meier, H.E.M., Hansson, U., Graham, L.P., 2002. The development of the regional coupled ocean-atmosphere model RCAO. Boreal Environ. Res. 7, 183–192.

Döscher, R., Wyser, K., Meier, H.E.M., Qian, M., Redler, R., 2010. Quantifying Arctic contributions to climate predictability in a regional coupled ocean-ice-atmosphere model. Clim. Dyn. 34, 1157–1176.

Garvine, R.W., 2001. The impact of model configuration in studies of buoyant coastal discharge. J. Mar. Res. 59, 193–225.

Horner-Devine, A.R., Fong, D.A., Monismith, S.G., 2008. Evidence for the inherent unsteadiness of a river plume: satellite observations of the Niagara River discharge. Limnol. Oceanogr. 53, 2731–2737.

Horner-Devine, A.R., Fong, D.A., Monismith, S.G., Maxworthy, T., 2006. Laboratory experiments simulating a coastal river discharge. J. Fluid Mech. 555, 203–232.

Höglund, A., Meier, H.E.M., Broman, B., Kriezi, E., 2009. Validation and correction of regionalised ERA-40 wind fields over the Baltic Sea using the Rossby Centre Atmosphere model RCA3.0., Oceanografi 97. SMHI, Norrköping, Sweden 46.

Huq, P., 2009. The role of Kelvin number on bulge formation from estuarine buoyant outflows. Estuaries Coasts 32, 709–719.

Janssen, F., Schrum, C., Backhaus, J., 1999. A climatological dataset of temperature and salinity for the North Sea and the Baltic Sea. Ger. J. Hydrogr. 9, 1–245.

Jurisa, J.T., Chant, R., 2012. The coupled Hudson River estuarine-plume response to variable wind and river forcings. Ocean Dyn. 62, 771–784.

Fujiwara, T., Sanford, L.P., Nakatsujic, K., Sugiyama, Y., 1997. Anticyclonic circulation driven by the estuarine circulation in a gulf type ROFI. J. Mar. Syst. 12, 83–99.

Lindström, G., Janssen, F., Schrum, C., Backhaus, J., 2010. Development and testing of the HYPE (Hydrological Predictions for the Environment) water quality model for different spatial scales. Hydrol. Res. 41, 295–319.

Malačič, V., Petelin, P., 2009. Climatic circulation in the Gulf of Trieste (northern Adriatic). J. Geophys. Res.—Oceans 114, http://dx.doi.org/10.1029/2008JC004904.

McClimans, T.A., Johnson, D.R., Krosshavn, M., King, S.E., Carroll, J., Grenness, O., 2000. Transport processes in the Kara Sea. J. Geophys. Res.—Oceans 105, 14,121–14,139.

Nielsen, M.H., 2005. The baroclinic surface currents in the Kattegat. J. Mar. Syst. 55, 97–121.

Osadchiev, A.A., Zavialov, P.O., 2013. Lagrangian model of a surface-advected river plume. Cont. Shelf Res. 58, 96–106.

Panteleev, G., Proshutinsky, A., Kulakov, M., Nechaev, D.A., Maslowski, W., 2007. Investigation of the summer Kara Sea circulation employing a variational data assimilation technique. J. Geophys. Res.—Oceans 112, http://dx.doi.org/10.1029/2006JC003728.

Passenko, J., Lessin, G., Raudsepp, U., Maljutenko, I., Neumann, T. and Laanemets, J., 2010. Analysis of temporal variability of measured and modeled vertical distributions of salinity and temperature in the Gulf of Finland during 10-year period. In: Baltic International Symposium (BALTIC), 2010 IEEE/OES US/EU. http://dx.doi.org/10.1109/BALTIC.2010.5621648.

Pietrzak, J., 1998. The use of TVD limiters for forward-in-time upstream-biased advection schemes in ocean modeling. Mon. Weather Rev. 126, 812–830.

Preisendorfer, R.W., Mobley, C.D., 1988. Principal Component Analysis in Meteorology and Oceanography. Elsevier, Amsterdam.

Raudsepp, U., Beletsky, D., Schwab, D.J., 2003. Basin-scale topographic waves in the Gulf of Riga. J. Phys. Oceanogr. 33, 1129–1140.

Raudsepp, U., 2001. Interannual and seasonal temperature and salinity variations in the Gulf of Riga and corresponding saline water inflow from the Baltic Proper. Nord. Hydrol. 33, 135–160.

Seifert, T., Tauber, F. and Kayser, B., 2001. A high Resolution Spherical Grid Topography of the Baltic Sea, revised ed. ⟨http:/www.io-warnemuende.de/admin/de_indexhtmel⟩.

Shchepetkin, A.F., McWilliams, J.C., 2003. A method for computing horizontal pressure-gradient force in an oceanic model with a nonaligned vertical coordinate. J. Geophys. Res.—Oceans 108, 347–404.

Simpson, J.H., 1997. Physical processes in the ROFI regime. J. Mar. Syst. 12, 3–15.

Soosaar, E., Sipelgas, L. and Raudsepp, U., 2010. Simple model calculations of the ice thickness for complementing satellite remote sensing of ice extent. In: Baltic International Symposium (BALTIC), 2010 IEEE/OES US/EU. http://dx.doi.org/10.1109/BALTIC.2010.5621637.

Stipa, T., Tamminen, T., Seppälä, J., 1999. On the creation and maintenance of stratification in the Gulf of Riga. J. Mar. Syst. 23, 27–49.

Stips, A., Bolding, K., Pohlmann, T., Burchard, H., 2004. Simulating the temporal and spatial dynamics of the North Sea using the new model GETM (general estuarine transport model). Ocean Dyn. 54, 266–283.

Umlauf, L., Burchard, H., 2005. Second-order turbulence closure models for geophysical boundary layers. A review of recent work. Cont. Shelf Res. 2, 795–827.

Wake, G.W., Ivey, G.N., Imberger, J., McDonald, N.R., Stocker, R., 2004. Baroclinic geostrophic adjustment in a rotating circular basin. J. Fluid Mech. 515, 63–86.

Wassman, P., Tamminen, T., 1999. Pelagic eutrophication and sedimentation in the Gulf of Riga: a synthesis. J. Mar. Syst. 23, 269–283.

Whitney, M.M., Garvine, R.W., 2006. Simulating the Delaware Bay buoyant outflow: comparison with observations. J. Phys. Oceanogr. 36, 3–21.

Yankovsky, A.E., Chapman, D.C., 1997. A simple theory for the fate of buoyant coastal discharges. J. Phys. Oceanogr. 27, 1386–1401.

Paper IV

Elken J, Raudsepp U, Laanemets J, Passenko J, Maljutenko I, Pärn O, Keevallik S. 2014. Increased frequency of wintertime stratification collapse events in the Gulf of Finland since the 1990s. J Mar Syst 129:47–55. Elsevier B.V. doi:10.1016/j.jmarsys.2013.04.015 (1.1)

Journal of Marine Systems 129 (2014) 47–55

Contents lists available at ScienceDirect

Journal of Marine Systems

journal homepage: www.elsevier.com/locate/jmarsys

Increased frequency of wintertime stratification collapse events in the Gulf of Finland since the 1990s

Jüri Elken *, Urmas Raudsepp, Jaan Laanemets, Jelena Passenko, Ilja Maljutenko, Ove Pärn, Sirje Keevallik

Marine Systems Institute at Tallinn University of Technology, Akadeemia 15a, EE12618 Tallinn, Estonia

ARTICLE INFO

Article history:
Received 10 January 2012
Received in revised form 23 April 2013
Accepted 24 April 2013
Available online 4 May 2013

Keywords:
Estuary
Wind-induced straining
Wind mixing work
Destratification
Wind regime change
Baltic Sea
Gulf of Finland

ABSTRACT

Since the 1990s, an increased frequency of stratification collapse events in the Gulf of Finland has been noticed, when the density difference between near-bottom and surface waters fell below 0.5 kg m^{-3}. Such stratification crashes occur in the winter months, from October–November to March–April, when saline and thermal stratification decrease compared to the summer period according to the well-known seasonal cycle. The stratification decay process is forced primarily by (1) the westerly-southwesterly wind stress, which causes anti-estuarine straining, and (2) direct wind mixing proportional to the wind speed cubed. The potential energy anomaly (PEA) is occasionally reduced from the average winter level of 70 J m^{-3} (per unit volume; 4.9 kJ m^{-2} per unit area of 70-m water column) to nearly zero, manifesting the stratification collapse, when the current-straining work and wind-mixing work significantly exceed their average levels. Increased collapse frequency is caused by the shift of wind forcing. Namely, the average bimonthly cumulative westerly-southwesterly wind stress in December and January has increased from 1.7 N m^{-2} d during 1962–1988 to 3.7 N m^{-2} d during 1989–2007, yielding a reduction in PEA during these two winter months of about 4.4 kJ m^{-2} between the periods. The other component of the reduction in PEA, wind mixing work per unit surface area, has also increased by 4.6 kJ m^{-2} since 1999 for these two months.

1. Introduction

Kullenberg (1981), among others, has noted that the Gulf of Finland (Fig. 1) is a "true estuarine embayment" of the Baltic Sea multi-basin brackish water system. With its dimensions (length of about 400 km and width from 48 to 135 km over most of the length), low salinity at the entrance (from 6–7 g kg^{-1}/on the reference-composition salinity scale, IOC et al., 2010/at the surface to 8–11 g kg^{-1} in the bottom layers below 80–100 m), and almost absent tides, the gulf is, however, quite unique among the world estuaries (Hansen and Rattray, 1966; see also the reviews by Alenius et al., 1998; MacCready and Geyer, 2010). In the west, the gulf has a free connection, 60 km wide and about 90 m deep, to the Baltic Proper, the central basin of a system that undergoes in its northern part large variations of the stratification (e.g. Elken et al., 2006; Matthäus, 1984). River discharge is concentrated in the eastern part of the gulf, where at the estuary head the Neva River drains an average of 2400 m^3 s^{-1} of freshwater, about two thirds of all of the freshwater imported to the gulf. Despite the large dimensions, compared to the internal Rossby radius (typical scales from 2 to 4 km, Alenius et al., 2003) and variable cyclonic circulation with a number of loops, eddies, fronts, and upwelling events (Andrejev et al., 2004; Elken et al., 2011; Lehmann et al., 2002; Lips et al., 2009; Pavelson et al., 1997, Zhurbas et al., 2008), the along-basin salinity and density gradients are still very profound, especially when studied on the basis of temporally mean values over the seasons.

Salinity and stratification of the Gulf of Finland undergo strong seasonal variations (Haapala and Alenius, 1994). In the period of highest thermal stratification in summer, after the spring maximum of freshwater discharge, the surface salinity is decreased from the winter values of about 6.5 g kg^{-1} down to about 5.5 g kg^{-1} in the central part of the gulf. At the same time, the deep salinity at around 90 m depth is increased from about 7.5 g kg^{-1} to about 10 g kg^{-1}, forming a kind of salt wedge. While a decrease of surface salinity during and after the period of high river discharge is a common feature of most of the estuaries (e.g. Hong et al., 2010; Kimbro et al., 2009; van Aken, 2008), a simultaneous increase of deep salinity is quite unique. The latter can be partly explained by the seasonal conditions of the adjacent larger sea basin, the Baltic Proper, where halocline goes deeper during the winter due to convection and entrainment from the layers above (e.g. Reissmann et al., 2009); in the Northern Baltic Proper deep salinity decrease in winter may exceed 1 g kg^{-1} below the halocline down to the bottom (e.g. Matthäus, 1984).

Interannual changes of the oceanographic conditions of the Gulf of Finland reflect the variations in the large-scale forcing factors. Regarding direct climate forcing, stronger zonal (westerly) winds have been identified in the 1990s and 2000s compared to the 1970s and 1980s. A number of climatic indices, including those at the regional level like the Baltic Sea Index (BSI, Lehmann et al., 2002, 2011) and the Baltic Winter Index (WIBIX, Hagen and Feistel, 2005) also reveal

* Corresponding author. Tel.: +372 26204302; fax: +372 620 4301.
E-mail address: juri.elken@msi.ttu.ee (J. Elken).

0924-7963/$ – see front matter © 2013 Elsevier B.V. All rights reserved.
http://dx.doi.org/10.1016/j.jmarsys.2013.04.015

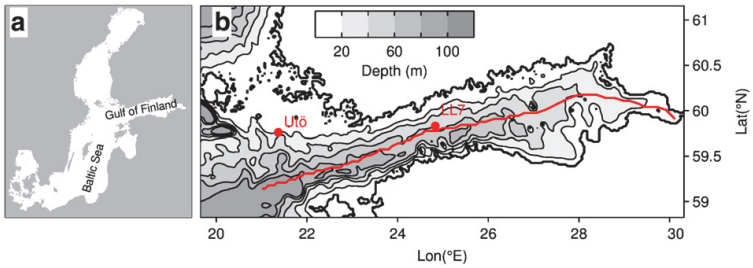

Fig. 1. A map of the Baltic Sea (a) and close-up of the Gulf of Finland (b). Locations of the HELCOM monitoring station LL7 (BMP F3), the Utö weather station, and the main axis of the Gulf (red line) are shown. The depth contours are drawn from the gridded topography (Seifert et al., 2001) in metres.

such a change. Combined with the changes in heat flux, net precipitation, freshwater discharge, and human impact, marine ecosystems have responded with variable regimes (e.g. Dippner et al., 2012, Voss et al., 2011).

A specific feature of the Baltic Sea is the intermittent nature of the large inflows of highly saline water from the North Sea (MBIs, Major Baltic Inflows, after Matthäus and Frank, 1992). With a stronger and shallower halocline in the Baltic Proper, more saline water can be transported to the Gulf of Finland, increasing the strength of stratification. The opposite occurs during the stagnation periods when MBIs are missing for many years. While deep layers of the Baltic Proper are supplied with oxygen only during MBIs by lateral advection, those of the Gulf of Finland are also ventilated during the stagnation periods when stratification is weaker (e.g. Conley et al., 2009, Kahru et al., 2000). As an example, on the basis of monitoring data for 1965–2000, Laine et al. (2007) have shown a decrease in salinity and density stratification until the early 1990s and a slight increase afterwards, while opposite changes in the oxygen content took place. Vermaat and Bouwer (2009) have proposed that a reduced ice extent during the recent period has favoured vertical mixing, causing a reduction of the extent of hypoxic bottoms.

Among the complex ventilation processes (Meier et al., 2006), convection due to surface cooling, turbulent erosion from surface towards deeper layers, and turbulent shear mixing are usually considered as most important in the Gulf of Finland. In summer, a significant decay of observed stratification has been explained by persistent southwesterly winds, creating a temporary estuarine circulation reversal (Elken et al., 2003). With reference to other estuaries, Blumberg and Goodrich (1990) showed for the Chesapeake Bay that wind-induced current shear is more effective in destratification than surface-generated turbulence. In the framework of estuarine dynamic concepts, Scully et al. (2005) presented a conceptual model for the exchange processes during up-estuary and down-estuary winds and pointed to the role of wind-induced current straining interacting with along-basin density gradients.

Observational data are quite rare for winter, during the period of the weakest stratification in the Gulf of Finland. Still, events of complete stratification collapse (reaching the well-mixed state) can be frequently observed during recent winters. These situations, when the bottom-to-surface density difference (and consequently, the potential energy anomaly) decreases drastically to almost zero, cannot persist over longer time periods since longitudinal gradients of mean density restore the stratification.

The aim of the paper is to study the stratification collapse events in the Gulf of Finland using observational data and to find the governing wind forcing mechanisms for such events. Further on, the purpose is to assess whether it is likely that the collapse events have also occurred during non-sampled times and whether there is a change of frequency of complete destratification related to the changing climate factors.

Our hypothesis is that purely vertical mixing processes in the Gulf of Finland are not always strong enough to cause complete destratification as observed, and wind-induced current straining is important. To evaluate the role of the different mechanisms, we use the balance for the potential energy anomaly (PEA), that is, the vertical integral of the potential energy density in reference to a well-mixed state (Burchard and Hofmeister, 2008; Simpson et al., 1990; Wang et al., 2011). The "normal" wintertime PEA values are determined from the hydrographic observations and they manifest the stratification under average forcing conditions. We further study changes in PEA due to straining by wind-induced currents and direct wind mixing using the data from long-term wind observations. The straining effect is estimated from the established correlation between the specific wind stress component and the time-dependent amplitude of the "strain" EOF mode of along-basin currents. The wind-to-EOF dependency is found from a numerical model. The effect of direct wind mixing is evaluated from the cubic relation to the wind speed. Changes in PEA are calculated for the ice-free periods of each winter. The paper ends with a discussion of the relation of PEA changes to the climatic forcing data.

2. Data and methods

2.1. Observational data

The basic data set describes stratification conditions in the Gulf of Finland. We used long-term data of hydrographic observations for the period 1900–2008 extracted from the ICES (International Council for the Exploration of the Sea) international database. The data are mainly from the standard depths (e.g. Haapala and Alenius, 1994; Janssen et al., 1999). Deeper layers have less data coverage than the surface, especially in the first half of the period. We focused on the data around HELCOM monitoring station BMP F3 (historically known also as LL7, $\varphi = 59.8465^\circ$ N, $\lambda = 24.8378^\circ$ E). This station is located in the deepest part of the central area of the gulf near the transect Tallinn-Helsinki, with a depth range of 80–110 m. For inclusion of the data we adopted a search radius of 15 km, well below the dimensions of the gulf. The ICES data were complemented with 38 profiles from the national CTD data set, observed since 1984. They were also converted to the standard depths to maintain homogeneity with historical data.

The main aim of the analysis was to characterize the strength of stratification over time, especially during the winter period. The basic approach is to investigate the near-bottom ρ_b to surface ρ_s density difference $\rho_b - \rho_s$, as can be found in many studies (e.g. Laine et al., 2007). For the deep values, we used the closest depth to 70 m below

that value. In total we obtained 47 values of $\rho_b - \rho_s$ in December and January since 1975.

The strength of variable stratification can be more precisely (in terms of dynamic equations) characterized by the PEA, the potential energy of the water column of a thickness H relative to the well-mixed state when the initial density ρ takes the depth-mean value (origin of vertical coordinate z is laid on the undisturbed sea surface and pointed upward).

$$\overline{\rho} = \frac{1}{H}\int_{-H}^{0} \rho\, dz \tag{1}$$

Following the definitions by for example Simpson (1981) and Simpson et al. (1990), PEA per unit volume of the water column (J m^{-3}), as work needed to convert the water column into a well-mixed state, is

$$\varphi = \frac{g}{H}\int_{-H}^{0} (\overline{\rho} - \rho)\, z\, dz \tag{2}$$

where g is the acceleration due to gravity.

PEA is zero for the well-mixed state and positive for stable stratification.

The main technical question in PEA calculation is to convert the data into fixed levels (compared to slightly variable levels in observational data). We used linear interpolation/extrapolation to the levels of 0 m and 70 m when the difference in depth from the sampled value did not exceed 5 m. Only profiles with at least seven data points between the surface and the 70 m depth were taken into account. Unfortunately, there were no data for 1915–1920 and 1940–1953 that could meet the above criteria.

For the evaluation of wind forcing we used the three-hour wind observations at the Utö meteorological station provided by the Finnish Meteorological Institute since 1961. The station is located on the island at the entrance to the Gulf of Finland (Fig. 1) and presents the wind conditions over the open part of the Gulf of Finland well (Soomere and Keevallik, 2003). In order to take into account variable ice conditions in transferring the wind force to the water surface, we used digitized ice charts (grid steps of 10′ latitude and 60′ longitude) from the archive of the Estonian Meteorological and Hydrological Institute (Pärn and Haapala, 2011).

2.2. Model data

We used the data from the 10-year simulation of 1997–2006 by the general estuarine transport model (GETM) described in detail by Burchard et al. (2004). The GETM model has numerous successful applications in the Baltic Sea, including a decadal high-resolution simulation of circulation in the Gulf of Finland (Maljutenko et al., 2010; Passenko et al., 2010). The present model setup used 25 sigma layers with a horizontal resolution of the model grid of two nautical miles for the whole Baltic Sea. The bathymetry has been interpolated on the computation grids from the digital topography by Seifert et al. (2001). Depths have been adjusted so that the maximum depth is 260 m. Initial temperature and salinity fields were constructed using the Data Assimilation System coupled with the Baltic Environmental Database at Stockholm University (http://nest.su.se/das). Atmospheric forcing (wind stress and heat flux components) with three-hour intervals was adopted from ERA40 re-analysis data dynamically downscaled with the help of the Rossby Centre Atmosphere Ocean model (Döscher et al., 2010). For sea level elevations at the open boundary in the northern Kattegat, one-hour averaged measurements at Smøgen (Sweden) were used. Salinity and temperature at the North Sea open boundary have been adopted from the climatological mean fields by Janssen et al. (1999). The model output during the long-term run was written with a one-day interval, which is adequate for temperature and salinity but does not represent short-term current variations.

Variations of currents and sea level were investigated from the results obtained from the operational HIROMB model (e.g. Lagemaa et al., 2011). The finest grid of the setup provided by the Swedish Meteorological and Hydrological Institute has a resolution of one nautical mile. Vertical fixed levels have variable layer thicknesses from 4 m near the sea surface to 15 m near 100 m depth. We used hourly output data for 2005–2009 to study the EOF modes of currents in relation to wind forcing.

3. Results

3.1. Observational evidence of temporary stratification collapse

Re-inspection of historical hydrographic time series from the Gulf of Finland has drawn our attention to the "missing stratification" profiles in winter. We collected the profiles from December and January as shown in Fig. 2. On the background of normal (weaker than in summer) stratification, several vertically nearly constant profiles can be identified. One can suspect instrument failure during ice conditions. According to the database, such unusual profiles were carefully checked. For example on 14 January 2000, the Finnish research vessel *Aranda* made three consecutive profiles at station BMP F3, all of which revealed the same stratification collapse. Such events of vertically well-mixed stratification conditions were occasionally observed during many winters, but they are not so easy to catch because of the historically low sampling frequency.

We define stratification collapse as an event where the bottom-to-surface density difference becomes less than 0.5 kg m^{-3}. A time series of bottom-to-surface density difference observed at station BMP F3 during December and January (Fig. 3) reveals 11 winters with collapse out of 26 winters with available observations. We note again the poor data availability in winter; several winters have no observations due to the hard navigation conditions during ice cover and/or winter storms. Also, collapse is a short-term event that may not be caught by irregular and sparse sampling.

In order to quantify the stratification collapse in terms of PEA, we calculated the PEA values in a 15 km radius around the station BMP F3 based on hydrographic observations from 1901 onwards. In summer the PEA values are higher than in winter, and the highest value of 360 J m^{-3} was found during the summer of 1930. Very high values, above 300 J m^{-3}, were also observed during the summers of 1970, 1973, 1980, 1983, 1988, 1994, and 2004–2006. Compared to the beginning of the twentieth century, the range of PEA variation has increased slightly: summer maximums have increased from 280 to 350 J m^{-3} and winter minimums have decreased from 20 J m^{-3} to nearly zero.

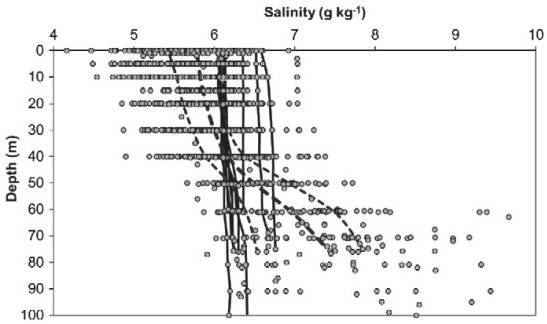

Fig. 2. Salinity values observed in the Gulf of Finland in 1900–2008 during winter (December–January) at station BMP F3 (dots), median and quartile profiles of all data (dashed lines), and profiles with collapsed stratification (solid lines).

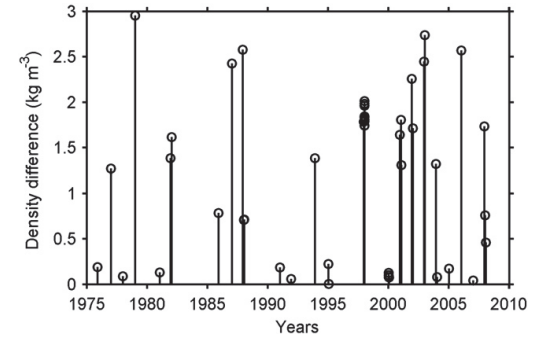

Fig. 3. Temporal course of winter (December–January) bottom-to-surface difference in water density calculated from HELCOM monitoring data at station BMP F3 for 1976–2008.

The seasonal PEA cycle for the whole observational data set is presented in Fig. 4. The monthly mean PEA in winter is about 70 J m^{-3} but the variation range is from nearly zero to 160 J m^{-3}. Stratification collapse may be defined as a PEA value below 30 J m^{-3}. Such values were observed 44 times during the low stratification season from October to April, most frequently in January (13 times).

3.2. Evaluation of wind-induced current straining and direct mixing

We are further interested in evaluating the role of different dynamical factors in creating wintertime destratification and eventual stratification collapses. Here we consider the main assumptions of potential energy conversion.

The temporal change in PEA is governed by the energy conversion budget (W m^{-3}):

$$\frac{\partial \varphi}{\partial t} = \frac{\partial \varphi_S}{\partial t} + \frac{\partial \varphi_W}{\partial t} + \frac{\partial \varphi_Q}{\partial t} + D_\varphi \tag{3}$$

where the terms of interest to us (further evaluated step by step) are as follows: φ_S is the work done by straining (time-dependent vertically differential lateral advection on the background of mean estuarine gradients), φ_W denotes the work executed by direct vertical (wind) mixing, φ_Q is the work done by heating or cooling at the sea surface, and D_φ reflects the power of other processes in changing the PEA. Concerning the derivation of complete PEA equation and interpretations we refer to Burchard and Hofmeister (2008).

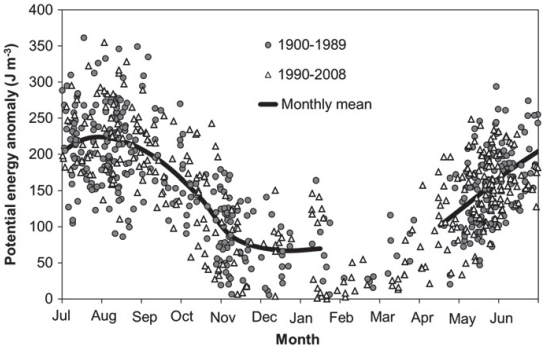

Fig. 4. Seasonal cycle of potential energy anomaly per unit water volume in the Gulf of Finland calculated from the data in a 15 km radius from the central station BMP F3. Data are from 1900 to 2008; the monthly mean over the whole period (February and March missing due to the low number of observations) and the individual data points of the two sub-periods are explained in the legend.

The power from straining (work per unit time) can be estimated sufficiently by

$$\frac{\partial \varphi_S}{\partial t} = \frac{g}{H}\frac{\partial \overline{\rho}}{\partial x}\int_{-H}^{0}(u-\overline{u})\,z\,dz \tag{4}$$

where

$$\overline{u} = \frac{1}{H}\int_{-H}^{0} u\,dz \tag{5}$$

is the vertical average (over depth H) of the along-basin velocity u. We have pointed the along-basin coordinate x in the up-estuary direction, i.e. looking from the open sea to the estuary head. Positive values of Eq. (4) describe an overall strengthening of stratification.

In Eq. (4) we assume a constant along-basin density gradient over the depth and time. Indeed, the long-term mean $\frac{\partial \overline{\rho}}{\partial x}$ is about $-4.5 \cdot 10^{-6}$ kg m^{-4} in the surface and deep layers, according to the results of climatic simulations using the GETM model, while somewhat smaller gradients are found in the mid-depths.

The long-term mean of the vertically averaged current $\langle\overline{u}\rangle$ originates from the river discharge and is distributed over the cross-sectional area of the basin. In the Gulf of Finland, taking the section area of 3 km^2 (Elken et al., 2011) and mean river discharge of 3600 $m^3\,s^{-1}$, the depth-mean current is only about 0.1 cm s^{-1}. On shorter time scales, variations of $\overline{u}$ are related to the basin volume changes due to fluctuating mean sea level. Within the time scales of weeks and months, the mean sea level of the Gulf of Finland may vary together with the overall Baltic sea level by about 0.5 m in 10 days (neglecting the short-term storm pulses and Baltic Sea seiches), yielding a variability range of $\overline{u}$ of about 0.5 cm s^{-1} (the gulf's surface area is about 29,500 km^2). Baroclinic currents show a much higher speed range of roughly 10–20 cm s^{-1}, and their contribution to the PEA change is of primary interest in the following.

Further we want to estimate time series of Eq. (4) over a long period using only the wind data. Elken et al. (2011) have shown that along-basin currents can be decomposed on the cross-basin transects of the Gulf of Finland by the EOF analysis into a "flat" barotropic mode (unidirectional over the whole water column, 23–42%, correlated with the short-term volume changes), a two-layer mode (surface Ekman transport with the deeper compensation flow, 19–22%, correlated with the southwesterly wind stress component), and a number of other modes whose correlation with the wind field was statistically insignificant. While the first, nearly barotropic mode resembles an analogue to the tidal motions, the second mode can produce wind-induced current straining. In order to evaluate the time- and depth-dependent along-basin current component $u(z,t)$ in Eq. (4), we recalculate the EOF modes (Fig. 5) from the hourly HIROMB model data at time moments t_n and discrete depths z_k over two winter months from December 2005 to January 2009. For that purpose we take the initial data as cross-basin averages of $u-\overline{u}$ over the deeper part of the basin with depths of more than 50 m in order to suppress the effects of coastal currents and upwelling processes. We use the decomposition

$$u(z_k,t_n) = \langle u\rangle_k + \sum_{m=1}^{M} A_m(t_n)\;F_m(z_k) \tag{6}$$

where $\langle u\rangle_k$ is the depth distributed mean vertical profile of current over a longer time period, $F_m(z_k)$ are dimensional EOF modes ($m = 1\ldots M$ is the mode number, with M equal to the number of vertical data points K, $k = 1\ldots K$), and $A_m(t_n)$ are non-dimensional amplitudes, to yield the unit standard deviation over the whole time period. We have calculated the EOF modes for two longitudinal sections along 23.65° E (section A, at the gulf entrance) and 24.38° E (section B, near BMP F3). The amplitude of the second mode $A_2(t_n)$ has a quite good correlation with the

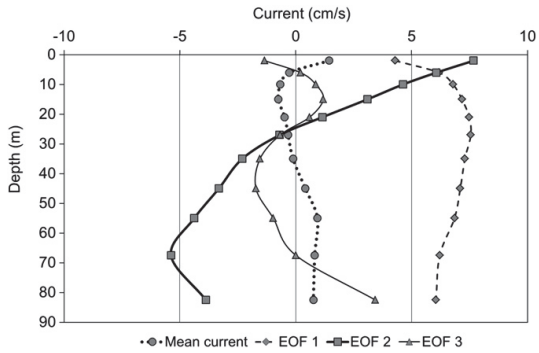

Fig. 5. Mean along-basin current and corresponding EOF modes which are dimensional to obtain unit standard deviations of time-dependent amplitudes along longitude 24.38° E for December and January during 2005–2009.

southwesterly wind stress component in both of the sections. Namely, in section B the correlation squared, R^2, is significantly above 0.5 for the wind direction range 190–250° (positive slope, maximum $R^2 = 0.60$ for directions 210–220°) and 10–60° (negative slope) and the correlation is missing (below 0.1) for directions 290–330° and 110–150°. Amplitudes from section A are highly correlated ($R^2 = 0.90$) with those from section B, due to the much larger spatial scale of overlying wind fields and the channel-like basin geometry. The corresponding wind stress regression is $A_m(t_n) = a_S\, c_D\, \rho_a\, W_{SW}(t_n)\, W(t_n)$, where a_S is the regressive slope (we determined 6.8 and 7.8 $m^2\ N^{-1}$ for A and B, respectively), W_{SW} is the southwesterly wind speed component, and W is scalar wind speed. We used common values for air density $\rho_a = 1.2\ kg\ m^{-3}$ and drag coefficient $c_D = 1.3 \cdot 10^{-3}$. The value of the integral in expression (4) over 90 m depth, using the second EOF mode as shown in Fig. 6, is about 78 $m^3\ s^{-1}$ for both of the sections (we note also that regression of EOF amplitudes on both of the sections yielded the ratio of 1.0). Consequently, power from wind straining (a corresponding temporal change of PEA over the whole water column) per unit surface area is

$$\frac{\partial \Phi_S}{\partial t} = H\frac{\partial \varphi_S}{\partial t} = A_S\, g\, \frac{\partial \overline{\rho}}{\partial x}\, c_D\, \rho_a\, W_{SW}\, W. \tag{7}$$

The site-specific value of A_S has been estimated empirically from the HIROMB model results. We adopt $A_S = 570\ m^4\ s\ kg^{-1}$ since the individual values on sections A and B are 530 and 610 $m^4\ s\ kg^{-1}$, respectively. Within this estimate, the southwesterly (nearly up-estuary) wind stress $\tau_{SW} = c_D\, \rho_a\, W_{SW}\, W$ of 0.1 $N\ m^{-2}$ (wind speed about 8 $m\ s^{-1}$) creates an anti-estuarine straining power of $-2.5 \cdot 10^{-3}\ W\ m^{-2}$, that is, weakening of stratification, since the density gradient is negative. The straining by mean current $\langle u \rangle_k$ favours re-stratification but its power is only $0.4 \cdot 10^{-3}\ W\ m^{-2}$ and we have omitted it in Eq. (7). During the EOF calculation period, the mean wind vector was from the southwest with a speed of 3.3 $m\ s^{-1}$, superimposed by isotropic wind vector variations with a standard deviation of 6.2 $m\ s^{-1}$. Therefore the mean eastward current at the surface as shown in Fig. 5 reflects the Ekman drift.

PEA is reduced by mixing through a chain of processes that depends on the wind (the term φ_W in Eq. (3)). Mixing power per unit

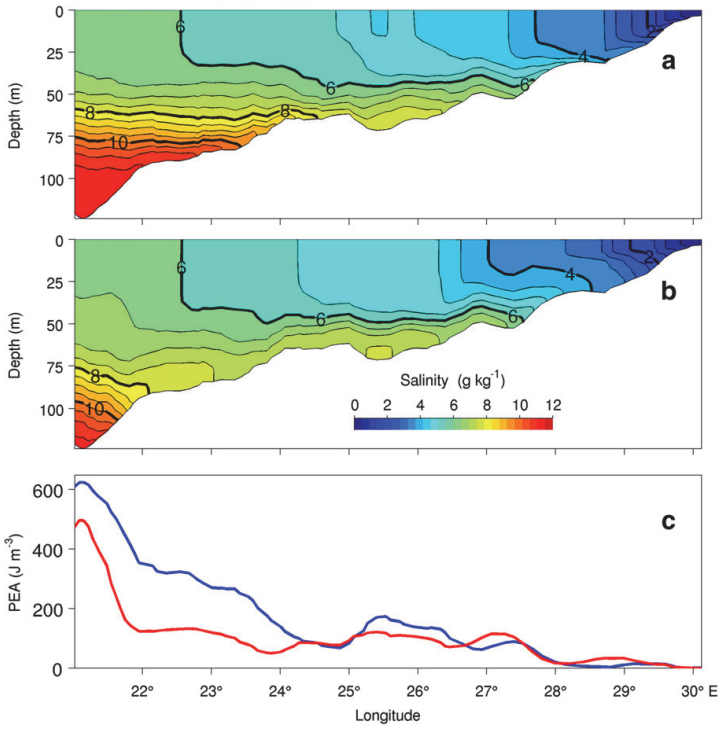

Fig. 6. Snapshot vertical transects of salinity along the main axis of the Gulf of Finland (see Fig. 1) on 27 November (a) and 12 December 1999 (b) and corresponding potential energy anomaly distributions (c) for 27 November (blue) and 12 December 1999 (red).

surface area, generated by the wind, fan be estimated in cubic formulation from the wind speed W:

$$\frac{\partial \Phi_W}{\partial t} = H\frac{\partial \varphi_W}{\partial t} = -\gamma c_D \rho_a W^3 \quad (8)$$

where $\gamma = 10^{-3}$ is a non-dimensional mixing efficiency parameter (see the discussion by Pavelson et al., 1997). As an example of the range of values, to reduce the average winter PEA level, 70 J m^{-3}, of the 70 m layer to zero in a weekly stormy period, (constant) W must exceed 17 m s^{-1}.

In winter, the temperature lies within a few degrees Celsius of the temperature of maximum density, about 2.5 °C in the western and 3.5 °C in the eastern part of the gulf (Alenius et al., 1998). Therefore changes in temperature have a negligible effect on water density, and the work done by heating or cooling of the water surface (φ_Q in Eq. (3)) may be omitted in the wintertime PEA balance.

According to the recent literature, the contribution of other wintertime processes (D_φ in Eq. (3)) is unknown in the Gulf of Finland. Later, we use the assumption that restoration of stratification by D_φ is, on average over time, in balance with the mean destratifying terms given by straining and wind mixing.

The relations (7) and (8) can be interpreted using a specific case of two stratification situations given in Fig. 6 along the main axis of the gulf, simulated using the GETM model. From 27 November to 12 December 1999, after 15 days of strong southwesterly winds with speeds of 10–15 m s^{-1} (according to the model forcing data), the salt wedge lying under the halocline was considerably pushed out from the gulf, and the halocline became deeper and/or disappeared. As calculated from the modelled density distributions, PEA was reduced at section A (23.65° E) by about 120 J m^{-3} but remained unchanged at section B (24.38° E) and eastward from it. The average PEA reduction in the western half of the Gulf of Finland can be estimated as 60 J m^{-3}; for the surface area of the whole water column this gives an estimate of 5.4 kJ m^{-2}. The southwesterly wind impulse (cumulative wind stress) was 1.2 N m^{-2} d, giving a PEA reduction due to wind straining of 2.6 kJ m^{-2}, according to Eq. (7). Time integration of Eq. (8) gave a PEA reduction due to direct wind mixing of 2 kJ m^{-2}. The sum of these two estimated amounts of work corresponds roughly to the calculated loss of PEA. From this example we conclude that expressions (7) and (8) do not resolve the details of the change in PEA in space and time but they can be used for gross estimates of PEA reduction due to anti-estuarine wind straining and direct wind mixing. We also found that in this particular model case the straining work slightly exceeded the wind mixing work.

3.3. Time series evaluation of wind effects on PEA

Based on the relations (7) and (8), we estimate the contributions of wind-induced current straining and direct wind mixing in changing PEA during the winter months from December to January. Based on the three-hour wind data observed at the Utö meteorological station during 1961–2007, we have made time integrations of wind-dependent terms for each winter.

According to Eq. (7), cumulative westerly-southwesterly wind stress (wind impulse)

$$T_{SW} = \int_0^t \tau_{SW} dt = c_D \rho_a \int_0^t W_{SW} W dt \quad (9)$$

generates a PEA change of $\Delta\Phi_S$ due to the work by straining

$$\Delta \Phi_S = A_S g \frac{\partial \overline{\rho}}{\partial x} T_{SW} \quad (10)$$

whereas the wind impulse of 1 N m^{-2} d creates a PEA reduction of about 2.2 kJ m^{-2}.

The wintertime bimonthly wind impulse time series (Fig. 7) reveal remarkable changes, from −2 to 8 N m^{-2} d. On average, the westerly-southwesterly wind impulse $T_{SW}(t)$ is positive. Exceptions are the winters of 1966 (winter is noted by the year of January), 1967, 1977, 1979, 1982, 1985, and 1987, when northeasterly wind stress dominated over this two-month period. Since the winter of 1988, the wind impulses have been only positive, favouring anti-estuarine transport in the Gulf of Finland. Because $T_{SW}(t)$ is changing over time, we have also found maximum positive values of $T_{SW}(t)$ corresponding to the maximum PEA reduction due to straining. From 1989 onwards, westerly-southwesterly winds have dominated throughout the winter and maximum $T_{SW}(t)$ values are found at the end of January.

We have kept the mean density gradient $\frac{\partial \overline{\rho}}{\partial x}$ in Eq. (10) constant over the whole period, since its relative variation between individual years is small compared to that of the wind impulse. Still, the effects of varying deep water density and halocline depth of the adjacent Baltic Proper, impacting on the PEA change in the Gulf of Finland may be in details more complex than given by the relation Eq. (10). As an example from the yearly mean data, during the period 1985–1995 the halocline in the Baltic Proper was exceptionally deep (e.g. Reissmann et al., 2009); observed salinities in the Gulf of Finland were generally lower than the long-term average both in the surface and bottom layers (Laine et al., 2007) but the strength of stratification in terms of bottom-to-surface density difference did not show a significant reduction.

Wind impulse changes were estimated using the sequential shift detection technique proposed by Rodionov (2004) based on successive t-tests. The estimated mean bimonthly westerly-southwesterly wind impulse is about 1.7 N m^{-2} d during 1962–1988 and about 3.7 N m^{-2} d during 1989–2007. For the regime shift detection, the cut-off length was set to 10 years and the Huber's weight parameter to 2. The latter means that the values exceeding two standard deviations from the regime are considered to be outliers and a certain weighing procedure is applied to them to estimate the average values of the regimes. In the present case, only one outlier was detected in the winter of 1992. Setting Huber's parameter to 1, the number of outliers increased to 12, but this procedure changed only the average values of the regimes and did not affect the switch-time of the shift. The method ensures that the regimes of periods longer than the cut-off length will certainly be determined with statistically significant differences of mean values, but detection of shorter regime periods is also possible.

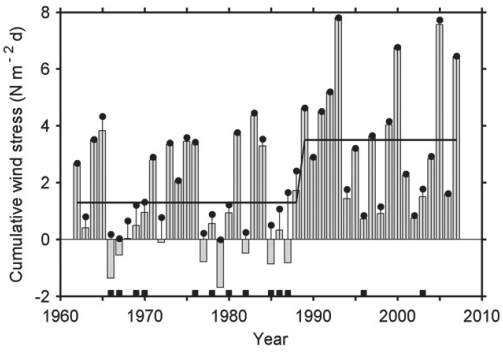

Fig. 7. Temporal course of the cumulative westerly-southwesterly component of wind stress (positive eastward) calculated from the Utö weather station data (filled bars) for the period December–January in 1962–2007. Filled circles mark maximum cumulative wind stress within the period December–January for each winter. The black bold line shows mean values with the 1987/89 regime shift identified by the technique proposed by Rodionov (2004). Filled boxes on the *x*-axis show the winters during which at least 50% ice cover appeared in December–January in the western Gulf of Finland.

An increase of the mean bimonthly westerly-southwesterly wind impulse by 2 N m^{-2} d corresponds to a PEA reduction in terms of $\Delta\Phi_S$ of about 4.4 kJ m^{-2} and might potentially cause full destratification of the water column under the assumption that stratification restoring factors and changes in mixing intensity are not important. Note that the observed average wintertime PEA level of 70–100 J m^{-3} per unit volume corresponds to 5–7 kJ m^{-2} per unit surface area of the 70 m water column.

PEA change due to direct wind mixing, $\Delta\Phi_W$, is estimated by time integration of the relation (8):

$$\Delta\Phi_W = -\gamma c_D \rho_a \int_0^t W^3 dt. \quad (11)$$

On average, the wintertime bimonthly wind mixing work (Fig. 8) for PEA reduction in terms of $\Delta\Phi_W$ is frequently 5–7 kJ m^{-2} but can exceed 15 kJ m^{-2}, as observed in 2000 and 2005. Higher $|\Delta\Phi_W|$ values were also observed in the winters of 1965, 1993, 2004, and 2007. The applied regime shift detection technique revealed that the mean value of about 7.5 kJ m^{-2}, which was evident for 1962–1998, increased to 12.1 kJ m^{-2} from 1999 onwards. However, this regime shift is less reliable than the change observed in the westerly-southwesterly wind stress.

The effects of ice cover on wind mixing and currents are not well known, because they depend on the ice concentration, ice types, vicinity of coasts, and so on. Zhang and Leppäranta (1995) have noted that in ice conditions, the piling-up of water decreases and the sea level slope, which forces the deep currents, may be reduced to one third of the value of an ice-free slope in similar wind conditions. For the rough calculation, we assumed that free atmosphere-to-sea transfer occurs if less than 50% of the western Gulf of Finland is covered by ice and blocking occurs when there is more extensive ice cover. The results given in Figs. 7 and 8 show that high values of $-\Delta\Phi_S$ and $-\Delta\Phi_W$ occurred in mild winters when the surface waters of the western gulf were nearly ice-free until the end of January. In severe winters, the PEA reduction by straining in terms of $\Delta\Phi_S$ was as a rule much lower than the average value for the period.

For the independent interpretation, the PEA time series calculated from the GETM model results for 1997–2006 showed minimum values in winter. The average PEA level per unit surface area was 5–7 kJ m^{-2}, well within the range of observed values, but remarkable changes occurred, from 1 to 19 kJ m^{-2}. The strongest stratification, with the highest PEA, was modelled for the severe winter of 2003 with early ice cover. Low PEA values were modelled for the winters of 1999, 2000, and 2005. During the winters of 2000 and 2005 the stratification collapse was observed (Fig. 3), validating the model performance, while observations were missing for the winter of 1999.

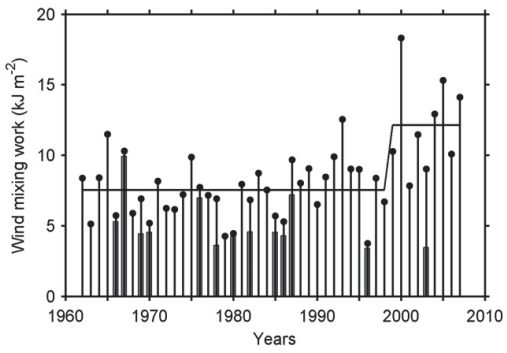

Fig. 8. Temporal course of wind mixing work over the period December–January (filled circles) calculated from the Utö weather station data for 1962–2007. The bold line corresponds to that in Fig. 7. Filled bars show wind mixing work over the period from the beginning of December until at least 50% of the western Gulf of Finland is covered by ice.

According to the model data, the low PEA periods were quite long, lasting several tens of days, and the along-basin extent of low PEA events was about 150 km (from about longitude 22° E to 25° E), which is considerably larger than the baroclinic Rossby deformation radius. According to these scale estimates, wintertime monitoring should be done with a weekly time interval, in order to avoid aliasing error. Unfortunately, historical monitoring was performed a few times per winter, while several years remained unsampled.

For full mixing of the water column, additional work of 5–7 kJ m^{-2} is needed to change the climatic situation. We assume that in the long-term average conditions, the PEA loss values over the water column $\langle\Delta\Phi_S\rangle \approx -6$ kJ m^{-2} and $\langle\Delta\Phi_W\rangle \approx -8$ kJ m^{-2} are balanced by PEA production due to the average freshwater discharge and average higher salinity/density of the inflowing open sea waters. For the collapse forcing criterion, we need to find the critical value of $\Delta\Phi_{cr}$ below which the PEA loss creates the event $\Delta\Phi_S + \Delta\Phi_w < \Delta\Phi_{cr}$. The best match with the observed cases was found for $\Delta\Phi_{cr} = -14$ kJ m^{-2}. Among the wintertime stratification observations in 23 winters during December and January, all the collapse cases satisfied this criterion, except for the winter of 1978. Therefore we consider that our approach to assessing the stratification collapses based only on the wind data is qualitatively workable.

Based on the episodic time series of wintertime stratification observations (Fig. 3), we have a very rough collapse frequency estimation: during 1975–1989, out of nine winters with available measurements, stratification collapse was evident during three winters, giving a collapse frequency of 1/3, whereas during 1990–2008 there were 14 observed winters, among which collapse was evident in seven, giving a frequency of 1/2. Within these low sample amounts, the frequency estimation is, however, quite arbitrary. The confidence of determination is increased by the inclusion of estimates of potential energy conversion from regular wind observations, presented above: we estimate an increase in wintertime collapse frequency from 40% to 60%.

4. Discussion and outlook

Although increased mixing in the Gulf of Finland has been briefly noted in several papers and data reports, the events of temporary stratification collapse have not received attention so far. The reasons for such ignorance could be (a) difficult wintertime sampling logistics due to ice cover and/or winter storms, and (b) problems of validating the numerical models in reproducing the short-term stratification events (except for upwelling, which is modelled adequately).

We have extended the knowledge from limited historical observations to the PEA changes using the relations to the wind forcing. One of the key findings is the approximate relation of PEA reduction to the impulse (cumulative wind stress) of westerly-southwesterly winds. This approach, derived from the EOF analysis of vertical current profiles and correlative relation of the "straining" EOF mode amplitude to the wind stress projection, is in agreement with earlier findings by Krauss and Brügge (1991). They found that the volume transported through the Stolpe Channel is proportional to the wind stress projected onto a specific (not necessarily along-channel) direction. For the Gulf of Finland, the importance of the southwesterly wind for the forcing of along-basin transport was discussed by Elken et al. (2003). While the deep transport is geostrophically adjusted to the cross-basin sea level slope over the deep area (generating the barotropic part of currents), the relation of the slope to the prevailing wind forcing remained unresolved in detail. In the present study we also had to use the site-specific constants in relation (7). Feng and Li (2010) have found that in estuaries with open mouths, both wind components cause nearly equal sea level changes. Their model is an extension of that by Garvine (1985). Forcing of sea level slopes in an elongated estuary has also been considered by Reyes-Hernandez and Valle-Levinson

(2010) and Hinata et al. (2010). These results partly explain the empirical wind direction relationship found and also motivate further studies of wind-forced motions in the Baltic Sea.

Considering the wintertime impulse of westerly-southwesterly winds, it becomes evident that a shift took place in 1989. The chosen cut-off length of 10 years ensures that the regimes whose duration exceeds this time interval will be detected with sufficient statistical confidence. The observed shift in wind regime supports the increase of temporary reversals of estuarine circulation in the Gulf of Finland. Such a change is caused by the larger scale climatic processes. Meier (2005) has found that average salinity of the Baltic is dependent on zonal winds: increase of westerly winds reduces average salinity. It is widely recognized that the western flow over northeast Europe has intensified during winter months. Keevallik (2011) has shown that this intensification can be partly ascribed to an abrupt increase in the upper-air zonal wind component in January and February around 1987. Such an increase is accompanied by a shift in the meteorological regime at the surface: during the period of 1987–1989 simultaneous shifts have taken place at the observation sites in Estonia, where the monthly mean zonal wind component, temperature, and precipitation have increased. Such findings are supported by other investigations that also suggest switch-like changes in meteorological regimes at the end of the 1980s (Kysely and Domonkos, 2006; Lehmann et al., 2011). Regarding the forcing of stratification collapse events by stronger winds and sea level gradients (of appropriate direction), further independent studies of the climatology of such forcing factors in the Gulf of Finland area in the context of large-scale patterns are needed.

The results in the present paper are based on the routine hydrography and wind observations and unfortunately lack any details of spatio-temporal features of stratification collapse events. Therefore several detailed studies of wintertime dynamics have just started or are in the planning phase. Consideration of the ecological effects of abrupt stratification dynamics is also of significant interest. During strong stratification, hypoxic conditions may develop near the bottom (Conley et al., 2009; Kahru et al., 2000; Laine et al., 2007), favouring the release of accumulated phosphorus from the sediments. But, how and by which processes is the new near-bottom phosphorus transported to the euphotic layer when the stratification is strong? Eventual collapse of stratification is likely to be one important process that brings the (before collapse) bottom-released nutrients back into the active ecological cycle, intensifying eutrophication and harmful algal blooms. On the other hand, if mixing throughout the water column is intensive over a longer period, hypoxia does not develop and benthic communities have favourable living conditions. We hypothesize that climatic change of the dominance of the two stratification collapse processes – wind-direction-dependent straining and direction-independent direct wind mixing – might have different consequences for the marine ecosystem health in the Gulf of Finland: the first one amplifying the eutrophication and the second one improving the living conditions for the benthic communities.

5. Conclusions

A measure of the stratification strength – potential energy anomaly (PEA) – has in the central and western parts of the Gulf of Finland an overall wintertime value of about 5 kJ m^{-2} per unit surface area of the water column of 70–80 m depth. There is some observational evidence that this PEA level could be balanced by the PEA production due to the freshwater discharge and inflow of open sea waters of higher salinity and density and by the PEA reduction due to the mixing at average forcing conditions. The PEA is occasionally reduced nearly to zero, manifesting the stratification collapse, when the wind mixing work and the work by wind-induced current straining (due to the up-estuary southwesterly winds) significantly exceed their average levels. On a bi-monthly scale, in December and January, the estimates for average work by straining and wind mixing are 6 and 8 kJ m^{-2}, respectively. These estimates are based on the observed time series of wind and the derived relations for PEA change. The relations are validated by the results from episodic hydrographic observations. During all the observed stratification collapse cases, the wind-dependent PEA reduction work, with reference to the long-term average work, exceeded the average PEA level. Since 1991, "overshoot" of PEA reduction compared to its average level increased, implying a longer duration of collapse events.

An analysis of wind data, using the derived and validated PEA relations, showed that since the 1990s the frequency of stratification collapse events and the duration of such events have both increased. This change is most probably related to an abrupt increase in the upper-air zonal wind component around 1987 in January and February over northeast Europe, which may form a significant part of the intensification of the western flow. As a result, since the late 1980s the winter season of the Baltic Sea area has tended to be warmer, with less ice cover and warmer sea surface temperatures. In Estonia, near the Gulf of Finland, an abrupt increase in the monthly mean zonal wind component and temperature has taken place in January and February.

Acknowledgements

The present study was initiated by the finding and interpretation of the "missing stratification" profiles, which were re-inspected in the course of preparing the model validation data set within the BONUS + ECOSUPPORT project. The study was supported by the Estonian Science Foundation grant nos. 7328 and 7467; the results were also used in the writing of the proposals for grant nos. 9278 and 9382 and preparing some results, the study was also supported by the Estonian national project "EstKliima".

References

Alenius, P., Myrberg, K., Nekrasov, A., 1998. The physical oceanography of the Gulf of Finland: a review. Boreal Environ. Res. 3, 97–125.
Alenius, P., Nekrasov, A., Myrberg, K., 2003. Variability of the baroclinic Rossby radius in the Gulf of Finland. Cont. Shelf Res. 23, 563–573.
Andrejev, O., Myrberg, K., Alenius, P., Lundberg, P.A., 2004. Mean circulation and water exchange in the Gulf of Finland — a study based on three-dimensional modelling. Boreal Environ. Res. 9, 9–16.
Blumberg, A.F., Goodrich, D.M., 1990. Modeling of wind-induced destratification in Chesapeake Bay. Estuaries 13 (3), 236–249.
Burchard, H., Hofmeister, R., 2008. A dynamic equation for the potential energy anomaly for analysing mixing and stratification in estuaries and coastal seas. Estuar., Coast. Shelf Sci. 77, 679–687.
Burchard, H., Bolding, K., Villarreal, M.R., 2004. Three-dimensional modelling of estuarine turbidity maxima in a tidal estuary. Ocean Dyn. 54, 250–265.
Conley, D.J., Björck, S., Bonsdorff, E., et al., 2009. Hypoxia-related processes in the Baltic Sea. Environ. Sci. Technol. 43, 3412–3420.
Dippner, J.W., Kornilovs, G., Junker, K., 2012. A multivariate Baltic Sea environmental index. Ambio. http://dx.doi.org/10.1007/s13280-012-0260-y.
Döscher, R., Wyser, K., Meier, H.E.M., Qian, M., Redler, R., 2010. Quantifying Arctic contributions to climate predictability in a regional coupled ocean–ice–atmosphere model. Clim. Dyn. 34, 1157–1176.
Elken, J., Raudsepp, U., Lips, U., 2003. On the estuarine transport reversal in deep layers of the Gulf of Finland. J. Sea Res. 49, 267–274.
Elken, J., Mälkki, P., Alenius, P., Stipa, T., 2006. Large halocline variations in the Northern Baltic Proper and associated meso- and basin-scale processes. Oceanologia 48 (S), 91–117.
Elken, J., Nõmm, M., Lagemaa, P., 2011. Circulation patterns in the Gulf of Finland derived from the EOF analysis of model results. Boreal Environ. Res. 16A, 84–102.
Feng, Z., Li, C., 2010. Cold-front-induced flushing of the Louisiana Bays. J. Mar. Syst. 82, 252–264.
Garvine, R.W., 1985. A simple model of estuarine subtidal fluctuations forced by local and remote wind stress. J. Geophys. Res. 90 (C6), 11945–11948.
Haapala, J., Alenius, P., 1994. Temperature and salinity statistics for the Northern Baltic Sea 1961–1990. Finn. Mar. Res. 262, 51–121.
Hagen, E., Feistel, R., 2005. Climatic turning points band regime shifts in the Baltic Sea region: the Baltic winter index (WIBIX) 1659–2002. Boreal Environ. Res. 10, 211–224.
Hansen, D.V., Rattray, M., 1966. New dimensions in estuary classification. Limnol. Oceanogr. 11 (3), 319–326.
Hinata, H., Kanatsu, N., Fujii, S., 2010. Dependence of wind-driven current on wind stress direction in a small semienclosed, homogeneous rotating basin. J. Phys. Oceanogr. 40, 1488–1500.

Hong, B., Panday, N., Shen, J., Wang, H.V., Gong, W., Soehl, A., 2010. Modeling water exchange between Baltimore Harbor and Chesapeake Bay using artificial tracers: seasonal variations. Mar. Environ. Res. http://dx.doi.org/10.1016/j.marenvres.2010.03.010.

IOC, SCOR, IAPSO, 2010. The International Thermodynamic Equation of Seawater — 2010: Calculation and Use of Thermodynamic Properties. Intergovernmental Oceanographic Commission, Manuals and Guides No. 56. UNESCO, Paris (English,196 pp., http://www.TEOS-10.org).

Janssen, F., Schrum, C., Backhaus, J., 1999. A climatological data set of temperature and salinity for the North Sea and the Baltic Sea. Dtsch. Hydrogr. Ztg. (Suppl. 9).

Kahru, M., Leppänen, J.M., Rud, O., Savchuk, O.P., 2000. Cyanobacteria blooms in the Gulf of Finland triggered by saltwater inflow into the Baltic Sea. Mar. Ecol. Prog. Ser. 207, 13–18.

Keevallik, S., 2011. Shifts in meteorological regime of the late winter and early spring in Estonia during recent decades. Theor. Appl. Climatol. 105 (1/2), 209–215.

Kimbro, D.L., Largier, J., Grosholz, E.D., 2009. Coastal oceanographic processes influence the growth and size of a key estuarine species, the Olympia oyster. Limnol. Oceanogr. 54 (5), 1425–1437.

Krauss, W., Brügge, B., 1991. Wind-produced water exchange between the deep basins of the Baltic Sea. J. Phys. Oceanogr. 21, 373–384.

Kullenberg, G., 1981. Physical oceanography. In: Voipoi, A. (Ed.), The Baltic Sea, 30. Elsevier Oceanography Series, pp. 135–218.

Kysely, J., Domonkos, P., 2006. Recent increase in persistence of atmospheric circulation over Europe: comparison with long-term variations since 1881. Int. J. Climatol. 26, 461–483.

Lagemaa, P., Elken, J., Kõuts, T., 2011. Operational sea level forecasting in Estonia. Estonian J. Eng. 17 (4), 301–331.

Laine, A.O., Andersin, A.B., Leinio, S., Zuur, A.F., 2007. Stratification-induced hypoxia as a structuring factor of macrozoobenthos in the open Gulf of Finland (Baltic Sea). J. Sea Res. 57, 65–77.

Lehmann, A., Krauss, W., Hinrichsen, H.H., 2002. Effects of remote and local atmospheric forcing on circulation and upwelling in the Baltic Sea. Tellus 54A, 299–319.

Lehmann, A., Getzlaff, K., Harlass, J., 2011. Detailed assessment of climate variability in the Baltic Sea area for the period 1958 to 2009. Clim. Res. 46, 185–196.

Lips, I., Lips, U., Liblik, T., 2009. Consequences of coastal upwelling events on physical and chemical patterns in the central Gulf of Finland (Baltic Sea). Cont. Shelf Res. 29, 1836–1847.

MacCready, P., Geyer, W.R., 2010. Advances in estuarine physics. Ann. Rev. Mar. Sci. 2, 35–58.

Maljutenko, I., Laanemets, J., Raudsepp, U., 2010. Long-term high-resolution hydrodynamical model simulation in the Gulf of Finland. Baltic International Symposium (BALTIC), 2010 IEEE/OES US/EU, 24–27 August 2010, Riga. http://dx.doi.org/10.1109/BALTIC.2010.5621641.

Matthäus, W., 1984. Climatic and seasonal variability of oceanological parameters in the Baltic Sea. Beiträge zur Meereskunde 51, 29–49.

Matthäus, W., Frank, H., 1992. Characteristics of major Baltic inflows — a statistical analysis. Cont. Shelf Res. 12, 1375–1400.

Meier, H.E.M., 2005. Modeling the age of Baltic Seawater masses: quantification and steady state sensitivity experiments. J. Geophys. Res. 110. http://dx.doi.org/10.1029/2004JC002607.

Meier, H.E.M., Feistel, R., Piechura, J., Arneborg, L., Burchard, H., Fiekas, V., Golenko, N., Kuzmina, N., Mohrholz, V., Nohr, C., Paka, V.T., Sellschopp, J., Stips, A., Zhurbas, V., 2006. Ventilation of the Baltic Sea deep water: a brief review of present knowledge from observations and models. Oceanologia 48, 133–164.

Pärn, O., Haapala, J., 2011. Occurrence of synoptic flaw leads of sea ice in the Gulf of Finland. Boreal Environ. Res. 16, 71–78.

Passenko, J., Lessin, G., Raudsepp, U., Maljutenko, I., Neumann, T., Laanemets, J., 2010. Analysis of temporal variability of measured and modeled vertical distributions of salinity and temperature in the Gulf of Finland during 10-year period. Baltic International Symposium (BALTIC), 2010 IEEE/OES US/EU, 24–27 August 2010, Riga. http://dx.doi.org/10.1109/BALTIC.2010.5621648.

Pavelson, J., Laanemets, J., Kononen, K., Nõmmann, S., 1997. Quasi-permanent density front at the entrance to the Gulf of Finland: Response to wind forcing. Cont. Shelf Res. 17, 253–265.

Reissmann, J.H., Burchard, H., Feistel, R., Hagen, E., Lass, H.U., Mohrholz, V., Nausch, G., Umlauf, L., Wieczorek, G., 2009. Vertical mixing in the Baltic Sea and consequences for eutrophication — a review. Prog. Oceanogr. 82, 47–80.

Reyes-Hernandez, C., Valle-Levinson, A., 2010. Wind modifications to density-driven flows in semienclosed, rotating basins. J. Phys. Oceanogr. 40, 1473–1487.

Rodionov, S.N., 2004. A sequential algorithm for testing climate regime shifts. Geophys. Res. Lett. 31. http://dx.doi.org/10.1029/2004GL019448.

Scully, M.E., Friedrichs, C., Brubaker, J., 2005. Control of estuarine stratification and mixing by wind-induced straining of the estuarine density field. Estuaries 28 (3), 321–326.

Seifert, T., Tauber, F., Kayser, B., 2001. A high resolution spherical grid topography of the Baltic Sea, Baltic Sea Science Congress, Stockholm, 25–29 November 2001. (Poster No. 147, Abstr. Vol.) 2nd edn. (http://www.io-warnemuende.de/iowtopo).

Simpson, J.H., 1981. The shelf-sea fronts: implications of their existence and behaviour. Philos. Trans. R. Soc. Lond. Ser. A 302, 531–546.

Simpson, J.H., Brown, J., Matthews, J., Allen, G., 1990. Tidal straining, density currents, and stirring in the control of estuarine stratification. Estuaries 13 (2), 125–132.

Soomere, T., Keevallik, S., 2003. Directional and extreme wind properties in the Gulf of Finland. Proc. Est. Acad. Sci. Eng. 9 (2), 73–90.

van Aken, H.M., 2008. Variability of the salinity in the western Wadden Sea on tidal to centennial time scales. J. Sea Res. 59, 121–132.

Vermaat, J.E., Bouwer, L.M., 2009. Less ice on the Baltic reduces the extent of hypoxic bottom waters and sedimentary phosphorus release. Estuar., Coast. Shelf Sci. 82, 689–691.

Voss, M., Dippner, J.W., Humborg, C., Hürdler, J., Korth, F., Neumann, T., Schernewski, G., Venohr, M., 2011. History and scenarios of future development of Baltic Sea eutrophication. Estuar., Coast. Shelf Sci. 92, 307–322.

Wang, B., Giddings, S.N., Fringer, O.B., Gross, E.S., Fong, D.A., Monismith, S.G., 2011. Modeling and understanding turbulent mixing in a macrotidal salt wedge estuary. J. Geophys. Res. 116. http://dx.doi.org/10.1029/2010JC006135.

Zhang, Z., Leppäranta, M., 1995. Modeling the influence of ice on sea level variations in the Baltic Sea. Geophysica 31 (2), 31–45.

Zhurbas, V., Laanemets, J., Vahtera, E., 2008. Modeling of the mesoscale structure of coupled upwelling/downwelling events and the related input of nutrients to the upper mixed layer in the Gulf of Finland, Baltic Sea. J. Geophys. Res. 113. http://dx.doi.org/10.1029/2007JC004280.

Paper V

Raudsepp U, Legeais J-F, She J, Maljutenko I, Jandt S. 2018. Baltic Inflows. In: von Schuckmann K, Pierre-Yves Le T, Smith N, Pascual A, Brasseur P, Fennel K, Djavidnia S, editors. Copernicus Marine Service Ocean State Report, Issue 2. Journal of Operational Oceanography. p. 107–111. (1.1)

Taylor & Francis
Taylor & Francis Group

Journal of Operational Oceanography

ISSN: 1755-876X (Print) 1755-8778 (Online) Journal homepage: http://www.tandfonline.com/loi/tjoo20

Copernicus Marine Service Ocean State Report

Karina von Schuckmann, Pierre-Yves Le Traon, Neville Smith (Chair), Ananda Pascual, Pierre Brasseur, Katja Fennel & Samy Djavidnia

To cite this article: Karina von Schuckmann, Pierre-Yves Le Traon, Neville Smith (Chair), Ananda Pascual, Pierre Brasseur, Katja Fennel & Samy Djavidnia (2018) Copernicus Marine Service Ocean State Report, Journal of Operational Oceanography, 11:sup1, S1-S142, DOI: 10.1080/1755876X.2018.1489208

To link to this article: https://doi.org/10.1080/1755876X.2018.1489208

Published online: 08 Sep 2018.

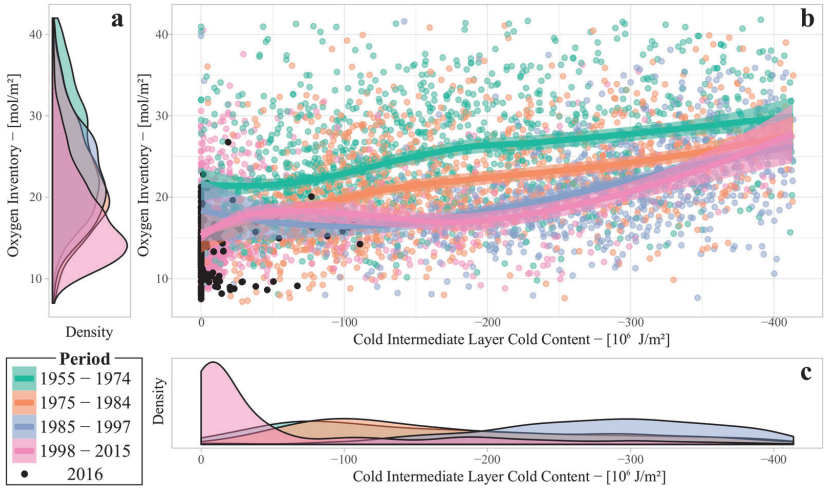

Figure 3.6.3. Estimates of the probability density function for (a) oxygen inventory and (c) cold content within the Cold Intermediate Layer, which is a proxy for convective dense water formation. Panel (b) highlights the ventilating role of cold water formation by depicting the relationship between cold water and oxygen content. Black dots locate the 2016 Argo profiles on this diagram.

is an urgent need to evaluate at regional and national levels the risk and consequences of further deoxygenation, and to measure the impact of global warming by quantifying the sources and sinks of the Black Sea oxygen budget and their respective variability. In particular, large fishes are known to avoid suboxic conditions (Stramma et al. 2012). In the Black Sea, studies suggest that zooplankton migrate to remain in oxic waters (Ostrovskii and Zatsepin 2011). We therefore suggest that habitat compression may have affected the Black Sea trophic web. Yet, to our present knowledge, the possible impact of deoxygenation-related habitat compression on Black Sea fisheries has not been documented.

3.7. Baltic inflows

Leading authors: Urmas Raudsepp, Jean-Francois Legeais, Jun She

Contributing authors: Ilja Maljutenko, Simon Jandt.

Statement of outcome: Major Baltic Inflows (MBI), which usually occur many years apart, bring saline and oxygenated water to the dead zones of the Baltic Sea. The MBI in December 2014 improved the bottom oxygen conditions in the Gotland Basin, but the oxygen concentrations started to decline quite rapidly after the inflow. More persistent salinity stratification favoured the saline and oxygenated water of the following inflows in winters 2016 and 2017, not even categorised as MBIs, to be easily transported to the downstream basins. The mean sea level of the Baltic Sea derived from satellite altimetry data can be used as proxy for the detection of saline water inflows to the Baltic Sea from the North Sea.

Products used:

Ref. No.	Product name & type	Documentation
3.7.1	BALTICSEA_ANALYSIS_FORECAST_PHYS_003_006 Model	PUM: http://marine.copernicus.eu/documents/PUM/CMEMS-BAL-PUM-003-006.pdf QUID: http://cmems-resources.cls.fr/documents/QUID/CMEMS-BAL-QUID-003-006.pdf
3.7.2	INSITU_BAL_NRT_OBSERVATIONS_013_032 *In situ*	PUM: http://marine.copernicus.eu/documents/PUM/CMEMS-INS-PUM-013.pdf QUID: http://marine.copernicus.eu/documents/QUID/CMEMS-INS-QUID-013-030-036.pdf
3.7.3	Merged sea level maps from Copernicus Climate Change Service (C3S)	http://climate.copernicus.eu/climate-data-store

The saline water inflows to the Baltic Sea through the Danish straits, especially the Major Baltic Inflows (MBI), shape hydrophysical conditions in the Baltic Sea, which in turn have a substantial influence on marine ecology. However, along with bringing oxygenated water to the dead zones of the Baltic Sea the displacement of old stagnated water can cause temporary anoxic conditions in the bottom layers of shallow downstream basins. The numerical experiments conducted by Lessin et al. (2014) have shown that absence of oxygenated saline inflows increased anoxia in the deep Gotland Basin of the Baltic Sea (see Figure 3.7.1(a) for geographical locations), while oxygen conditions in the Gulf of

Finland (shallower downstream basin) improve due to weaker vertical stratification. The MBI in December 2014, which reached the Gotland Basin in March 2015 (Raudsepp et al. 2016) improved the bottom oxygen conditions there, but the effect was temporary (Neumann et al. 2017).

The MBIs occur seldom, usually many years apart, (e.g. Matthäus and Franck 1992; Schimanke et al. 2014) being initiated by a special sequence of large-scale meteorological events (Schinke and Matthäus 1998), p. 1) prior to the inflow, in many cases, there is an outflow from the Baltic Sea and a decrease of the mean sea level in response to the easterly winds and barotropic pressure gradient from the Arkona Basin towards the Kattegat (Mohrholz et al. 2015, p. 2) the following change of easterly winds to westerlies causes the inflow of saline water to the Baltic Sea and the increase of the mean sea level (Lass & Matthäus 1996).

Lehmann et al. (2017) have defined large volume changes (LVC) of the Baltic Sea as a change between local minimum and maximum sea level at the Landsort (Figure 3.7.1(a)) over a certain time period, subtracted by the corresponding runoff over the same period, with the predefined threshold of 60 km^3. Not all LVCs are categorised as MBIs. Thus, LVCs/MBIs can be qualitatively expressed as a sequence of sea level changes consisting of 'decrease-increase' pattern of the Baltic mean sea level.

We use time series of the mean sea level averaged over the Baltic Sea area (including Kattegat at 57.5°N and from 10.5°E to 12°E) from product reference 3.7.3, and compare these basin wide changes with the bottom salinity of the Arkona Basin and Bornholm Basin from Copernicus Marine and Environment Monitoring Service (NRT CMEMS) product (3.7.1). The mean sea level time series has been computed with the altimeter two-satellites merged sea level maps produced by the

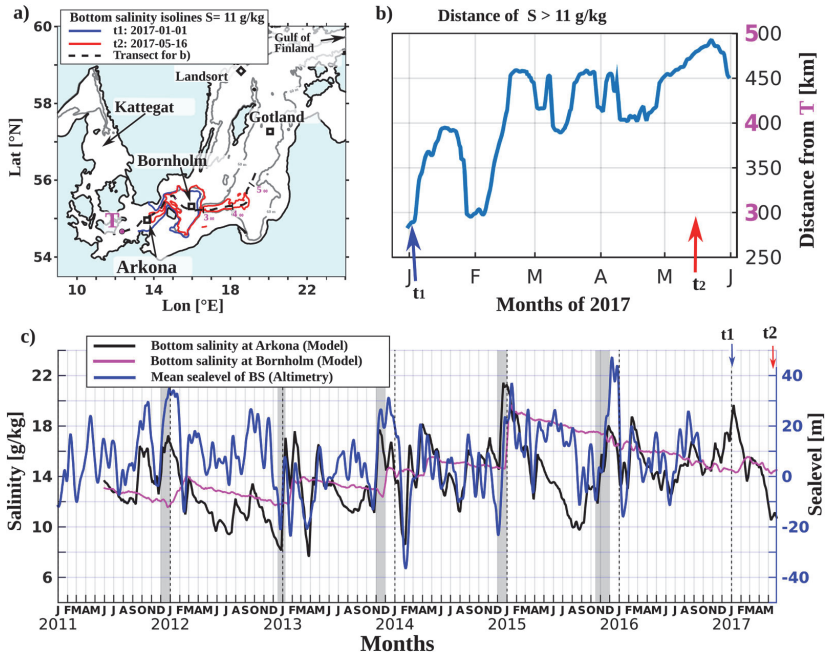

Figure 3.7.1. (a) Map of the Southern Baltic Sea showing locations of the basins. 60 m isodepth is marked with grey line. Blue and red contours show isohalines of the bottom salinities from the regional NRT CMEMS product (3.7.1) for the 1st January (t1) and for the 16th May (t2) of the year 2017. (b) Time series of the maximum distance of the water with salinity greater than 11 g/kg. The distance is shown along the black dashed line starting from point T on subplot (a). Dates t1 and t2 with arrows correspond to dates t1 and t2 on subplots (a) and (c). (c) Time series of basin wide daily mean sea level of the Baltic Sea area derived from the satellite data product (3.7.3) and bottom salinity in the Arkona and Bornholm Basins from the regional NRT CMEMS product reference 3.7.1, smoothed using a 12 day running mean. The grey shaded areas correspond to the winter periods when rapid sea level changes and subsequent inflows occurred. Dates t1 and t2 with arrows correspond to dates t1 and t2 on subplots (a) and (b).

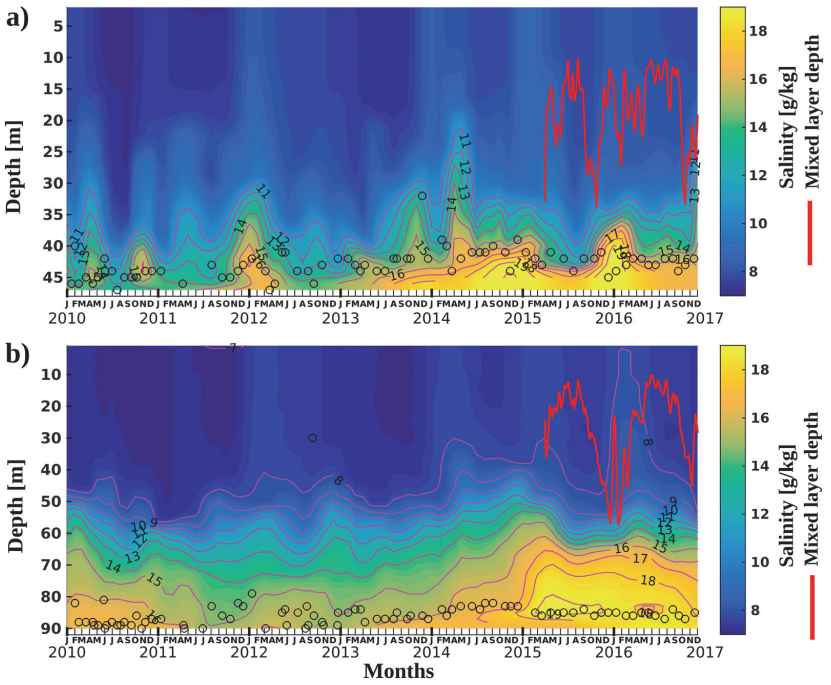

Figure 3.7.2. Hovmöller diagram (time-depth) of salinity in (a) the Arkona Basin and (b) Bornholm Basin from *in situ* measurements product reference 3.7.2. Black circles show the locations of the deepest measurements at specific date. Red line shows the depth of the mixed layer (smoothed using a 14 day running mean) calculated using modelled density from the product reference 3.7.2 at the respective locations.

Copernicus Climate Change Service (C3S) (product reference 3.7.3).

The saline water inflows, i.e. increase of bottom salinity in the Arkona Basin, are pronounced in late autumn and winter (Figure 3.7.1(c) and Figure 3.7.2 (a)), which is consistent with the previous results on the temporal occurrence of LVCs (Lehmann et al. 2017). The abrupt change of mean sea level from decrease to increase is evident during the winter inflows (shaded areas in Figure 3.7.1(c)). The salinity signal of winter inflows can be traced downstream to the Bornholm Basin every year (Figures 3.7.1(c) and 3.7.2 (b)). There are two exceptional cases: 1) increase of bottom salinity in the Bornholm Basin in May 2014 next to the salinity increase due to inflow in 2013/2014; 2) absence of the bottom salinity increase following the inflow in winter 2015/2016 (Figure 3.7.1(c)). The former case corresponds to the exceptionally low mean sea level in February 2014 (Figure 3.7.1(c)). Afterwards the Arkona Basin was filled in with saline water (Figure 3.7.2(a)), a part of which spread to the Bornholm Basin (Figure 3.7.2(b)). In the latter case, the bottom layer of the Bornholm Basin was already filled in with the saline water that entered the Arkona Basin (Figures 3.7.1(c), 3.7.2(a) and 3.7.2(b)). In that case, we suggest that water transported to the Bornholm Basin slipped over the saline water beneath there.

The smaller inflows in 2011/2012 and earlier did not reach the Gotland Basin. The 2013/2014 winter inflow resulted in a bottom layer salinity increase from 15.5 to 16.5 g/kg in the Bornholm Basin (Figure 3.7.2(b)). The salinity started to increase in the Gotland Basin since February 2014 (Figure 3.7.3(a)). The main water masses of the MBI in December 2014 filled the Bornholm Basin on the 26th of December 2014 with maximum salinity of 19.5 g/kg and reached the Gotland Basin in March 2015 (Raudsepp et al. 2016). Neumann et al. (2017) report that maximum oxygen concentrations were measured at the beginning of April in 2015. There is a data gap of bottom layer oxygen in April and May 2015 in *in situ* measurements, product reference 3.7.2. Yet, the measurements show that oxygen conditions improved in the deep layer between about 140 m and the bottom (Figure 3.7.3(c)) in 2015. There was still an anoxic intermediate layer between 80 and 140 m. Anoxic conditions reappeared by the end of December 2015, which is

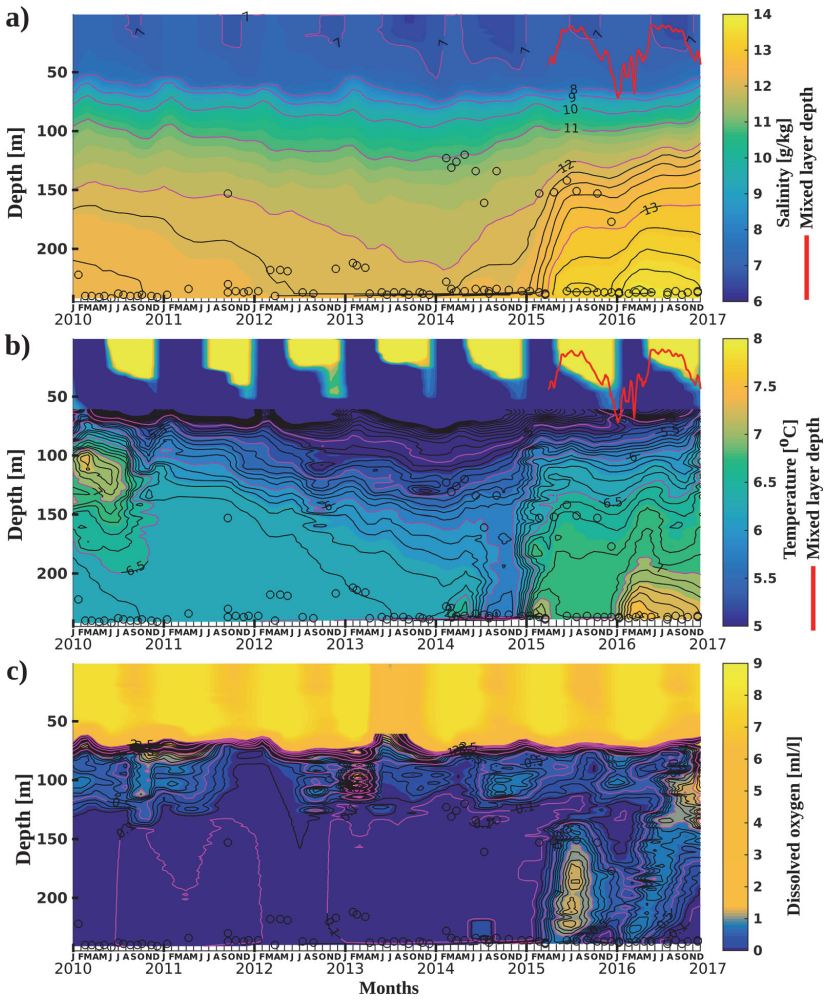

Figure 3.7.3. Hovmöller diagram (time-depth) of (a) salinity, (b) temperature and (c) dissolved oxygen concentration in the Gotland Basin from the in situ measurements product reference 3.7.2. Black circles show the locations of the deepest measurements at specific date. Time series of the mixed layer depth (smoothed using a 14 day running mean) at the Gotland Basin calculated from modelled density in the product reference 3.7.2 are superposed with red line.

consistent with the result by Neumann et al. (2017), who reported almost zero oxygen concentrations in November 2015. In time, oxygen concentrations started to decline simultaneously from the intermediate anoxic layer and the bottom. The former suggests the effect of water advection in the intermediate layer from adjacent areas where anoxic water was pushed by inflowing water. The latter indicates potential effect of local biogeochemical processes. Myllykangas et al. (2017) reported strong aerobic oxidation rates for CH_4 below 70 m in the Gotland Deep, depleting the oxygen pool by August 2015. Hypoxic conditions initiated nitrification and denitrification processes, which led to high N_2O concentration in the Gotland Deep.

The small inflow events that follow the main MBI are very important for improved oxygen conditions in the deep basins of the Baltic Sea, as emphasised by Neumann et al. (2017). The salinity stratification showed rather persistent pattern over the year of 2015 in the Bornholm and Gotland Basin (Figures 3.7.2(b) and 3.7.3(a)). Thus, the MBI in December 2014 filled the deep basins of the Baltic Sea, which enabled the dense salty water of the

following inflows, not even categorised as MBIs, to be easily transported to the downstream basins.

Consequently, smaller inflows in December 2015 and in February 2016 as indicated by time series of mean sea level and bottom salinity in the Arkona Basin (Figure 3.7.1(b)) could supply saline and oxygenated water to the downstream basins. Since the beginning of 2016 the bottom salinity and oxygen concentration started to increase in the Gotland Basin (Figure 3.7.3(c)). Bottom salinity reached values of 14 g/kg and oxygen conditions improved. The oxygen concentrations remained lower than during the inflow in December 2014, but extended vertically to the permanent halocline. The peculiarity of the inflow in 2015/2016 was the much higher temperature of the saline water reaching the Gotland Basin, when compared to the previous case (Figure 3.7.3(b)). The latter may indicate that the water that reached the Gotland Basin may not be completely fresh from the North Sea. Oxygen concentrations started to decline quite rapidly after the inflow (Figure 3.7.3(c)). The decline started in the bottom layer and extended upward in time, which indicates the effect of local biogeochemical processes. Besides being important for supplying of fresh oxygenated water with high density to the Baltic Sea, the inflows have an effect on vertical stratification of the Baltic Sea sub-basins. Being important in determination of the halocline depth and the stratification beneath, the inflows affect even the temporal changes of the mixed layer depth (MLD). In the Bornholm and Gotland Basin the MLD has well defined seasonal cycle, while in the Arkona Basin frequent inflows may surpass seasonal changes (Figures 3.7.2 and 3.7.3).

Our study shows that the mean sea level of the Baltic Sea derived from satellite altimetry data can be used as proxy for the detection of saline water inflows to the Baltic Sea from the North Sea. Relative changes of the mean sea level between local minimum and maximum could be used as an indicator of the strength of the Baltic inflows and, in the future in conjunction with numerical modelling and *in situ* measurements, for the prediction of vertical stratification, deep water oxygen conditions and marine ecology in the Baltic Sea. However, it should be kept in mind that the Baltic Sea is a region where the uncertainty of the altimeter sea level measurements is particularly high because of the errors of the instrument and the altimeter geophysical corrections and also due to the large internal variability of the observed ocean (see Section 1.5). Recent measurements at the MARNET station in the Arkona Basin show an inflow in January 2017 with instantaneous maximum salinity of 23–25 g/kg (not shown). As saline water is still present in the deep layers of downstream basins, the inflow in 2016/2017 could contribute to the following oxygenation of the bottom water in the Gotland Basin. Operational models with their NRT products could be a valuable tool to observe the pathways of inflowing water and the changes of oxygen conditions in the Baltic Sea. Preliminary results from the CMEMS NRT model (product reference 3.7.1) show spreading of 2016/2017 inflow water into the southern Gotland Basin (Figure 3.7.1(a,b)).

3.8. Eutrophication and hypoxia in the Baltic Sea

Leading authors: Urmas Raudsepp, Jun She.

Contributing authors: Vittorio E. Brando, Mariliis Kõuts and Priidik Lagemaa, Michela Sammartino, Rosalia Santoleri.

Statement of outcome: HELCOM assessment characterises the Baltic Sea as a eutrophicated marine area, which is caused by a combination of anthropogenic over-enrichment and climate change. Nutrient inputs have decreased in the last two decades but no decline in eutrophication effects has been documented with high concentrations of chlorophyll-a still observed every summer. Hypoxia is one of the most severe consequences of eutrophication. While Major Baltic Inflows bring new, oxygen enriched water into the deep areas of Baltic Sea, the conditions are improved only for a short period, as was the case in the study period of 2014–2016.

Products used:

Ref. No.	Product name & type	Documentation
3.8.1	OCEANCOLOUR_BAL_CHL_L3_REP_OBSERVATIONS_009_080 Remote sensing	PUM: http://marine.copernicus.eu/documents/PUM/CMEMS-OC-PUM-009-ALL.pdf QUID : http://marine.copernicus.eu/documents/quid/cmems-oc-quid-009-080-097.pdf
3.8.2	OCEANCOLOUR_BAL_OPTICS_L3_REP_OBSERVATIONS_009_097 Remote sensing	PUM: http://marine.copernicus.eu/documents/PUM/CMEMS-OC-PUM-009-ALL.pdf QUID: http://marine.copernicus.eu/documents/quid/cmems-oc-quid-009-080-097.pdf
3.8.3	BALTICSEA_ANALYSIS_FORECAST_BIO_003_007 Model	PUM: http://marine.copernicus.eu/documents/PUM/CMEMS-BAL-PUM-003-007.pdf QUID: http://marine.copernicus.eu/documents/QUID/CMEMS-BAL-QUID-003-007.pdf

Eutrophication in the Baltic Sea is mainly caused by anthropogenic enrichment of the nutrients as well as climate change (HELCOM 2014). The nutrient over-

Mediterranean outflow. Geophys Res Lett. 44:5665–5672. doi:10.1002/2017GL072615.
Sammartino S, García Lafuente J, Naranjo C, Sánchez Garrido JC, Sánchez Leal R, Sánchez Román A. 2015. Ten years of marine current measurements in Espartel Sill, Strait of Gibraltar. J Geophys Res Ocean. 120.
Schroeder K, Chiggiato J, Bryden HL, Borghini M, Ben Ismail S. 2016. Abrupt climate shift in the Western Mediterranean Sea. Sci Rep. 6:23009. http://www.ncbi.nlm.nih.gov/pmc/articles/PMC4786855/.
Schroeder K, Ribotti A, Borghini M, Sorgente R, Perilli A, Gasparini GP. 2008. An extensive western Mediterranean deep water renewal between 2004 and 2006. Geophys Res Lett. 35:L18605. doi:10.1029/2008GL035146.
Simoncelli S, Fratianni C, Pinardi N, Grandi A, Drudi M, Oddo P, Dobricic S. 2014. Mediterranean Sea physical reanalysis (MEDREA 1987-2015) (version 1) [dataset]. Copernicus Monitoring Environment Marine Service (CMEMS). doi:10.25423/medsea_reanalysis_phys_006_004.
Zunino P, Schroeder K, Vargas-Yáñez M, Gasparini GP, Coppola L, García-Martínez MC, Moya-Ruiz F. 2012. Effects of the Western Mediterranean transition on the resident water masses: pure warming, pure freshening and pure heaving. J Mar Syst. 96:15–23. http://www.sciencedirect.com/science/article/pii/S0924796312000280.

Section 3.6

Capet A, Stanev E, Beckers JM, Murray J, Grégoire M. 2016. Decline of the Black Sea oxygen inventory. Biogeosciences. 13:1287–1297.
Capet A, Troupin C, Carstensen J, Grégoire M, Beckers JM. 2014. Untangling spatial and temporal trends in the variability of the Black Sea cold intermediate layer and mixed layer depth using the DIVA detrending procedure. Oce Dyn. 64(3):315–324.
Garcia HE, Locarnini RA, Boyer TP, Antonov JI, Mishonov AV, Baranova OK, Zweng MM, Reagan JR, Johnson JR. 2013. World Ocean Atlas 2013. Vol. 3: dissolved oxygen, apparent oxygen utilization, and oxygen saturation. S. Levitus, editor; Mishonov A, Technical editors. NOAA Atlas NESDIS 75, 27 pp.
Jaccard P, Norli M, Ledang AB, Hjermann DØ, Reggiani E R, Sørensen K, Wehde H, Kaitala S, Folkestad A. 2015. Real time quality control of biogeochemical measurements, version 2.5. My Ocean document.
Konovalov S, Murray JW. 2001. Variations in the chemistry of the Black Sea on a time scale of decades (1960–1995). J Marine Syst. 31:217–243.
Murray J, Jannasch H, Honjo S, Anderson R, Reeburgh W, Top Z, Friederich G, Codispoti L, Izdar E. 1989. Unexpected changes in the oxic/anoxic interface in the Black Sea. Nature. 338:411–413.
Ostrovskii A, Zatsepin A. 2011. Short-term hydrophysical and biological variability over the northeastern Black Sea continental slope as inferred from multiparametric tethered profiler surveys. Ocean Dyn. 61:797–806.
Özsoy E, Ünlüata Ü. 1997. Oceanography of the Black Sea: a review of some recent results. Earth Sci Rev. 42(4):231–72.
Schmechtig C, Thierry V and the Bio Argo Team. 2015. Argo quality control manual for biogeochemical data. doi:10.13155/40879.
Stanev E, He Y, Grayek S, Boetius A. 2013. Oxygen dynamics in the Black Sea as seen by Argo profiling floats. Geophys Res Lett. 40(12):3085–3090.
Stramma L, Prince ED, Schmidtko S, Luo J, Hoolihan JP, Visbeck M, Wallace DW, Brandt P, Körtzinger A. 2012. Expansion of oxygen minimum zones may reduce available habitat for tropical pelagic fishes. Nat Clim Change. 2 (1):33–7.
Tugrul S, Basturk O, Saydam C, Yilmaz A. 1992. Changes in the hydrochemistry of the Black Sea inferred from water density profiles. Nature. 359:137–139.

Section 3.7

Lass HU, Matthäus W. 1996. On temporal wind variations forcing salt water inflows into the Baltic Sea. Tellus A. 48:663–671.
Lehmann A, Höflich K, Post P, Myrberg K. 2017. Pathways of deep cyclones associated with large volume changes (LVCs) and major Baltic inflows (MBIs). J Mar Syst. 167:11–18.
Lessin G, Raudsepp U, Stips A. 2014. Modelling the influence of major Baltic inflows on near-bottom conditions at the entrance of the Gulf of Finland. PLoS ONE. 9(11):e112881.
Matthäus W, Franck H. 1992. Characteristics of major Baltic inflows – a statistical analysis. Cont Shelf Res. 12:1375–1400.
Mohrholz V, Naumann M, Nausch G, Krüger S, Gräwe U. 2015. Fresh oxygen for the Baltic Sea – an exceptional saline inflow after a decade of stagnation. J Mar Syst. 148:152–166.
Myllykangas J-P, Jilbert T, Jakobs G, Rehder G, Werner J, Hietanen S. 2017. Effects of the 2014 major baltic inflow on methane and nitrous oxide dynamics in the water column of the Central Baltic Sea. Earth Syst Dynam Discuss. doi:10.5194/esd-2017-14.
Neumann T, Radtke H, Seifert T. 2017. On the importance of Major Baltic Inflows for oxygenation of the central Baltic Sea. J Geophys Res Oceans. 122:1090–1101.
Raudsepp U, Axell L, Almoroth-Rosell E, Viktorsson L. 2016. Baltic Sea. In: von Schuckmann K. et al. 2016. The Copernicus Marine Environment Monitoring Service ocean state report. J Oper Oceanogr. 9 Suppl:S235–320.
Schimanke S, Dieterich C, Meier HEM. 2014. An algorithm based on sea-level pressure fluctuations to identify major Baltic inflow events. Tellus A. 66:21.
Schinke H, Matthäus W. 1998. On the causes of major Baltic inflows – an analysis of long time series. Cont Shelf Res. 18:67–97.

Section 3.8

Brewin R, Sathyendranath S, Müller D, Brockmann C, Deschamps P-Y, Devred E, Doerffer R, Fomferra N, Franz B, Grant M, et al. 2015. The ocean colour climate change initiative: III. A round-robin comparison on in-water bio-optical algorithms. Remote Sens. Environ. 162:271–294. doi:10. 1016/j.rse.2013.09.016.
Carstensen J, Sanchez-Camacho M, Duarte CM, Krause-Jensen D, Marbà N. 2011. Connecting the dots: responses of coastal ecosystems to changing nutrient concentrations. Environ Sci Technol. 45:9122–9132.
Funkey CP, Conley DJ, Reuss NS, Humborg C, Jilbert T, Slomp CP. 2014. Hypoxia sustains cyanobacteria blooms in the Baltic Sea. Environ Sci Technol 48:2598–2602.

Curriculum vitae

Personal data

Name:	Ilja Maljutenko
Date of birth:	03.12.1986
Place of birth:	Russia
Citizenship:	Estonian

Contact

E-mail:	ilja.maljutenko@taltech.ee

Education

2011–2019	Tallinn University of Technology, Earth Sciences — PhD
2009–2011	Tallinn University of Technology, Earth Sciences — MSc
2006–2009	Tallinn University of Technology, Engineering Physics — BSc
2003–2006	Tallinn Nõmme Gymnasium, High school

Language competence

Estonian:	Native speaker
English:	Fluent
Russian:	Intermediate

Professional employment

2017–	Tallinn University of Technology, Department of Marine Systems, Junior Researcher
2011–2016	Tallinn University of Technology, Marine Systems Institute, Junior Researcher
2009–2011	Tallinn University of Technology, Marine Systems Institute, Technician

Supervised theses

2017	Joann Gustav Arro	BSc thesis, defended in Tallinn University of Technology
2016	Meri Liis Treimann	BSc thesis, defended in Tartu University
2015	Marili Viitak	MSc thesis, defended in Tallinn University of Technology

Scientific work

1.1 *(Articles indexed by the ISI WEB of Science)*

Maljutenko I, Raudsepp U. 2019. Long-term mean, interannual and seasonal circulation in the Gulf of Finland — The wide salt wedge estuary or gulf type ROFI. J Mar Syst 195:1–19. Elsevier. doi:10.1016/J.JMARSYS.2019.03.004

Raudsepp U, Maljutenko I, Kõuts M, Granhag L, Wilewska-Bien M, Hassellöv I-M, Eriksson KM, Johansson L, Jalkanen J-P, Karl M, et al. 2019. Shipborne nutrient dynamics and impact on the eutrophication in the Baltic Sea. Sci Total Environ 671:189–207. The Authors. doi:10.1016/j.scitotenv.2019.03.264

Raudsepp U, Legeais J-F, She J, Maljutenko I, Jandt S. 2018. Baltic Inflows. In: von Schuckmann K, Pierre-Yves Le T, Smith N, Pascual A, Brasseur P, Fennel K, Djavidnia S, editors. *Copernicus Marine Service Ocean State Report,*Issue 2. Journal of Operational Oceanography. p. 107–111.

Kotta J, Herkül K, Jaagus J, Kaasik A, Raudsepp U, Alari V, Arula T, Haberman J, Järvet A, Kangur K, et al. 2018. Linking atmospheric, terrestrial and aquatic environments: Regime shifts in the Estonian climate over the past 50 years. PLoS One 13(12). doi:10.1371/journal.pone.0209568

Sildever S, Kremp A, Enke A, Buschmann F, Maljutenko I, Lips I. 2017. Spring bloom dinoflagellate cyst dynamics in three eastern sub-basins of the Baltic Sea. Cont Shelf Res 137:46–55. doi:10.1016/j.csr.2016.11.012

Viitak M, Maljutenko I, Alari V, Suursaar Ü, Rikka S, Lagemaa P. 2016. The impact of surface currents and sea level on the wave field evolution during St. Jude storm in the eastern Baltic Sea. Oceanologia 58(3). doi:10.1016/j.oceano.2016.01.004

Soosaar E, Maljutenko I, Uiboupin R, Skudra M, Raudsepp U. 2016. River bulge evolution and dynamics in a non-tidal sea – Daugava River plume in the Gulf of Riga, Baltic Sea. Ocean Sci 12(2):417–432. doi:10.5194/os-12-417-2016

Erm A, Maljutenko I, Buschmann F, Suhhova I, Meerits A. 2014. Stormwater impact on the coastal area of the Tallinn Bay. 2014 IEEE/OES Baltic International Symposium (BALTIC):1–15. IEEE. doi:10.1109/BALTIC.2014.6887867

Lessin G, Raudsepp U, Maljutenko I, Laanemets J, Passenko J, Jaanus A. 2014. Model study on present and future eutrophication and nitrogen fixation in the Gulf of Finland, Baltic Sea. J Mar Syst 129:76–85. Elsevier B.V. doi:10.1016/j.jmarsys.2013.08.006

Erm A, Maljutenko I, Buschmann F, Suhhova I, Meerits A. 2014. Stormwater impact on the coastal area of the Tallinn Bay. Measuring and Modeling of Multi-Scale Interactions in the Marine Environment - IEEE/OES Baltic International Symposium 2014, BALTIC 2014. doi:10.1109/BALTIC.2014.6887867

Elken J, Raudsepp U, Laanemets J, Passenko J, Maljutenko I, Pärn O, Keevallik S. 2014. Increased frequency of wintertime stratification collapse events in the Gulf of Finland since the 1990s. J Mar Syst 129:47–55. Elsevier B.V. doi:10.1016/j.jmarsys.2013.04.015

Soosaar E, Maljutenko I, Raudsepp U, Elken J. 2014. An investigation of anticyclonic circulation in the southern Gulf of Riga during the spring period. Cont Shelf Res 78:75–84. Elsevier. doi:10.1016/j.csr.2014.02.009

Raudsepp U, Laanemets J, Maljutenko I, Hongisto M, Jalkanen J. 2013. Impact of ship-borne nitrogen deposition on the Gulf of Finland ecosystem : an evaluation. Oceanologia 55(4):1–21. doi:10.5697/oc.55-3.000

3.1 *(Articles in proceedings indexed by the ISI WEB of Science)*

Maljutenko I, Raudsepp U. 2014. Validation of GETM model simulated long-term salinity fields in the pathway of saltwater transport in response to the Major Baltic Inflows in the Baltic Sea. Carroll J, editor. 2014 IEEE/OES Baltic International Symposium (BALTIC):23–31. Tallinn: IEEE/OES. doi:10.1109/BALTIC.2014.6887830

Erm A, Maljutenko I, Buschmann F, Suhhova I, Meerits A. 2014. Stormwater impact on the coastal area of the Tallinn Bay. Measuring and Modeling of Multi-Scale Interactions in the Marine Environment - IEEE/OES Baltic International Symposium 2014, BALTIC 2014. doi:10.1109/BALTIC.2014.6887867

Maljutenko I, Laanemets J, Raudsepp U. 2010. Long-term high-resolution hydrodynamical model simulation in the Gulf of Finland. 2010 IEEE/OES Baltic International Symposium (BALTIC):1–7. IEEE. doi:10.1109/BALTIC.2010.5621641

Passenko J, Lessin G, Raudsepp U, Maljutenko I, Neumann T, Laanemets J. 2010. Analysis of temporal variability of measured and modeled vertical distributions of salinity and temperature in the Gulf of Finland during 10-year period. 2010 IEEE/OES Baltic International Symposium (BALTIC):1–8. IEEE. doi:10.1109/BALTIC.2010.5621648

Selected projects

Advanced modeling tool for scenarios of the Baltic Sea ecosystem to support decision making (ECOSUPPORT), 2009–2011

SNOOP – Shipping-induced NOx and SOx emissions - OPerational monitoring network, 2009–2012

Assessment of possible changes of Estonian climate and environmental status on the basis of dynamical modeling of atmosphere, ocean and river runoff (EstKliima), 2012 – 2014

Investigations of the seabed sediments and environmental impacts during the time of construction near the site of the shipwreck "TVER" and of the unknown object in the southern part of the Tallinn Bay, 2017

Sustainable Shipping and Environment of the Baltic Sea region, 2015–2018

Multi-scale physical processes controlling the biogeochemical signal dynamics in the stratified Baltic Sea, 2014–2019

Copernicus Marine Environment Monitoring Service's at Baltic Monitoring and Forecasting Centre, 2018–2021

Elulookirjeldus

Isikuandmed

Nimi:	Ilja Maljutenko
Sünniaeg:	03.12.1986
Sünnikoht:	Venemaa
Kodakondsus:	Eesti

Kontaktandmed

E-post:	ilja.maljutenko@taltech.ee

Hariduskäik

2013– 2019	Tallinna Tehnikaülikool, Maa-teadused – PhD
2011–2013	Tallinna Tehnikaülikool, Maa-teadused – MSc
2008–2011	Tallinna Tehnikaülikool, Tehniline füüsika – BSc
2004–2007	Tallinna Nõmme gümnaasium, keskharidus

Keelteoskus

Eesti keel:	emakeel
Inglise keel:	kõrgtase
Vene keel:	kesktase

Teenistuskäik

2017–	TTÜ, meresüsteemide instituut, nooremteadur
2011–2017	TTÜ, Meresüsteemide Instituut, nooremteadur
2009–2011	TTÜ, Meresüsteemide Instituut, tehnik

Juhendatud lõputööd

2017	Joann Gustav Arro	BSc, kaitstud Tallinna Tehnikaülikoolis
2016	Meri Liis Treimann	BSc, kaitstud Tartu Ülikoolis
2015	Marili Viitak	MSc, kaitstud Tallinna Tehnikaülikoolis

Teadustegevus

Publikatsioonid Eesti Teadusinfosüsteemi klassifikaatori 1.1 ja 3.1 järgi ning valitud projektid on ülaltoodud inglise keelses CVs.